NASA CR-121214
AiResearch 74-9874-1

DESIGN OF H_2-O_2 SPACE SHUTTLE APU

(VOLUME 1 - APU DESIGN)

January 1974

by E. Harris and Staff

AIRESEARCH MANUFACTURING COMPANY
OF CALIFORNIA,
A DIVISION OF THE GARRETT CORPORATION

Prepared for

NATIONAL AERONAUTICS AND SPACE ADMINISTRATION

NASA Lewis Research Center

Contract NAS 3-15708

(NASA-CR-121214) DESIGN OF H2-02 SPACE SHUTTLE APU. VOLUME 1: APU DESIGN (AiResearch Mfg. Co., Torrance, Calif.) 278 p HC $16.00 CSCL 10A

N74-15737

Unclas
G3/03 27646

1. Report No.	2. Government Accession No.	3. Recipient's Catalog No.
NASA CR-121214		

4. Title and Subtitle	5. Report Date
DESIGN OF H_2-O_2 SPACE SHUTTLE APU (VOLUME 1 - APU DESIGN)	January 1974
	6. Performing Organization Code
7. Author(s)	8. Performing Organization Report No.
E. Harris and Staff	74-9874-1
	10. Work Unit No.
9. Performing Organization Name and Address	11. Contract or Grant No.
AiResearch Manufacturing Company of California A Division of The Garrett Corporation Torrance, California 90509	NAS 3-15708
	13. Type of Report and Period Covered
12. Sponsoring Agency Name and Address	Contractor Report
National Aeronautics and Space Administration Washington, D. C. 20546	14. Sponsoring Agency Code

15. Supplementary Notes

Project Manager, H. M. Cameron, NASA-Lewis Research Center, Cleveland, Ohio 44135

16. Abstract

The H_2-O_2 Space Shuttle auxiliary power unit (APU) program is a NASA-Lewis effort aimed at hardware demonstration of the technology required for potential use on the Space Shuttle. It has been shown that a hydrogen-oxygen power unit (APU) system is an attractive alternate to the Space Shuttle baseline hydrazine APU system for minimum weight. It has the capability for meeting many of the heat sink requirements for the Space Shuttle vehicle, thereby reducing the amount of expendable evaporants required for cooling in the baseline APU. Volume I of this report covers preliminary design and analysis of the current reference system and detail design of the test version of this reference system. Combustor test results are also included. Volume II contains (1) the results of the analysis of an initial version of the reference system in Appendix A and (2) the computer printouts of system performance in Appendix B. The APU consists of subsystems for propellant feed and conditioning, turbopower, and control. Propellant feed and conditioning contains all heat exchangers, valves, and the combustor. The turbopower subsystem contains a two-stage partial-admission pressure-modulated, 400-hp, 63,000-rpm turbine, a 0- to 4-g lubrication system, and a gearbox with output pads for two hydraulic pumps and an alternator (alternator not included on test unit). The electronic control functions include (1) regulation of speed and system temperatures; and (2) start-and-stop sequences, overspeed (rpm) and temperature (TIT) limits, fail-safe provisions, and automatic shutdown provisions.

17. Key Words (Suggested by Author(s))	18. Distribution Statement
Auxiliary Power Unit Hydrogen-Oxygen	Unclassified-unlimited

19. Security Classif. (of this report)	20. Security Classif. (of this page)	21. No. of Pages	22. Price*
Unclassified	Unclassified	273	

* For sale by the National Technical Information Service, Springfield, Virginia 22151

FOREWORD

The H_2-O_2 Space Shuttle auxiliary power unit (APU) program is a NASA-Lewis effort aimed at hardware demonstration of the technology required for potential use on the Space Shuttle. Use of such a system on the Space Shuttle would provide significant cost and weight advantages over the current baseline design.

This program is being conducted under the direction of Harry M. Cameron, Project Manager. It is a follow-on effort to two study programs conducted by NASA-Lewis under Contracts NAS 3-14407 and NAS 3-14408. The results of these studies were reported in the following NASA Contractor Reports: NASA CR-2001 and NASA CR-1994, 1995, 1996, 1997, 1993, and 1928.

This report is submitted in two volumes. Volume I covers the work to date in the design of the APU. Volume II contains the appendixes. Initial activities showed that the initial reference APU design could be modified to reduce system uncertainties; these analyses for the initial reference system are summarized in Appendix A. A new reference system was defined; this design, along with that of the test unit, is described in Volume I of this report. Appendix B of Volume II contains the steady-state system analysis.

The requirements of NASA Policy Directive NPD 2220.4 (September 14, 1970) regarding the use of SI units have been waived in accordance with the provisions of paragraph 5d of that Directive by the Director of Lewis Research Center.

Distribution of this report is provided in the interest of information exchange. Responsibility for the contents resides in the author or organization that prepared it.

CONTENTS

ILLUSTRATIONS

ILLUSTRATIONS (Continued)

ILLUSTRATIONS (Continued)

ILLUSTRATIONS (Continued)

ILLUSTRATIONS (Continued)

ILLUSTRATIONS (Continued)

ILLUSTRATIONS (Continued)

TABLES

(TABLES) Continued

(TABLES) Continued

SECTION 1

INTRODUCTION AND SUMMARY

SECTION 1

INTRODUCTION AND SUMMARY

Two study programs performed under Contracts NAS 3-14407 and NAS 3-14408 for the NASA-Lewis Research Center showed a hydrogen-oxygen auxiliary power unit (APU) system to be an attractive alternate to the Space Shuttle baseline hydrazine APU system for minimum weight. In addition to providing a low specific propellant consumption relative to hydrazine, an APU system using cryogenic hydrogen has the capability for meeting many of the heat sink requirements for the Space Shuttle vehicle, thereby greatly reducing the amount of water or other expendable evaporant that must be provided with the baseline APU for cooling. Effective utilization of this cooling capacity requires careful attention to design of the thermal management and control provisions. Digital computer modeling techniques have been developed and applied to handle both problems simultaneously.

This report covers preliminary design and analysis of the current reference system and detail design of the test version (APU-T) of this reference system. A summary of the test system combustor test results is also included.

The reference system is intended to be a preliminary design of a flight prototype APU. The test system is a close-coupled experimental test version of the reference system. The APU-T incorporates all significant reference system design features as well as additional options to be investigated and includes instrumentation to allow investigation and development of the technology required to develop a flight-qualified APU design. It contains "flight-type" components, which have appropriate dynamic characteristics and have received sufficient evaluation to provide reasonable assurance of being qualified for flight application with some modification.

Early studies performed under NAS 3-14408 yielded a system design that incorporated a recycle loop driven by a jet pump to maximize the amount of available cooling. The work under the current program started with approximately that design. A steady-state digital computer program was formulated and a large matrix of flight conditions, power settings, and design variables such as turbine temperature, hydraulic cooling load, and system sizing was examined. Although these design studies showed the operation of the system to be feasible, there were performance prediction uncertainties associated with the jet pump operation over a wide range of conditions. A new reference system was then studied in which the jet pump was replaced by a new heat exchanger called the regenerator, which also maximized the amount of available cooling. The feasibility studies of this new reference system were based upon a modification of the steady-state digital computer system analysis program. Again, a large matrix of operating and design conditions was evaluated. These steady-state system design study results were used to define component design specifications.

The steady-state system computer program then was modified for transient analysis. Transients such as starting, load applications and removals, etc. were evaluated to define the control requirements and further refine the system design. A mathematical model of the control requirements was converted into a breadboard circuit design through further analysis and laboratory work.

The preliminary design of the reference system served as a basis for the detail design of the test system. The test system assembly was packaged with emphasis on accessibility. Special features were added to the control for turbine calibration and system development. In addition, some cost saving modifications were made where they would not affect the technical objectives.

The results of the Task I initial reference system (jet pump) analysis and preliminary design are documented in Appendix A, as the initial design is now of secondary interest. A tabulation of steady-state computer results applicable to the current system is included in Appendix B.

Both appendixes are being published in Volume II, NASA CR-134485.

SECTION 2

SYSTEM DESCRIPTION

SECTION 2

REFERENCE SYSTEM

Reference System Description

The reference system, shown in fig. 2-1, consists of a propellant feed and conditioning subsystem, turbopower subsystem, and control system. The propellant feed and conditioning system begins at the outlet of the high-pressure propellant tanks and contains all heat exchangers, valves, and the combustor. The turbopower subsystem contains a two-stage partial-admission pressure-modulated 400-hp turbine, a 0- to 4-g lubrication system, and a zero-g gearbox with multiple output pads to accommodate two hydraulic pumps and an alternator.

The cold hydrogen is first heated in a hydrogen preheater by hydrogen from the recuperator. Secondly, it flows through a regenerator where it receives heat from the reentrant hydrogen flow that has been the sink for hydraulic pump case drain waste heat. Out of the regenerator both hydrogen streams are now between 400° and 460°R, controlled by the preheater bypass loop. One stream flows through the hydraulic cooler; the other through the lube cooler and the recuperator. The last pass is through the hydrogen-oxygen temperature equalizer where the oxygen is conditioned to be close to the hydrogen temperature. Except for the flow bypass, one around the recuperator, the other around the preheater that acts as flow divider, the hydrogen describes a single path through the propellant conditioning system.

The preheater bypass loop flow is controlled to maintain the lube oil temperature below the maximum permissible operating temperature, but above the congealing temperature, and preferably in the range between 650° and 700°R. As shown on the temperature schedule (inset in fig. 2-1), when the lube oil temperature is 650°R the hydrogen temperature out of the first preheater pass will be controlled by an appropriate preheater bypass flow rate to 460°R. As the lube oil temperature increases (usually at low power output), the hydrogen temperature will be controlled down to 400°R (but not lower, to avoid local congealing).

The preheater bypass loop flow increases with higher hydraulic and lube cooler heat loads. In those cases, most of the preheating will occur in the regenerator. The bypass flow also will increase with increasing hydrogen fluid temperatures. This is the case with a thermally pressurized supercritical tank supply.

The reference system only provides case drain hydraulic fluid cooling. Additional cooling of the hydraulic fluid can be accommodated by routing the hydrogen flow through a full-flow hydraulic fluid cooler and by regenerative utilization of the rejected heat in the tank thermal pressurization system. This leads to a naturally stable tank pressurization system since the fluid withdrawal rates are always directly proportional to the hydraulic waste heat.

The recuperator bypass loop flow is controlled by the hydrogen temperature downstream of the temperature equalizer, attempting to maintain 750°R combustor inlet. At high power levels, the engine operates more efficiently

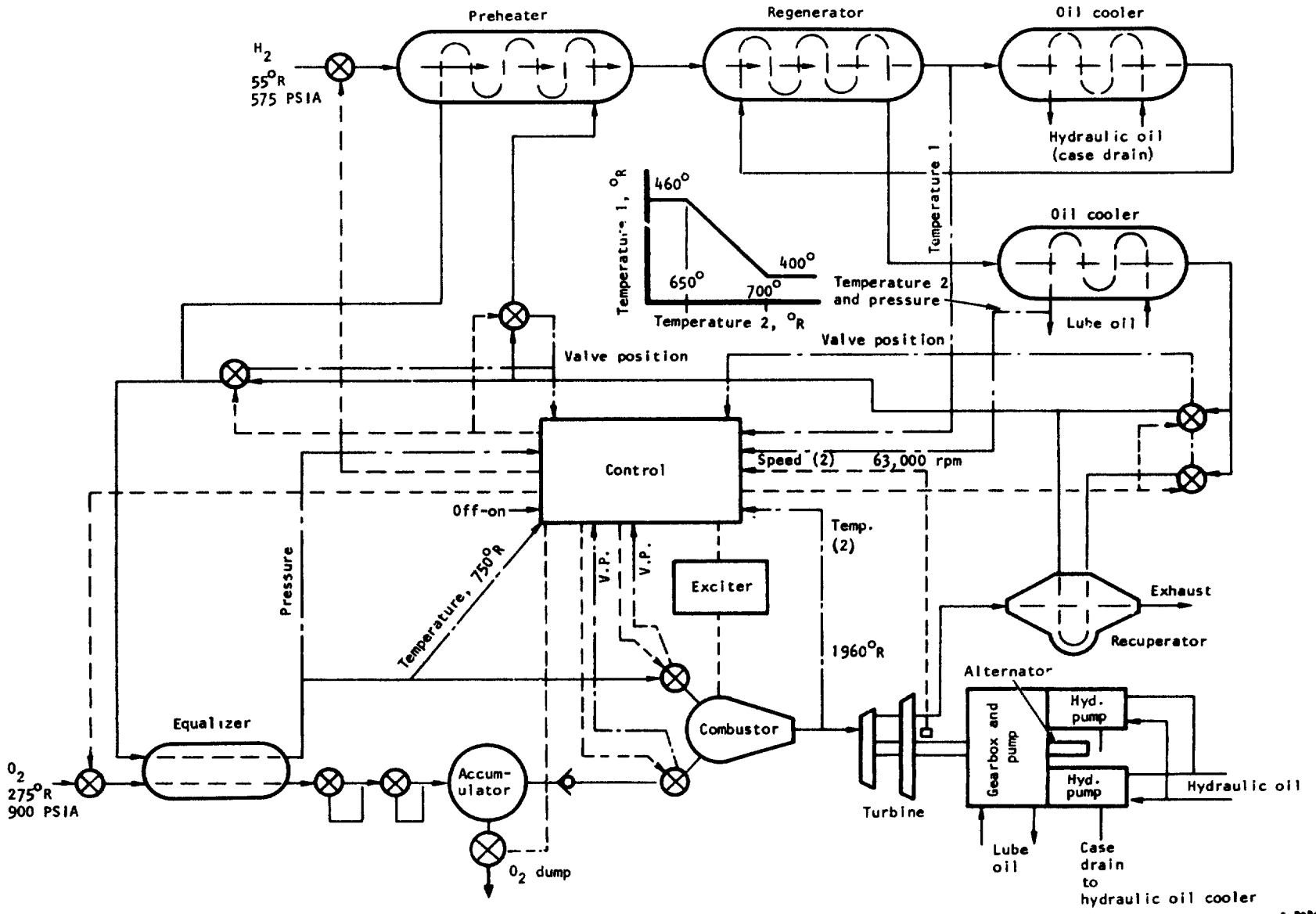

Figure 2-1.--Reference System.

and insufficient heat is available in the recuperator to attain this temperature even at zero bypass. Computer simulation shows, however, that with 55°R hydrogen inlet and full power combustor, inlet temperature will be no lower than 680°R.

Each bypass loop is controlled by two butterfly valves, one in series, the other in parallel with the heat exchanger throughflow. The two valves in each loop are linked electronically so they act like a three-way valve. The two valve sets are also electronically coupled in the control to prevent undesirable interaction. It may be advantageous later actually to replace two butterflies with a single three-way to achieve system simplification; however, the system operation may be more forgiving of single valve failures with the present design.

Two redundant pressure regulators are employed in the oxygen circuit, since a single one sticking open would result in an overtemperature. They are both located downstream of the temperature equalizer in order to maintain supercritical pressure and avoid two-phase flow in the equalizer.

An accumulator is located downstream of the regulators in order to provide more equal stiffness in the hydrogen and oxygen control system, compensating for a somewhat slow pressure regulator response (100 msec). The accumulator has a dump valve that opens on shutdown signal to vent the oxygen. This is an emergency provision in the event of an electrical failure in which the oxygen control valve fails in its nearly closed position and the hydrogen valve fails open. Without oxygen dump, with both shutoff valves closed, a high O/F would result at the end of the hydrogen run-out. In a later modification, both the accumulator and the dump valve may be designed out of the system if fast electronic regulators are substituted for the now specified mechanical one.

A check valve is located downstream of the oxygen accumulator to prevent hydrogen backflow into the accumulator during starting, as hydrogen lead is used in starting to prevent overtemperature. The hydrogen and oxygen control valves are electrically linked in the control. An exciter is used to energize the combustor spark plug during start and whenever the turbine temperature is 100°R below the set point, and the system is turned on. The combustor delivers hydrogen-rich combustion products to the turbopower subsystem.

The turbine is a two-stage supersonic axial-flow design. The design speed is 63,000 rpm with a turbine inlet temperature (TIT) of 1960°R using V-57 alloy turbine wheels. The turbine is so designed that it can be retrofitted with U-700 wheels and operated at 70,000 rpm and 2060°R TIT. The case drain oil from the hydraulic pumps mounted on the turbine gearbox is cooled by hydrogen in the hydraulic oil cooler; the turbine gearbox oil is cooled by hydrogen in the lube oil cooler.

The electronic control functions can be divided into primary and secondary. The primary control functions are to hold the TIT, rpm, and equalizer outlet temperature constant by modulation of the hydrogen bypass and control valves. The secondary control functions are start-and-stop sequences, overspeed (rpm) and temperature (TIT) limits, fail-safe provisions, and automatic

shutdown provisions including lube pressure and temperature, hydrogen underpressure, turbine overspeed, and control internal monitoring. The description of the components design and their function is treated in detail in the pertinent section of this volume of the report. The system specifications are summarized in Table 2-1.

TABLE 2-1

SUMMARY OF SYSTEM SPECIFICATIONS

Peak power:	400 hp gearbox shaft output
Minimum power:	0 hp gearbox shaft output
Output pads:	2 pump pads at 5,000 rpm 1 generator pad at 12,000 rpm
Turbine speed:	63,000 rpm ±1 percent steady state ±5 percent transient
Turbine inlet temperature:	1960°R
Hydrogen inlet temperature to APU:	55° to 560°R
Hydrogen inlet pressure:	575 psia
Oxygen inlet temperature to APU:	275° to 560°R
Oxygen inlet pressure:	900 psia
Design life:	1,000 hr hot operation (900 cycles) and 2,000 hr on inert gas checkout (600 cycles)
Cooling capability at 400 hp (heat sink for hydraulic system):	5,000 Btu/min
Potential cooling with integrated tank pressurization at 400 IP:	15,000 Btu min
Estimated dry weight:	280 lb

Test System Description

The auxiliary power test unit (APU-T) is schematicall the same as shown in fig. 2-1 and is a close-coupled experimental test versio. of the reference system. To allow the investigation and demonstration of the technology required for a flight-type APU, special design features and contr.l options have been added.

Provisions in the controller permit variations in the rpm, TIT, and combustor pressure to permit initial APU operation to be conducted at moderate speeds and temperatures. The capability to improve system efficiency by increasing the combustor inlet temperature from 750° to 900° R has also been provided.

The APU-T system has been protected through automatic shutdown in the event of exceedance of control values or component failures that are not necessarily critical or do not give cause for shutdown of the flight system.

The APU-T utilizes all "flight-type"* components except as listed below:

(1) The turbine bearing seal has been changed from a face seal to a labyrinth seal with externally supplied nitrogen buffer gas in order to avoid seal development.

(2) An external lube oil pump supplies the turbine and gearbox

(3) Heat soakback problem at shutdown was solved in the reference turbine design but was not carried through into the -T turbine since lubricant flow from an external source can be maintained after shutdown.

(4) The gearbox has not been designed for zero-g flight capability and has two pump pads but no alternator pad.

(5) The recuperator had to be designed for ground test in which internal pressure is reduced to vacuum and the external one is at the ambient pressure of the test environment.

The APU-T shown in fig. 2-2 was packaged for ease of component and instrumentation accessibility and installation, without strict regard to weight and volume. The controller is not included in the package because it is located in the control room and is connected to the APU-T by an umbilical cable.

*"Flight-type" components are similar in size, weight, and dynamic characteristics and have received sufficient evaluation to provide reasonable assurance that they are capable of being qualified for the required flight application with only minor modifications.

The APU-T assembly is built by brazing the following two major subassemblies into a single unit:

(1) Turbine-gearbox-pump assembly, which also will contain the combustor and oxygen flow control valves, the oxygen check valve and accumulator, and the oxygen regulators. All these components will be mounted on the gearbox support structure.

(2) The heat exchanger assembly, which will include all heat exchangers and bypass valves. This assembly includes a separate support structure.

The above two subassemblies then will be combined into the complete APU-T by brazing three interface joints: the oxygen line, the hydrogen line, and the turbine exhaust duct. The entire assembly will be mounted on a base structure that will serve both as a test stand and a structure to support the assembly during transit and handling by forklift.

All joints in the hydrogen and oxygen circuits in the entire APU-T are welded or brazed. Some mechanically sealed joints exist in the turbine, valves, and certain instrumentation connections. Two hydroformed bellows are used in the duct between the turbine discharge and the recuperator to allow for thermal expansion. All other piping expansions are compensated by loops and bends in the piping. Each heat exchanger is mounted by a single fixed point, with other support points flexible to allow for expansion. All components are mounted for a one-g, one-direction environment.

The APU-T components and piping are so located that there is adequate access for instrumentation and application of a 1-in. layer of insulation material (Johns-Manville CRF-800 felted refractory insulation) that will be applied after preliminary checkout testing.

The location of the instrumentation is shown in fig. 2-3.

FOLDOUT FRAME

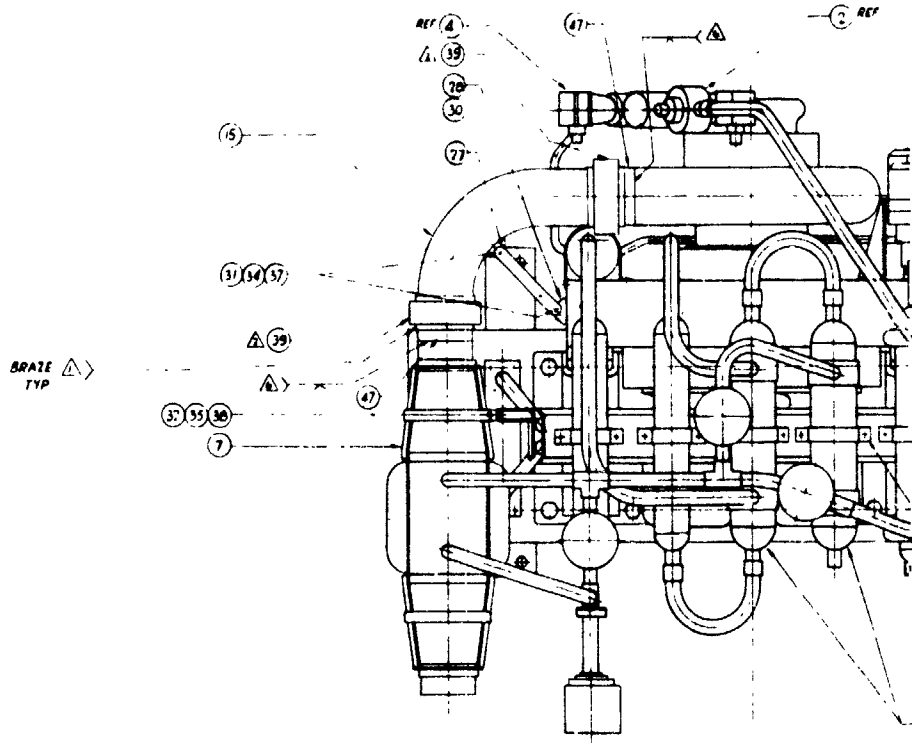

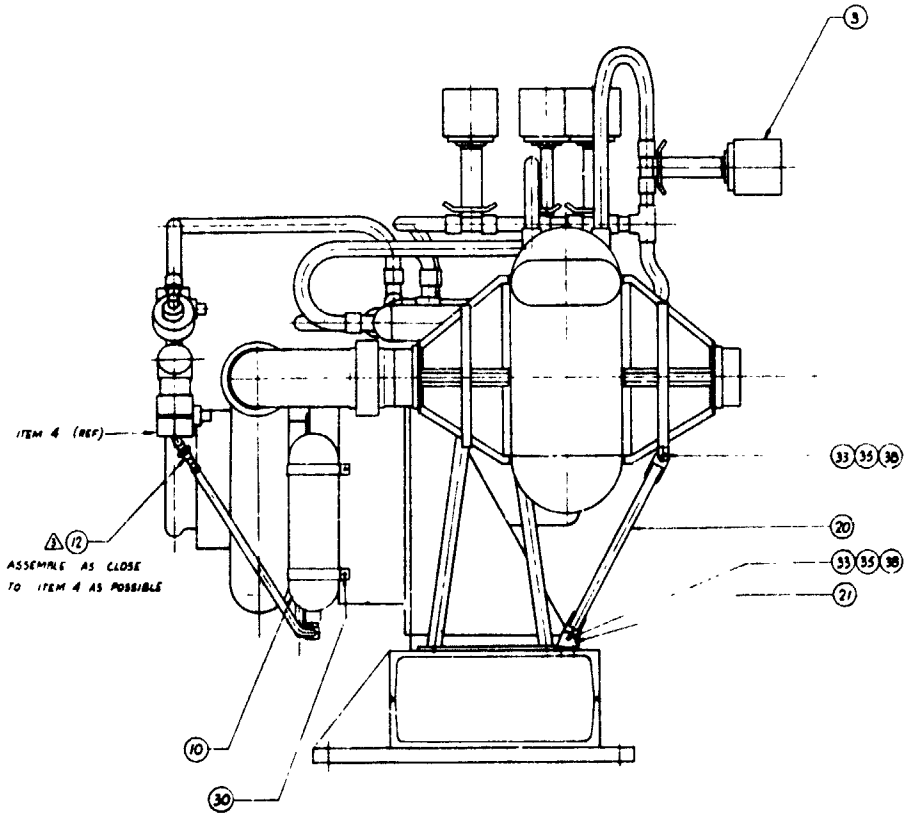

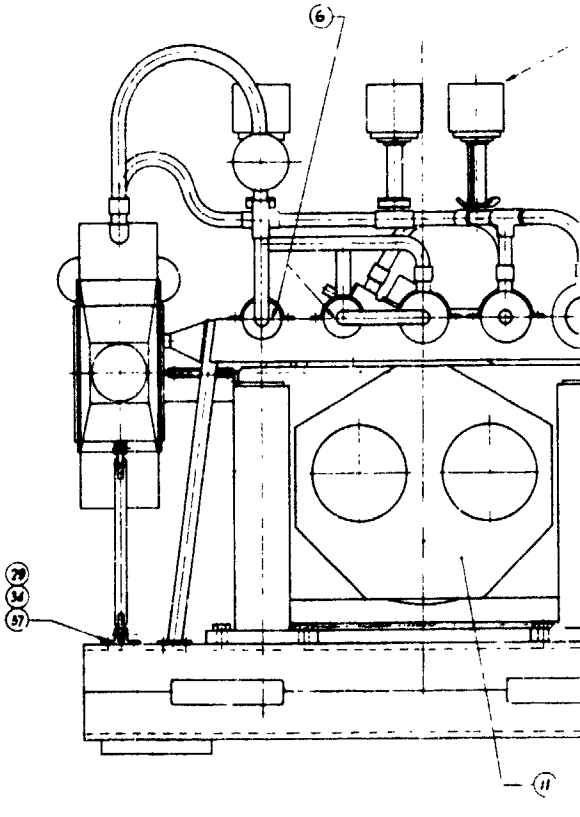

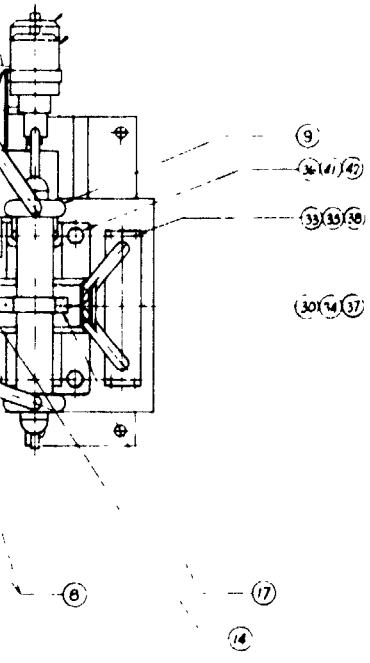

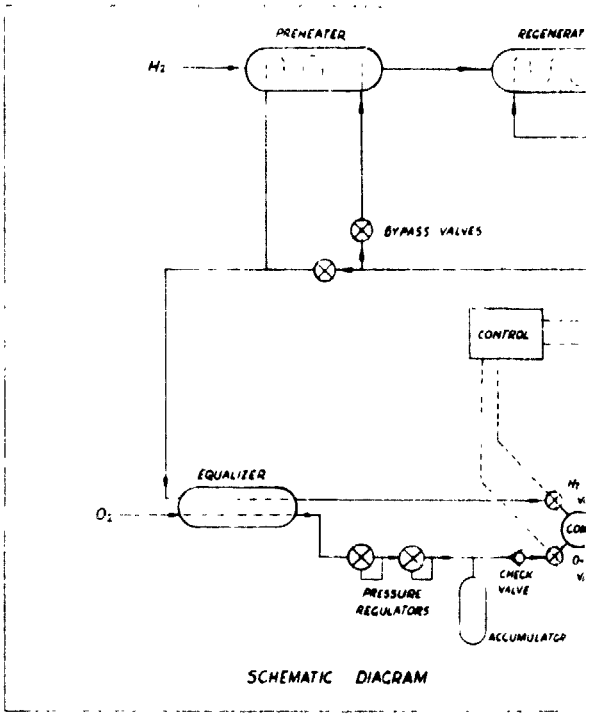

SCHEMATIC DIAGRAM

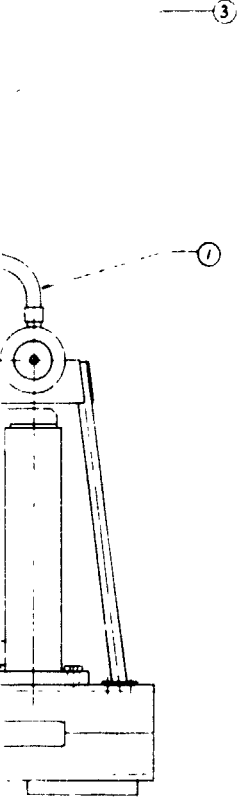

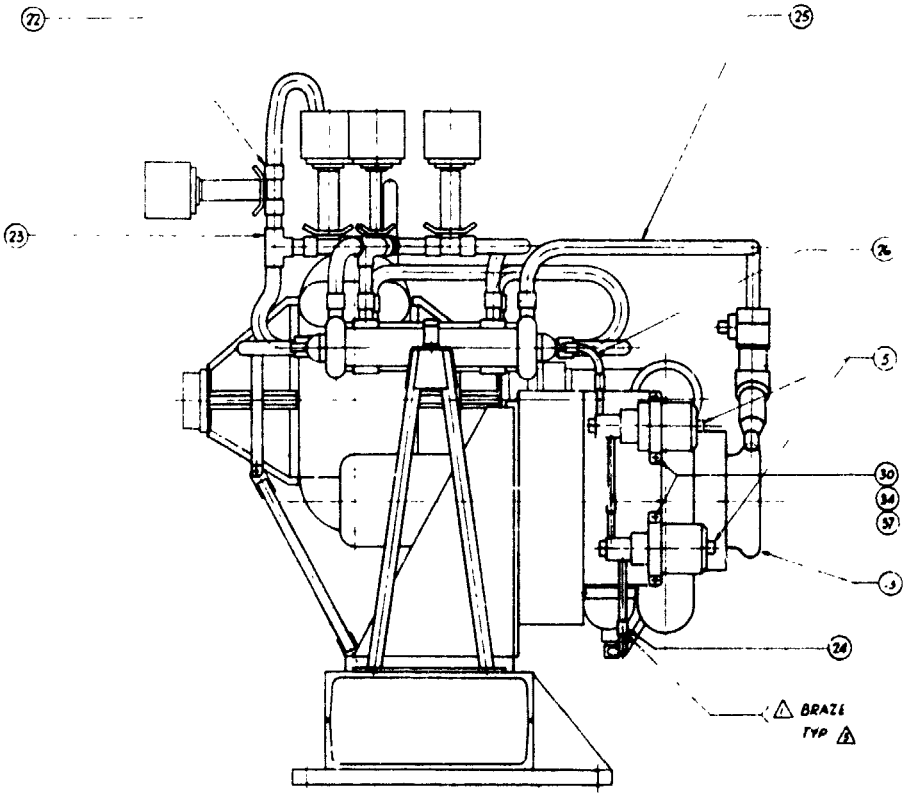

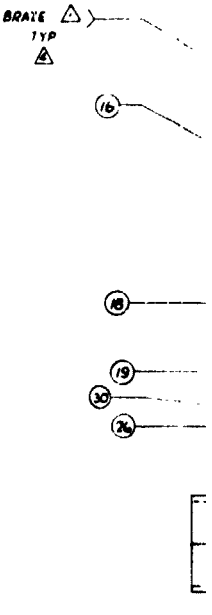

4 MAY BE OBTAINED FROM PURITAN ZEP., EL SEGUNDO, CA

5 WELD PER AIR SPEC WBS 18

6 ALL JOINT ENDS OF ITEM 26 TO BE SWAGED TO .491/.489 DIA FOR .50 MIN LENGTH REF

7 ALL JOINT ENDS OF ITEM 25 TO BE SWAGED TO .994/.989 DIA FOR .50 MIN LENGTH REF

FOLDOUT FRAME

FOLDOUT FRAME

3

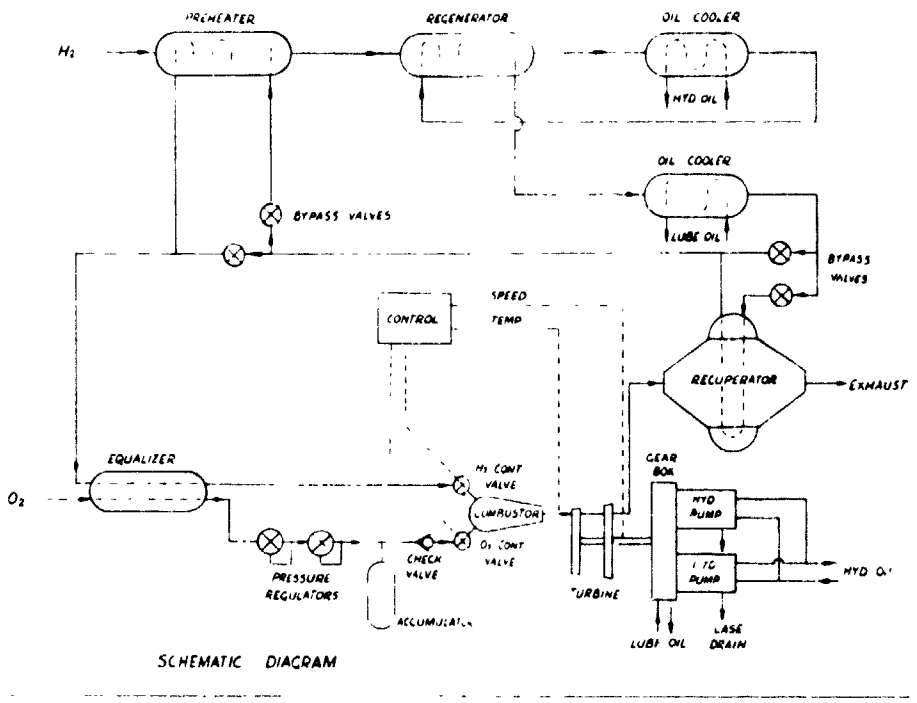

SCHEMATIC DIAGRAM

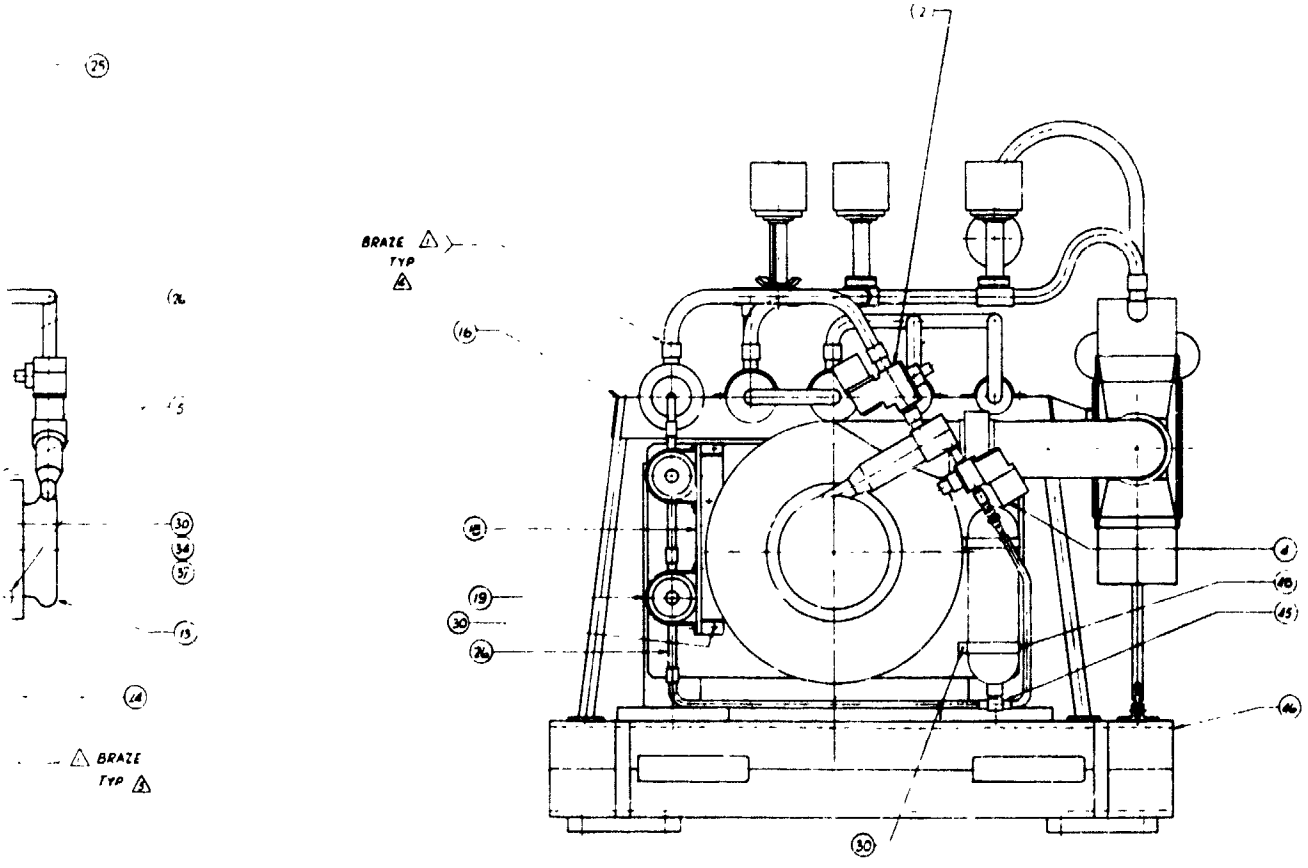

MAY BE OBTAINED FROM PURITAN ZEP, EL SEGUNDO CA

WELD PER AIR SPEC WBS 18

ALL JOINT ENDS OF ITEM 26 TO BE SWAGED TO .491/.489 DIA FOR .50 MIN LENGTH BEFORE BRAZING

ALL JOINT ENDS OF ITEM 25 TO BE SWAGED TO .994/.989 DIA FOR .50 MIN LENGTH BEFORE BRAZING

△1 MAY BE OBTAINED FROM CRISSAIR INC EL SEGUNDO CA

△1 MAY BE OBTAINED FROM GARDNER BELLOWS CORP VAN NUYS CA

△ INDUCTION BRAZE PER AIR SPEC WBS 27 USING BRAZING ALLOY ITEM (40)

NOTES: UNLESS OTHERWISE SPECIFIED

Figure 2-2.--H_2O_2 APU-T Assembly.

FOLDOUT FRAME

1

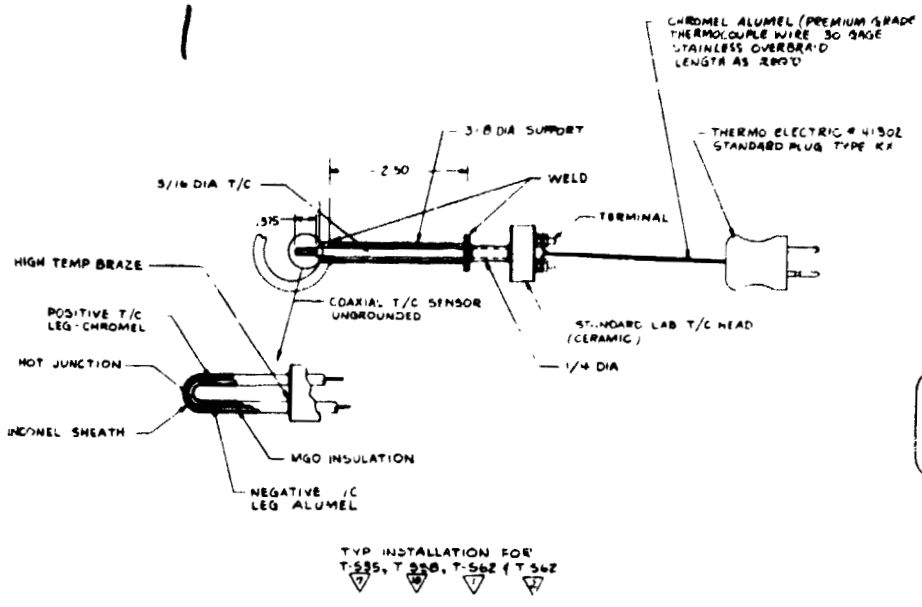

TYP INSTALLATION FOR
T-535, T-538, T-562 & T-562
(7) (8) (7) (7)

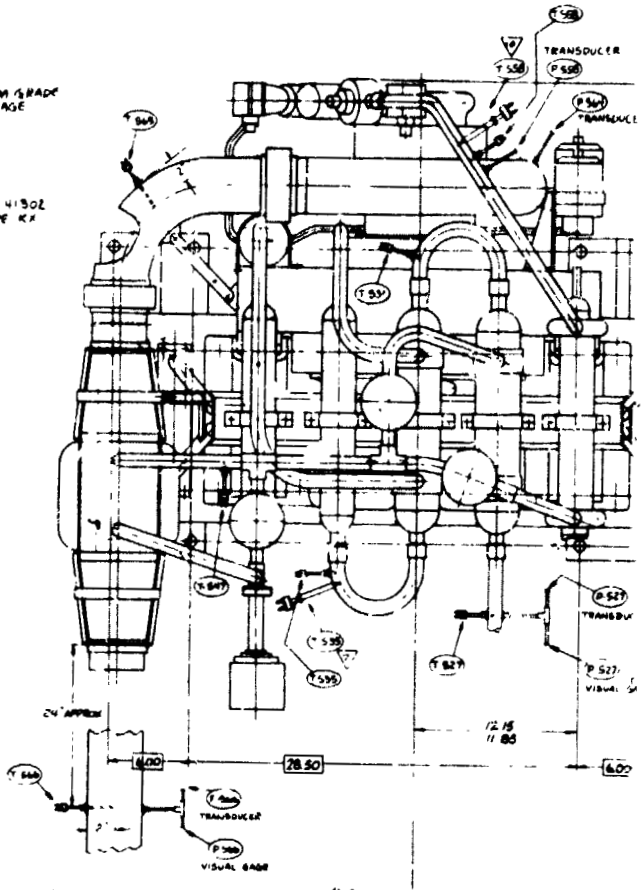

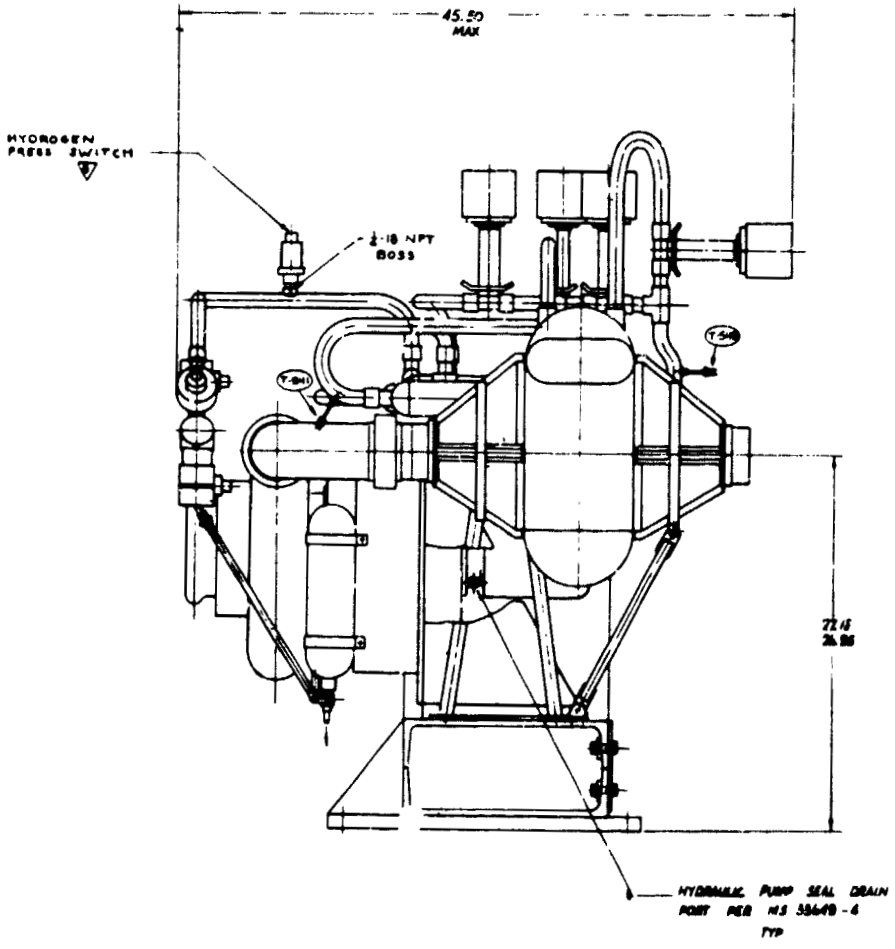

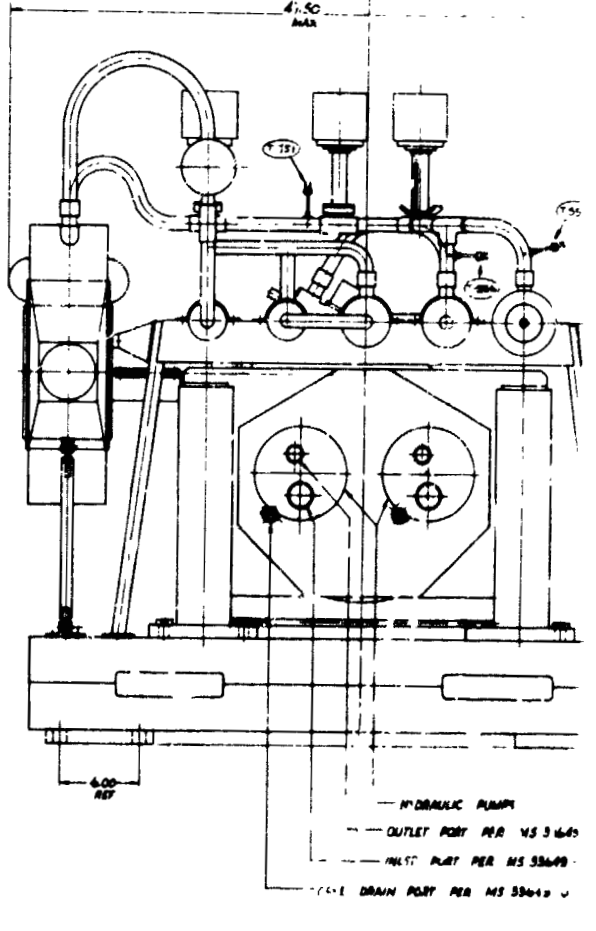

FOLDOUT FRAME

2

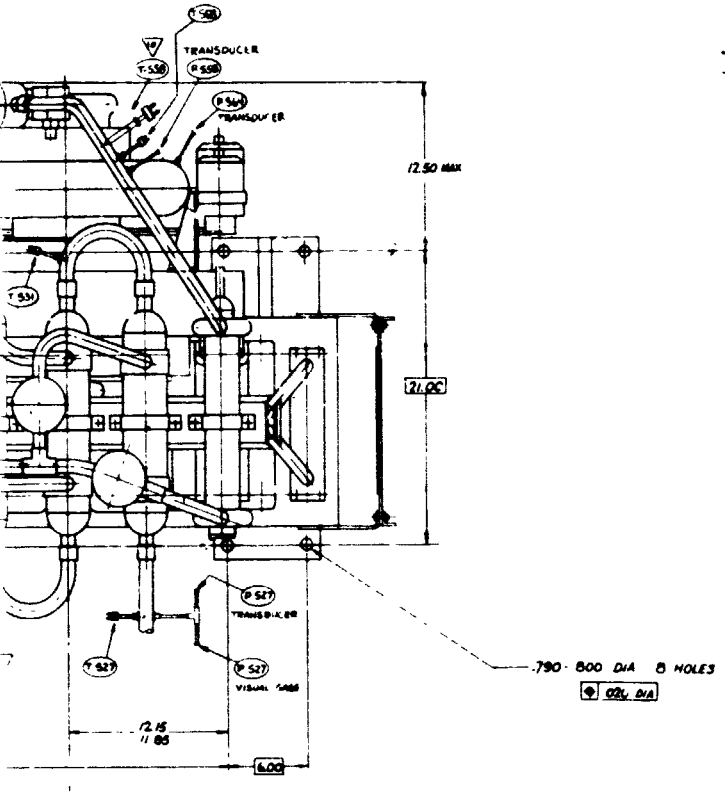

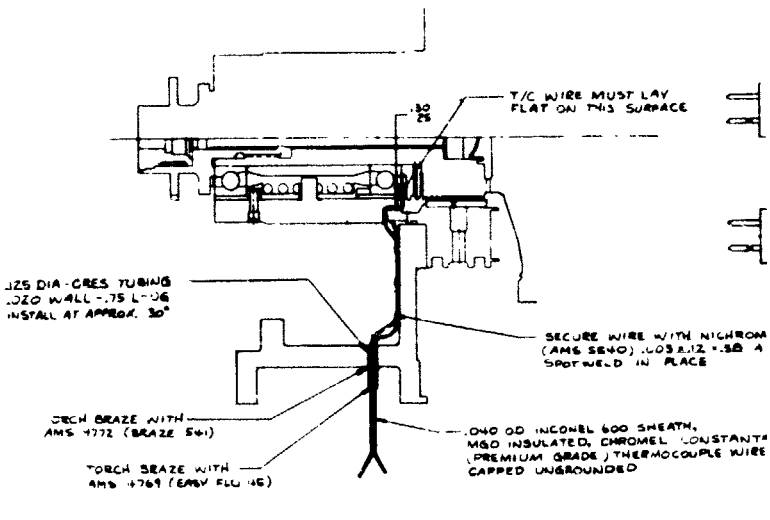

BEARING TEMP INSTALLATION
ASSEMBLE T/C WIRE AT 75° & 255° AT SUB ASSY
581273. T/C WIRE MUST BE TUCKED IN SLOT UNTIL
ROTATING ASSY IS INSTALLED INTO HOUSING

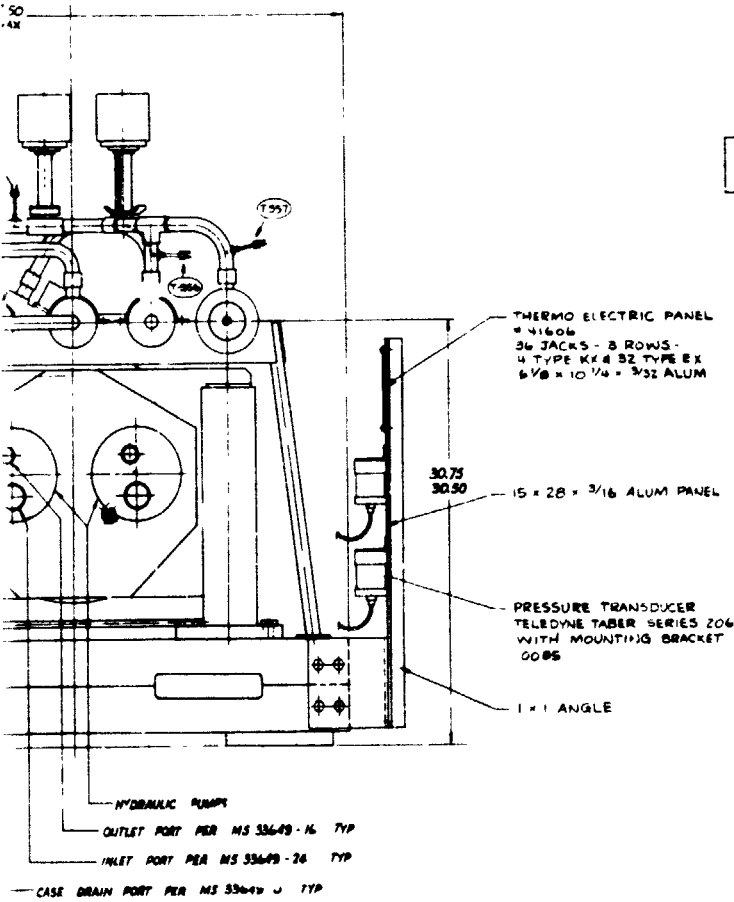

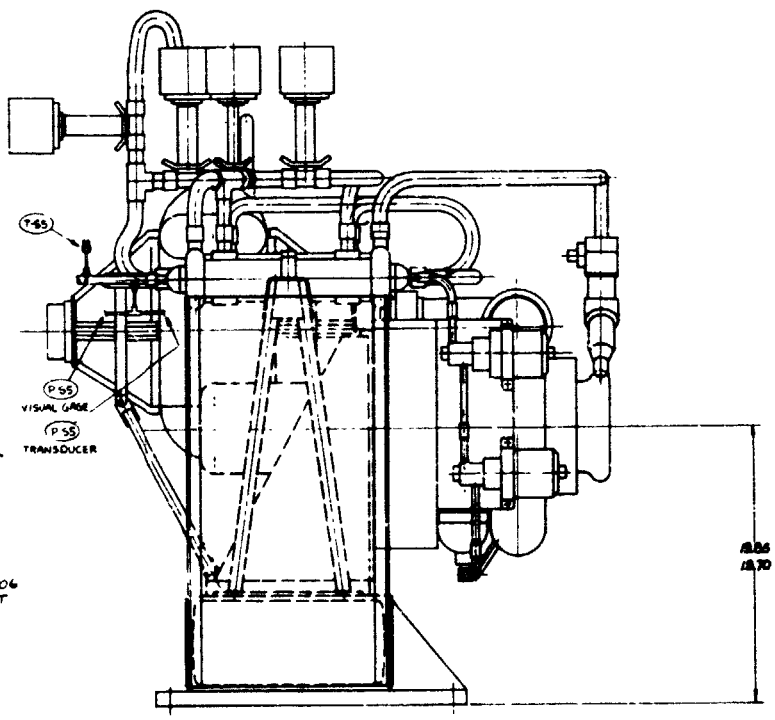

FOLDOUT FRAME

3

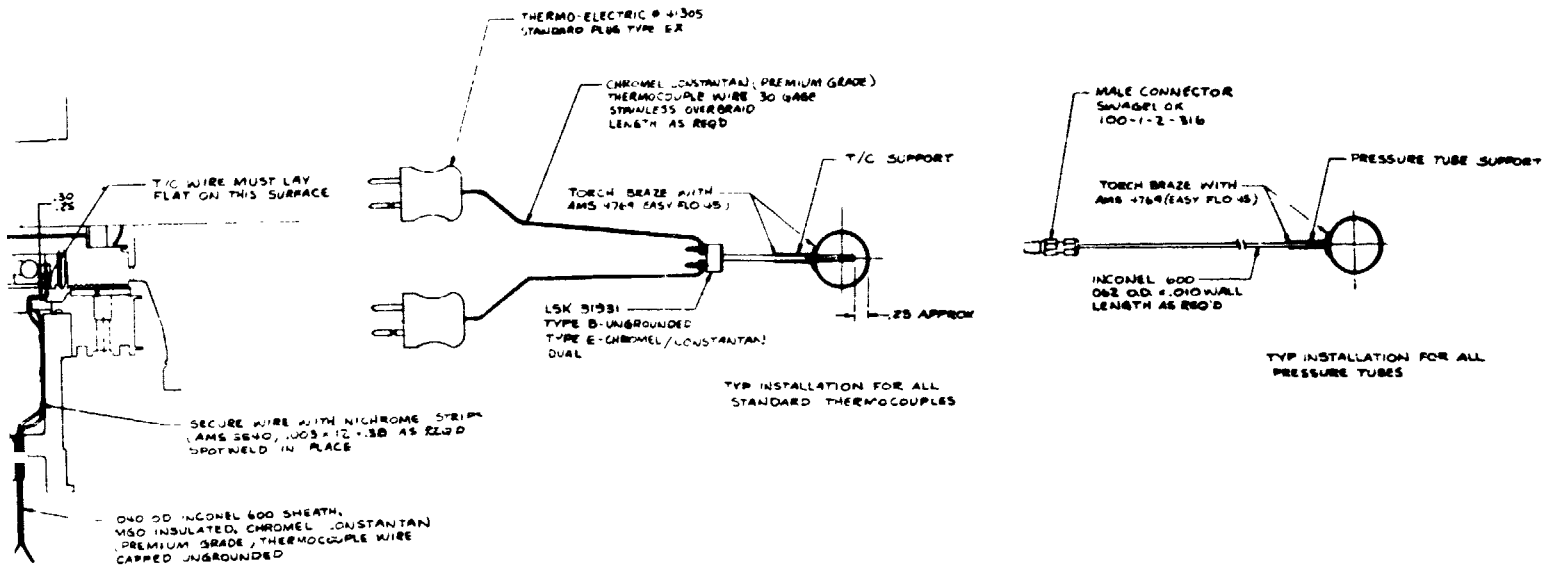

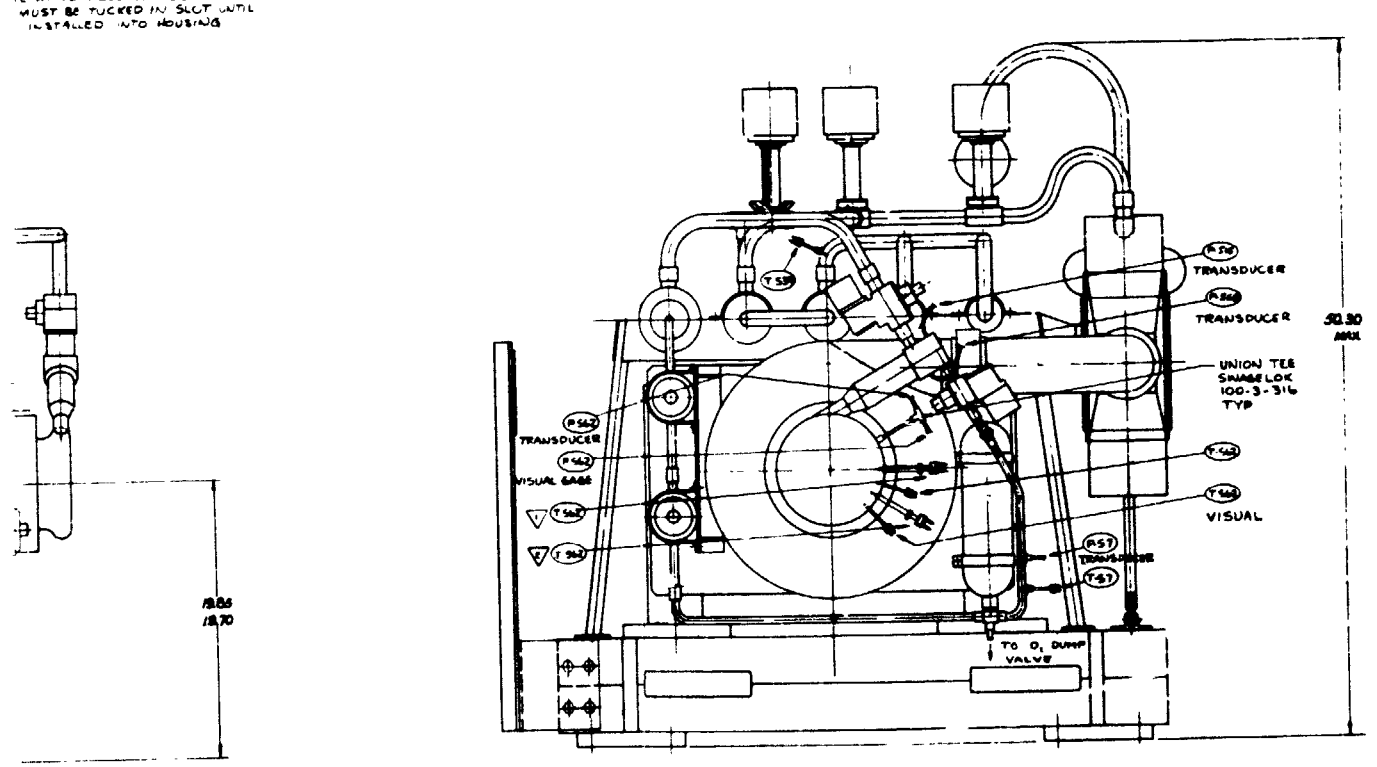

SEE DATA STATION LIST & SYSTEM TEST SCHEMATIC
FOR LEGEND AND DESCRIPTION OF INST. POINTS

Figure 2-3.--Installation APU-T H_2O_2

2-9/2-10

SECTION 3

SYSTEM ANALYSIS

SECTION 3

SYSTEM ANALYSIS

The system analysis was based on the reference system, utilizing the component dynamic characteristics, which were also valid for the test systems.

The system was analyzed using a digital computer simulator. The computer simulator is used in both steady-state and transient analysis to size and evaluate the performance of the various components for the complete system operating range. The sizing of the components requires that the nonlinear effects of the components be used, including major second-order component effects within the system.

The resulting digital model must have sufficient transient accuracy to permit identification of the system transfer functions. These transfer functions are necessary to design the APU control. The resulting control design, schematically shown in Fig. 3-1, is mechanized in the simulator to verify stability and predict transient performance of the control interacting with the nonlinear system.

Computer Program Description

The simulator is constructed using a main subroutine (MAINSR) that reads the control data cards. The data cards are of two types: (1) data to be used during a solution, and (2) solution types (by-pass, no-bypass, design point, off-design). The mode for data (to be used during a solution) is used to define boundary conditions or to scale particular components within the system. Solution-type data are used to select the dependent relationships to be satisfied and the independent parameters to be manipulated to satisfy the dependent conditions.

The steady-state solutions (fig. 3-2) are obtained by using the boundary specified by various data cards and the required conditions for the particular solution desired. The main subroutine (MAINSR) then dimensions the matrix required for the solution as well as establishing the particular independent variables (XEQ) and dependent relations (CLXEQ) to be used during the solution. The next step is to call a subroutine that solves a set of algebraic equations using a modified Newtonian technique (NEWTON). This in turn calls an external subroutine (SSAPUT), which is specified in its argument list to determine the algebraic relationships between the various independent and dependent variables. The dependent relations are written in a form that allows NEWTON to drive the dependent vector to the origin.

When the solution has been obtained, control is returned to MAINSR, which in turn calls FINAL to print the solution. Finally, MAINSR reads another card for instructions pertaining to the next case to be run.

The two primary uses for steady-stage solutions are (1) initial design performance of the system and (2) to set the initial conditions for a transient

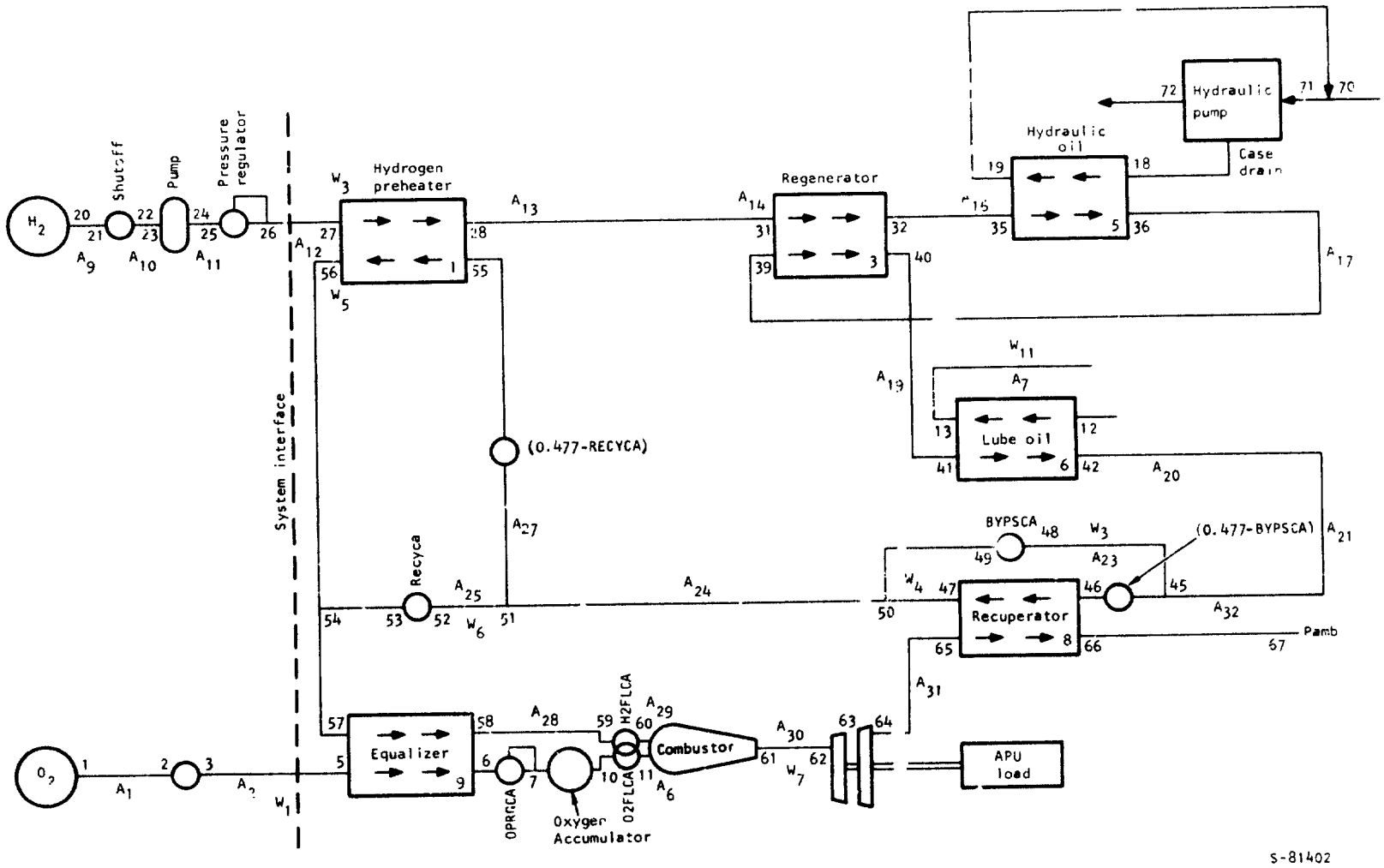

Figure 3-1.--H_2-O_2 APU Computer Program Notation.

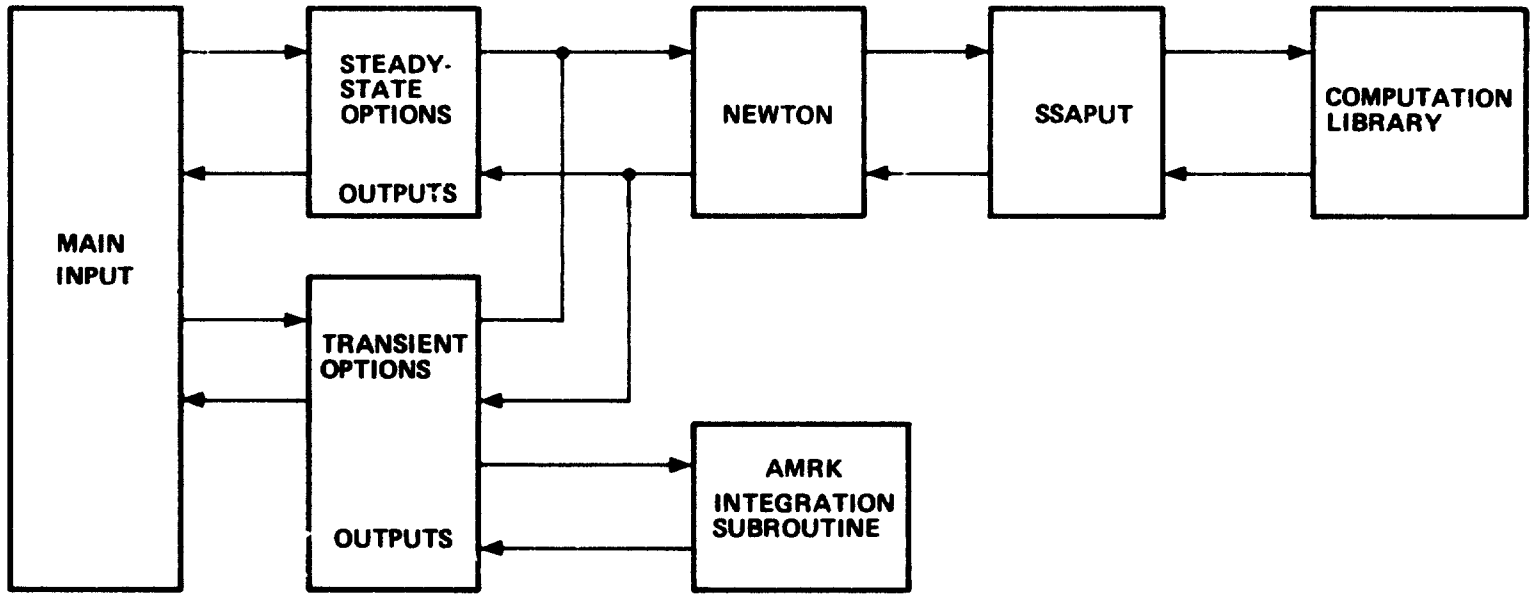

Figure 3-2.--Simulator Topology.

solution. Design match (DMATCH) is the first steady-state solution usually sought in the simulator program. It allows for a solution where some of the variables are the geometric characteristics of the engine. This particular option is reprogrammed for various solutions as the design proceeds, and finally is eliminated altogether as the APU design becomes finalized. The following paragraphs describe the use of the program to determine desirable component and system characteristics and design points.

Flow Control Valve Sizing

This option was programmed to size the hydrogen flow control valve (H2FLCA) and compared the turbine acceleration to a reference acceleration. The controlled closure errors were the turbine inlet temperature, turbine acceleration, combustor inlet temperature, and the hydrogen temperature at the inlet 63,000 rpm, sea level. Solutions were obtained at 1000 rpm/sec intervals (1000 rpm/sec, 2000 rpm/sec, 3000 rpm/sec, etc.) until the flow control valves no longer had controllable pressure drop. This set of runs was plotted versus time for the turbine to change 1000 rpm against the resulting hydrogen flow control valve area and oxygen flow control valve area.

The curves (figs. 3-3 and 3-4) show a sharp knee as the pressure drops across the valve diminish to zero. This knee is dependent on the pressure drop in the system between the propellant supply pressure and the inlet to the first-stage turbine nozzle. The location on the curve chosen for the electrical valve limit was an area equivalent to 10,000 rpm/sec, with a 350-hp load. This acceleration cannot be obtained at 60,000 rpm because of the constant horsepower characteristic of the load, which results in a higher torque requirement at lower speeds. However, sufficient acceleration capability in the system exists to provide acceptable response to system transients.

With the maximum valve area established, the option was run at minimum horsepower extraction at minimum altitude to determine the minimum valve areas (figs. 3-5 and 3-6). The system was run at various decelerations from -1000 rpm/sec until the flow control valves become completely closed. The minimum electrical limits on the valves were selected to yield a deceleration of -5000 rpm/sec.

The selection of a lower limit for the deceleration as compared to the acceleration limit is related to the load characteristics at each operating limit. The maximum horsepower end of the spectrum has a load characteristic that is primarily determined by the hydraulic pump characteristic. As the speed increases, the pump does not need as much stroke to maintain the hydraulic oil pressure; therefore, the pump stroke decreases, resulting in a decreased torque. The decrease in the required torque for the pump is greater than the decrease in the turbine torque due to the increased speed, which makes the system open loop unstable. At the other end of the load spectrum, the load is determined by the hydraulic oil pump losses and the gearbox losses. This load characteristic results in an increasing load horsepower with increasing speed, and furthermore, an increasing load torque with an increase in turbine speed. The turbine characteristic is similar to the high-power case, but is open-loop stable. The range of operation that requires the largest

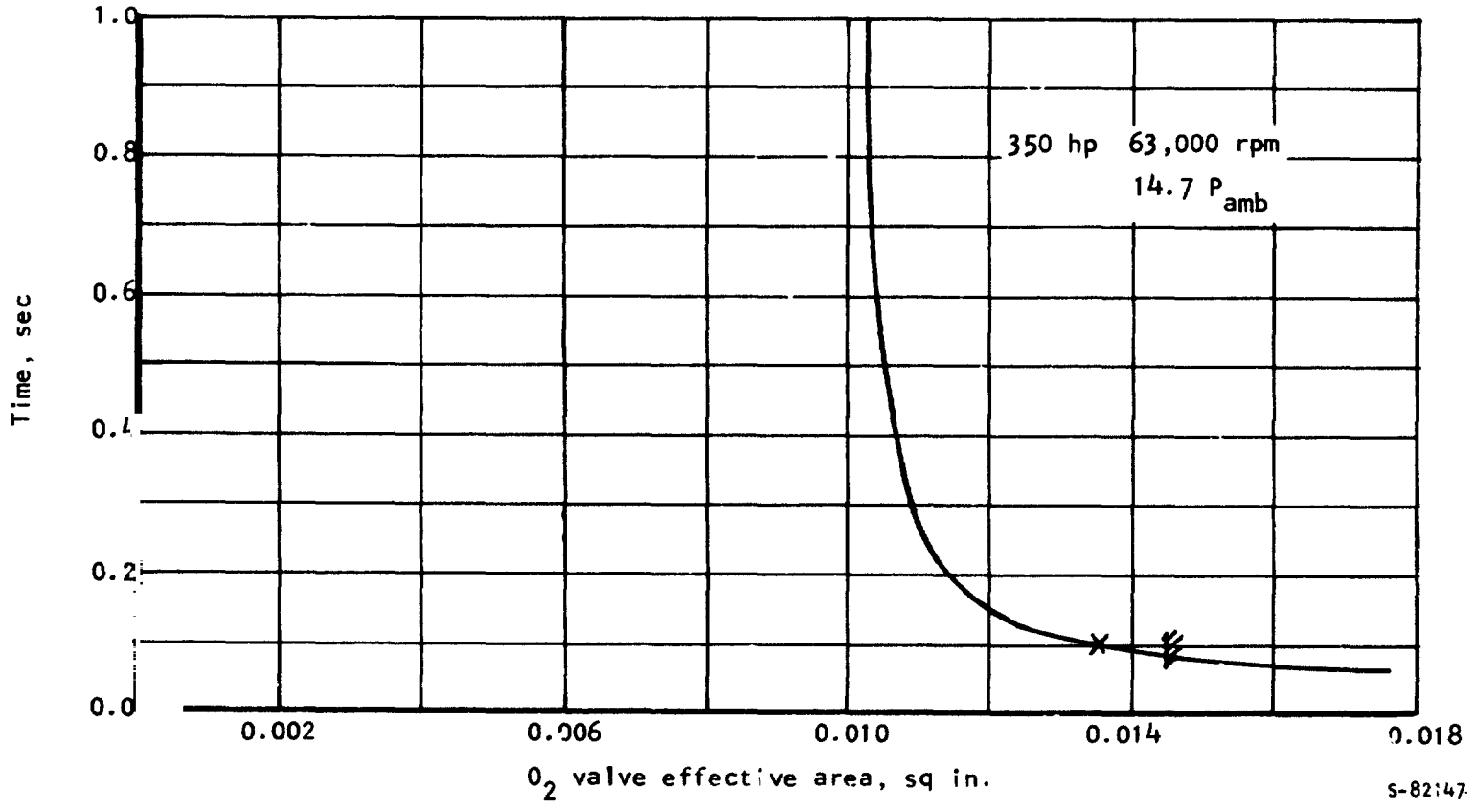

Figure 3-3.--Time to Acceleration 1,000 rpm vs O_2 Effective Valve Area.

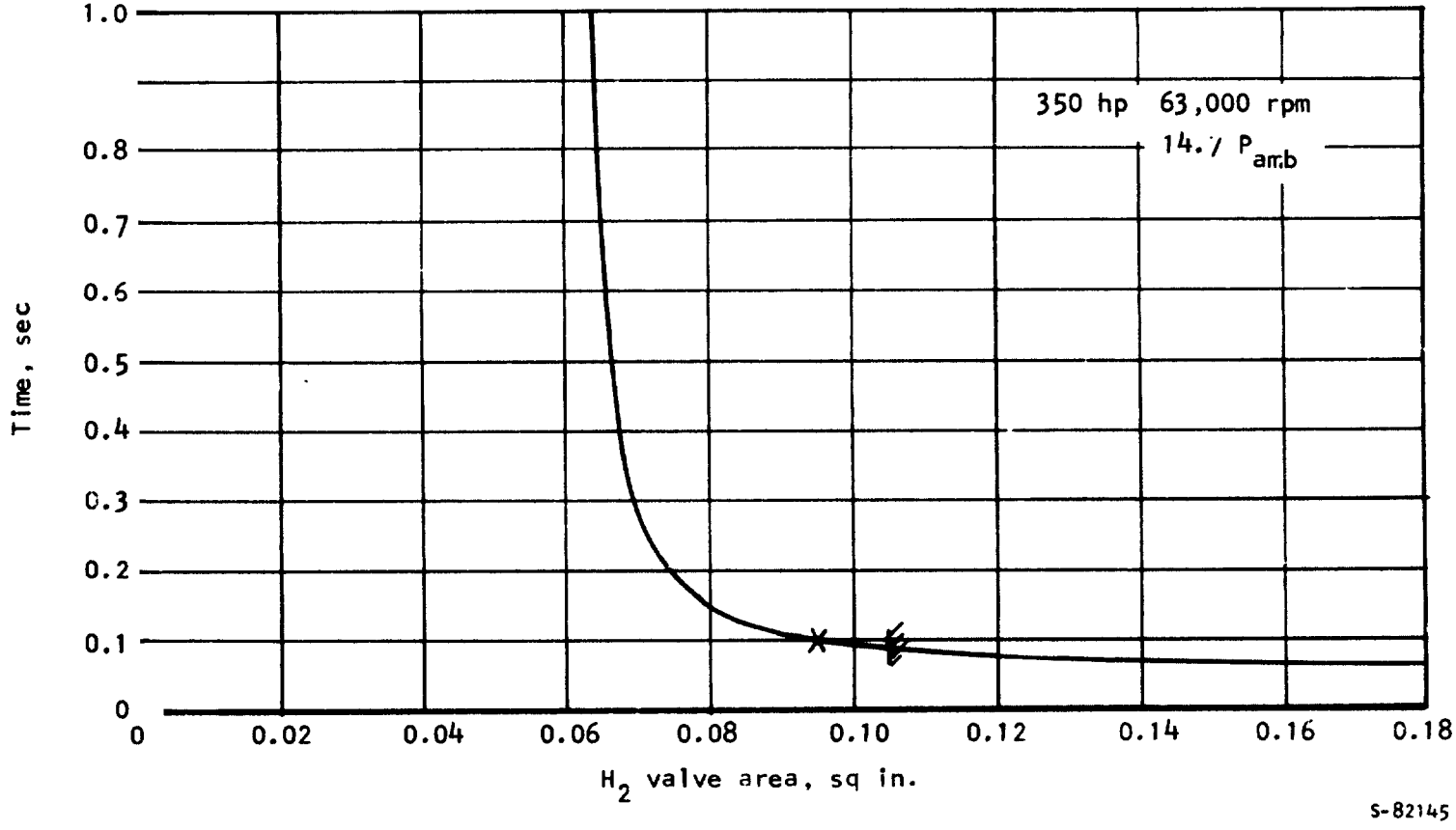

Figure 3-4. --Time to Acceleration 1,000 rpm vs Effective Valve Area.

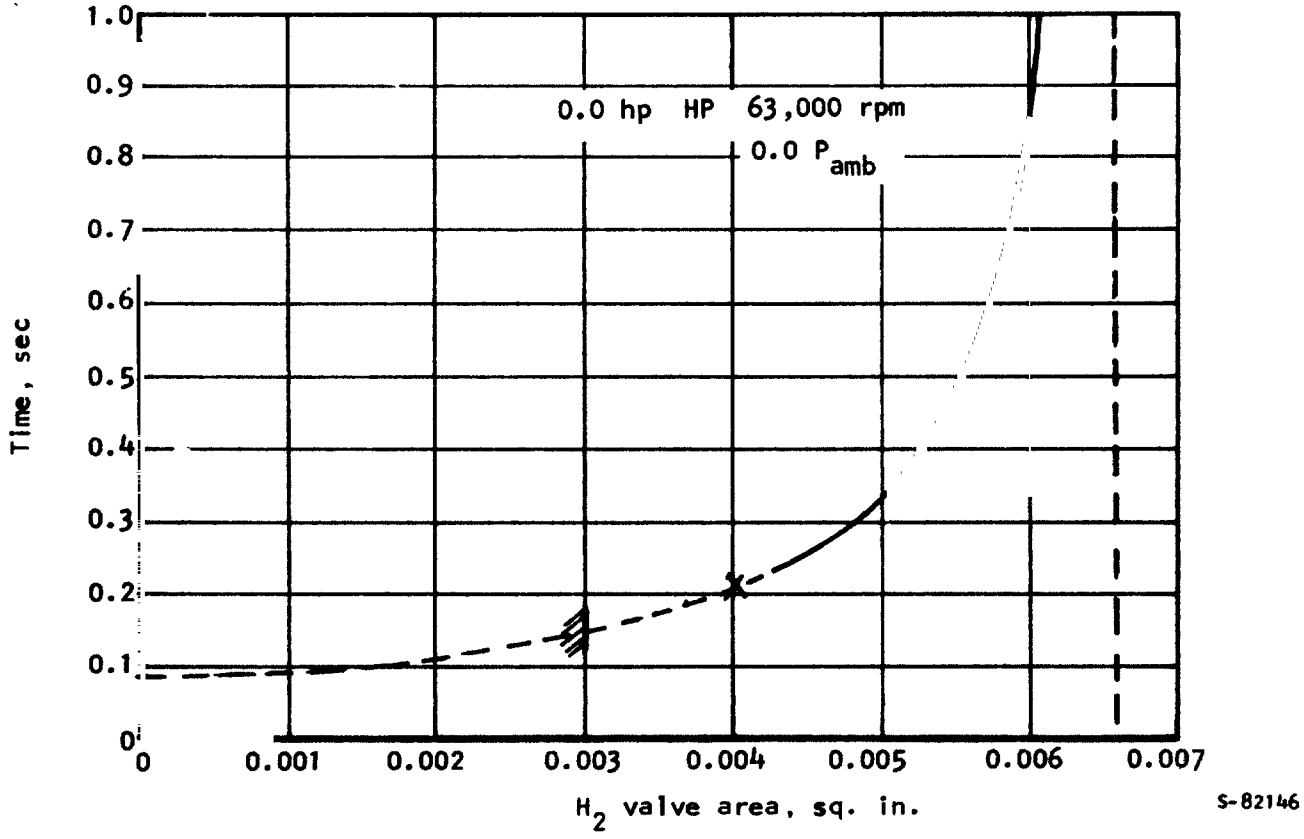

Figure 3-5. --Time to Deceleration 1,000 RPM vs Hz Control Valve Effective Area.

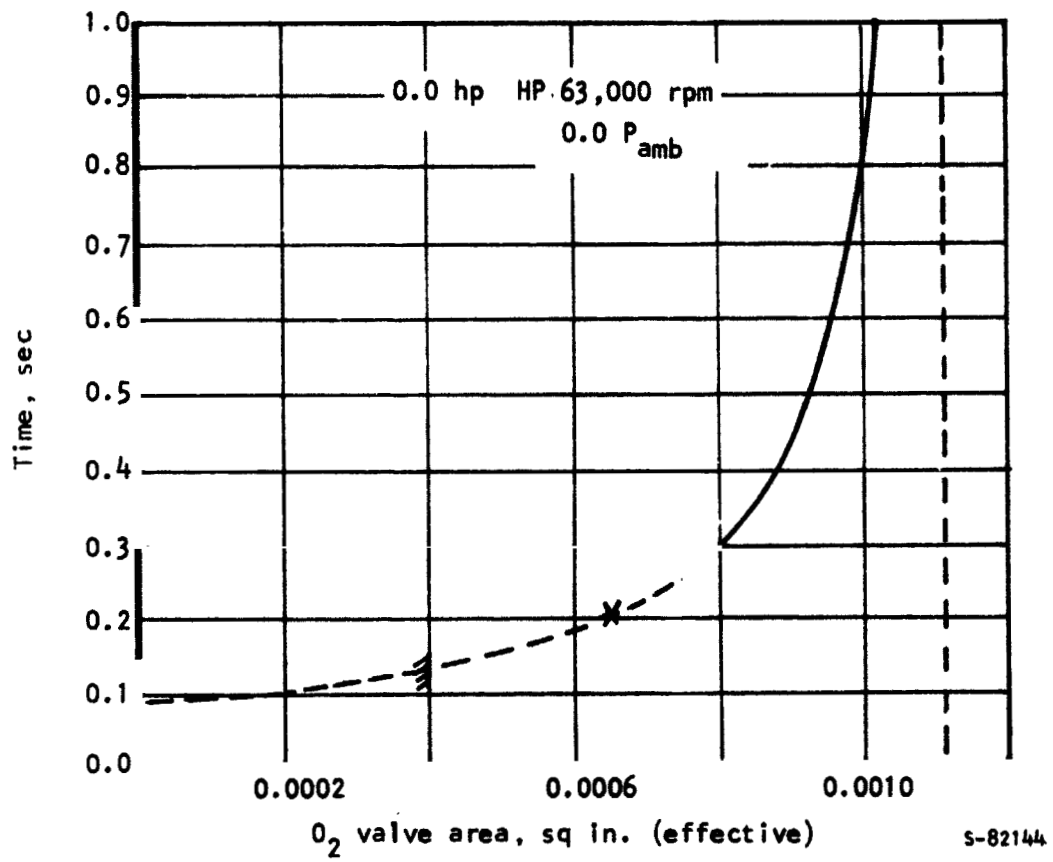

Figure 3-6.--Time to Deceleration, 1,000 rpm vs O_2 Effective Valve Area.

adjustment for a corrective change is in the region of open-loop instability; thus, the valve area selected corresponds to 10,000 rpm/sec acceleration capability fully loaded and -500 rpm/sec minimum load.

Bypass Option

The bypass option is one of the two options used to evaluate the steady-state performance of the APU. The option uses four control variables for a solution; the recuperator bypass to control the hydrogen temperature at the inlet to the combustor, the preheater bypass valve to control the hydrogen temperature at the inlet of the hydraulic oil cooler, the hydrogen flow control valve to control the turbine speed, and the oxygen flow control valve to control the turbine inlet temperature. The remaining fifteen of nineteen variables (listed in Table 3-1) are to satisfy various boundary conditions throughout the system.

No-Bypass Option

The no-bypass option is used when energy in the system is insufficient to bring the temperature of hydrogen out of the equalizer up to 750°R. If a bypass option is used for such a case, the dependent variables cannot all be satisfied. The recuperator bypass valve area and the flow split recuperator bypass valve are dropped from the independent vector. The controlled hydrogen temperature at station 58 (fig. 3-6) and the pressure balance at station 50 between the heat exchanger flow and the bypass valve flow are eliminated from the dependent vector. The no-bypass option is needed when the APU hydrogen flow has more cooling capability than the system has waste heat to bring up the temperature. The system approaches this condition as the horsepower output is increased above 250 hp.

Transient program.--The transient options of the APU simulator were developed for the controls analysis work. The options were used to identify the control transfer functions of the APU (H2FLCA, O2FLCA, RECYCA, BYPSCA). The control verification and the dynamic performance parametric studies were used to establish the sufficiency of the various control systems and to study the effects of various components on the APU performance (START, TRANS).

H2FLCA.--This particular option was written to identify the transfer functions of the speed control. The option is used by first establishing the initial conditions of the APU by running a BYPASS or a NO BYPASS solution. This

TABLE 3-1

INDEPENDENT VARIABLES AND DEPENDENT RELATIONSHIPS

Independent Variable	Dependent Relationship
Oxygen flow to combustor	Hydrogen pressure difference between the injector exit pressure and the combustor pressure
Hydrogen flow to combustor	The difference between the combustor flow and the flow through the first stage of the turbine
Preheater bypass flow	The difference in pressure between the preheater exit and the preheater bypass valve exit
Hydrogen flow control valve area	Torque balance between the turbine and load
Oxygen flow control valve area	The temperature error of the hydrogen entering the hydraulic oil heat exchanger and the scheduled temperature due to lube oil temperature
Preheater bypass valve area	The difference between the guessed mixed temperature from the recuperator and the calculated temperature
Hydrogen temperature at the recuperator exit	The difference between the calculated recuperator exit pressure and the guessed
Hydrogen pressure at the recuperator exit	The difference between the guessed and the calculated temperature of the hydrogen at the hydraulic oil cooler exit
Hydrogen temperature at the hydraulic cooler exit	The difference between the calculated and guessed pressure of the hydrogen at the hydraulic oil cooler exit
Hydrogen pressure at the hydraulic cooler exit	The oxygen flow difference between the temperature equalizer and the flow control valve
Oxygen inlet pressure to combustor	The difference between the first-stage turbine flow and the second-stage flow
Turbine interstage static pressure	If the exhaust duct is not choked, the closure error between the static pressure at the end of the exhaust duct and ambient pressure; if the exhaust duct is choked, matching the corrected flow at the inlet to the exhaust duct compared to the corrected flow required to make the duct choke
Turbine exhaust static pressure	The exhaust gas pressure at the exit to the recuperator compared with the independent variable
Recuperator exhaust products exit pressure	Heat balance in the lube oil loop
Inlet lube oil temperature	The temperature generated by the combustion of the hydrogen and oxygen compared to the desired control temperature.
Recuperator bypass valve area	The temperature of the hydrogen entering the combustion chamber compared to the desired controlled temperature
Recuperator bypass flow	The pressure at the exit of the recuperator bypass valve compared to the pressure from the recuperator exit
Inlet hydraulic fluid temperature	The temperature at the hydraulic pump case return compared to the temperature of the hydraulic pump entering the hydraulic cooler
Oxygen accumulator pressure	The difference between the oxygen flow through the temperature equalizer and the flow through the pressure regulator

provides a solution with the flow control valves in the correct position to balance the load torque and the turbine power. The system is then perturbed by increasing the hydrogen flow control valve 5 percent while holding the heat exchanger bypass valves in their initial positions. An ideal turbine inlet temperature control is used to manipulate the oxygen flow control valve. Turbine acceleration as a function of time was used to determine the Laplace transforms that would yield this type of step response. The transfer functions were established at various operating points, and a nonlinear element in series with the valve (as well as the required transfer functions for the control) were determined.

The H2FLCA option uses a 12-by-12 Jacobian matrix during the transient portion of the operation. The reduced complexity of the Jacobian is a result of some of the independent variables becoming state-variables (described by differential equations instead of algebraic equations). Also, the bypass controls have been frozen in their last position, which results in a further reduction in the Jacobian size (Table 3-2).

Hydrogen accumulation effects.--The H2FLCA option also was used to evaluate the effect of the hydrogen accumulation on the dynamics of the APU. To raise the pressure in a heat exchanger, the hydrogen mass in the heat exchanger must increase; this is the "gas bag" effect. The model used was to calculate the mass of the hydrogen in the APU from the shutoff valve through the hydrogen-hydraulic oil heat exchanger. Then, an accumulation was selected that would hold the same mass of hydrogen as the expected pressure and temperature found at the hydraulic oil heat exchanger exit. Thus, the pressure in this accumulator and the pressure out of the hydrogen shutoff valve become the boundary conditions, which determines the hydrogen flow from station 26 to station 36 within the APU. Similarly, an accumulator was placed between the temperature equalizer and the hydrogen flow control valve, which held the same mass of hydrogen as the lines and heat exchangers between station 36 and station 58. The combustor accumulator was removed from the deck to provide a comparison base without dynamics. The base acceleration was a step in turbine acceleration from 0 to 2672 rpm/sec. The actual run (figs. 3-7 and 3-8) shows that the acceleration peaks initially to 2880 rpm/sec (+7.8 percent) and then decays to 2624 rpm/sec (-1.8 percent) at 5.6 msec. The response reaches steady state at 16.8 msec. The disturbance from the nominal was very small and the duration is shown, which verified the initial assumption that the "gas bag" effect was not significant.

O2FLCA.--The option to identify the characteristics of the system for the temperature control is based on the coupled response of the speed control. The speed control was mechanized to control the hydrogen flow control valve (fig 3-9). The oxygen flow control was set at a fixed ratio of the hydrogen flow control valve. This option is run after an initial bypass condition. The heat exchanger bypass valves were held in the initial position during the transient. The

TABLE 3-2

H2FLCA OPTION: INDEPENDENT VARIABLES AND DEPENDENT RELATIONSHIPS

Independent Variable	Dependent Relationship
Oxygen flow to combustor	Hydrogen pressure difference between the injector exit pressure and the combustor pressure
Hydrogen flow to combustor	
Preheater bypass flow	The difference in pressure between the preheater exit and the preheater bypass valve exit
Oxygen flow control valve area	The difference between the calculated recuperator exit pressure and the guessed
Hydrogen pressure at the recuperator exit	The difference between the calcuiated and guessed pressure of the hydrogen at the hydraulic oil cooler exit
Hydrogen pressure at the hydraulic cooler exit	The oxygen flow difference between the temperature equalizer and the flow control valve
Oxygen inlet pressure to combustor	The difference between the first-stage turbine flow and the second-stage flow
Turbine interstage static pressure	If the exhaust duct is not choked, the closure error between the static pressure at the end of the exhaust duct and ambient pressure; if the exhaust duct is choked, matching the correct flow at the inlet to the exhaust duct compared to the corrected flow required to make the duct choke
Turbine exhaust static pressure	The exhaust gas pressure at the exit to the recuperator compared with the independent variable
Recuperator exhaust products exit pressure	The temperature generated by the combustion of the hydrogen and oxygen compared to the desired control temperatures
Recuperator bypass flow	The pressure at the exit of the recuperator bypass valve compared to the pressure from the recuperator exit
Inlet hydraulic fluid temperature	The temperature at the hydraulic pump case return compared to the temperature of the hydraulic pump entering the hydrauiic cooler
	The difference between the oxygen flow through the temperature equalizer and the flow through the pressure regulator

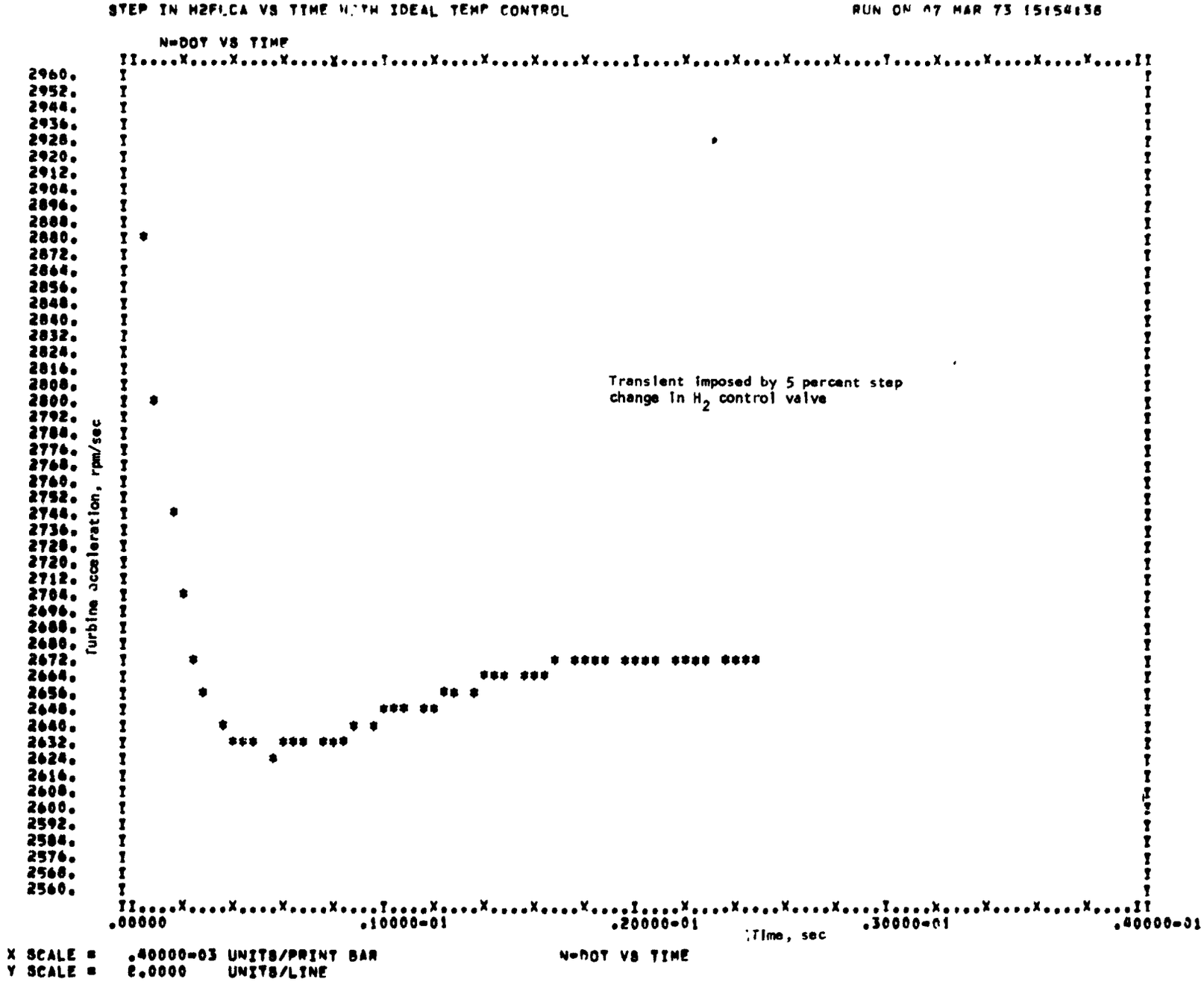

Figure 3-7.--Turbine Acceleration During Transient (With Accumulators).

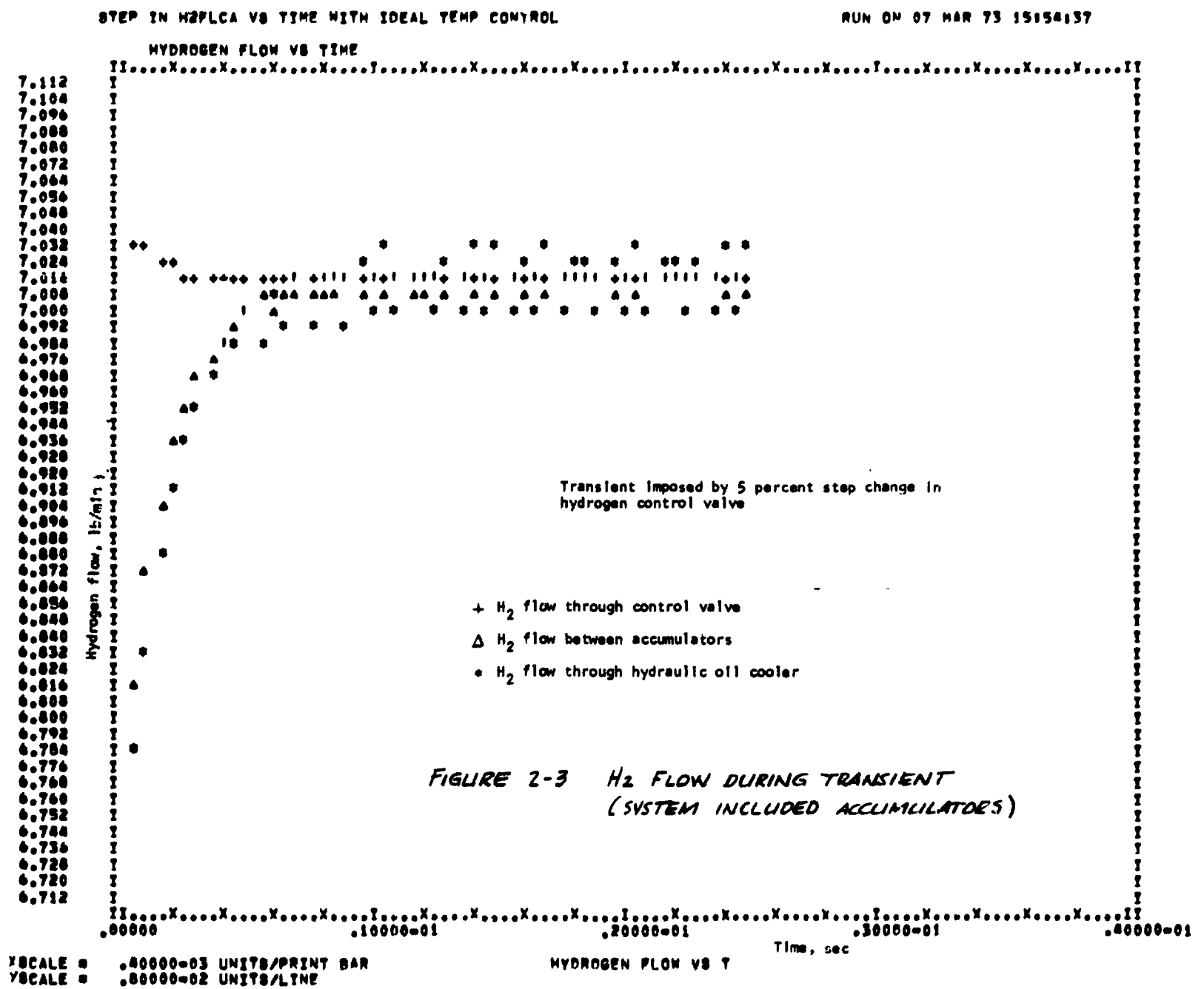

FIGURE 2-3 H_2 FLOW DURING TRANSIENT (SYSTEM INCLUDED ACCUMULATORS)

Figure 3-8.--Hz Flow During Transient (System Included Accumulators).

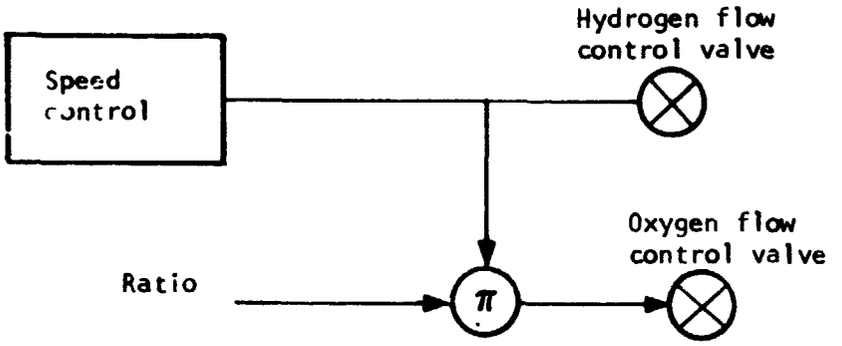

Figure 3-9.--Mechanization of O2FLCA Computer Option.

ratio of the oxygen flow control valve area to hydrogen flow control valve area was the initial condition ratio plus 1 percent (i.e., if the initial conditions indicated that the O_2 valve was 18.4 percent of the H_2 valve, then the transient would be run with an O_2/H_2 area ratio of 19.4 percent. The effect of this change in ratio is an increase in the turbine inlet temperature, which provides more energy to the turbine, and the speed control changes the valve areas to maintain turbine speed. The temperature control is identified with the interaction of the speed control because the speed control reacts faster than the temperature control. This results in a temperature control that mainly has a trimming function.

Bypass Control

The RECYCA option was used to determine the response of the hydrogen temperatures throughout the system to a step in the preheater bypass control valve area. The preheater bypass valve area and the preheater series valve have complementary areas, thus acting as a three-way valve. The hydrogen temperatures at stations 32 and 58 were determined with the turbine speed control and the turbine inlet temperature controls operable.

The procedure used to acquire the identifying transient was to step the valve area and record the resulting temperature transients (fig. 3-10 and 3-11). Similarly, the reaction of the system to a step in recuperation bypass (BYPSCA) valve area was performed (figs. 3-12 and 3-13).

It is required to identify the transfer function from both valve area changes to each of the temperatures to be controlled because there is a considerable amount of interaction between the control loops.

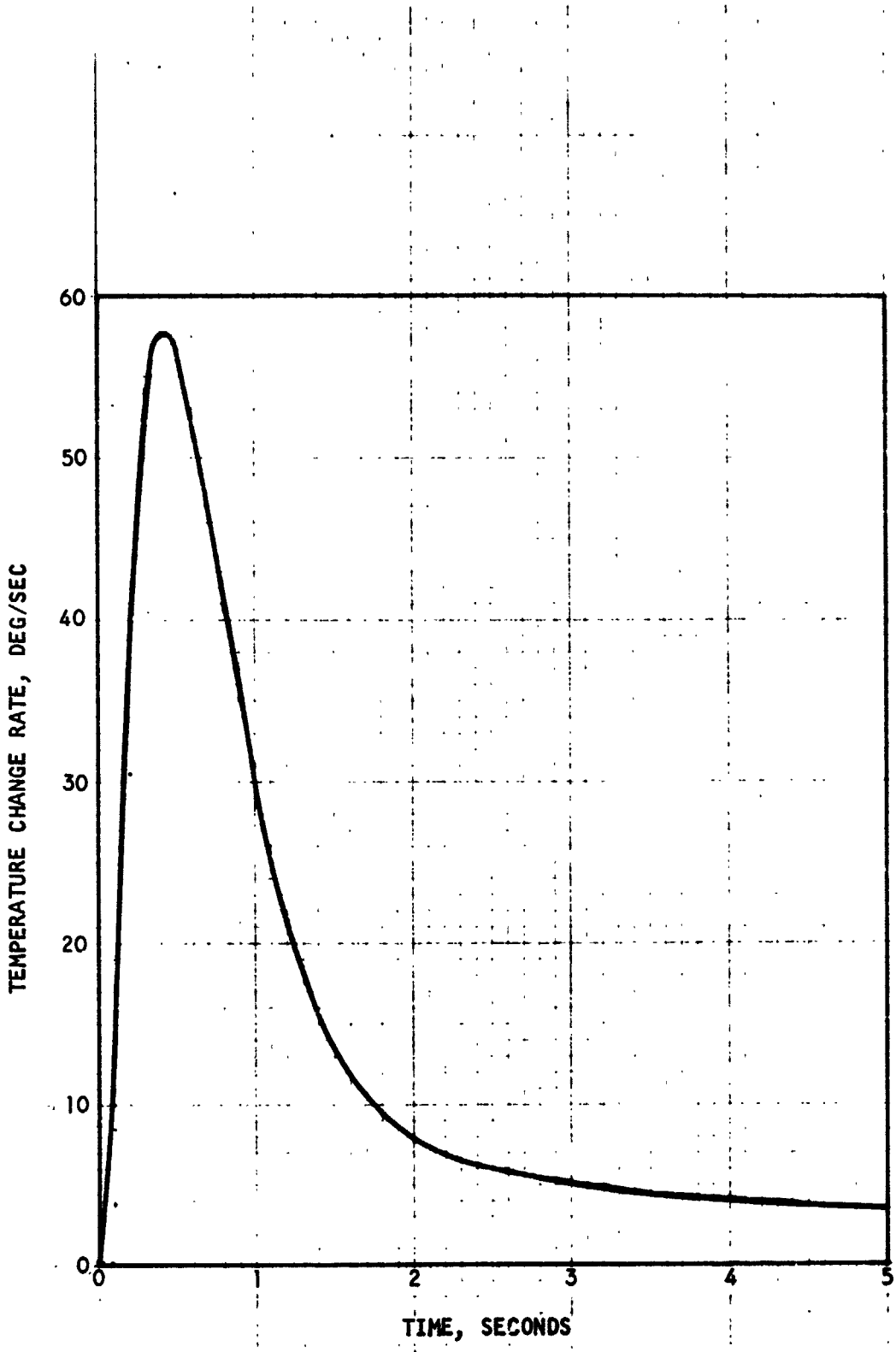

Figure 3-10.--Rate of Change of H_2 Temperature at Hydraulic Oil Cooler Inlet Due to Preheater Bypass Valve Step.

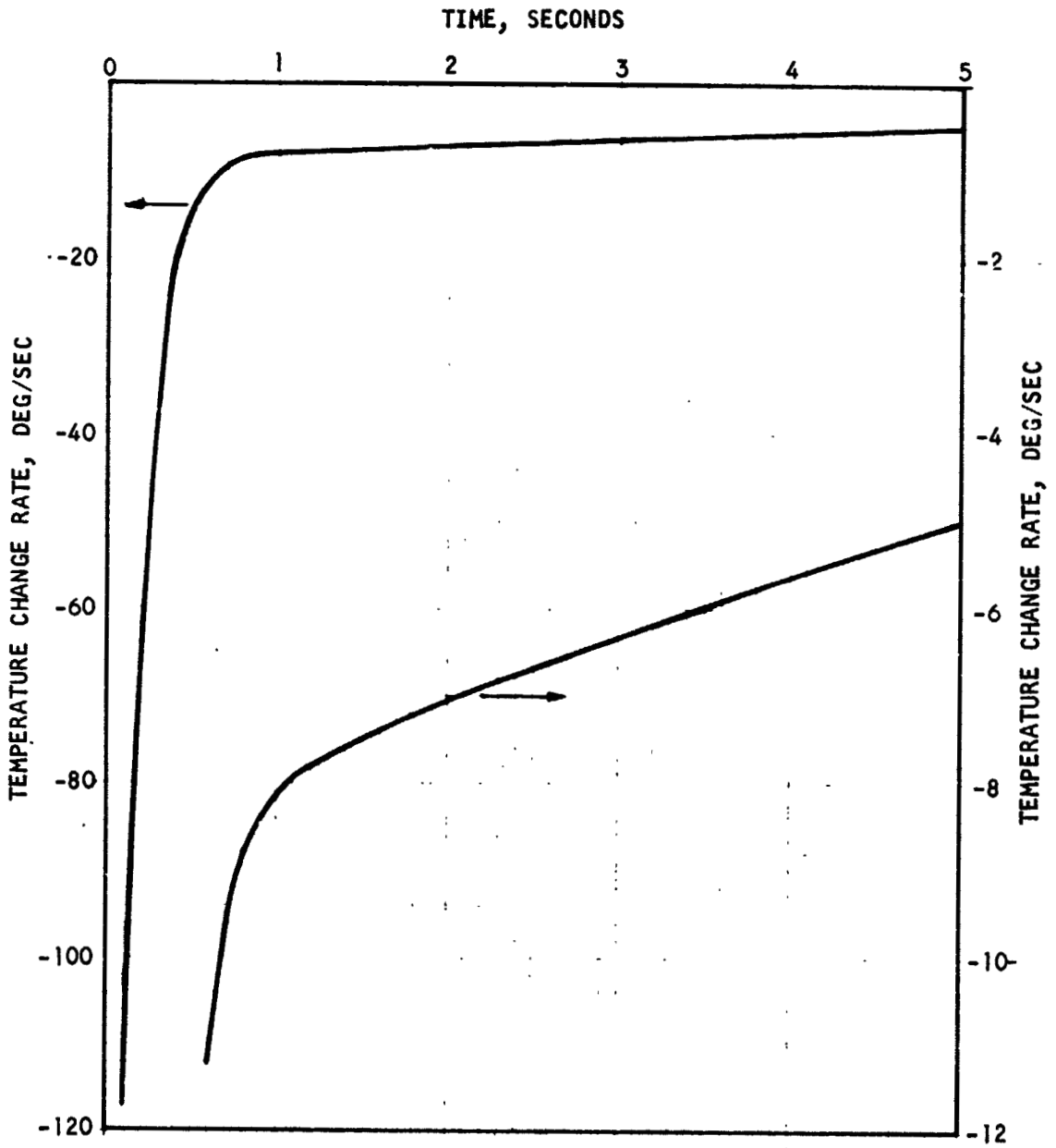

Figure 3-11.--Rate of Change of H_2 Temperature at Equalizer Exit Due to Preheater Bypass Valve Step.

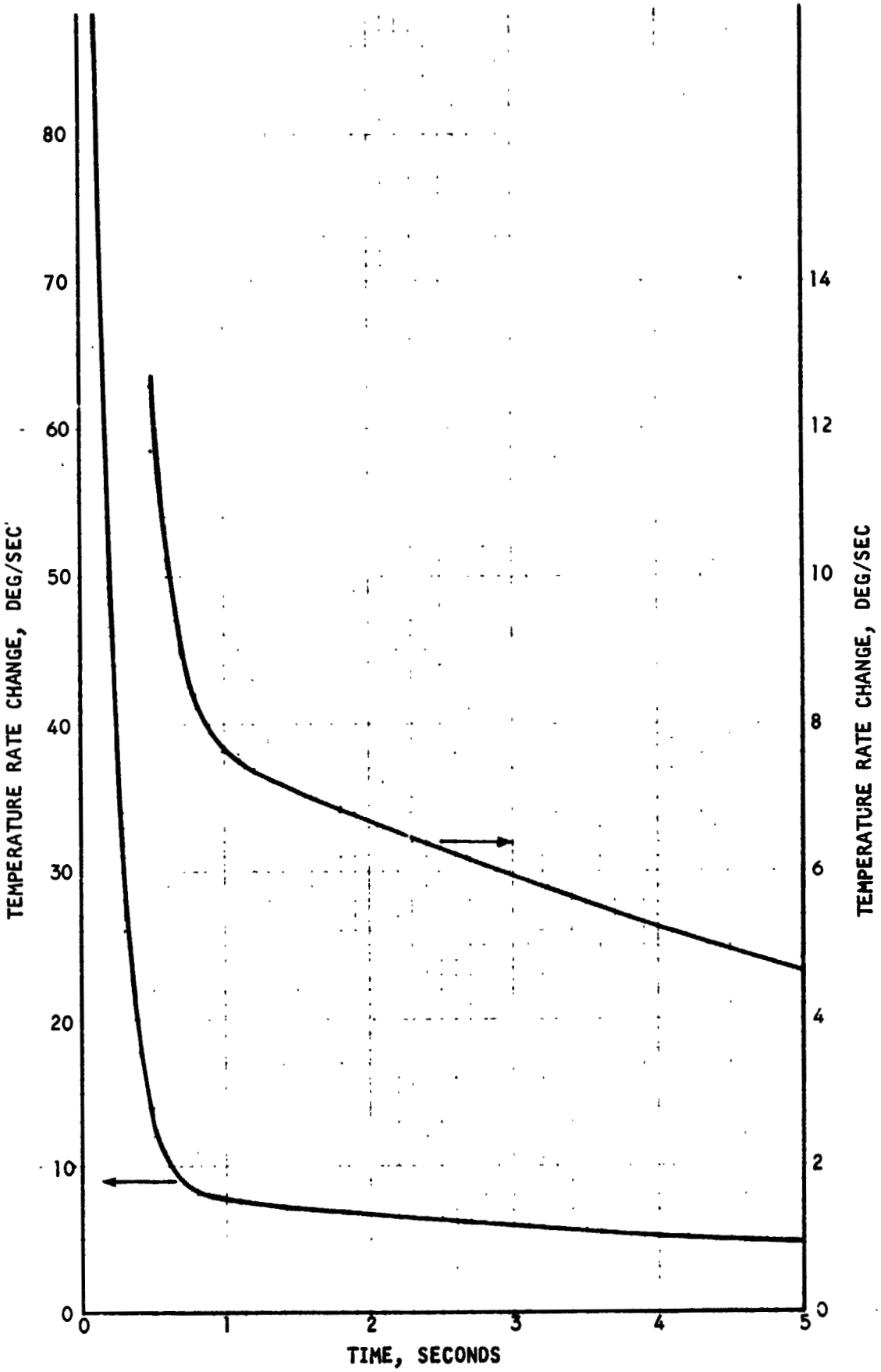

Figure 3-12.--Rate of Change of H_2 Temperature at Equalizer Exit Due to Recuperator Bypass Valve Step.

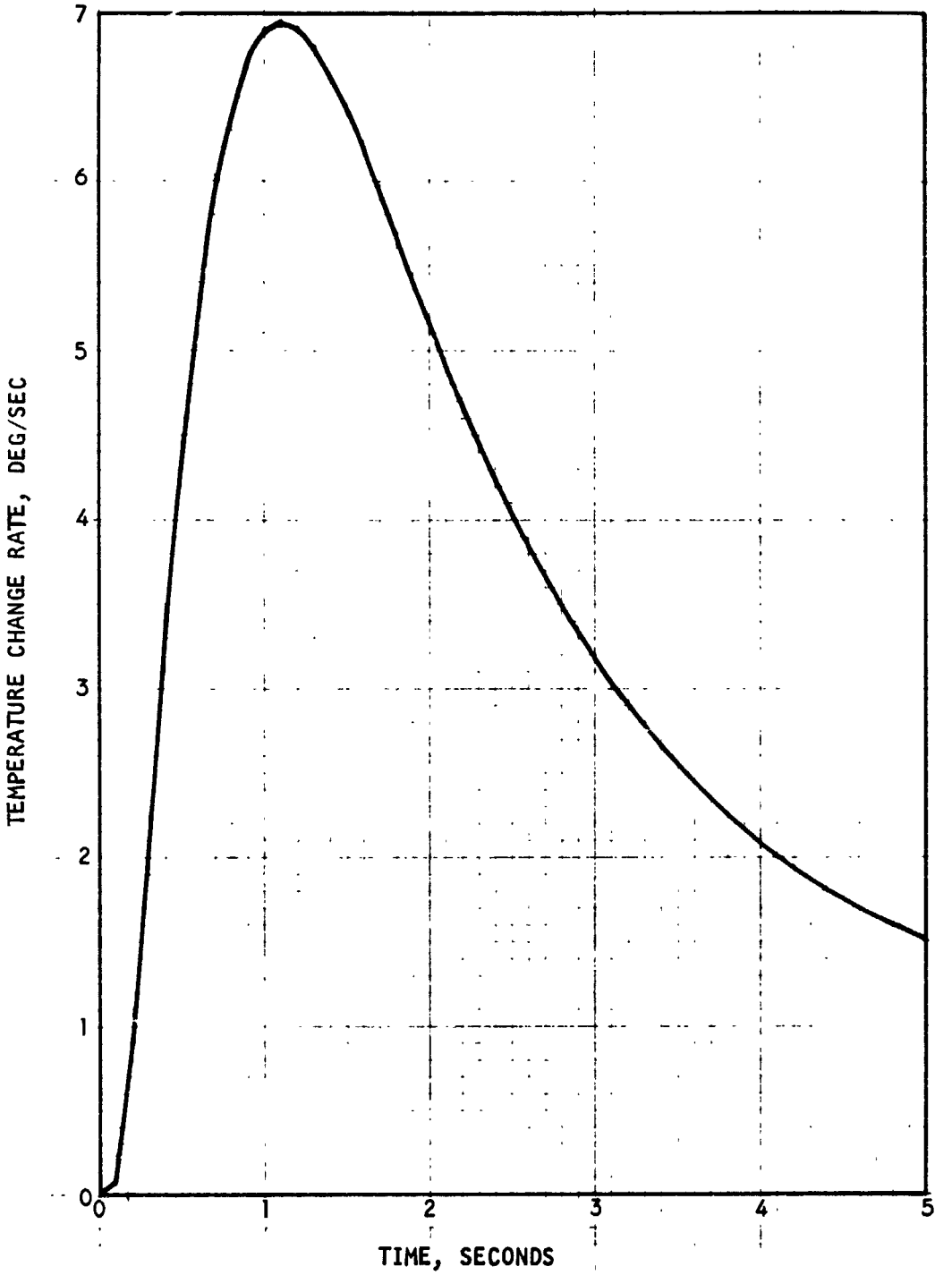

Figure 3-13.--Rate of Change of H_2 Temperature at Hydraulic Oil Cooler Due to Recuperator Bypass Valve Step.

Transient

The transient (TRANS) option in the MAINSR was used to evaluate the performance of the control system to various disturbances. An example of the performance of the system to a 1-sec maximum power pulse and then returning to idle is shown in fig. 3-14. The response of the speed control is very symmetric at high and low power; this is due to the nonlinearity placed in the speed control. The variation in response rate of T(32) between high and low power is due to the variation in hydrogen flow.

The TRANS option also was used to evaluate the variation in turbine inlet temperature control as a function of accumulator volume and oxygen pressure regulator characteristics.

Turbine Control Variations

Turbine speed and temperature controls were analyzed to evaluate performance during transient operation. Several different system configurations were run through the transient imposed by changing from idle power to full power in 75 msec at sea level. The first system was considered the "base" system and the other configurations were changes to the base. In each change, only one characteristic was different from the base. The systems are listed in table 3-3. Performance comparisons based on the several system configurations are shown in figs. 3-15 through 3-19.

TABLE 3-3

SYSTEM CONFIGURATIONS FOR TRANSIENT ANALYSIS

	Base System	Change Number			
		1	2	3	4
O_2 regulator response, msec	200	200	200	100	200
O_2 accumulator volume, cu in.	100	25	100	100	100
O_2 flow valve maximum area	--Per Specification --				115 Percent of Spec
O_2 regulator setting, psig	550	550	565	550	550

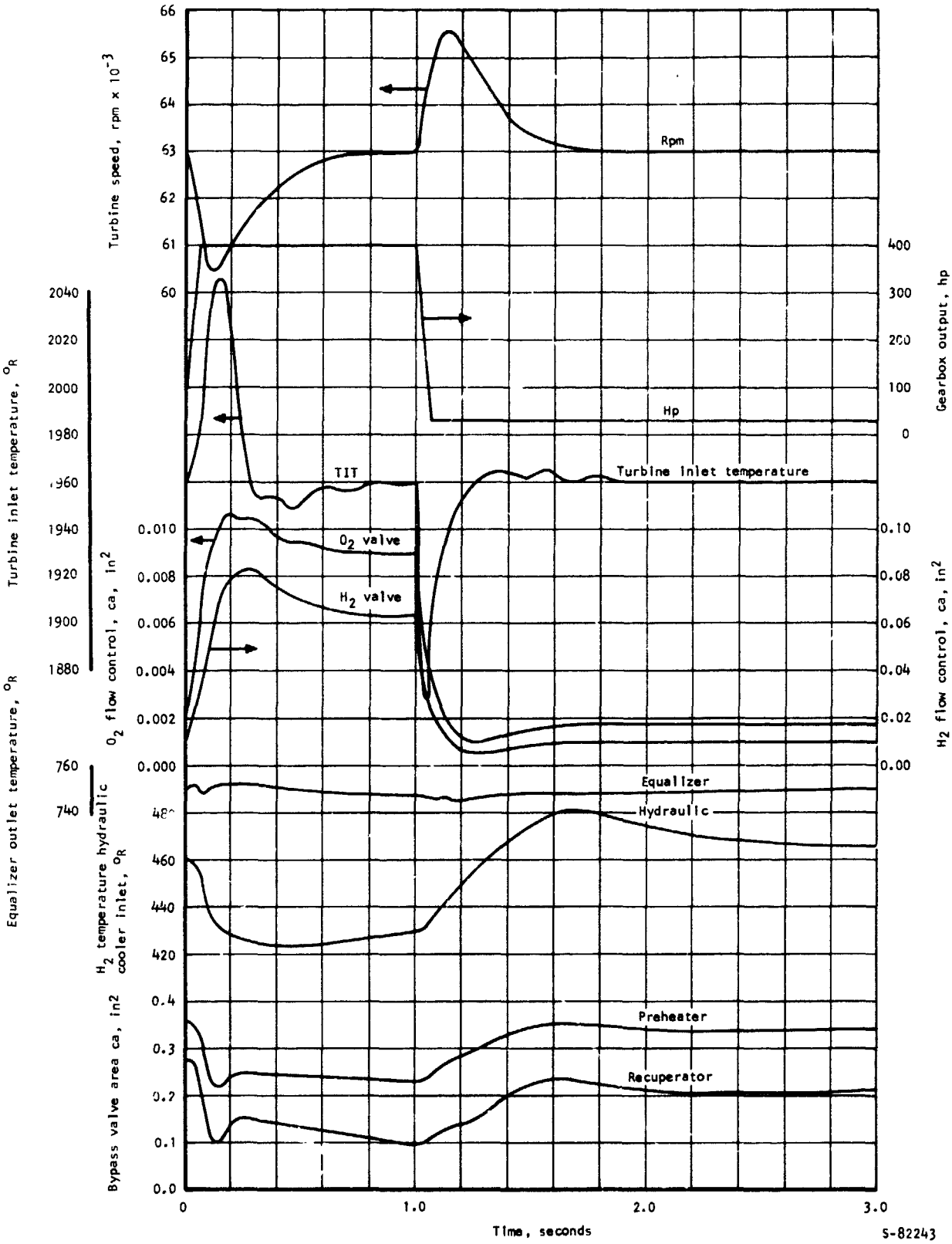

Figure 3-14.--Performance During Load Transient

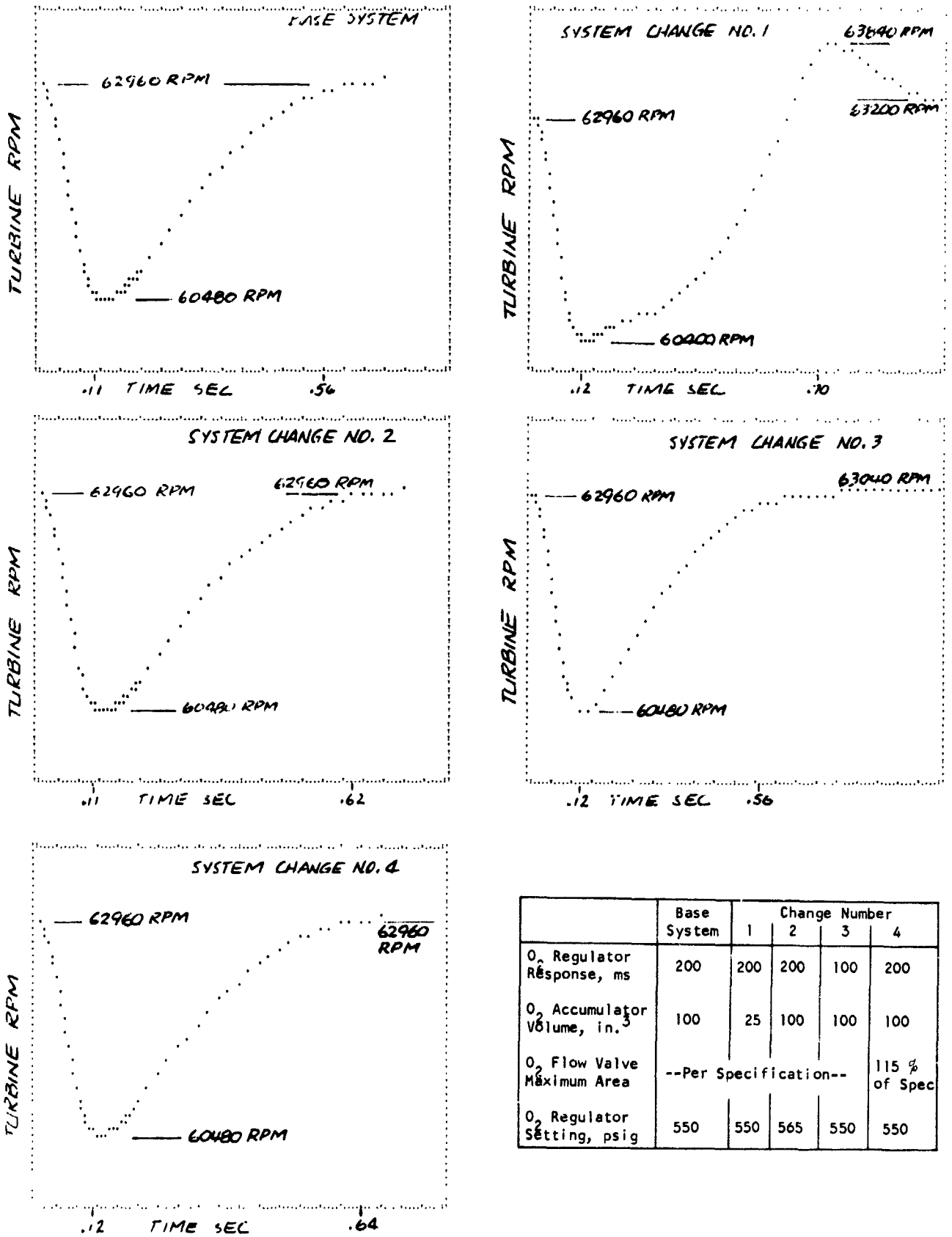

	Base System	Change Number 1	2	3	4
O_2 Regulator Response, ms	200	200	200	100	200
O_2 Accumulator Volume, $in.^3$	100	25	100	100	100
O_2 Flow Valve Maximum Area	--Per Specification--				115 % of Spec
O_2 Regulator Setting, psig	550	550	565	550	550

Figure 3-15.-- Turbine Speed During Idle to Full Power Transient.

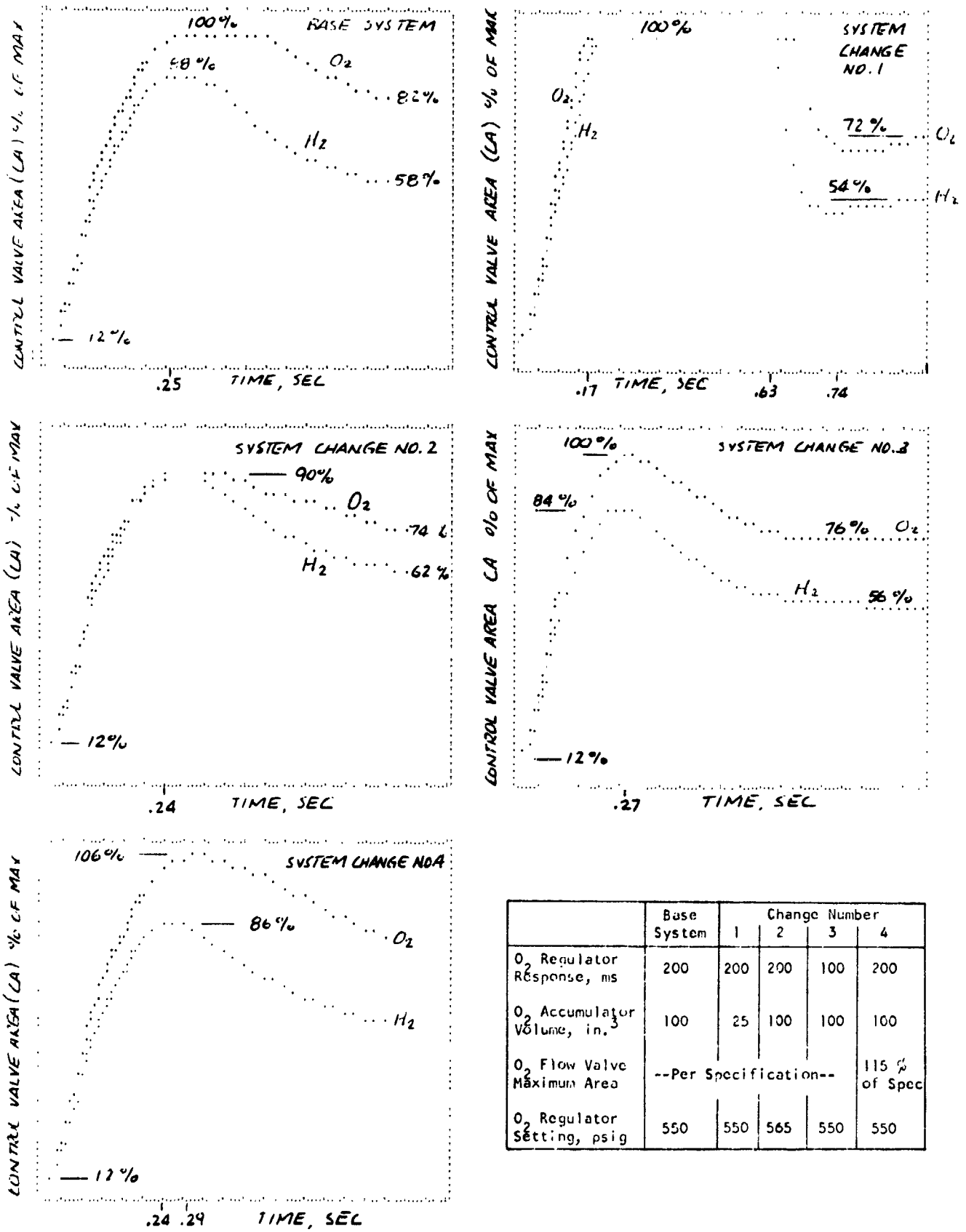

	Base System	Change Number 1	2	3	4
O_2 Regulator Response, ms	200	200	200	100	200
O_2 Accumulator Volume, $in.^3$	100	25	100	100	100
O_2 Flow Valve Maximum Area	--Per Specification--				115 % of Spec
O_2 Regulator Setting, psig	550	550	565	550	550

Figure 3-16.-- Area (CA) of H_2 and O_2 Flow Control Valves During Idle to Full Power Transient.

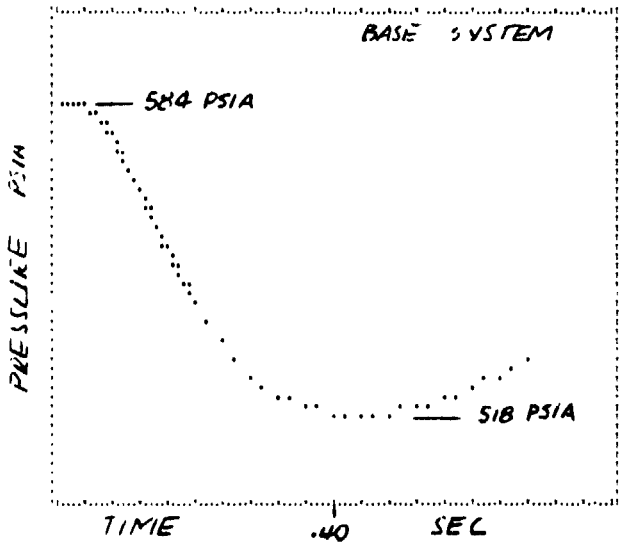

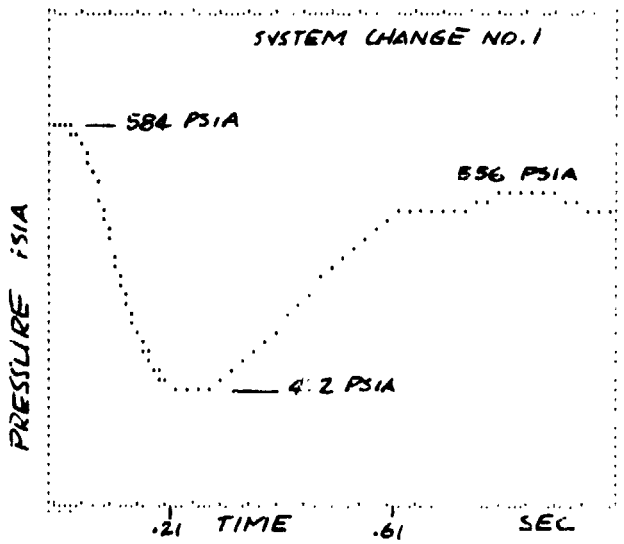

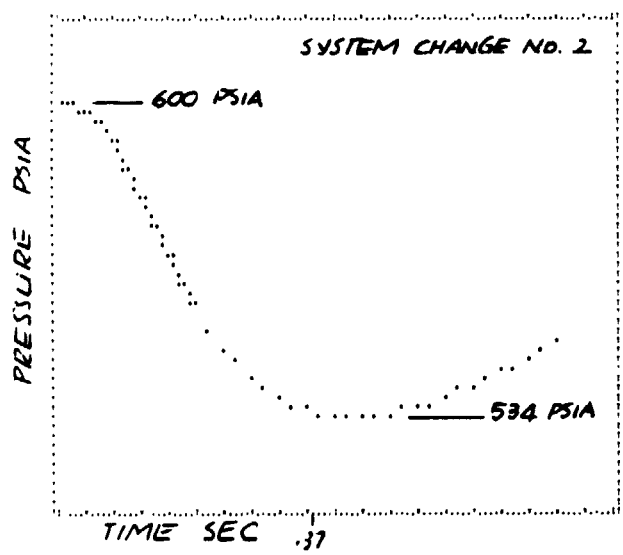

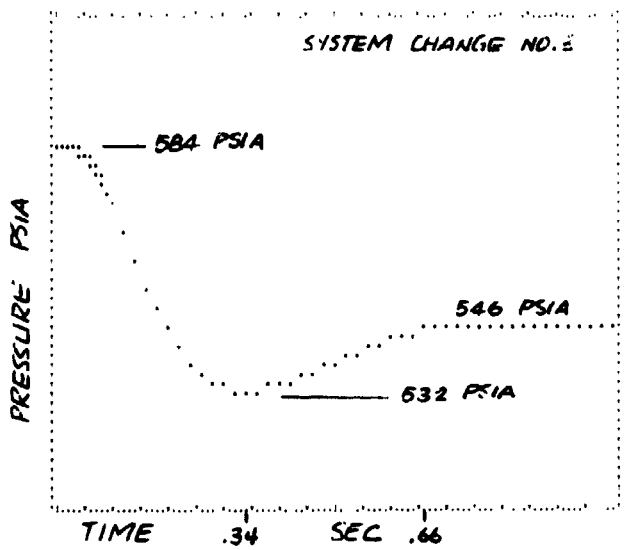

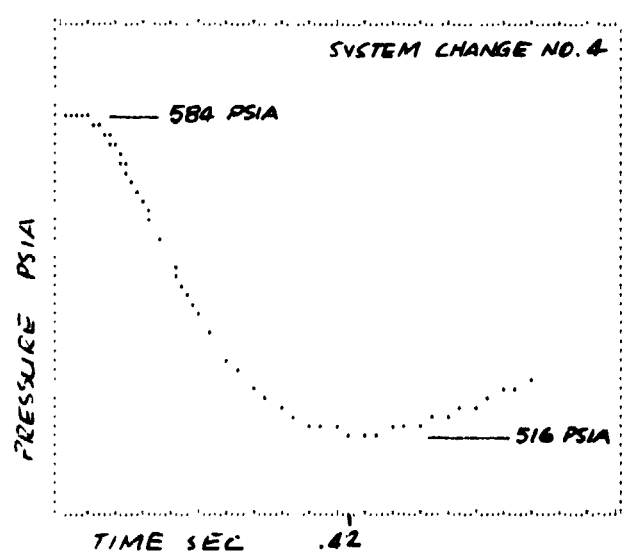

	Base System	Change Number 1	2	3	4
O_2 Regulator Response, ms	200	200	200	100	200
O_2 Accumulator Volume, $in.^3$	100	25	100	100	100
O_2 Flow Valve Maximum Area	--Per Specification--				115 % of Spec
O_2 Regulator Setting, psig	550	550	565	550	

Figure 3-17.-- Oxygen Accumulator Pressure During Idle to Full Power Transient.

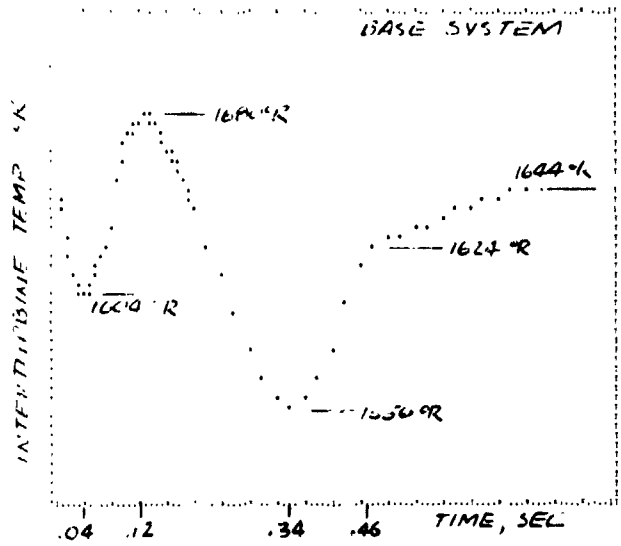

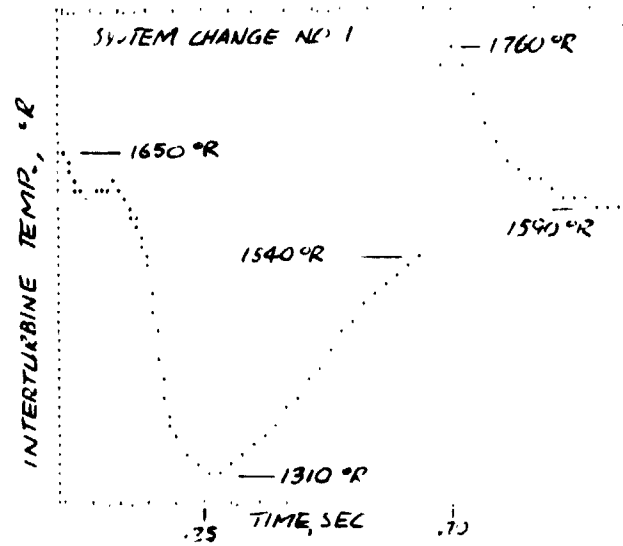

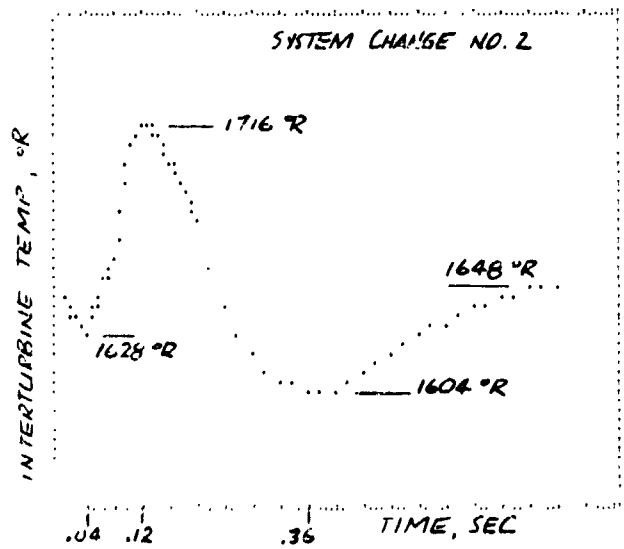

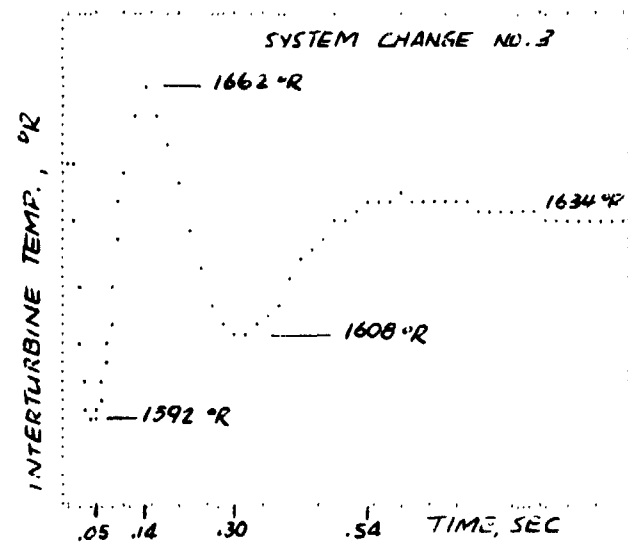

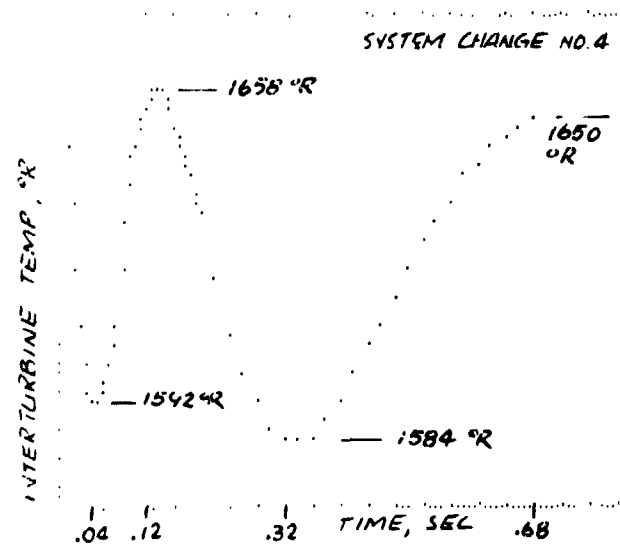

	Base System	Change Number 1	2	3	4
O_2 Regulator Response, ms	200	200	200	100	200
O_2 Accumulator Volume, $in.^3$	100	25	100	100	100
O_2 Flow Valve Maximum Area	--Per Specification--				115 % of Spec
O_2 Regulator Setting, psig	550	550	565	550	550

Figure 3-18.--Interturbine Temperature During Idle to Full Power Transient.

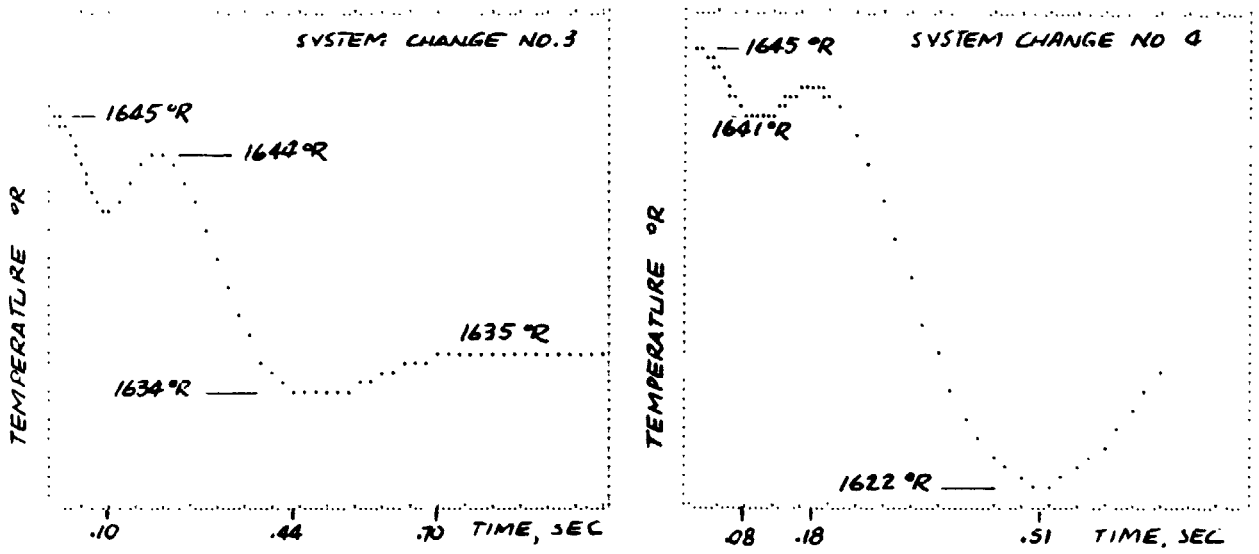

	Base System	Change Number 1	2	3	4
O_2 Regulator Response, ms	200	200	200	100	200
O_2 Accumulator Volume, $in.^3$	100	25	100	100	100
O_2 Flow Valve Maximum Area	--Per Specification--				115 % of Spec
O_2 Regulator Setting, psig	550	550	565	550	550

Note: Thermocouple data not plotted for Base System and Changes 1 and 2.

Figure 3-19.--Interturbine Thermocouple Temperature Indication During Idle to Full Power Transient.

Start

The start option was written to evaluate the performance of the control system during the start of the APU. The primary concern was the amount of turbine speed overshoot that would be experienced. For the initial conditions, all heat exchanger temperatures were set to 519°R, and the turbine speed was set to 100 rpm.

Component Definitions

Two aspects of component descriptions are (1) the verification that the results of the performance of the analysis model are compatible with more sophisticated analysis techniques, and (2) the effect of the simulator analysis on the component requirements.

The primary concern in the heat exchanger analysis is the transient characteristic of the heat exchanger as compared to performance of the same component using more sophisticated models. The recuperator start transient was considered to be the condition that would define the heat exchanger thermal stress specification. The start transient was performed using a 144-mode thermal analyzer program. The results closely matched the four-mode model used in the system simulator (fig. 3-20).

In the base run the oxygen flow control valve hit the full-open stop, and the result was a drop in combustor temperature. The reason that the oxygen valve hit the limit was that the maximum flow requirement of the speed control corresponded to the minimum pressure of the oxygen regulator-accumulator subsystem.

The first change to the base system was to drop the oxygen accumulator volume to 25 cu in. so as to reach a minimum sooner and recover before the flow requirement of the speed control reached the maximum point. The smaller accumulator did result in a faster subsystem but the disturbance amplification resulted in a response that was unacceptable.

For the second change the pressure regulator was set to a nominal 565 psig. This provided sufficient pressure across the oxygen flow control valve that travel was not limited. The increased pressure across the valve did result in a 112.9°R range in the combustor temperature. The increased range is due to the fact that change in oxygen flow with respect to combustor pressure is reduced and the short-term temperature gain of the combustor is increased. It was this phenomenon which originally caused the introduction of the pressure regulator to the system.

The third change to the system was to increase the response of the O_2 pressure regulator to 100 msec. The oxygen flow control valve did not hit the limit and the temperature variation was 69.5°R. This change does not compromise any other operating condition and it is accomplished by sizing the orifice into the bellows chamber of the pressure regulator.

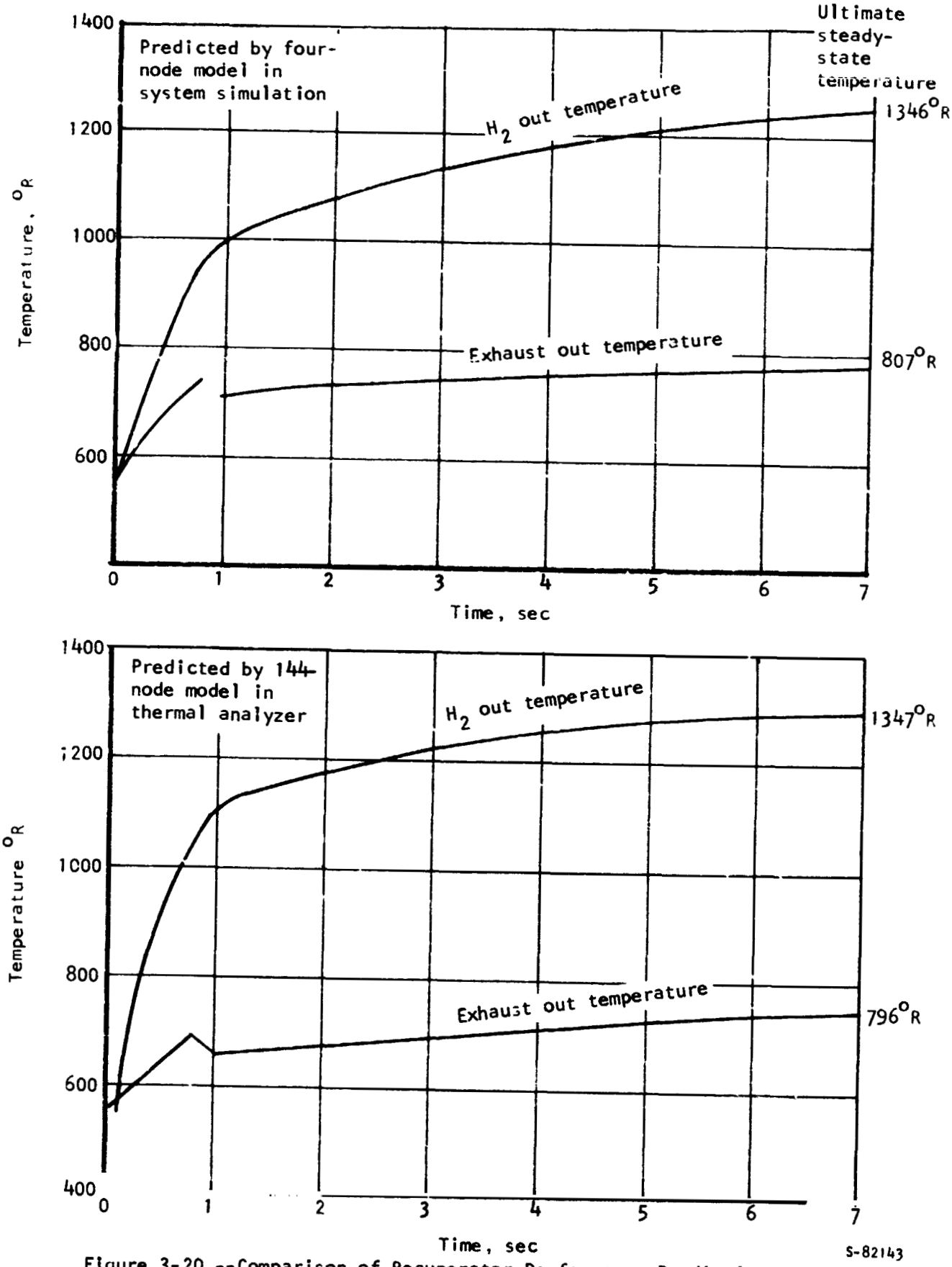

Figure 3-20.--Comparison of Recuperator Performance Predictions for Start Transient.

The last change to the system was to raise the oxygen flow control valve area limit to 115 percent of the specification requirement. The temperature range of the combustor during the transient was 74.1°R. The increase in the oxygen flow control valve area requires that the oxygen flow control valve have a larger turn-down ratio, which would increase the difficulty in producing the valve.

The selected configuration is the third change--O_2 regulator response changed from 200 to 100 msec.

Flow Control Valves

The flow control valve requirements were defined from the digital computer simulator. The speed of response was determined from the H2FLCA identification runs, whereas the temperature extremes were derived from the BYPASS and NO BYPASS options. The critical parameter, which was the size required for control, was derived by use of a special control valve option. The valves were sized such that the maximum acceleration under maximum load was greater than the maximum deceleration under minimum load.

Bypass Valves

The simulator provided information on the size of the heat exchanger bypass valves. Initially, 1-sq-in. valves were used to control the temperature. By performing parametric studies on the valves, control of the flow split of the hydrogen was shown to be ineffective with bypass areas of greater than 0.5 sq in. This, coupled with the requirement of raising the hydrogen inlet temperatures to ambient test conditions, resulted in the incorporation of series valves in the system to provide the capability of 100 percent bypass of both the preheater and the recuperator. The valves are driven to provide complementary areas (i.e., the sum of the area of the preheater bypass valve and the preheater series valve is a constant).

The required response of the bypass valves was determined by the required bandwidth of the bypass controls. The speed required by the valves can be seen from the valve movement required during load transients.

Oxygen Pressure Regulator

The oxygen pressure regulator initially was incorporated in front of the temperature equalizer, but was moved to prevent two-phase flow in the valve. The response and sizing of the pressure regulator were initially prepared by the valve group. With the regulator dynamics incorporated in the system simulator, it was decided to lower the spring rate of the regulator. This reduced ringing in the regulator and caused it to damp out faster.

Oxygen Accumulator

The oxygen accumulator was added to the basic system to provide inherent stability of the turbine inlet temperature. The oxygen pressure source is from a supercritical oxygen tank at 900 psia, whereas the hydrogen source pressure is 575 psia. This results in partial oxygen flow with respect to the combustor pressure. The pressure in the combustion chamber is determined by the primary flow rates of the hydrogen and oxygen and the oxygen-hydrogen ratio (O/F, oxygen/fuel ratio). At a particular level of flow through the combustor, the primary driving force on the combustor pressure is the temperature of the combustion products. As shown in fig. 3-21, the pressure increases as the square root of the temperature; then the temperature will increase if a disturbance occurs, and the temperature increase will increase pressure. Thus, if

$$\frac{\frac{\partial W_H}{\partial P_c}/W_H}{\frac{\partial W_o}{\partial P_c}/W_o} > 1.0 \qquad (3\text{-}1)$$

For no interaction between pressure and temperature, equation 3-1 must equal 1. To accomplish this, the oxygen pressure regulator pressure should be set such that the pressure ratio across the hydrogen flow control valve is equal to the pressure ratio across the oxygen flow control valve.

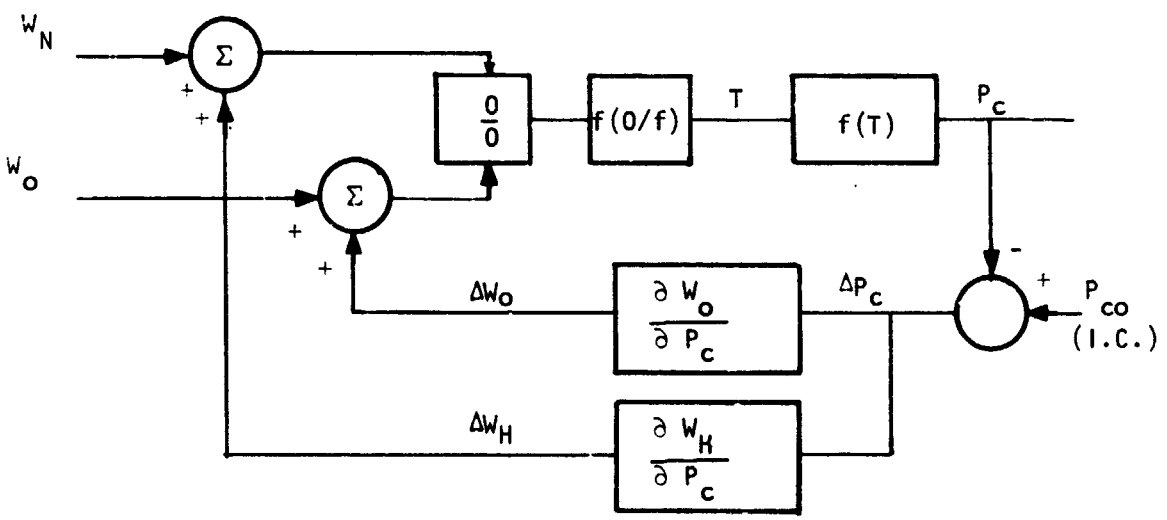

Figure 3-21.--Combustor Pressure and Temperature.

The pressure regulator set point is at the hydrogen pressure source less the pressure drop through the hydrogen temperature conditioning hardware. The pressure regulator will tend to provide a stable temperature at low frequencies, but as the disturbance becomes fast or contains high frequencies (which are higher than the regulator reaction rate), combustion temperature variations occur. To minimize this effect, the oxygen accumulator was incorporated. The accumulator provides the pressure stability to higher frequency disturbances and thus, coupled with the pressure regulator, provides a system with much less interaction between combustion pressure and temperature.

Check Valve

The oxygen check valve was introduced upon analysis of the start transient. The hydrogen pressure in the combustor increases until back flow from the combustor to the oxygen accumulator is eliminated. This results in an explosive H_2-0_2 mixture being passed through the ignitor spark gap with the possibility of a flashback into the oxygen accumulator. The check valve between the oxygen accumulator and the oxygen flow control valve will prevent this.

SECTION 4

CONTROL SUBSYSTEM

SECTION 4

CONTROL SUBSYSTEM

The control subsystem comprises two types of controls: primary and secondary. The primary controls are the dynamic control loops that position the flow control valves and the bypass control valves. The secondary controls are the logic circuitry required for system startup, shutdown, and monitoring. These are discussed in this section.

The breadboard control functions as a flight-type controller would, but contains certain features desirable for development that would not be incorporated into a flight design. The combustor pressure and temperature, turbine speed, and equalizer outlet temperature can be adjusted to various set points other than the design values. This permits great flexibility in initial testing. Design values will be used as confidence is gained in operation at reduced values.

Primary Controls

The primary controls are shown in Figure 4-1. These include:

(a) Turbine speed control

(b) Turbine temperature control

(c) Bypass controls

Turbine speed control.--The turbine speed control requires the transfer function from hydrogen flow control valve area to turbine speed, and was identified by use of the H2FLCA simulator option. The identification was performed at several points throughout the operating range. Three of these conditions (defined in figs. 4-2 and 4-3) are described to show the variation in the dynamics.

Condition 1 could have had a pole in the right-hand plane. The acceleration was increasing with almost immeasurable positive jerk. Since the pole was at a low enough frequency, an integrator was assumed for control design. This results in a linear system model for which minimum phase control design techniques can be used (such as Bode analysis).

A nonlinearity is placed between the linear portion of the control and the valve position loop to provide a more uniform gain for the complete range of operating conditions. With the addition of an integrating control with lead for stability, the control characteristics given in fig. 4-4 (in the form of a Bode plot) are obtained.

Turbine inlet temperature control.--In determining the coupling between the speed control and the temperature control, the speed control was mechanized with an ideal temperature control, and full load change transients were run.

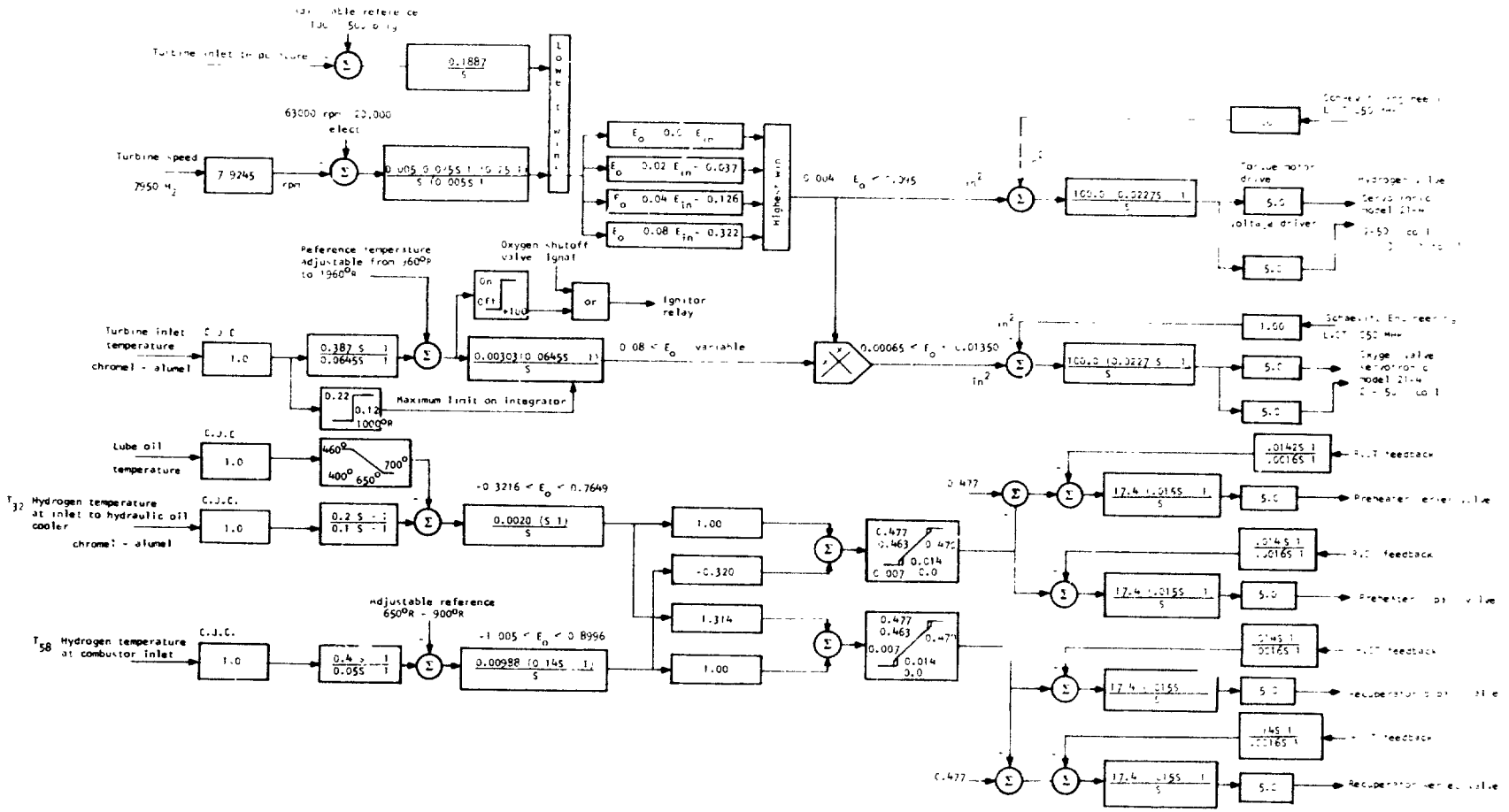

Figure 4-1.--H_2-O_2 Space Shuttle APU Primary Controls

Condition 1--350-hp hydraulic output at 14.7-psia ambient pressure

Condition 2- Zero hydraulic output at zero ambient pressure

Condition 3--270-hp hydraulic output at 14.7-psia ambient pressure

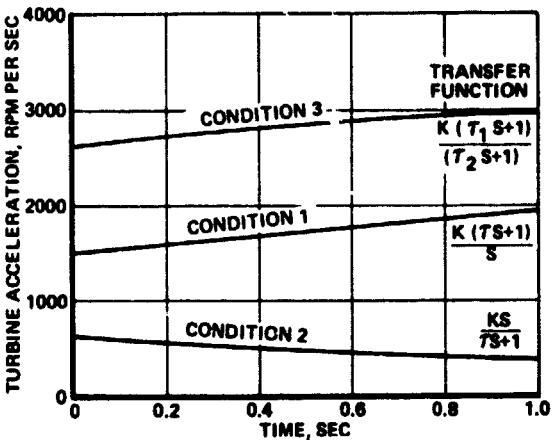

Figure 4-2.--Typical Response to 5 Percent Step Change in Hydrogen Flow Control Valve Area.

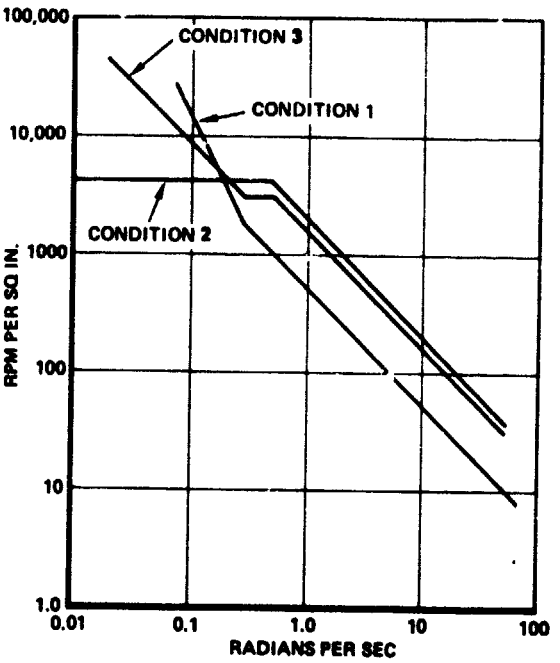

Figure 4-3.--Speed Control Transfer Func ions.

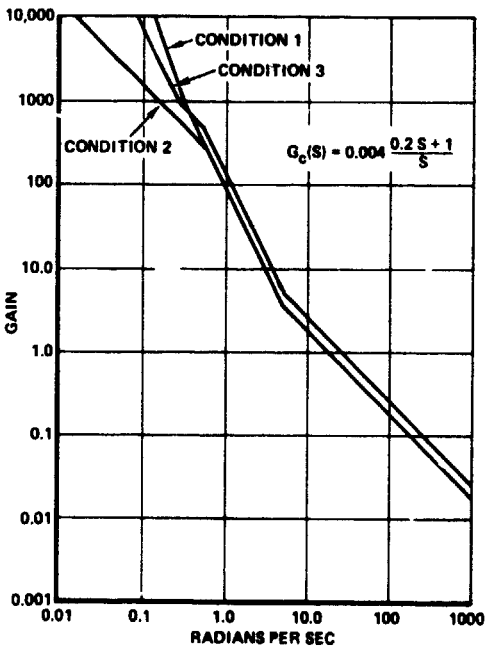

Figure 4-4.--Open-Loop Gain Characteristics of Speed Control.

The hydrogen flow control valve area was plotted against the oxygen flow control valve area (fig. 4-5). This indicated a fixed relationship between the two areas during the initial portion of the transient. Consequently, it was decided to mechanize the turbine temperature loop output as a ratio of oxygen flow control valve area to hydrogen flow control valve area. That is, with a change in the position of the hydrogen flow control valve (as determined by the speed control), the position of the oxygen flow control valve is changed simultaneously to maintain essentially the same valve area ratio during the initial part of the transient. Oxygen valve position is subsequently trimmed by the turbine inlet temperature control as required. In this way, close temperature control can be maintained during a load transient using a temperature sensor with relatively slow response. At the same time, the accuracy of a closed-loop control is obtained for steady-state operation at any load condition essentially independent of ambient conditions or propellant inlet temperature.

The O2FLCA option was used to identify the transfer function from the oxygen valve/hydrogen valve area ratio to the turbine inlet temperature. The conditions used for the control design were sea-level, maximum power and maximum altitude, minimum power. The control loop uses a lead-lag network in the feedback to provide some measure of thermocouple compensation, and an integration with a lead in the feed forward. At minimum power the thermocouple is undercompensated, which results in a controlled gas temperature that is high when the temperature of the thermocouple is low. As the thermocouple approaches steady state, the gas temperature also approaches steady state, while at maximum power the opposite occurs.

Bypass control.--The bypass controls were identified using the RECYCA and PYPSCA transient options. The transfer functions for both T_{58} and T_{32} (fig. 3-1) for each of the valve disturbances were identified. The requirement for both temperatures is due to the interaction of both temperatures with a change of either valve. The control loops for each of the temperatures were designed using a lead-lag feedback and an integrating control. The control loops are followed by a nondynamic cross-coupling of the bypass and series valves to provide a minimum interaction between the control loop and the expected crossover frequencies.

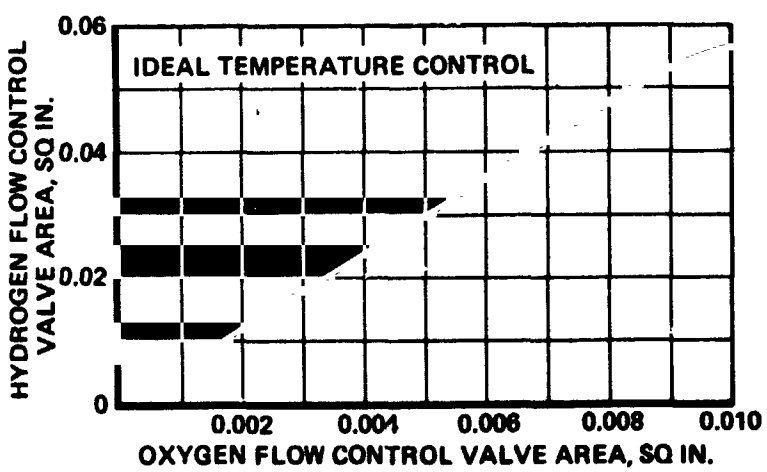

Figure 4-5.--Oxygen and Hydrogen Flow Control Valve Area Relationships for Speed Control with Ideal Temperature Control.

Secondary Controls

The startup and shutdown logic shown in fig. 4-6 is primarily designed to prevent an oxygen-rich mixture from passing over the hot turbomachinery. This requires that the hydrogen shutoff valve be opened first. After the hydrogen pressure is obtained, and the hydrogen flow is established, the oxygen valve is opened.

For shutdown, the oxygen shutoff valve is closed. To detect that the oxygen flow has been interrupted, the turbine inlet temperature sensor is used. The hydrogen shutoff valve remains open until the temperature of the overtemperature thermocouple is below 900°R; this temperature was selected because the turbine inlet temperature control point can be selected as low as 960°R.

Monitor

The monitor philosophy of the APU system has been to look at selected parameters and to initiate a normal shutdown upon detection of a possible failure. The parameters were selected by weighing two factors: (1) the criticality of the parameter, and (2) the ease of obtaining the data. Special sensors were incorporated into the system to obtain independent measurement of the turbine speed and the turbine inlet temperature. The difference in turbine inlet temperature as measured by the two thermocouples is accomplished by the incorporation of an amplifier and two diodes. The approach has been to set the failure limits conservatively with the hazard of unnecessary shutdowns. The system is shut down and then the problem is determined. The limits are shown in fig. 4-6. If one of the monitored parameters is consistently shutting down the system, the parameter limit can be changed or the monitoring of that particular point can be deleted.

Sensors

The three types of sensors used to provide information to the controller are (1) speed, (2) temperature, and (3) pressure.

Two speed sensors are used. The first counts the passage of the teeth of the pump drive gear, which has 95 teeth, rotates at 5020 rpm, and provides a nominal 7948-Hz signal to the controller for the primary speed control. A second identical sensor is located so as to count a 60-tooth disk on the turbine shaft. It provides a nominal 63,000-Hz signal that is used to detect an overspeed condition. These sensors are described in fig. 4-7.

Four thermocouples are used to monitor gas temperatures in the system. These thermocouples are of a special design to combine high response with resistance to the effects of hot hydrogen gas and a vibratory environment. The thermocouple joint is supported in a magnesium oxide insulation swaged in an 0.032-in.-dia inconel tube. This design will provide a time constant of approximately 0.2 to 0.4 sec, depending upon the gas flow rates. This type of thermocouple is illustrated in fig. 4-8.

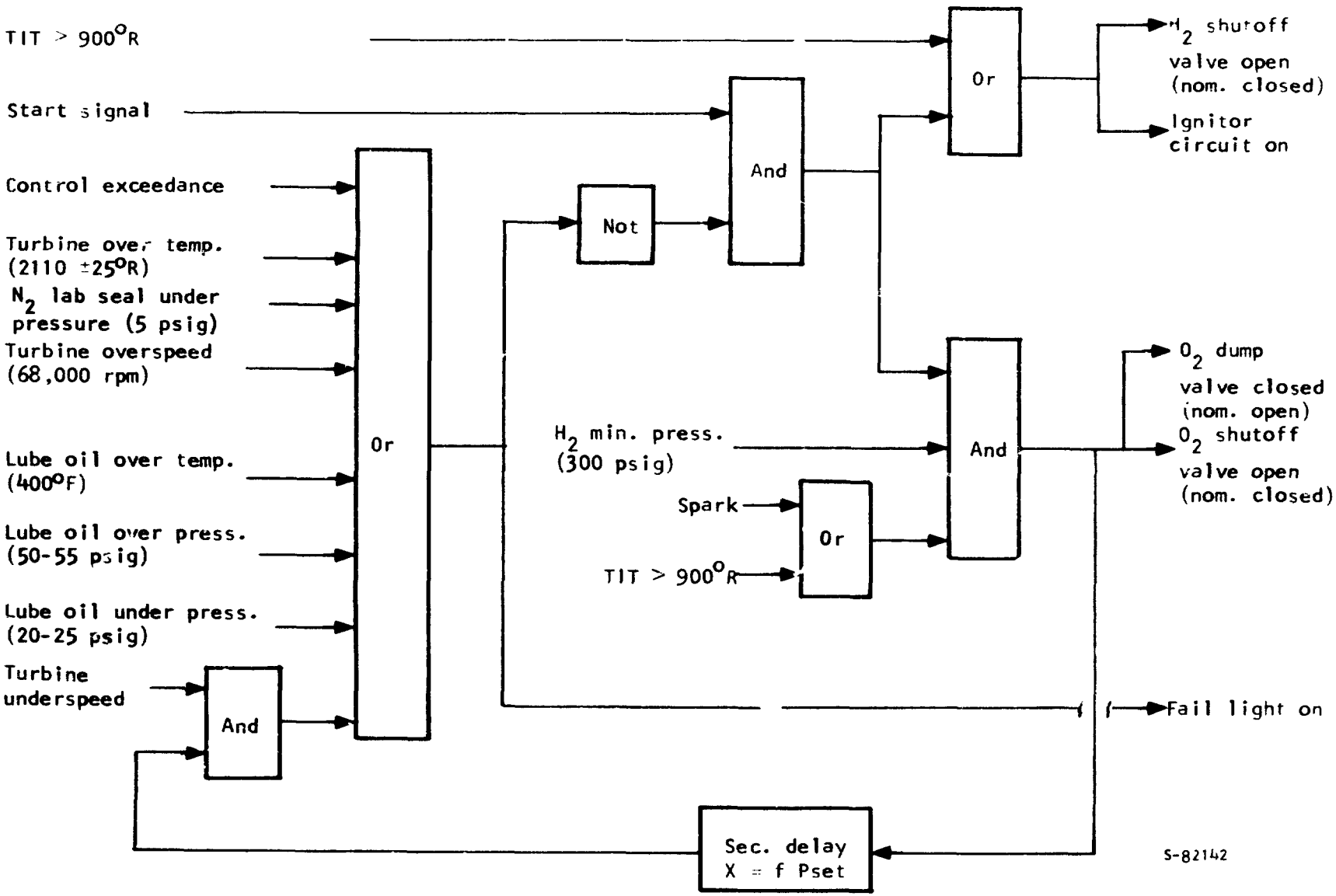

Figure 4-6.--H_2-O_2 APU Startup and Shutdown Control Logic.

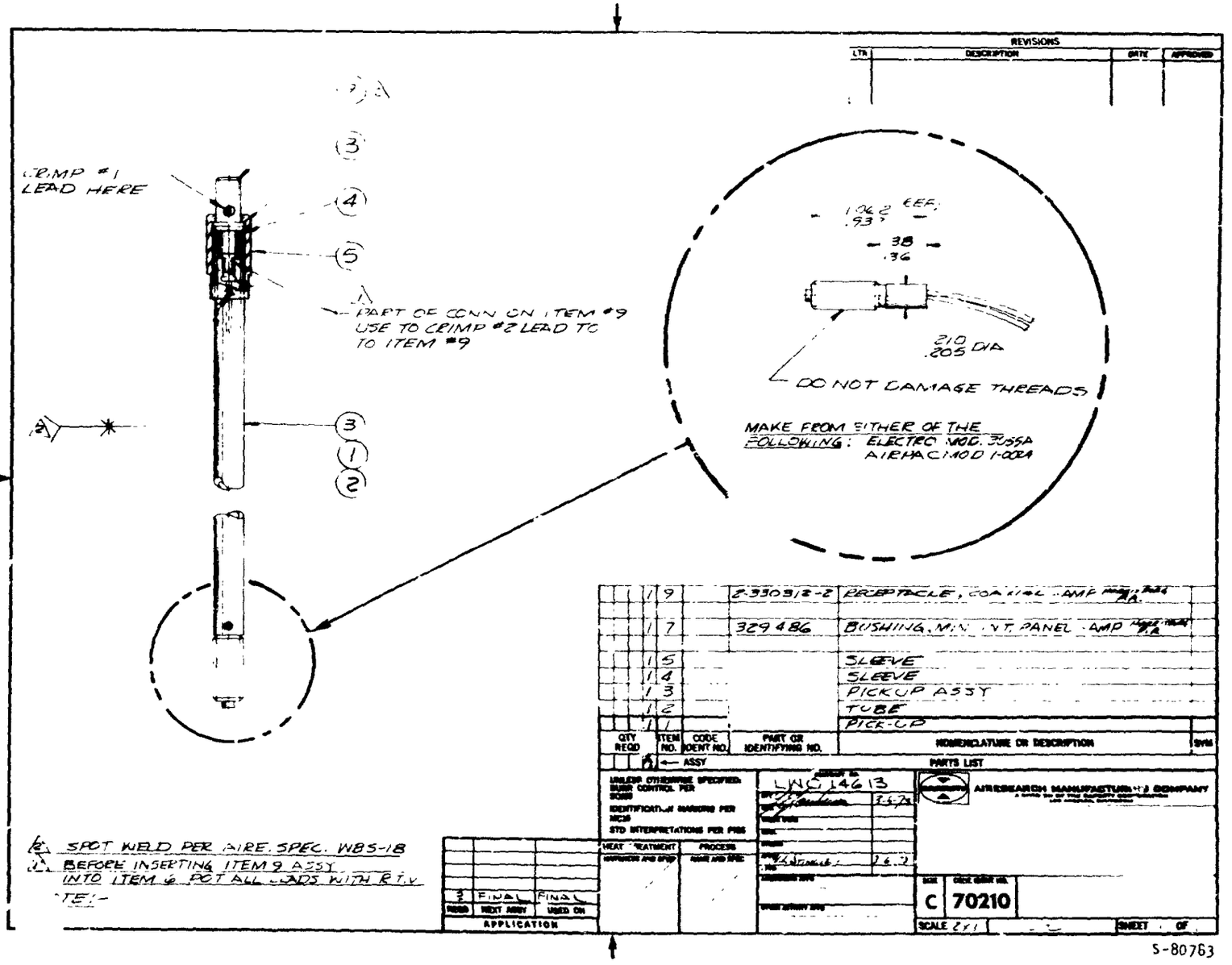

S-80763

Figure 4-7.--Speed Pickup Probe, Gearbox, Space Shuttle Turbine.

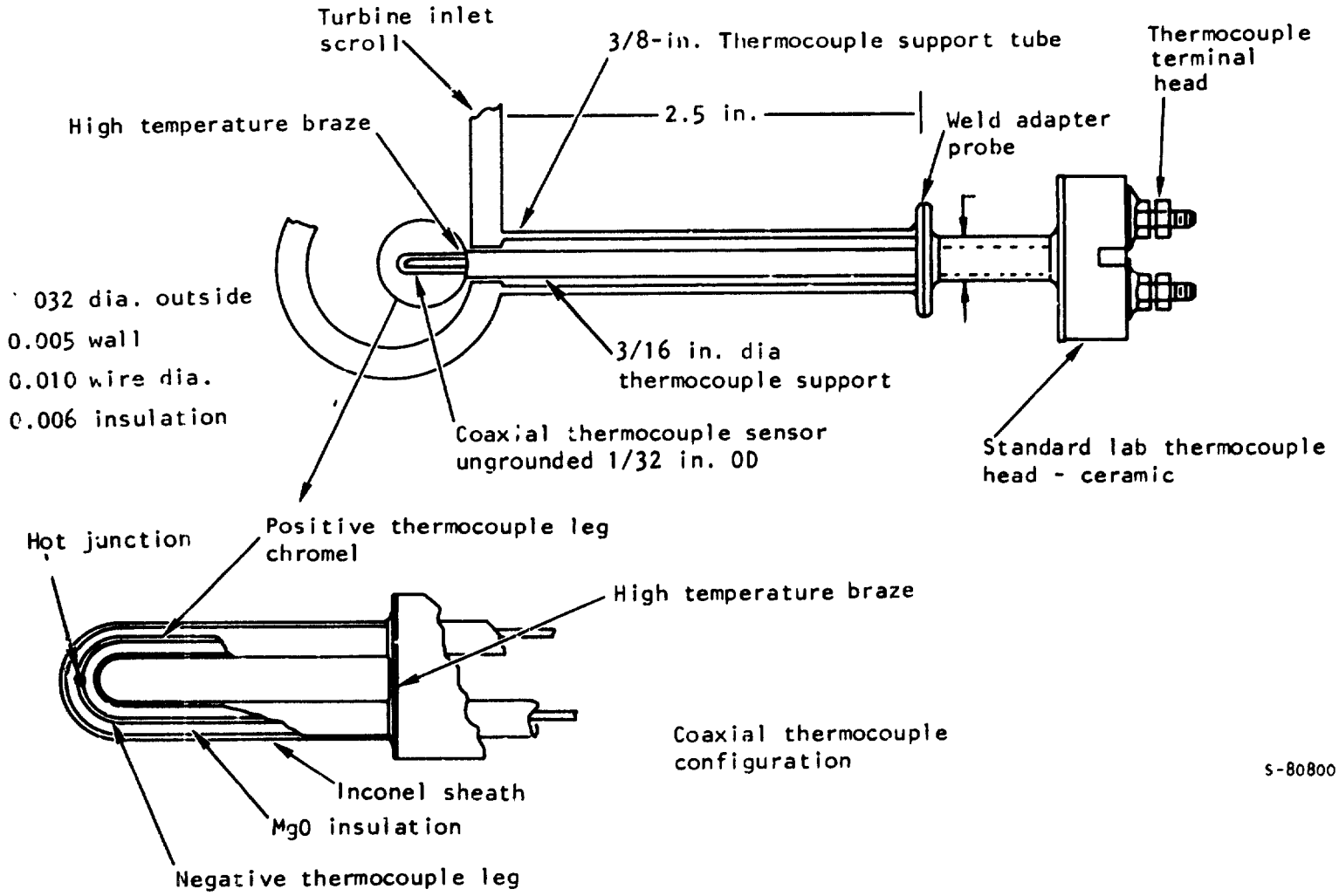

Figure 4-8.-- H_2-O_2 APU Turbine Inlet Thermocouple.

Two pressure switches are used to provide a switched signal to the controller in the event of over- or underpressure in the lubrication system. An overpressure condition could occur if the oil in the oil cooler congealed sufficiently to block the flow. These commercially available switches are described in fig. 4-9.

Control Circuit Design

In the following discussion, examples of portions of the electronic control circuit design and the effects of selected component failures are presented.

Thermocouple amplifier and cold junction compensation.--The schematic for turbine inlet control and overtemperature thermocouple amplifier is shown in fig. 4-10. The type of thermocouple to be used is chromel-alumel.

The combination Z_1, Z_2, and Z_4 comprises the turbine inlet control thermocouple signal conditioning. The cold junction compensation amplifier Z_1 compensates the cold junction formed when the chromel-alumel wires are terminated at the circuit board in the control system. The cold junction senses the ambient temperature of the circuit board. Since the ambient temperature is not constant, Z_1 and its associated circuitry provide a voltage that compensates for the cold junction through the use of thermistor R_7 (C-P nickel). The temperature coefficient of the thermistor approximates the voltage versus temperature properties of a chromel-alumel junction when the thermistor is properly biased. This compensation can be repeated consistently to $\pm 3^{\circ}F$ for ambient temperature changes of $150^{\circ}F$.

Operational amplifier Z_2 is a high-voltage gain amplifier used to condition the voltage from the chromel-alumel thermocouple. This amplification is necessary because the thermocouple has a low voltage versus temperature profile. The gain of the thermocouple is approximately 23 $\mu v/^{\circ}F$. In the case of an open-circuit thermocouple, the combination of R16 to R19 provides a low-voltage bias that will cause the output of Z_2 to exceed its normal operating range. When this exceedance occurs, a shutdown signal is provided to the shutdown logic through CR2.

Z_4 is used to level shift and buffer the amplified thermocouple voltage to its desired voltage scaling and level. The turbine inlet control will have a final scaling of 10.0 $mv/^{\circ}R$ and have an output voltage of 5.000 v at temperatures equal to $2000^{\circ}R$. The combination of Z_5 and Z_3 performs the same function as Z_2 and Z_4, except that these condition the overtemperature thermocouple.

The purpose of Z_6 is to compare the difference between the two conditioned thermocouple signals and to provide a shutdown signal for the shutdown logic if the difference exceeds a predetermined value. The purpose of Z_7 and Z_8

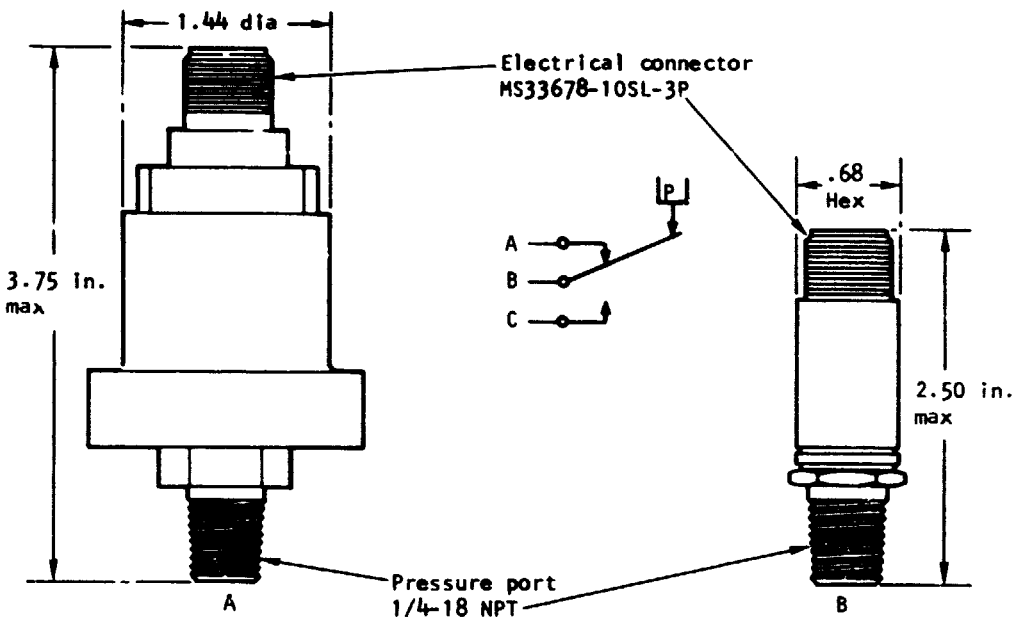

Switch application	Figure	Set point
Lube oil overpressure	A	Opens (pins A-B) on increasing pressure 50-55 psig
Lube oil underpressure	A	Opens (pins B-C) on decreasing pressure 25-20 psig
Hydrogen supply pressure	B	Closes (pins B-C) on increasing pressure 280-310 psig
Nitrogen underpressure	A	Opens (pins B-C) on decreasing pressure 5-4 psig

S-82237

Figure 4-9.--Pressure Switches Used on the H_2-O_2 APU-T P/N 581170-1-1

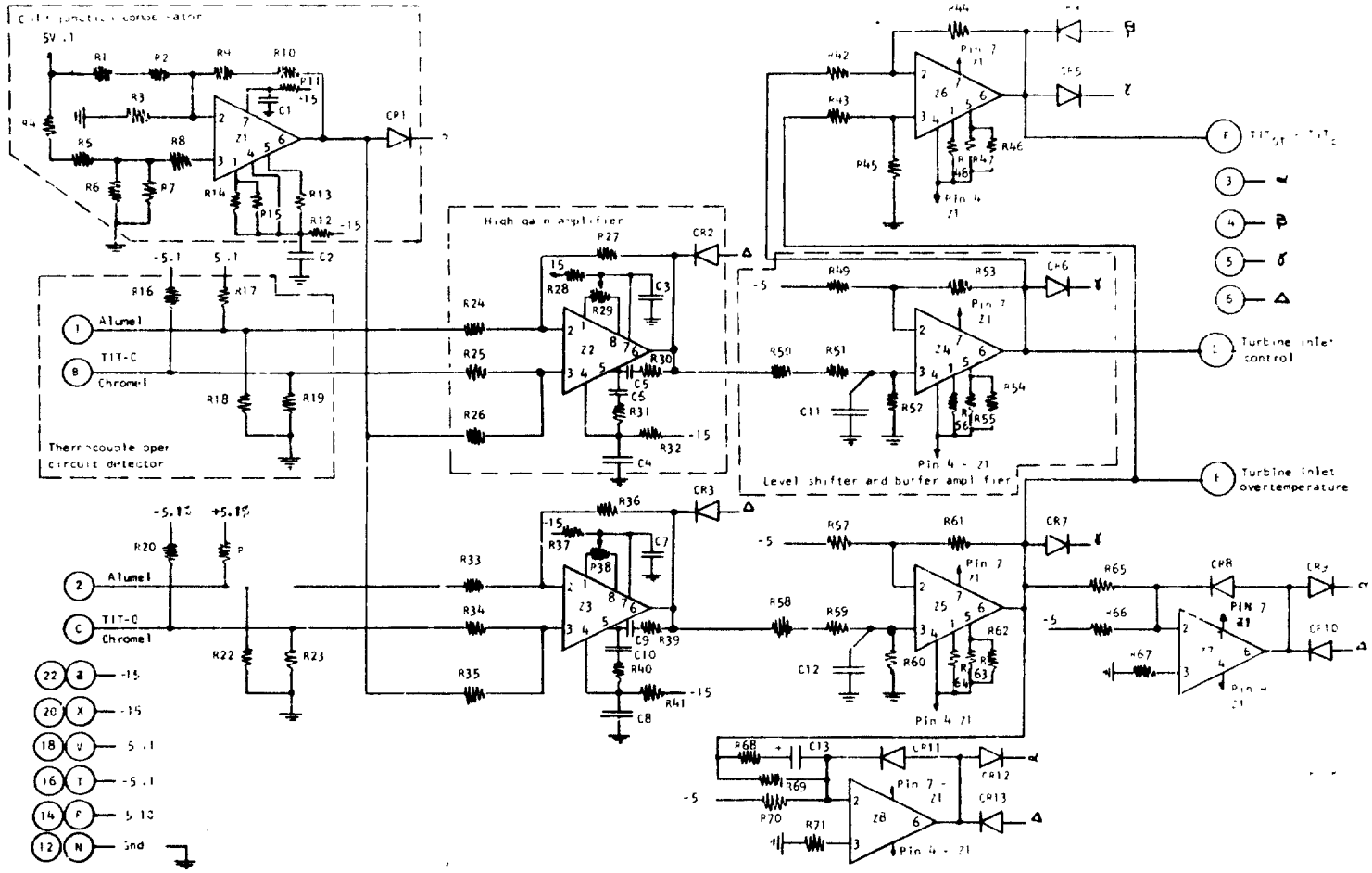

Figure 4-10.--Turbine Inlet Control and Overtemperature Thermocouple Amplifiers.

is to provide overtemperature shutdown; Z_7 provides a steady-state limit, while Z_8 takes into account the thermocouple dynamics to protect against overtemperature during transient conditions.

Frequency to direct current converters.--A schematic diagram of the frequency-to-dc converters is shown in fig. 4-11. The schematic includes the converters for both the control conditioner and the overspeed conditioner; both circuits are identical. The block diagram of the frequency-to-dc converter is shown below.

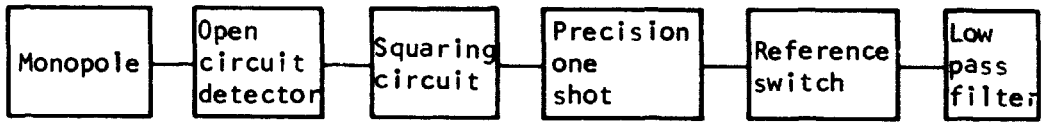

Each of these functional blocks is discussed below.

To sense an open circuit monopole, a dc current is passed through the monopole as shown in fig. 4-11. If the monopole has electrical continuity, Q_1 will remain in the saturated, or nonfailed, condition. If the monopole becomes an electrical open circuit, the base current, which ensures that Q_1 is saturated, will drop to a level that will allow Q_1 to turn off. This sequence sill provide a shutdown signal to the shutdown logic through CR1.

The squaring circuit conditions the output voltage from the monopole to a signal level and amplitude compatible with the voltage levels and power required to supply the precision one-shot. The amplitude of an unconditioned monopole would be unacceptable due to its variation in amplitude versus frequency characteristic; therefore, the high gain squaring circuit eliminates this restriction.

The precision one-shot is used to generate a stable time period. The operation of the frequency-to-dc converter is based on the principle that the average dc voltage level of a train of rectangular pulses is proportional to the amplitude and to the period of the pulses, and is inversely proportional to the time between pulses (see below).

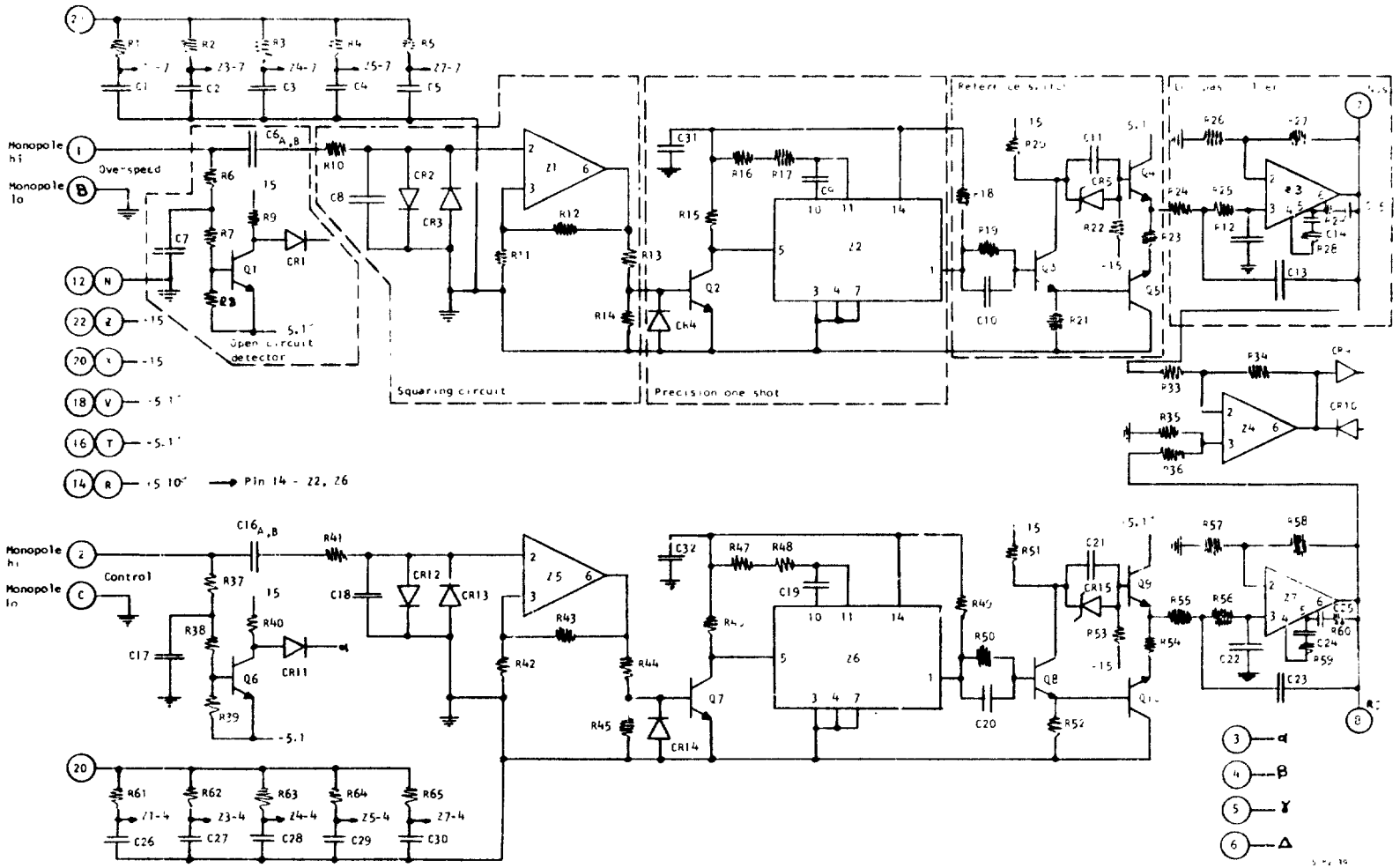

Figure 4-11.--Frequency-to-dc Converters.

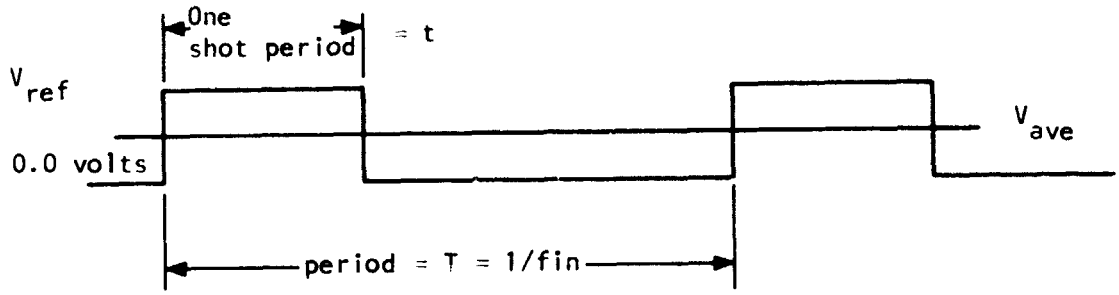

$$V_{ave} = \frac{1}{T}\int_0^T v(t)dt = \frac{1}{T}\left[\int_0^t V_{ref}dt + \int_t^T odt\right]$$

$$= \frac{1}{T}\left[V_{ref}t\right]_0^t = \frac{V_{ref}t}{T}$$

: where V_{ref} is provided by the reference switch.

If the pulse width t and amplitude V_{ref} are held constant, and the period between pulses (T_{in}) is equal to the period of the input frequency that is being converted, then

$$V_{ave} = \frac{V_{ref(t)}}{T_{in}}, \text{ and since } \frac{1}{T_{in}} = \text{input frequency,}$$

then $$V_{ave} = \text{(constant)} \times \text{(input frequency)}$$

therefore, the average dc voltage is linearly proportional to the input frequency.

The active filter serves to extract the average dc component from the pulse train provided from the reference switch. It also serves to amplify the average dc voltage to suitable scale factor. The dc gain of the active filter is chosen so that the output voltage level varies from 0 to 5 v for a 0 to 100 percent change in input frequency. The ac gain characteristics of the active filter are such that the output response time, phase shift, and ripple voltage in the dc output signal are controlled to acceptable limits.

Z_4 is used to compare the two conditioned speed signals. If the difference between these exceeds an allowable limit, (as shown in fig. 4-12) a shutdown signal is supplied to the shutdown logic.

Hydrogen valve control loop.--The schematic of the hydrogen valve control loop is shown in fig. 4-12. This control loop receives electrical inputs from the conditioned P_{61} (combustor pressure) signal conditioner, N_c (turbine speed), ΔP_{61} (external adjustment for varying P_{61} control level), and speed select (for selecting turbine speed control point). The circuit provides an electrical signal that commands hydrogen valve position. A block diagram of the control loop is shown below.

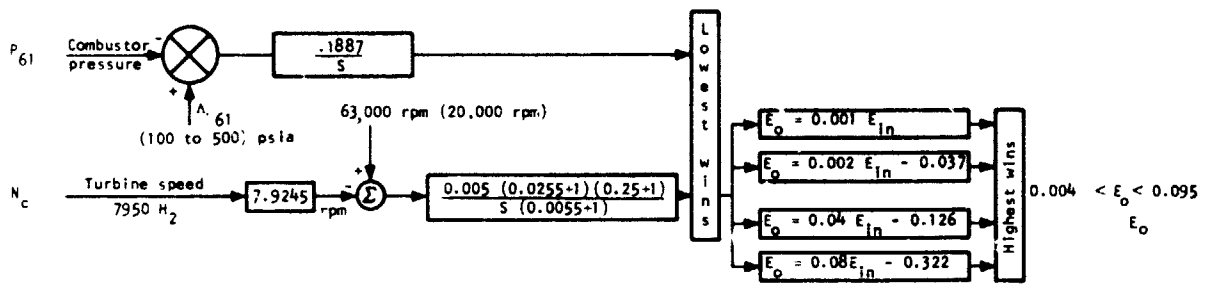

Hydrogen Valve Control Loop

The actual electronic circuit mechanization is included in fig. 4-13. The mechanization contains two function generators designed to fit the required type of curve by appropriate use of amplifiers in shunt and by discriminating with diodes.

In figs. 4-12 and 4-13, the areas designated ① are used to provide the necessary loop dynamics as required for loop stability. These dynamics are specified elsewhere. The two control modes (speed and pressure) must be bounded limits to eliminate integrater windup. This is accomplished by the function generator shown in fig. 4-13, which has a common feedback point for the operational amplifiers to ensure that the integrating capacitors for the speed and pressure loops have the same initial conditions. The mechanization of the four-segment function generator indicated in the valve control loop is shown in fig. 4-13 ②. A graph of the required function is as follows:

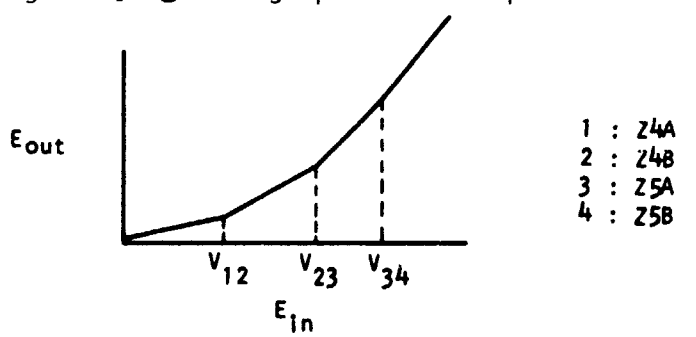

Function generator

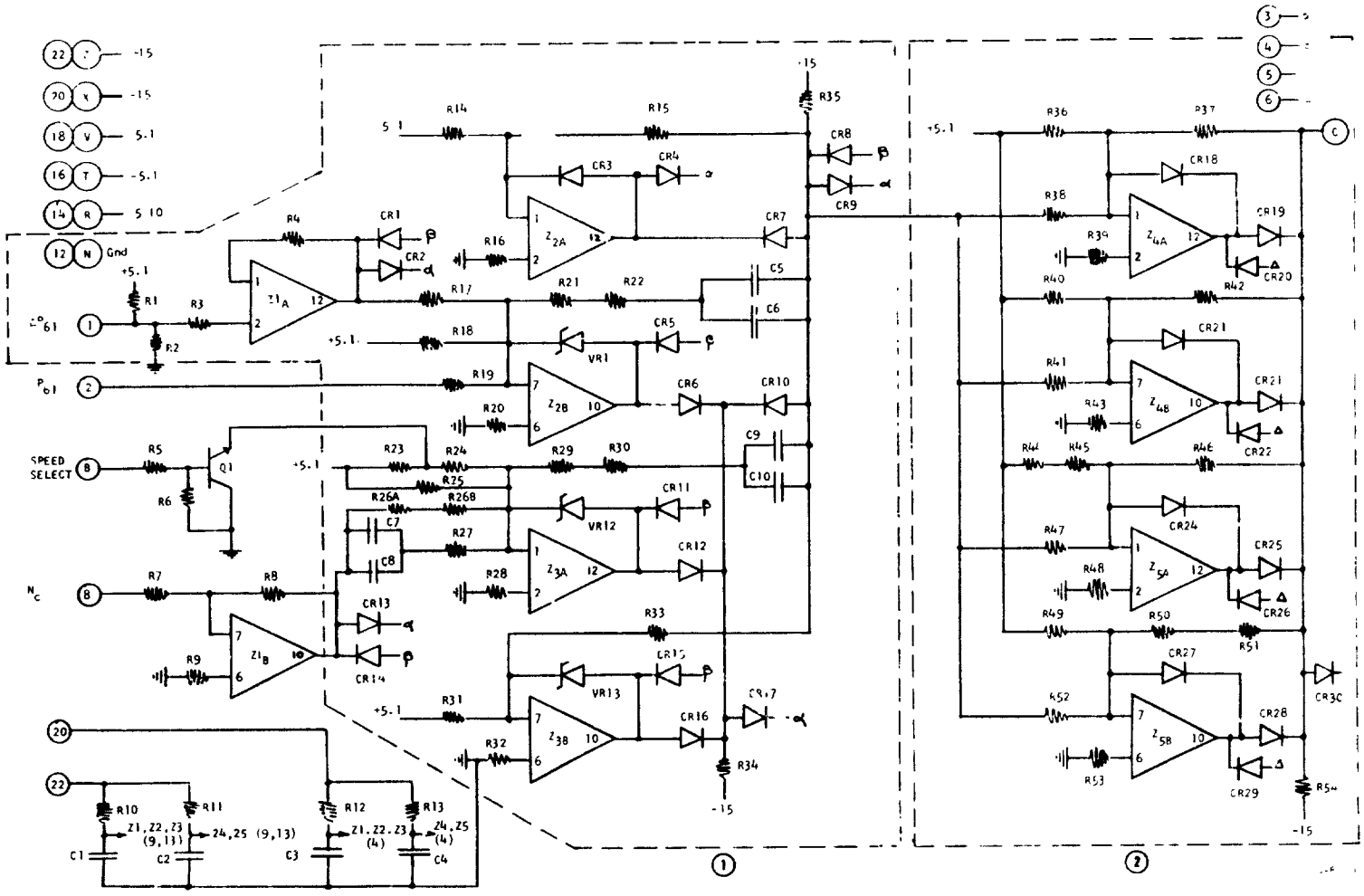

Figure 4-12.--Hydrogen Valve Control Loop.

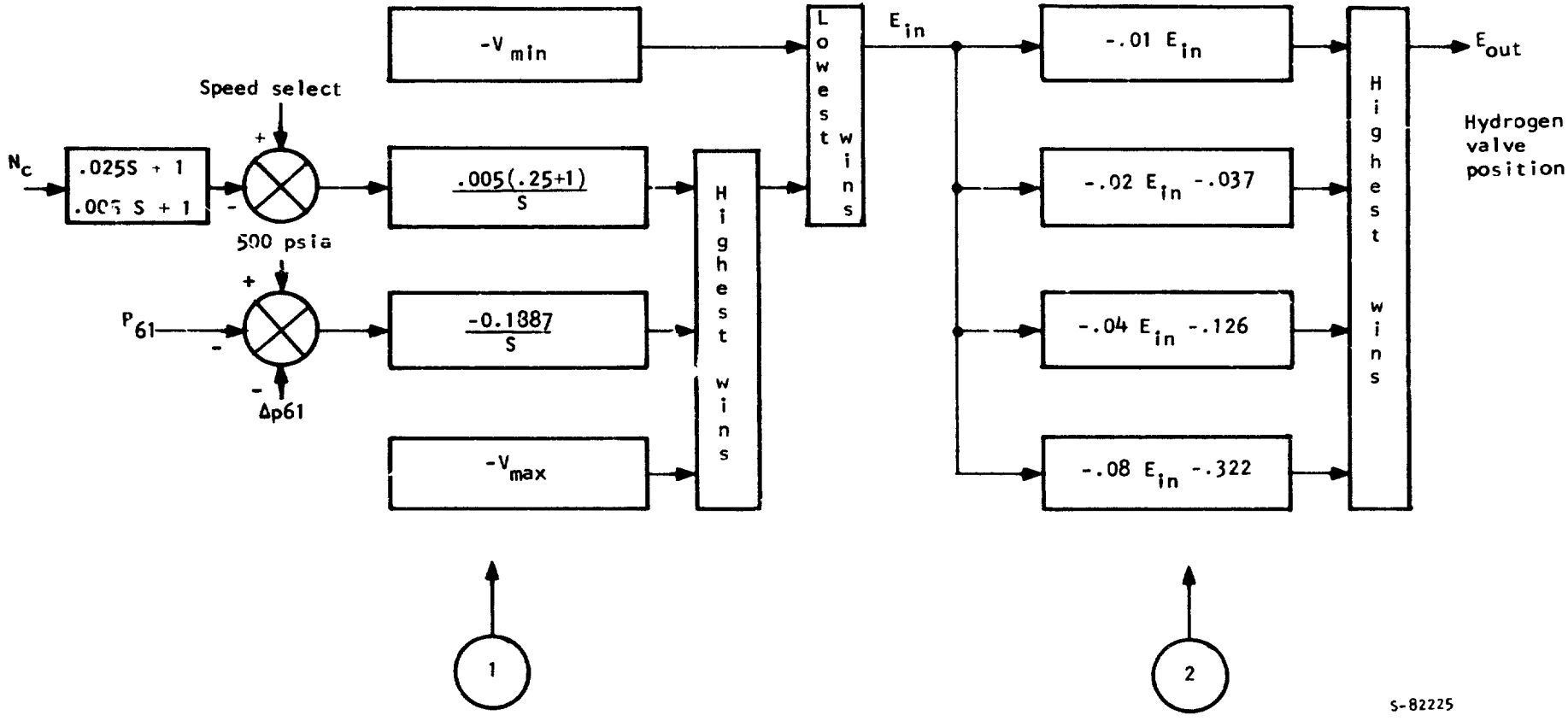

Figure 4-13. Circuit Mechanization of Control Loop.

Each of the four distinct segments shown above is mechanized by an operational amplifier. The individual characteristic of each amplifier is shown in the required function plot. Since the outputs of each amplifier are OR'ed together through CR19, CR22, CR25, and CR28, Z4A prevails until E_{in} approaches V_{12}. Z4B, Z5A, and Z5B are in negative saturation of the appropriate interloop diodes. When E_{in} exceeds V_{12}, Z4B predominates because Z4A, Z5A, and Z5B cannot control the output at a lower voltage than desired by Z4B. This same concept applies to the remaining segments. This approach was extended to high and low discriminator along the same lines as shown in fig. 4-1.

Response of system with failed components.--This discussion shows how the changes in specific components affect the system. Components discussed are (1) hydrogen flow control valve, (2) oxygen flow control valve, (3) preheater bypass valve, (4) recuperator bypass valve, (5) monopole, (6) pressure sensor, (7) temperature sensor, and (8) power supply.

Hydrogen flow control valve: The hydrogen flow control valve is primarily coupled to turbine speed and temperature control loops. The two types of hard-over failures of the hydrogen flow control valve are (1) a speed control failure causing both oxygen and hydrogen valves to be driven, and (2) a failure that drives only the hydrogen flow control valve. If both the hydrogen valve and the oxygen valve are driven into the limit at the same time, the turbine will start to accelerate. This provides considerable energy for turbine acceleration, but the turbine inlet temperature is kept within a reasonable limit. The turbine inlet temperature will drop if the hydrogen flow control valve opens without the oxygen flow control valve moving. The energy available with this failure is less than the energy with both valves opening, but the turbine will still start to accelerate.

The hydrogen flow control valve is designed to return to half stroke under loss of electrical power. The valve uses a dual-wound torque motor as the prime mover. Each of the coils is driven separately; however, if one coil opens, the other coil can drive the valve from less than 25 percent stroke to more than 75 percent stroke. Thus, an inoperable valve is not a complete failure. Under certain circumstances it may permit limited or even full utilization of the system.

If the oxygen valve is also driven closed when the hydrogen valve is driven full closed, the flame goes out and the turbine decelerates. If the hydrogen valve is driven closed and the oxygen valve remains in the last position, the combustor will become oxygen rich and the turbine inlet temperature will exceed maximum allowable temperature as the mixture passes through stoichiometric.

Oxygen flow control valve: The temperature will rise and the turbine will start to accelerate if the oxygen flow control valve becomes fully opened. The opposite occurs if the valve is closed.

Preheater bypass valve: The preheater bypass valve and the preheater series valve should be considered at the same time. The control is mechanized so that the valve areas are complementary. For the first failure characteristics,

the valves are assumed operating in a complementary fashion and the command is erroneous. If the preheater bypass valve is fully opened, the hydrogen entering the lube oil cooler and the hydraulic oil cooler will drop. This may cause the viscosity of the lube oil to become high enough to trip the lube oil overpressure switch. If the overpressure does not trip before zone congealing in the oil cooler, the lube oil temperature will start to rise. This is because the remaining area in the cooler becomes small enough and the boundary layer becomes viscous enough that the primary flow does not have a chance to transfer the heat. As a result, the lube oil will become excessively hot.

When the preheater bypass valve is fully closed, the hydrogen temperature into the hydraulic oil cooler and the lube oil cooler will increase.

Recuperator bypass valve: The recuperator bypass and recuperator series valves are complementary-coupled in a similar manner to the preheater bypass valve. When the recuperator bypass valves are commanded full-open or full-closed, the temperature equalizer drifts down or up, respectively. The system monitoring is not set up to detect this temperature drift. However, the temperature change is slow enough to allow an operator to detect the condition and shut down the system. Over most of the operating range of the APU, the full closure of the recuperator bypass valve would not result in damage to the system hardware. At no time would the complete loss of recuperation (recuperator bypass valve fully open) result in hardware damage.

Monopole failure: The monopole is used as a speed sensor. If the sensor were shorted, the signal level would drop below the level of detectability by the control. If this were to happen to the overspeed protection sensor, it would shut down the system as an underspeed. If the control sensor were to fail, then the control would allow the turbine to overspeed and shut down. Another failure would occur when the signal path opens; this type of failure is monitored and will cause a shutdown.

Pressure sensor: The pressure sensor is not needed for normal control, but is used for turbine calibration. If the pressure sensor erroneously indicates an overpressure, turbine power will be lost and the turbine will underspeed. If the pressure sensor erroneously indicates that the pressure is zero, the system pressure control will not function. This would result in the APU operating in the same manner as when the pressure control set point is 500 psi.

Temperature sensors: The critical temperature control for the APU is the turbine inlet temperature. This temperature is measured using redundant temperature sensors. The monitor is designed to shut down the system if one of the following conditions occurs: (1) the difference between the two sensors is greater than 50°, (2) the overtemperature sensor indicates a temperature greater than $1990^{\circ}R$, (3) the frequency compensated temperature output is greater than $2060^{\circ}R$.

Power supply: Power is obtained from the facility power source. Loss of facility power results in loss of the shutdown logic, which positions the system valves as follows:

Valve	Position
Hydrogen shutoff valve	Closed
Oxygen shutoff valve	Closed
Oxygen dump valve	Open
Hydrogen flow control valve	Mid position
Oxygen flow control valve	Minimum stop (mechanical)
All hydrogen bypass and series valves	Last position

The position of the flow control valves during loss of facility power will cause the turbine inlet temperature to drop. The oxygen dump valve prevents the gas mixture in the combustor from becoming oxygen rich as propellants empty from the system. The oxygen check valve prevents the combustion products (especially hydrogen) from flowing back into the oxygen accumulator.

System Valve Specifications

The valve specifications resulting from the preliminary design system are presented here and are applicable to both the reference system and test system valves. Specifications are presented for:

(1) Hydrogen bypass valve

(2) Oxygen pressure regulator

(3) Hydrogen flow control valve

(4) Oxygen flow control valve

APU-T HYDROGEN BYPASS VALVE REQUIREMENTS

General

It is the purpose of this document to define the requirements of the hydrogen bypass valve for NASA approval and valve and data procurement.

Description

The valve shall be a butterfly type valve which is used to bypass the pre-heater and recuperator heat exchangers. The valve element shall be driven by an available torque motor. A LVDT or RVDT shall be incorporated in the design for positive feedback. The valve shall tend to fail closed upon loss of power. The hardware shall be developed in accordance with "research" requirements of Garrett Operational Procedure 10.6.

Data Requirements

A design schedule is required prior to authorization to proceed with design. This schedule should give sufficient visibility to show major design activities. Percent completion and technical status reports will be required by the end of each month. A schedule of planned expenditures and actual expenditures will also be required monthly. Upon completion of the design a complete set of drawings, and a design development description outlining the design and future activities (i.e., stress and performance analysis, development plan, test plan, anticipated problems, fabrication and development schedule, estimate to complete and planned expenditures vs. time), shall be required prior to authorization to proceed with fabrication and development.

Upon authorization to proceed with fabrication, monthly reporting will be required as described above. A development log book will be prepared as the hardware is fabricated, inspected, and tested. All pertinent engineering records (i.e., inspection of critical dimensions by Q.C., rework activity, assembly notes, and test data), shall be recorded in this log book for ultimate delivery to NASA. Critical dimensions will be defined by AiResearch and approved by NASA. An informal test report showing compliance with and deviation from the valve specification shall be submitted separately. Valve performance test shall be conducted with air (room temperature and 1350°R).

Hardware Requirements

Four functional valves are required for APU-T system test. Long lead time and critical details should be fabricated or ordered in sufficient quantity so as to meet the requirements of the schedule.

APU-T HYDROGEN BYPASS VALVE SPECIFICATION

	H_2	EQUIVALENT AIR 1350°R	EQUIVALENT AIR 520°R
Design Conditions			
Maximum design pressure, psia	600		
Design ambient pressure, psia	0-15		
Proof pressure, psia	900		
Maximum design temp., °R	1350*		
Minimum design temp., °R	400		
Performance Requirements			
**Maximum flow, lb/min	7.83	18.5	29.8
Delta P, psi	0.8	0.8	0.8
Temperature, °R	520	1350	520
Pressure in, psia	541	541	541
Pressure out, psia	540	540	540
CA (reference), in.^{2}	0.477	0.477	0.477
*Minimum flow, lb/min	0.0288	0.0703	0.113
Delta P, psi	0.6	0.6	0.6
Temperature, °R	550	1350	520
Pressure in, psia	563	563	563
Pressure out, psia	562	562	562
CA (reference), in.^{2}	0.0022	0.0022	0.0022

LVDT resolution ±0.5 percent

Response time = 200 ms from min.-to-max. condition

Life: 1000 Hours

**NOTE: Set inlet and outlet conditions and measure flow at minimum and maximum operating position.

General Requirements

Line size = 1.0 in. O.D.

Electrical requirements, TBD by available parts

External leakage: Lab. Std. practice (NASA to check 10^{-6} sccm H_e)

Valve stability -- consistent with operation over the anticipated range without undesirable oscillations.

*NOTE: A new requirement -- previous maximum temperature was .075°R.

Rev. 1 - 3/7/73

APU-T OXYGEN PRESSURE REGULATOR VALVE REQUIREMENTS

General

It is the purpose of this document to define the requirements of the oxygen pressure regulator valve for NASA approval and valve and data procurement.

Description

The valve shall be a pneumatically actuated, differential pressure regulator. Its function is to regulate oxygen from the equalizer to the oxygen control valve. The design shall include provisions to prevent the outlet pressure from exceeding the specified maximum value during fouled or failed conditions. The hardware shall be developed in accordance with "research" requirements of Garrett Operational Procedure 10.6.

Data Requirements

A design schedule is required prior to authorization to proceed with design. This schedule should give sufficient visibility to show major design activities. Percent completion and technical status reports will be required by the end of each month. A schedule of planned expenditures and actual expenditures will also be required monthly. Upon completion of the design a complete set of drawings, and a design development description outlining the design and future activities (i.e., stress and performance analysis, development plan, test plan, anticipated problems, fabrication and development schedule, estimate to complete and planned expenditures vs. time), shall be required prior to authorization to proceed with fabrication and development.

Upon authorization to proceed with fabrication, monthly reporting will be required as described above. A development log book will be prepared as the hardware is fabricated, inspected, and tested. All pertinent engineering records (i.e., inspection of critical dimensions by Q.C., rework activity, assembly notes and test data), shall be recorded in this log book for ultimate delivery to NASA. Critical dimensions will be defined by AiResearch and approved by NASA. An informal test report showing compliance with and deviation from the valve specification shall be submitted separately. Valve performance test shall be conducted with air (room temperature and 750°R), with an inlet pressure of 900 psia.

Hardware Requirements

Two functional valves are required for APU-T system test. Long lead time and critical details should be fabricated or ordered in sufficient quantity so as to meet the requirements of the schedule.

O_2 REGULATOR VALVE SPECIFICATION

Design Conditions	O_2
Maximum design inlet pressure, psia	900
Maximum design outlet pressure, psia	650
Design ambient pressure, psia	0 -15
Proof pressure, psia	1350
Maximum design temperature, ^0R	900
Minimum design temperature, ^0R	400
Performance Requirements	
Regulated outlet pressure ~ psig	550 ± 25
Maximum flow, lb/min (ref)	6.62
Inlet pressure, psia	878
Temperature ~ ^0R	663
CA (reference), $in.^2$	0.00587
Minimum flow, lb/min (ref)	0.454
Inlet pressure, psia	900
Temperature ~ ^0R	750
CA (reference), $in.^2$	0.00072

Response Time 100 MS

Life 1000 hours

General Requirements

Line size = 1/2 in. OD

External Leakage: Lab standard practice at AiResearch (NASA to check to 10^{-6} sccm He)

Valve stability: Consistent with operation over the anticipated range without undesirable oscillations

Rev. 1 - 3/7/73

APU-T HYDROGEN CONTROL VALVE REQUIREMENTS

General

It is the purpose of this document to define the requirements of the hydrogen control valve for NASA approval and valve and data procurement.

Description

The valve shall be a balanced poppet design which is electrically linked to the oxygen control valve in the electronic APU-T control. The valve element shall be driven by an available dry-type linear displacement torque motor. A LVDT shall be incorporated in the design for positive feedback. The valve shall fail open upon loss of power. A mechanical stop shall be provided to prevent full closure of the valve. The hardware shall be developed in accordance with "research" requirements of Garrett Operational Procedure 10.6.

Data Requirements

A design schedule is required prior to authorization to proceed with design. This schedule should give sufficient visibility to show major design activities. Percent completion and technical status reports will be required by the end of each month. A schedule of planned expenditures and actual expenditures will also be required monthly. Upon completion of the design a complete set of drawings, and a design development description outlining the design and future activities (i.e., stress and performance analysis, development plan, test plan, anticipated problems, fabrication and development schedule, estimate to complete and planned expenditures vs time), shall be required prior to authorization to proceed with fabrication and development.

Upon authorization to proceed with fabrication, monthly reporting will be required as described above. A development log book will be prepared as the hardware is fabricated, inspected, and tested. All pertinent engineering records (i.e., inspection of critical dimensions by Q.C., rework activity, assembly notes, and test data), shall be recorded in this log book for ultimate delivery to NASA. Critical dimensions will be defined by AiResearch and approved by NASA. An informal test report showing compliance with and deviation from the valve specification shall be submitted separately. Valve performance test shall be conducted with air (room temperature and 750°R), with a choked nozzle (effective area = 0.0655 $in.^2$), downstream of the valve.

Hardware Requirements

One functional valve is required for APU-T system test. Long lead time and critical details should be fabricated or ordered in sufficient quantity so as to meet the requirements of the schedule.

H_2 CONTROL VALVE SPECIFICATION

	H_2	EQUIVALENT AIR	
		750°R	520°R
Design Conditions			
Maximum design pressure, psia	600		
Design ambient pressure, psia	0-15		
Proof pressure, psia	900		
Maximum design temperature, °R	900		
Minimum design temperature, °R	400		
Maximum system test temperature, °R	TBD**		
Performance Requirements			
Maximum flow, lb/min (reference)	9.02	34.4	41.8
Delta P, psi, max.	45.3	51	51
Temperature, °R	693	750	520
Pressure in, psia	506	506	506
Pressure out, psia	461	455	455
CA* (reference), $in.^2$	0.0950	0.0950	0.0950
Minimum flow, lb/min (reference)	0.701	2.64	3.21
Delta P, psi, min.	540	540	540
Temperature, °R	750	750	520
Pressure in, psia	575	575	575
Pressure out, psia	35	35	35
CA* (reference), $in.^2$	0.00400	0.00400	0.0040
LVDT resolution ±0.5 percent Response time = 40 ms from min.-to-max. condition Life: 1000 hours	NOTE: See outlet pressure and temperature and measure ΔP at minimum and maximum operating position.		

General Requirements

Line size = 1.0 in. OD

Mechanical stops:

Full open, Reference CA = 0.1050 $in.^2$ (110 percent of maximum operating)

Full close, Reference CA = 0.0030 $in.^2$ (75 percent of minimum operating)

Electrical requirements: TBD by available parts.

External leakage: Lab standard practice at AiResearch (NASA to check to 10^{-6} sccm He)

Valve Stability: Consistent with operation over the anticipated range without undesirable oscillations.

* Actual CA variation vs LVDT position shall be linear to within ±5%.

** A system test case not a design requirement, max. valve will take for limited testing.

Rev. 1 3/7/73

APU-T OXYGEN CONTROL VALVE REQUIREMENTS

General

It is the purpose of this document to define the requirements of the oxygen control valve for NASA approval and valve and data procurements.

Description

The valve shall be a balanced poppet design which is electrically linked to the hydrogen control valve in the electronic APU-T control. The valve element shall be driven by an available dry-type linear displacement torque motor. A LVDT shall be incorporated in the design for positive feedback. The valve shall fail closed upon loss of power. A mechanical stop shall be provided to prevent full closure of the valve. The hardware shall be developed in accordance with "research" requirements of Garrett Operational Procedure 10.6.

Data Requirements

A design schedule is required prior to authorization to proceed with design. This schedule should give sufficient visibility to show major design activities. Percent completion and technical status reports will be required by the end of each month. A schedule of planned expenditures and actual expenditures will also be required monthly. Upon completion of the design a complete set of drawings, and a design and development description outlining the design and future activities (i.e., stress and performance analysis, development plan, test plan, anticipated problems, fabrication and development schedule, estimate to complete and planned expenditures vs time), shall be required prior to authorization to proceed with fabrication and development.

Upon authorization to proceed with fabrication, monthly reporting will be required as described above. A development log book will be prepared as the hardware is fabricated, inspected, and tested. All pertinent engineering records (i.e., inspection of critical dimensions by Q. C., rework activity, assembly notes and test data), shall be recorded in this log book for ultimate delivery to NASA. Critical dimensions will be defined by AiResearch and approved by NASA. An informal test report showing compliance with the deviation from the valve specification shall be submitted separately. Valve performance test shall be conducted with air (room temperature and 750°F), with a choked nozzle (effective area = 0.0109 $in.^2$), downstream of the valve.

Hardware Requirements

One functional valve is required for APU-T system test. Long lead time and critical details should be fabricated or ordered in sufficient quantity so as to meet the requirements of the schedule.

Rev. 1 3/7/73

O_2 CONTROL VALVE SPECIFICATION

	O_2	EQUIVALENT AIR	
		750°R	520°R
Design Conditions			
Maximum design pressure, psia	600		
Design ambient pressure, psia	0-15		
Proof pressure, psia	1350		
Minimum design temperature, °R	400		
Maximum design temperature, °R	900		
Performance Requirements			
Maximum flow, lb/min (reference)	6.62	5.98	7.50
Delta P, psi, max.	61.8	62.8	62.8
Temperature, °R	663	750	520
Pressure in, psia	532	532	532
Pressure out, psia	470	469	469
CA* (reference), $in.^2$	0.0135	0.0135	0.0135
Minimum flow, lb/min (reference)	0.454	0.433	0.544
Delta P, psi, min.	536	536	536
Temperature, °R	750	750	520
Pressure in, psia	570	570	570
Pressure out, psia	34	34	34
CA* (reference), $in.^2$	0.00065	0.00065	0.00065

LVDT resolution ±0.5 percent

Response time = 40 ms from min.-to-max. condition

Life: 1000 Hours

NOTE: Set outlet pressure and temperature and measure ΔP at minimum and maximum operating position.

General Requirements

Line size = 1/2 in. OD

Mechanical stops:

Full open, Reference CA = 0.0145 $in.^2$ (107.5 percent of maximum operating)

Full close, Reference CA = 0.0004 $in.^2$ (62 percent of minimum operating)

Electrical requirements: TBD by available parts.

External leakage: Lab standard practice at AiResearch (NASA to check to 10^{-6} sccm He)

Valve stability: Consistent with operation over the anticipated range without undesirable oscillations.

* Actual CA variation versus LVDT position shall be linear to within ±5 percent.

System Valve Design

The APU-T system valves include the following:

- Four identical hydrogen bypass valves
- Two identical oxygen pressure regulators
- A hydrogen flow control valve
- An oxygen flow control valve

All but the oxygen regulator are controlled by electrical signals from the APU-T controller. The valves are designed to conform to reference system specifications as a minimum but are not flight weight.

Hydrogen bypass valve.--The function and a description of the hydrogen bypass valve are presented below.

Function: The four identical hydrogen bypass valves in the system operate in response to electrical drive signals from the system controller. Two of the valves control bypass flow around the recuperator, and two of the valves control bypass flow around the preheater. The bypass flow around these two heat exchangers is varied as required to control hydrogen temperature at the combustor inlet and at the inlets to the hydraulic and lube oil coolers.

Description: The basic components of the bypass valve (see fig. 4-14) are (1) a flat-plate butterfly valve and shaft (2) a dc, dry-type, rotary displacement torque motor (Inland Motor Division, Kollmorgen Corporation PN NT-2943B, rated at 0.90 lb-ft, 77 w), and (3) a rotary variable displacement transformer (RVDT) (Schaevitz Engineering PN R30A). The valve has been designed to meet the requirements of the bypass valve specification. Average power consumption of the torque motor will be approximately 10 w.

The valve modulates hydrogen flow by rotation of a circular flat plate in the flow duct. The plate is attached to a shaft that is connected to the torque motor. Application of current to the torque motor causes the valve to move toward open. With increasing current, the valve will continue to open, with the travel limited to 80 deg by a mechanical stop. In the closed position, the valve does not seal leak-tight.

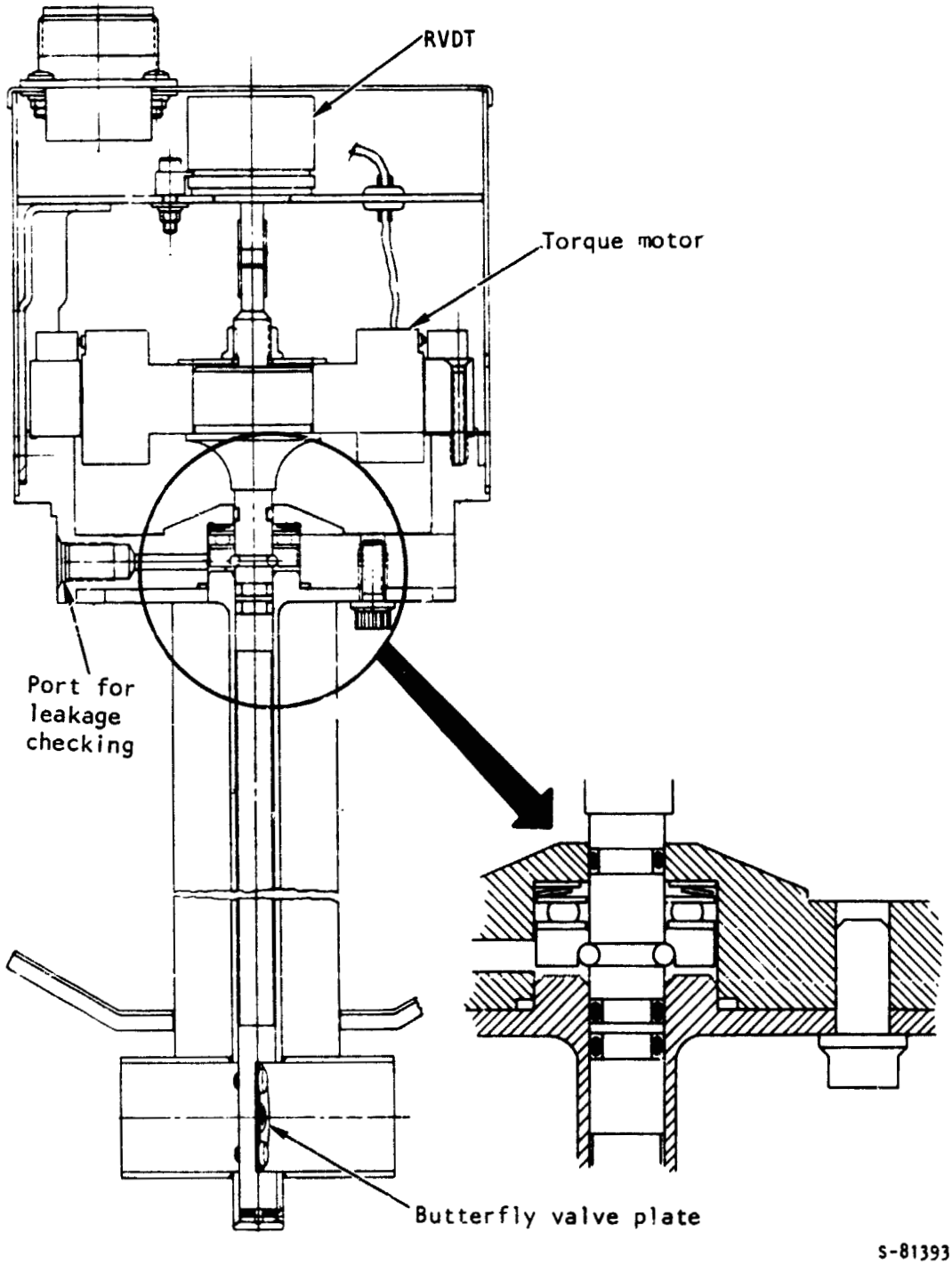

Figure 4-14.--H_2 Bypass Valve.

for use on the current APU-T being built for laboratory testing. In a flight-type design, it is anticipated that active cooling (possibly incoming cryogenic hydrogen) would be used to protect the torque motor and RVDT.

To prevent H_2 leakage along the valve shaft, redundant seals are included at the upper end of the shaft (near the torque motor). A port is provided in the valve body for checking and venting any hydrogen leakage that might get past the redundant seals. A single seal is included between the port and torque motor.

In the current APU-T, two-valves are used for each of the heat exchanger bypass circuits: one in series with the heat exchanger and one in parallel. As one valve opens the other closes. In a flight-type design, each pair of valves would be replaced by a three-way modulating valve.

Oxygen pressure regulator.--The function and a description of the oxygen pressure regulator are presented below.

Function: The oxygen regulator regulates oxygen pressure at the inlet to the combustor.

Description: In the oxygen pressure regulator, a ceramic ball-poppet valve is positioned by a calibration spring and differential pressure acting on a bellows actuator (see fig. 4-15). The regulator has been designed to meet the requirements of the oxygen regulator specification.

The regulator is normally full-open. As downstream pressure reaches the regulation band, the downstream pressure, which is vented to one side of the bellows actuator, overcomes an opposing load due to the calibration spring plus ambient pressure acting on the other side of the actuator. The actuator moves and allows a spring to move the ball-poppet toward the closed position. The balance of forces--downstream pressure on one side of the actuator and the calibration spring and ambient pressure on the other--maintains the poppet position required for regulation.

To achieve stable operation, the downstream pressure is sensed at a point approximately 4-1/4 in. downstream of the poppet instead of at a point close to the poppet. If pressure were sensed in the area close to the poppet valve discharge, flow turbulence could cause undesirable pressure fluctuations. Although an orifice in the sensing passage would dampen fluctuations, it would increase response time. The design does include a sensing passage in the valve body immediately downstream of the poppet. However, this passage will be sealed with a plug, which, if necessary at some future time, could be modified by drilling an orifice.

A port is provided on the top of the valve body for connecting the regulator to ambient. If oxygen internal leakage should occur, it would be ducted overboard (to ambient).

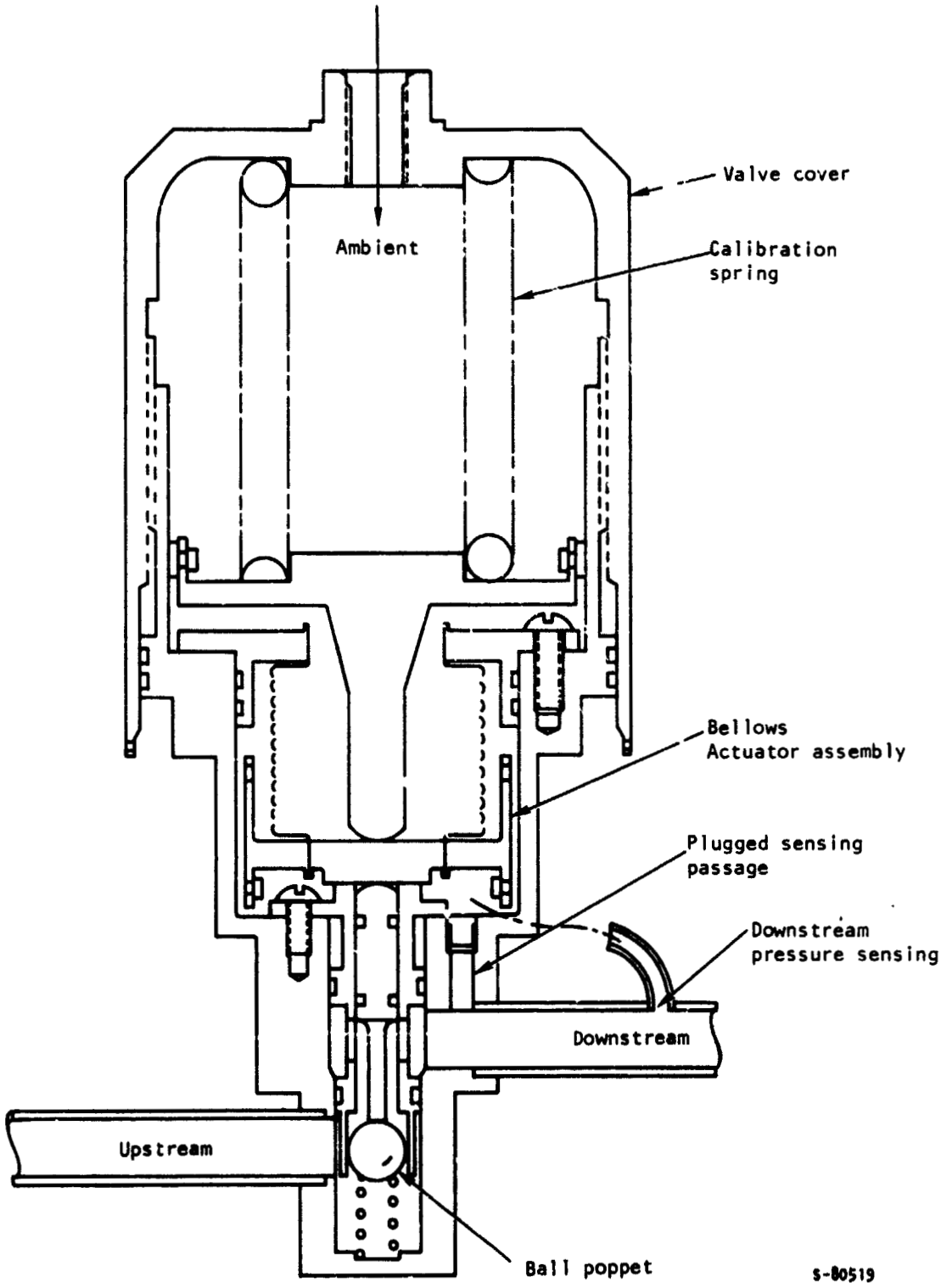

Figure 4-15.--Oxygen Pressure Regulator.

Two identical regulators will be connected in series, with the downstream regulator set 50 psi higher than the other. The downstream unit, therefore, protects against an open failure of the prime unit without interfering with normal regulation.

Hydrogen flow control valve.--The function and a description of the hydrogen flow control valve are presented below.

Function: The hydrogen control valve modulates hydrogen flow to the combustor in response to electrical control signals, and maintains constant turbine speed under varying APU loads and system conditions.

Description: The basic components of the hydrogen flow control valve (fig. 4-16) are (1) a dual-poppet assembly, (2) a dc, dry-type linear displacement torque motor (Servotronics PN 99-D0202), and (3) a linear variable displacement transformer (LVDT) (Schaevitz Engineering Type 050 MHR). The valve has been designed to meet the requirements of the hydrogen flow control valve specification.

Electrical input signals from the control are applied to the torque motor, which is connected to one end of a pivoted lever. The opposite end of the lever is attached to the poppet valve shaft on which dual poppets are mounted.

The normal (deenergized) position of the torque motor output shaft is held at the midstroke position of the torque motor by a high spring-rate torque tube in the motor. This position corresponds to the midstroke of the poppet valves. Upon application of polarized current (corresponding to a "close valve" signal) to the torque motor, the valve poppets are forced against the poppet spring toward the closed position. As current is increased, poppet movement continues until the poppet shaft is against a mechanical stop (valve nearly closed). As current is decreased, the valve moves back toward the central position. A change in torque motor polarity drives the poppets toward the full-open position. This motion is assisted by the poppet spring.

Poppet arrangement on a common shaft provides pressure force balancing to minimize power requirements of the actuating torque motor. Because of the large flow area of the hydrogen control valve, a velocity effect occurs that unbalances the poppets toward the closed position. To restore poppet balance, a deflector is mounted in the discharge path of one poppet to react with flow forces.

Poppet position is fed back to the control circuitry by means of a 400-Hz LVDT. The LVDT case is attached to the valve [illegible]e and the movable core is threaded to the poppet shaft. The position of the poppet is thus registered within the control logic for control monitoring.

At the suggestion of NASA, gold plating is specified for the rubbing surfaces of several parts in lieu of a dry-film lubricant. The parts to be

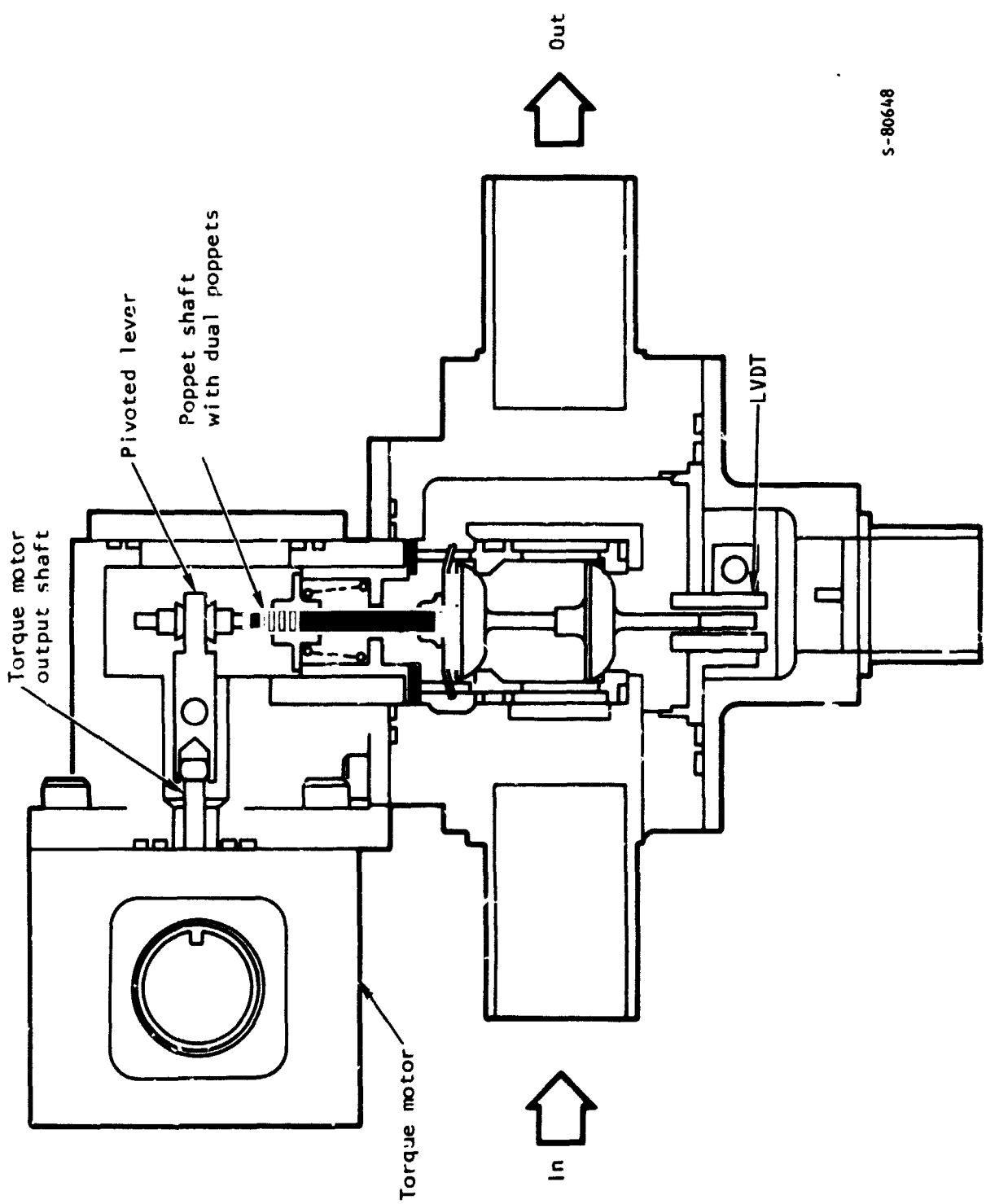

Figure 4-16.--Hydrogen Flow Control Valve.

plated are the pivoted lever at the area of contact with the spherical nut on the valve shaft, the spherical nut, and the pin on which the lever pivots. Gold plating will be applied in accordance with MIL-G-45204, Type I, Class 2.

Oxygen flow control valve.--The function and a description of the oxygen flow control valve are presented below.

Function: This valve modulates oxygen flow to the combustor in response to electrical control signals, and maintains turbine inlet temperature constant with varying load and system conditions.

Description: The basic components of the oxygen flow control valve (fig. 4-17) are (1) a dual-poppet assembly, (2) a dc, dry-type, linear displacement torque motor (Servotronics Part Number 99-D0201), and (3) an LVDT (Schaevitz Engineering Type 050 MHR). The valve has been designed to meet the requirements of the oxygen flow control valve specification.

Electrical input signals from the control are fed to the torque motor, which is directly coupled to the dual poppet valve shaft. As torque motor current is increased from zero, the spring-loaded-closed poppet assembly is displaced off its stop. This admits gaseous oxygen into the combustor. Gas flow increases as current is increased until the flow reaches a maximum value at the full open position of the dual poppets.

Poppet arrangement on a common shaft provides pressure force balancing to minimize power requirements of the actuating torque motor. Because of this balance effect, the torque motor output directly drives the poppet assembly.

An additional advantage of the dual poppets is the high gain relationship between the valve stroke and gas flow. In this unit, where the required flow is minimal, the resulting short valve stroke is within the stroke capability of the torque motor, and no additional linkage is required between the driving and driven members.

Poppet position is fed back to the control circuitry by means of a 400-Hz LVDT. The LVDT case is attached to the valve case, and the movable core is threaded to the poppet shaft. The position of the poppet is thus registered within the control logic for control monitoring.

The torque motor assumes the closed valve position with zero electrical current input. An additional magnetic closing force exists at the zero current conditions. The separate poppet closing spring acts to force the poppets closed. Thus, the oxygen control valve has redundant forces in the closing position in the event of power loss.

At NASA suggestion, gold plating is specified for the spherical nut, which is the rubbing surface in the connection between the torque motor output and the poppet shaft. The gold plating is intended as the lubricant and will be applied in accordance with MIL-G-45204, Type I, Class 2.

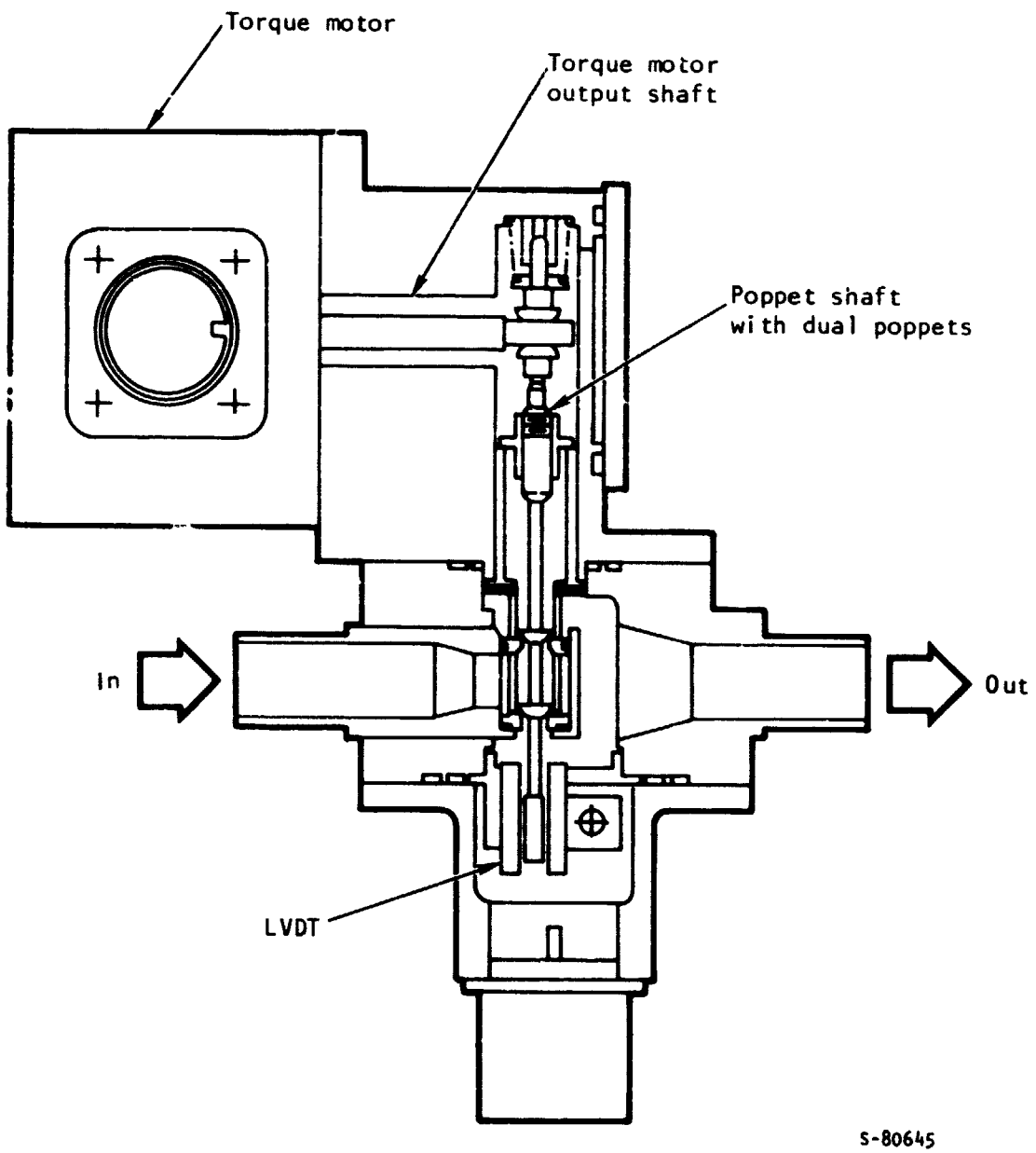

Figure 4-17.--Oxygen Flow Control Valve.

SECTION 5

TURBINE AND GEARBOX DESIGN

SECTION 5

TURBINE AND GEARBOX DESIGN

In this section, the aerodynamic design of the reference and test system turbine is discussed; the turbine mechanical design is presented; the turbine thermal analysis is presented; turbine stress and dynamics are analyzed; and the design of the gearbox is described.

Drawing L-208529 shows the reference turbine design layout as it existed prior to the design simplifications made to the T-system turbine (581192). The aerodynamic design is the same for both.

It was initially intended that the design of the APU-T turbine would be the same as the reference system turbine; however, following the final design review of the turbine layout, it became clear that the fabrication of that design would exceed the allowed budget. Further, the bearing cartridge face seal that seals hydrogen-water vapor mixture from the bearings would require a normal development with extensive turbine testing and several assembly-disassembly cycles. Too, the thermal isolation package that reduces to acceptable limits the heat soakback from the turbine to the bearing cartridge after shutdown requires some additional normal development. The decision was, therefore, made to design a simplified turbine.

The thermal and stress analysis were both made for the initial design, but on reevaluation showed themselves to be valid for the revised design.

The major changes from the reference to test system turbine gearbox design are as follows: a nitrogen gas buffer seal replaces a rubbing seal; an anti-heat soakback thermal barrier has been removed; the mounting structure for the turbine off the gearbox has been simplified, and the zero-g gearbox has been replaced by a more conventional type. The description and discussion differentiates between these two designs in the affected areas.

Turbine Aerodynamic Design

The system considerations that set the design point gas conditions and performance requirements are presented in table 5-1. The turbine fulfilling these requirements is a two-stage pressure-compounded axial-impulse turbine. In the meridianal flow path layout illustrated in fig. 5-1, the gas flows from left to right. It expands through the first-stage nozzles into the first rotor, and then enters the second-stage nozzles through an interstage plenum. The six first-stage nozzles are axisymmetric, while the second-stage nozzles are of two-dimensional design. The gas is at an intermediate pressure when entering the second-stage nozzles, where it expands again to the outlet pressure level flowing through the buckets of the second-stage wheel. Leaving the wheel, the gas enters the discharge plenum through a channel, providing some diffusion recovery of the rotational energy in the medium.

FOLDOUT FRAME

1

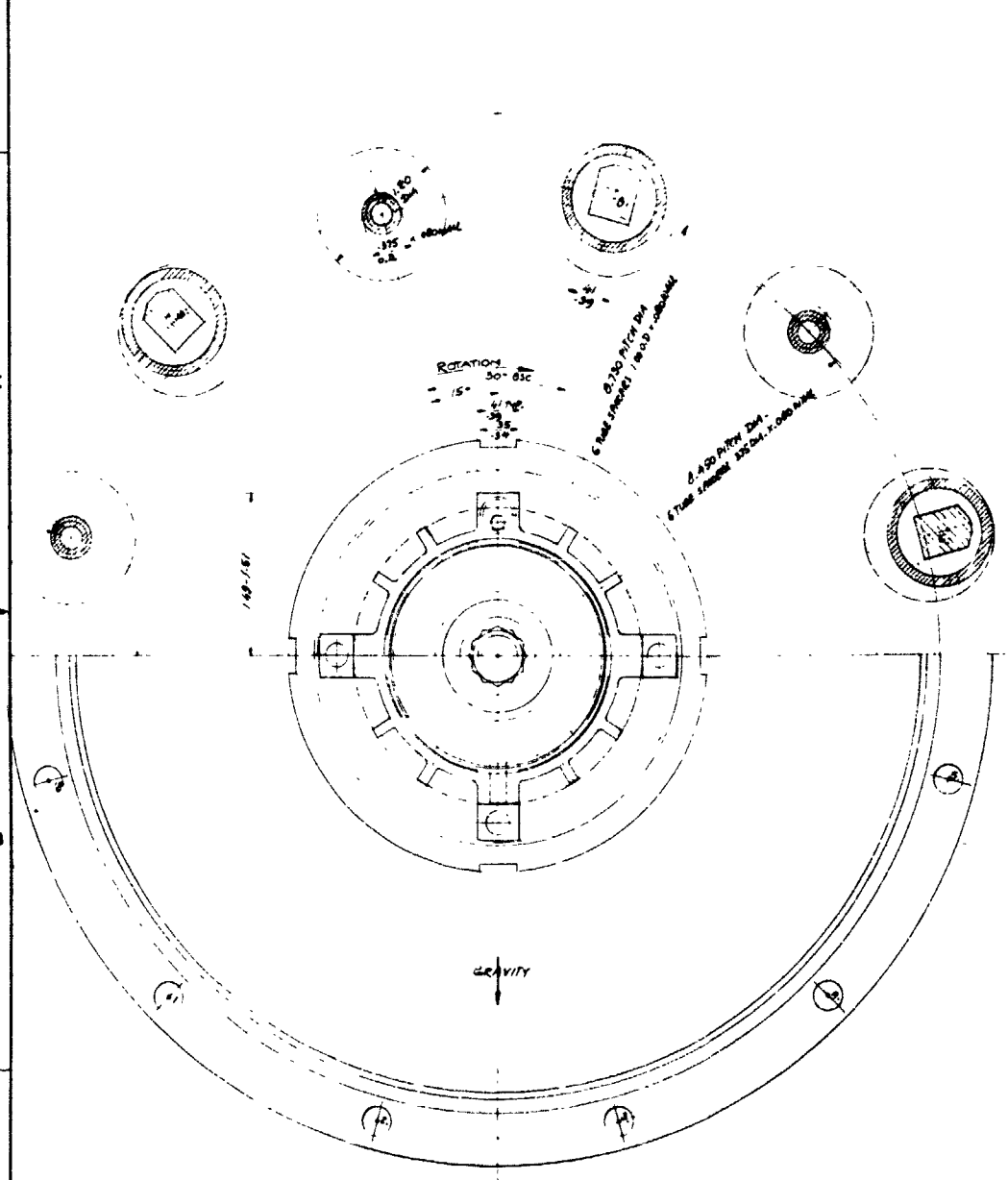

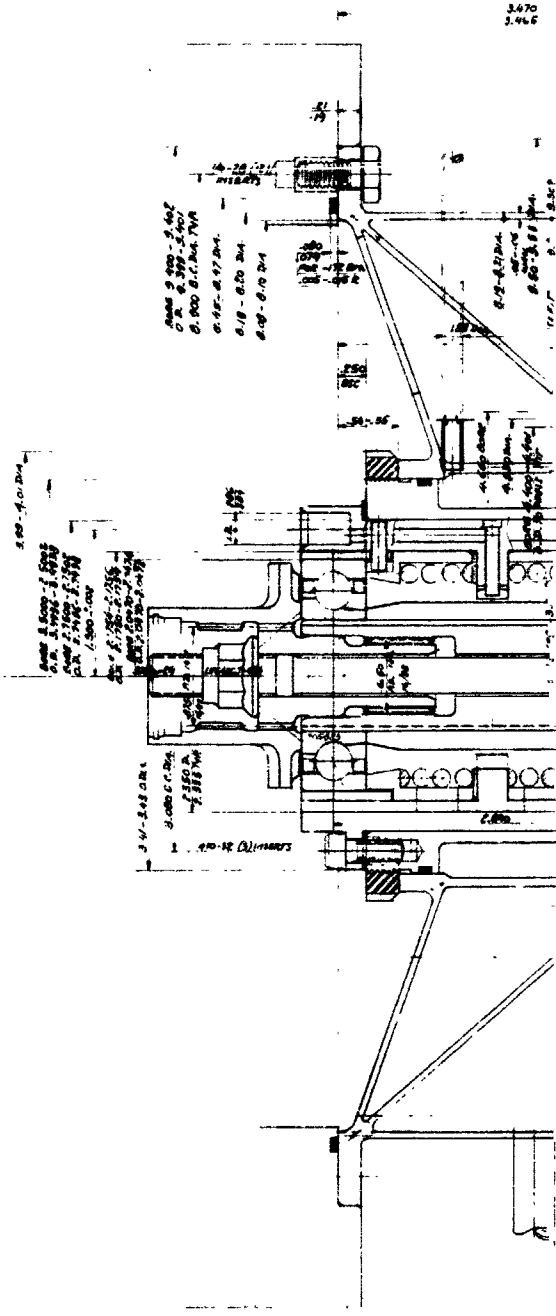

5 4 3

FOLDOUT FRAME

2

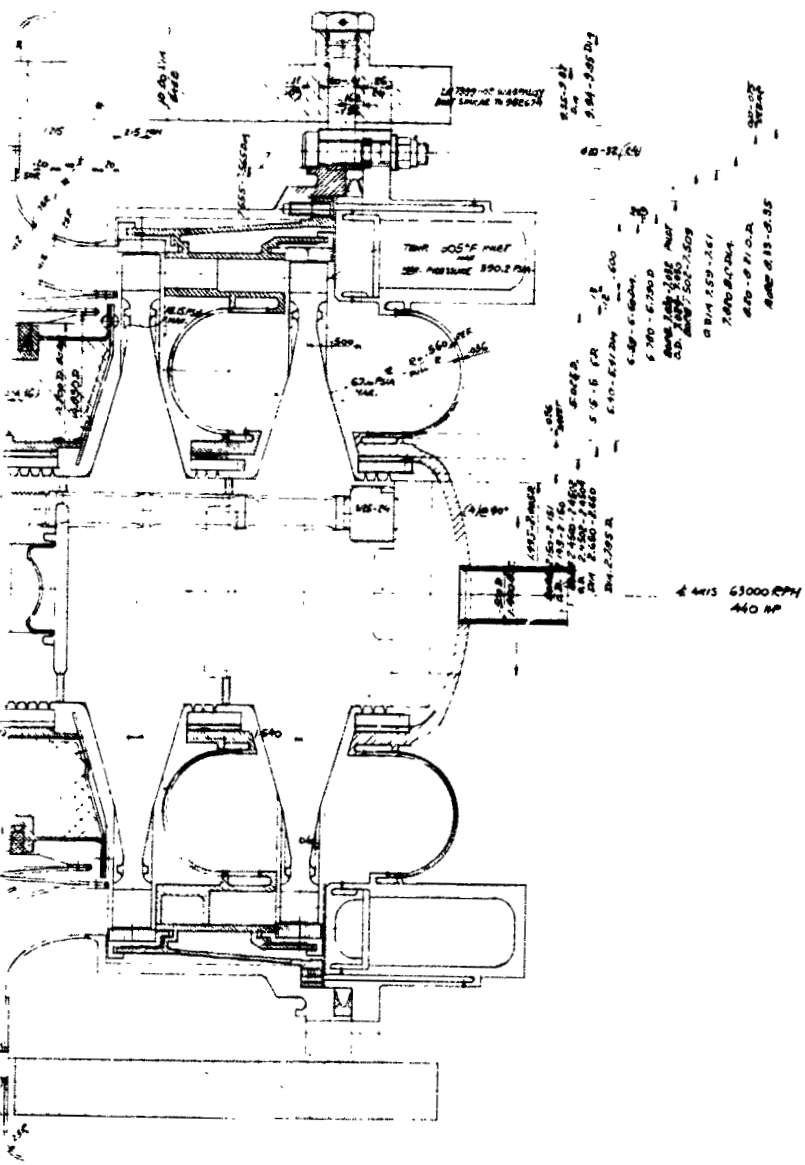

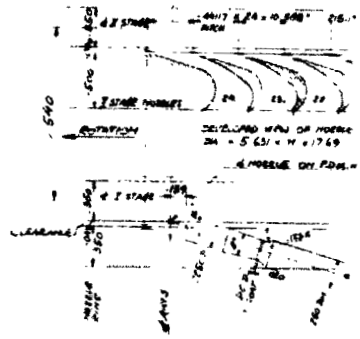

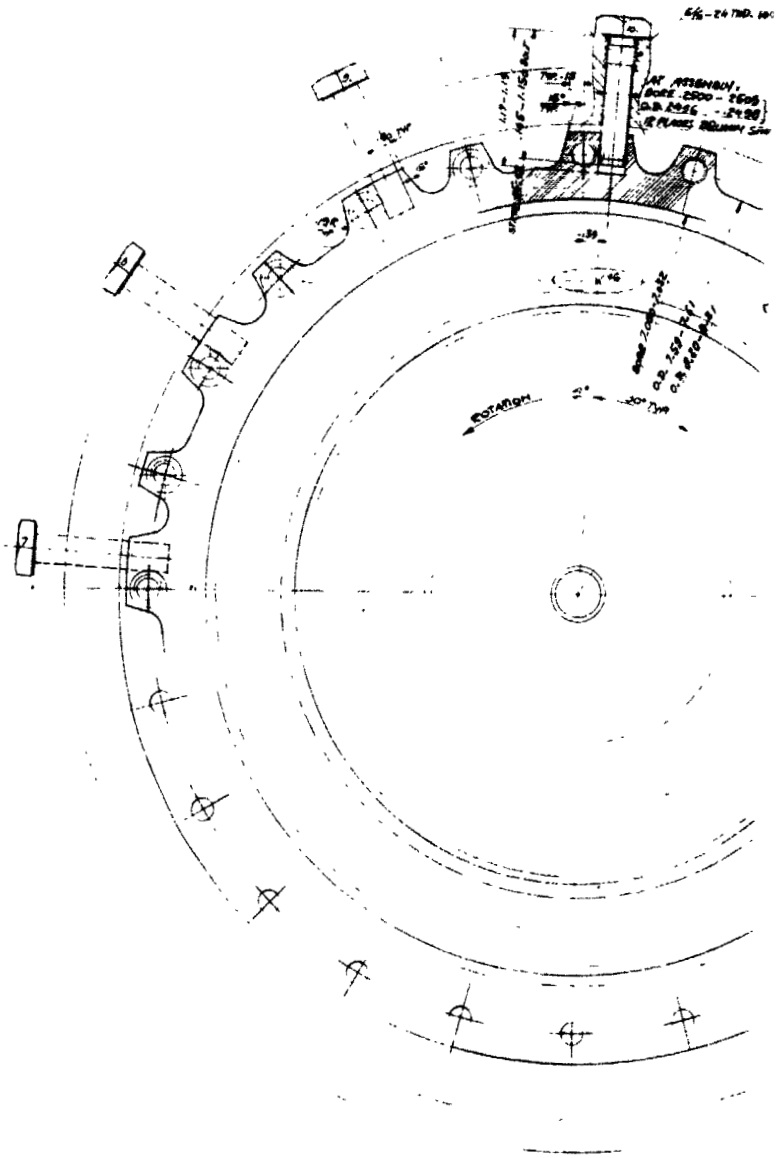

FOLDOUT FRAME

3

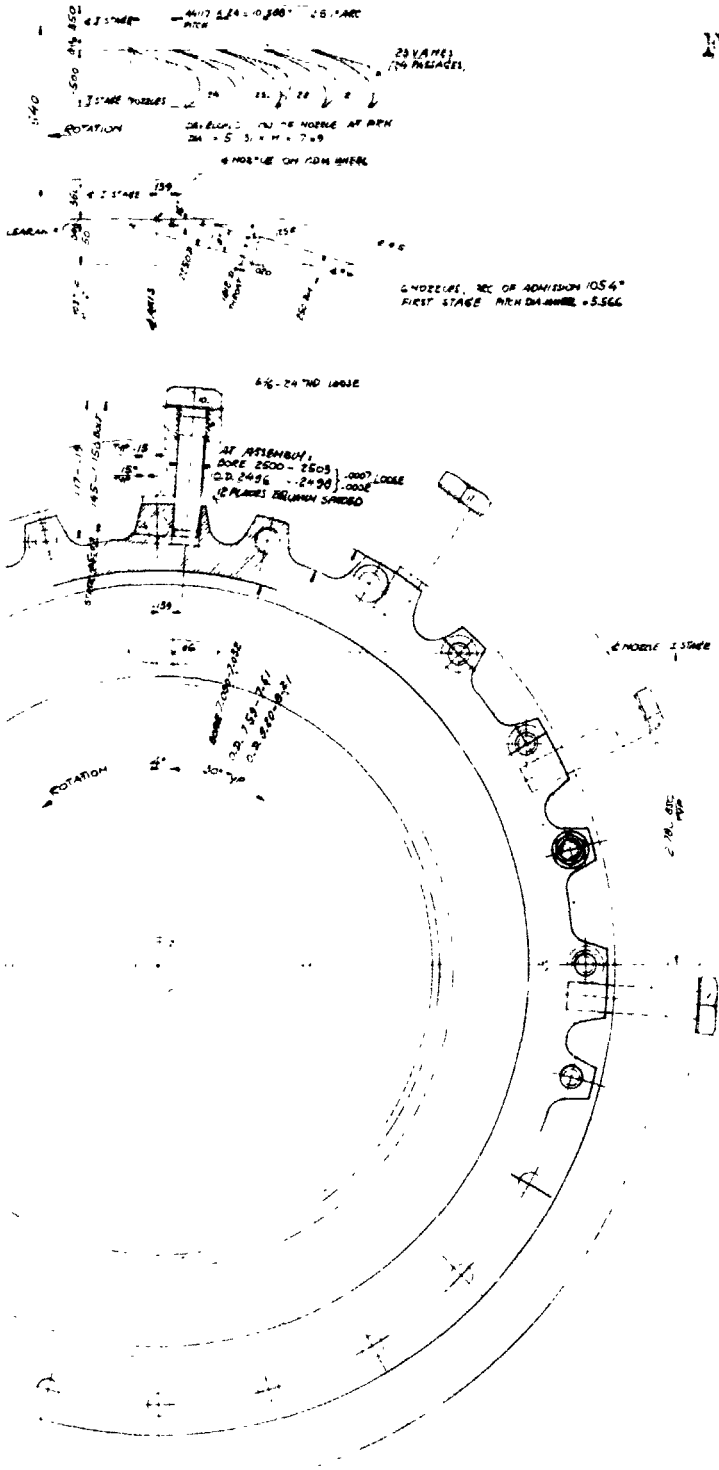

NOTES: UNLESS OTHERWISE SPECIFIED

1. SIMILAR TO PROPOSAL LAYOUT PER SK-39901 OF 11-19-71

REVISIONS				
SYM	LTR	DESCRIPTION	DATE	APPROVED

QTY REQD	ITEM NO.	PART OR IDENTIFYING NO.	NOMENCLATURE OR DESCRIPTION	MTRL SPEC
			PARTS LIST	

APPLICATION

ROCKWELL INTERNATIONAL CORPORATION
LAYOUT OF POWER UNIT
SPACE SHUTTLE APU

SIZE	CODE IDENT NO.	DRAWING NO.
J	70210	L-208529

SCALE 2/1 SHEET OF

L-208529

5-3/5-4

TABLE 5-1

DESIGN POINT CONDITIONS

Gas: H_2/O_2 combustion product
O/F ratio: 0.6
Gas exponent: $\gamma = 1.357$
Gas constant: $R = 455.85$ ft-lb/lb-^{o}R
Inlet total pressure: $P_{IN} = 390.2$ psia
Inlet total temperature: $T_{IN} = 1962.6\ ^{o}R$
Discharge static pressure: $P_{OUT} = 18.15$ psia
Exit duct area: $A_{EX} = 8$ sq in.
Power required: HP = 400 hp
Shaft speed: N = 63,000 rpm
Tip Clearance 0.010 in.

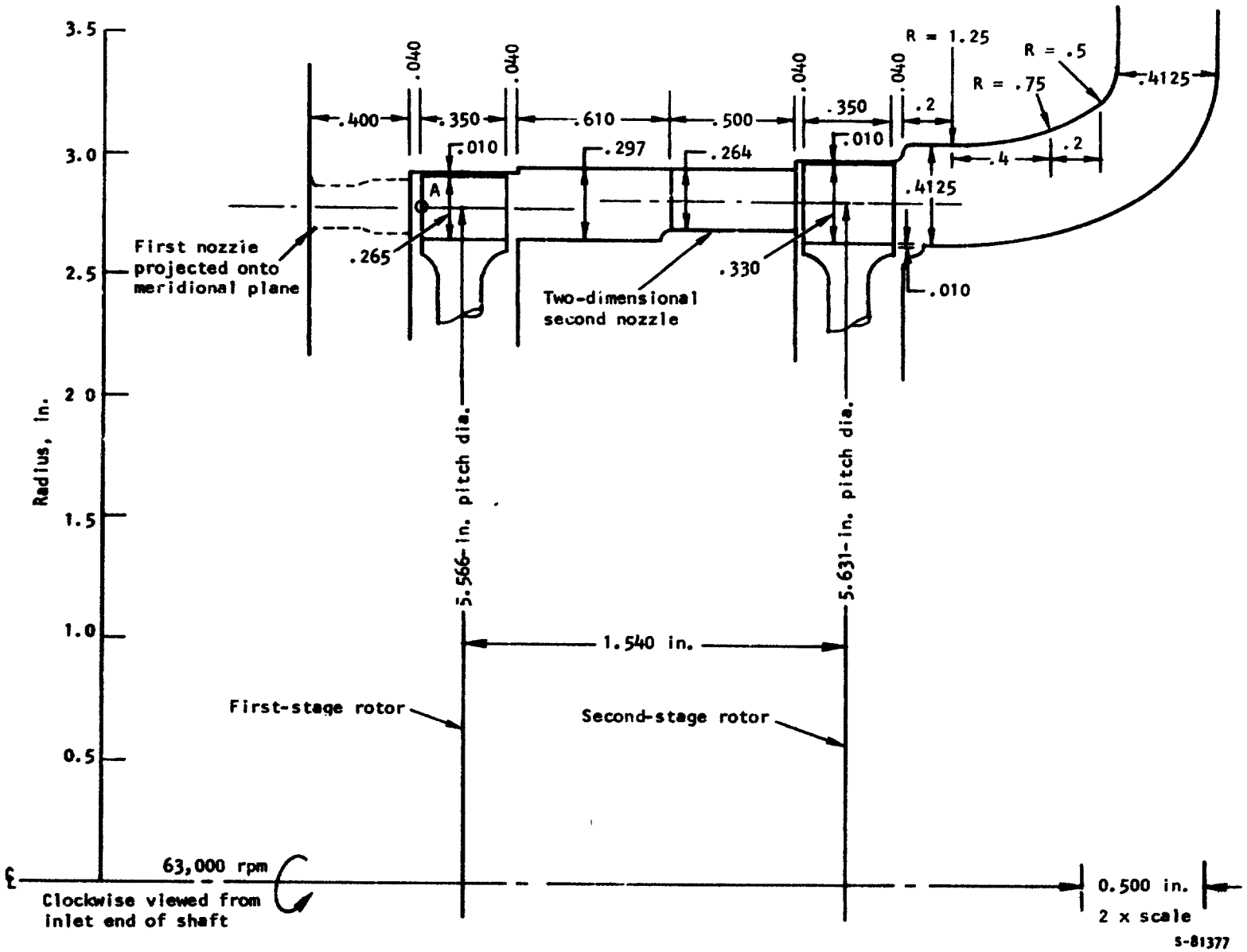

Figure 5-1.-- NASA H_2-O_2 APU Turbine Meridional Plane Aerodynamic Design.

The design characteristics of the turbine are summarized in table 5-2 in terms of the major geometric parameters of the two stages. The turbine design point velocity triangles along the mean flow path are shown in fig. 5-2, with schematic representations of nozzles and buckets.

The design of a first-stage nozzle is given in fig. 5-3. The nozzle is axisymmetric and of the conical supersonic design. An 8-deg cone connects the throat with the exit diameter. The area ratio is 1.539, which is about the theoretical value required by a 4.6 pressure ratio. This can be accomplished because the first-stage pressure ratio remains constant at an overall pressure ratios of about 7.5, as shown in fig. 5-4.

The design of the bucket is shown in fig. 5-5. This design is common for both stages, and it is presented at the pitch diameter of the first stage. The profile is assumed constant along the length of the bucket, and the channel between blades will be divergent about the radius of the wheel. The middle point of the blade radius is exactly radial. The design of the buckets on both wheels are identical; only the outside diameter of the wheels is trimmed to the required measurements. The profile of the bucket represents the high Mach number supersonic design, with the wedge transition into a constant radius turn providing constant supersonic turning of the flow without the development of shock fronts.

The design of the second-stage nozzles is shown in fig. 5-6. The nozzles are two-dimensional. The profile shown represents the cross-section at the pitch diameter of the second stage. There are 24 nozzle channels. Since the flow coming from the first stage has considerable velocity energy, the profiles should allow recovery of the major portion of it. It is assumed that 50-percent pressure recovery will occur at the entry of the nozzles. The nozzles are designed for 1.10 area ratio, giving good performance at a wide range of operating conditions. The relative positions of the first- and second-stage nozzles are shown in fig. 5-7; those positions are important to secure maximum inlet efficiency. The velocity distribution on the nozzle pressure and suction surfaces is shown in fig. 5-8.

Performance of Turbine

To predict the design point and off-design performance of this two-stage axial-impulse turbine, a computer program named TMAP has been used.

The printout of the results of the computer calculation for the design point performance is presented in fig. 5-9. To evaluate the overall performance capabilities of the turbine, off-design performance calculations have been run with the TMAP program. The pressure ratio distribution between the first and second stage is given in fig. 5-4 as a function of overall pressure ratio.

TABLE 5-2

TURBINE DESIGN PARAMETERS

	First Stage	Second Stage
Effective nozzle throat area, sq in.	0.1517	0.6300
Nozzle exit area, sq in.	0.2335	0.6930
Nozzle type	Axisymmetric	Two-dimensional
No. of nozzles	6	24
Admission, percent	29	60
Bucket height, in.	0.265	0.330
Axial chord length, in.	0.350	0.350
No. of blades	85	85
Pitch diameter, in.	5.566	5.631
Nozzle angle, deg	16.0	16.0
Bucket inlet angle, deg	23.0	23.0
Bucket exit angle, deg	21.7	21.7

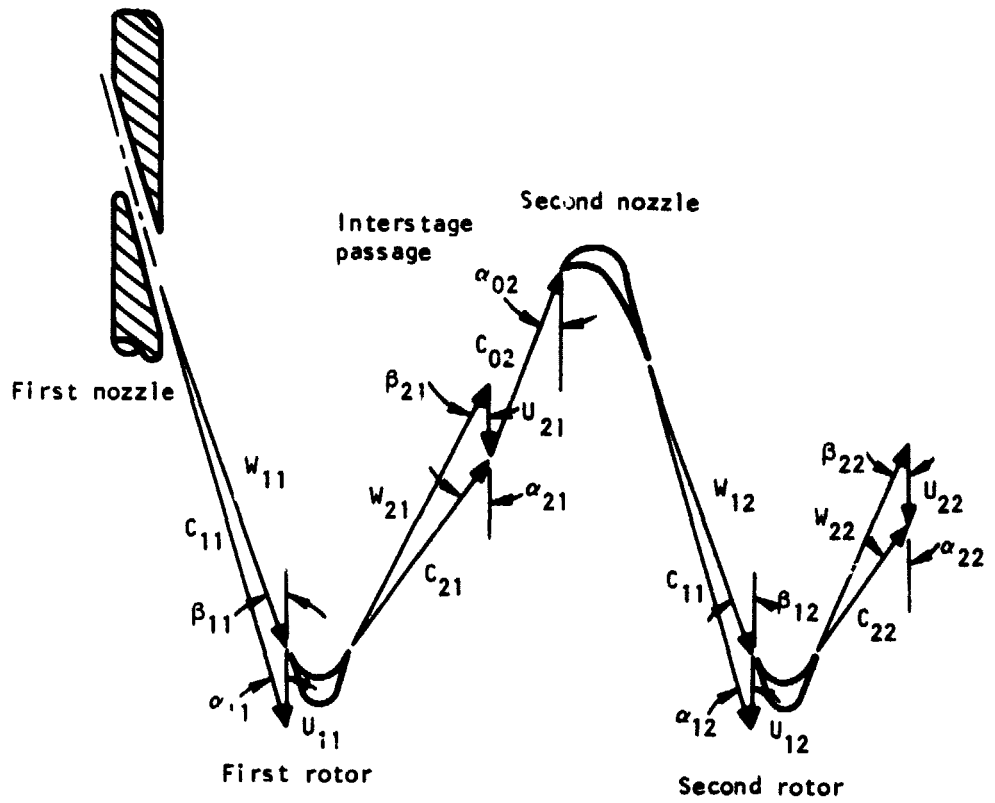

C_{11} = 8637.8	C_{21} = 4534.5	C_{02} = 3630	C_{12} = 7402.6	C_{22} = 3306.3
α_{11} = 16°	α_{21} = 38.9°	α_{02} = 16.1°	α_{12} = 16°	α_{22} = 39.6°
W_{11} = 7178.3	W_{21} = 5806.7		W_{12} = 5928.9	W_{22} = 4607.2
β_{11} = 19.4°	β_{21} = 26.1°		β_{12} = 20.1°	β_{22} = 24.6°
U_{11} = 1531.3	U_{21} = 1531.3		U_{12} = 1549.1	U_{22} = 1549.1

C, W, and U in ft/sec

s-81394

Figure 5-2.--NASA H_2-O_2 APU Turbine Velocity Triangles Sea Level Full Power Design Point.

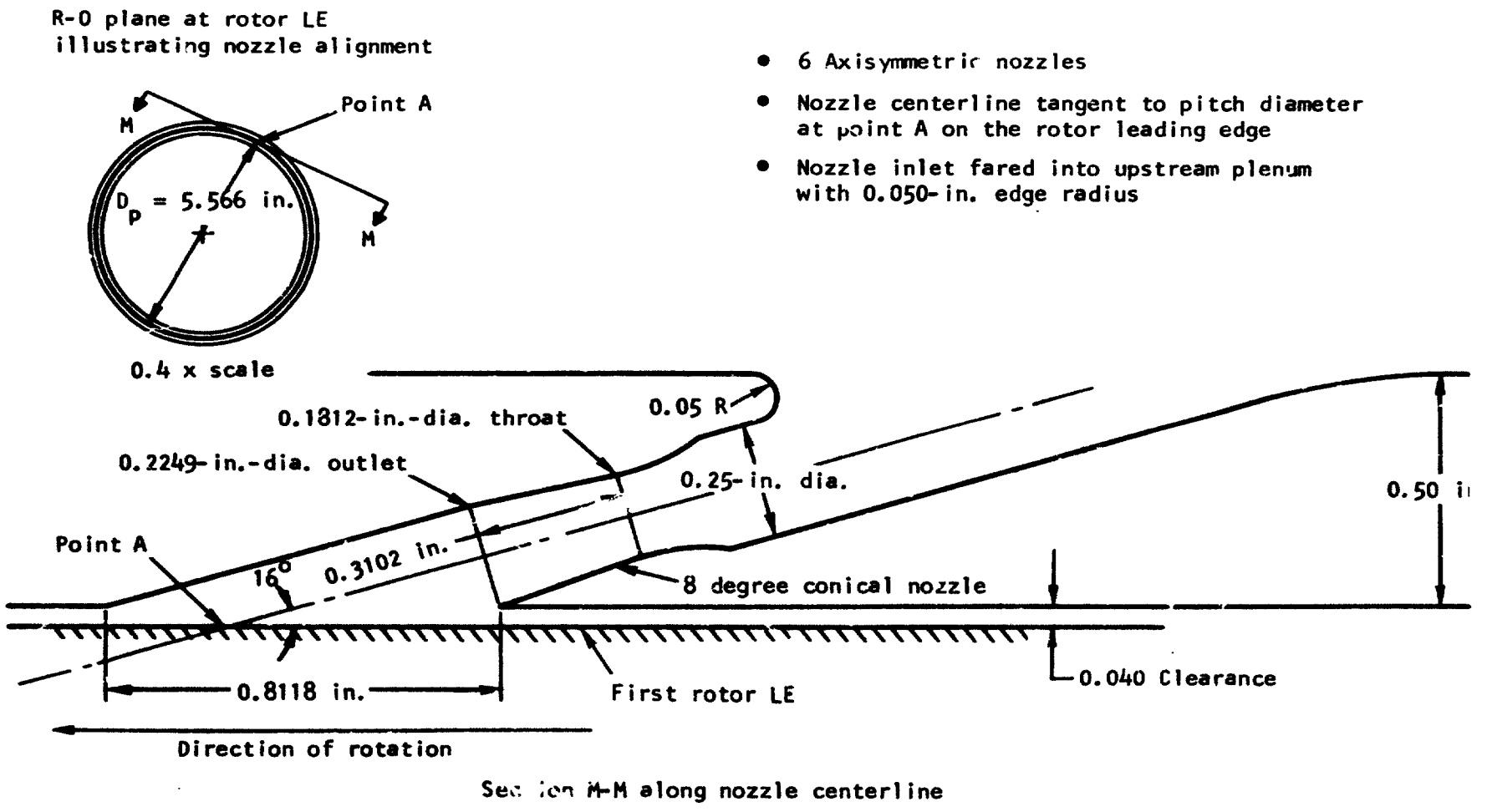

Figure 5-3.--NASA H_2-O_2 APU Turbine First-Stage Nozzle Design.

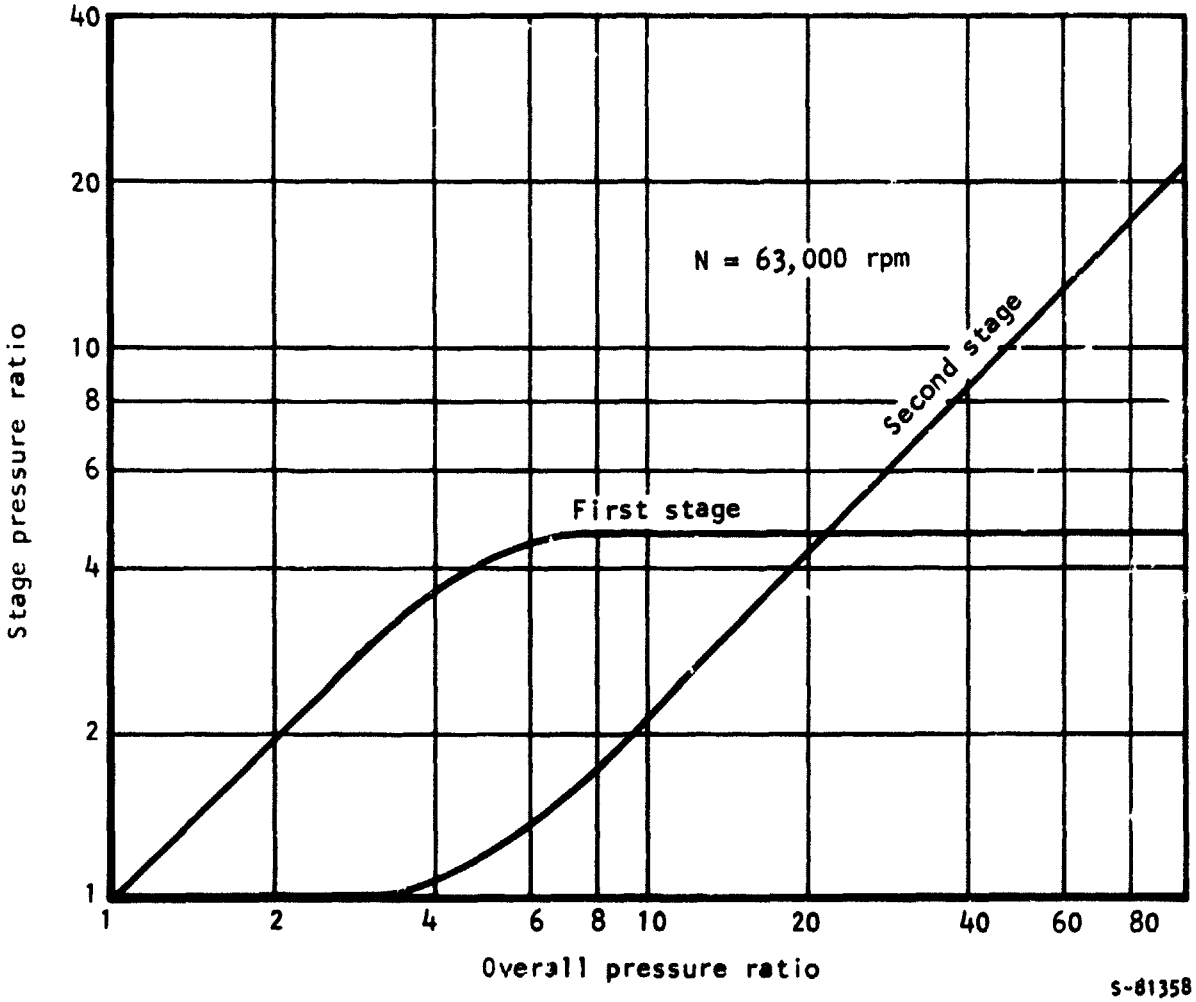

Figure 5-4.--Stage Pressure Ratios at Various Overall Pressure Ratios.

- LE thickness = 0.086 in., TE thickness = 0.056 in.
- "H-plane" section at pitch diameter

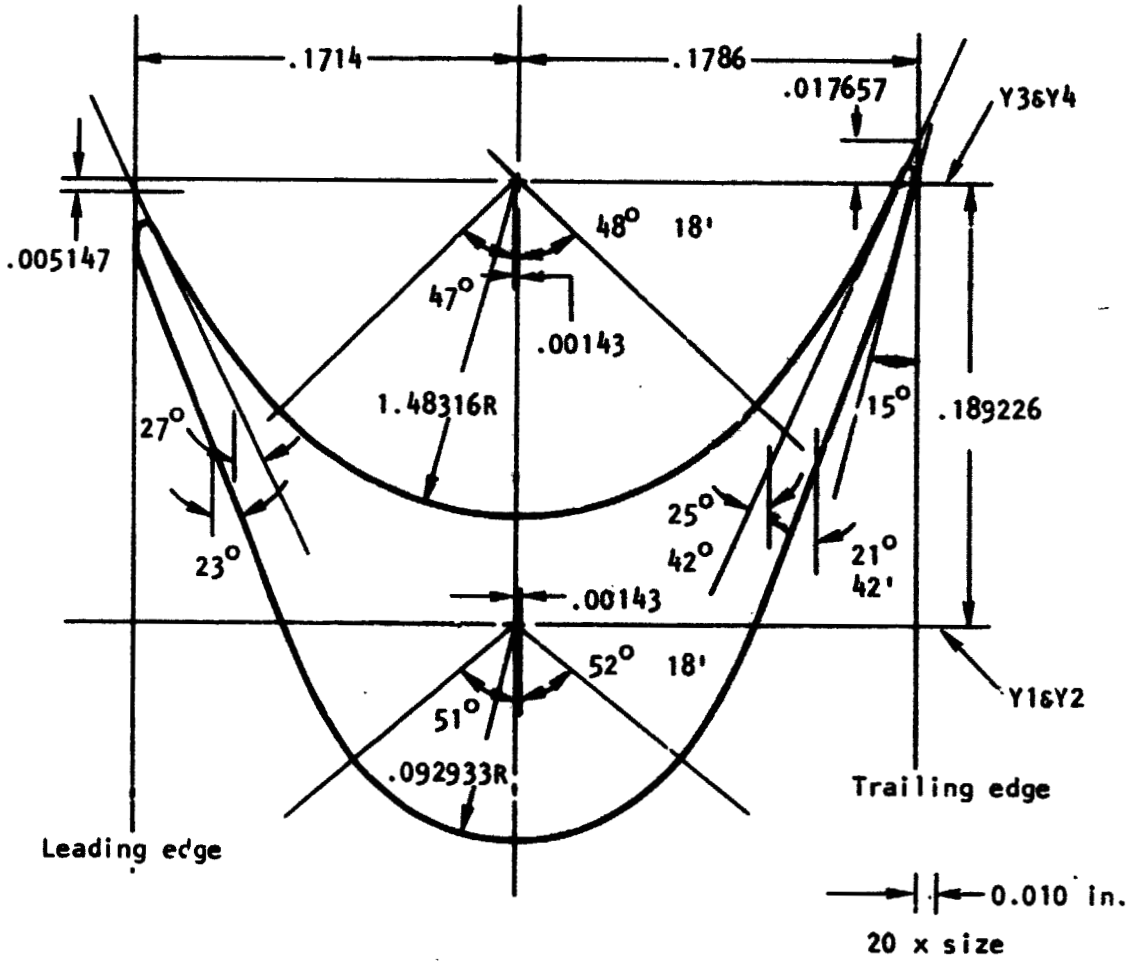

Figure 5-5.--NASA H_2-O_2 APU Turbine Rotor Blade Section.

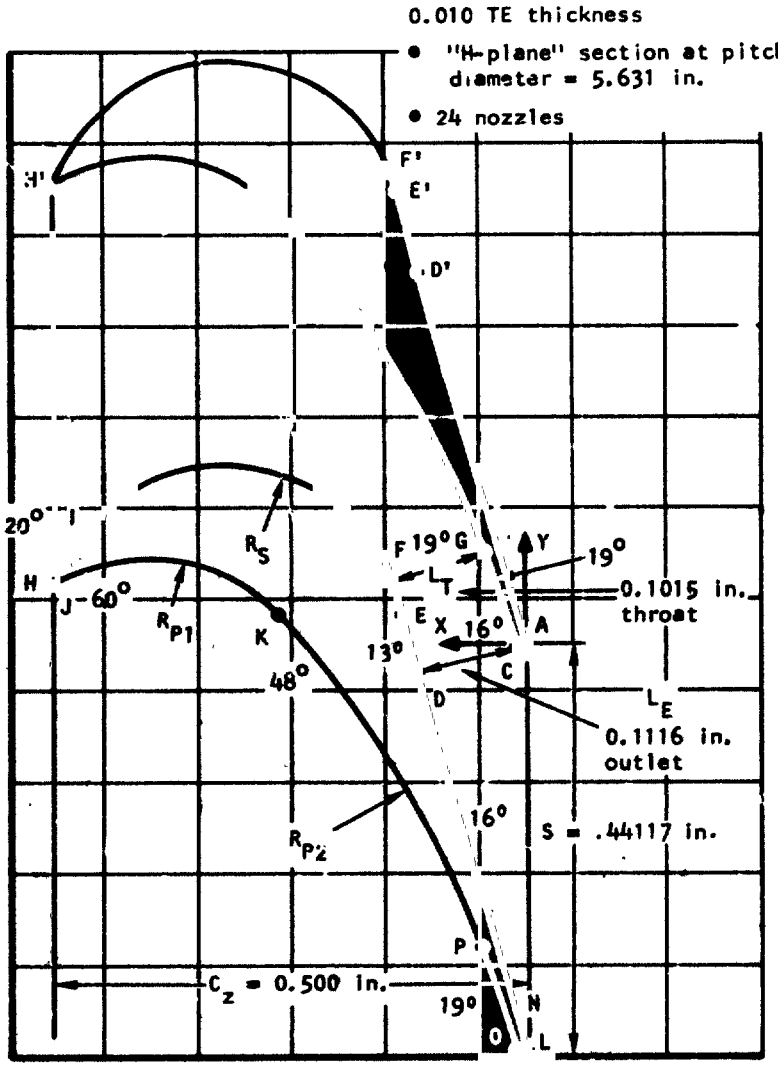

NASA H_2-O_2 Turbine Second-Stage Nozzle Design

Point	Coordinates in. X,	Y
A	0,	0
C	.00973,	-.00163
D	.11701,	-.03239
E	.13618,	.05063
F	.14166,	.06975
G	.04569,	.10279
H	.5 ,	.07202
I	.49985,	.07288
J	.49625,	.06985
K	.26454,	.03315
L	0 ,	-.44117
N	.00019,	-.43979
O	.00973,	-.44280
P	.04569,	-.33838
Upper Blade		
H'	.5 ,	.51319
K'	.26334,	.47432
D'	.11701,	.40878
E'	.13618,	.49180
F'	.14166,	.51092

R_S = .19000
L_S = .08520
L_P = .11044
R_{F1} = .18639
R_{P2} = 1.08141
L_T = .1015
L_E = .1111
R_{LE} = .0025
R_{TE} = .005
C_Z = .5
α_K = 48°
α_{LE} = 20° and 60°
α_{TE} = 19° and 16°
α_T = 19°
α_E = 16°
α_{SS} = 13°

S = - Y_L = .44117 = pitch

S-81392

Figure 5-6.--NASA H_2-O_2 Turbine Second-Stage Nozzle Design

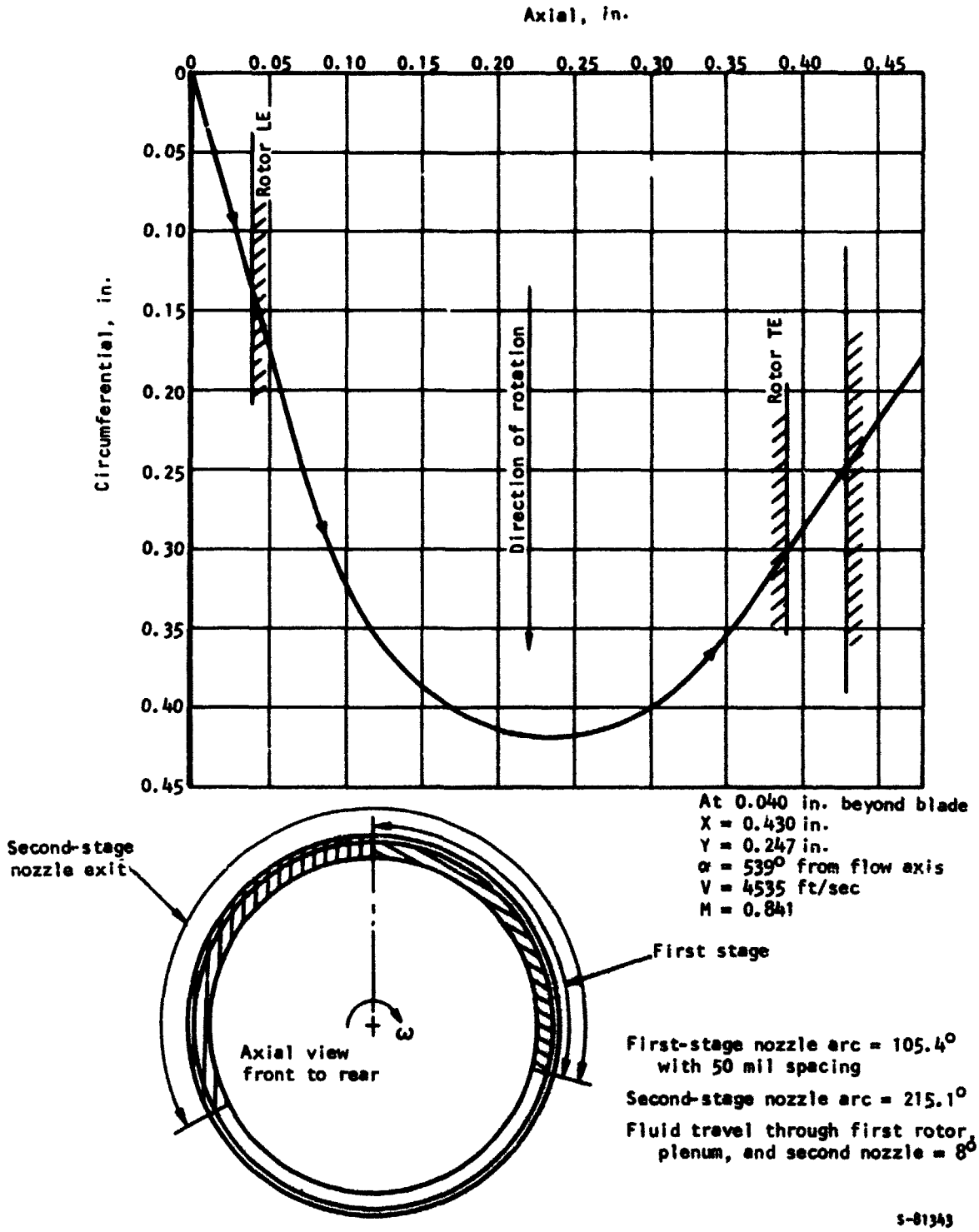

Figure 5-7.--NASA H_2-O_2 APU Turbine Circumferential Alignment First-Stage Streamline in Fixed Coordinates Admission Arcs for First and Second Stages.

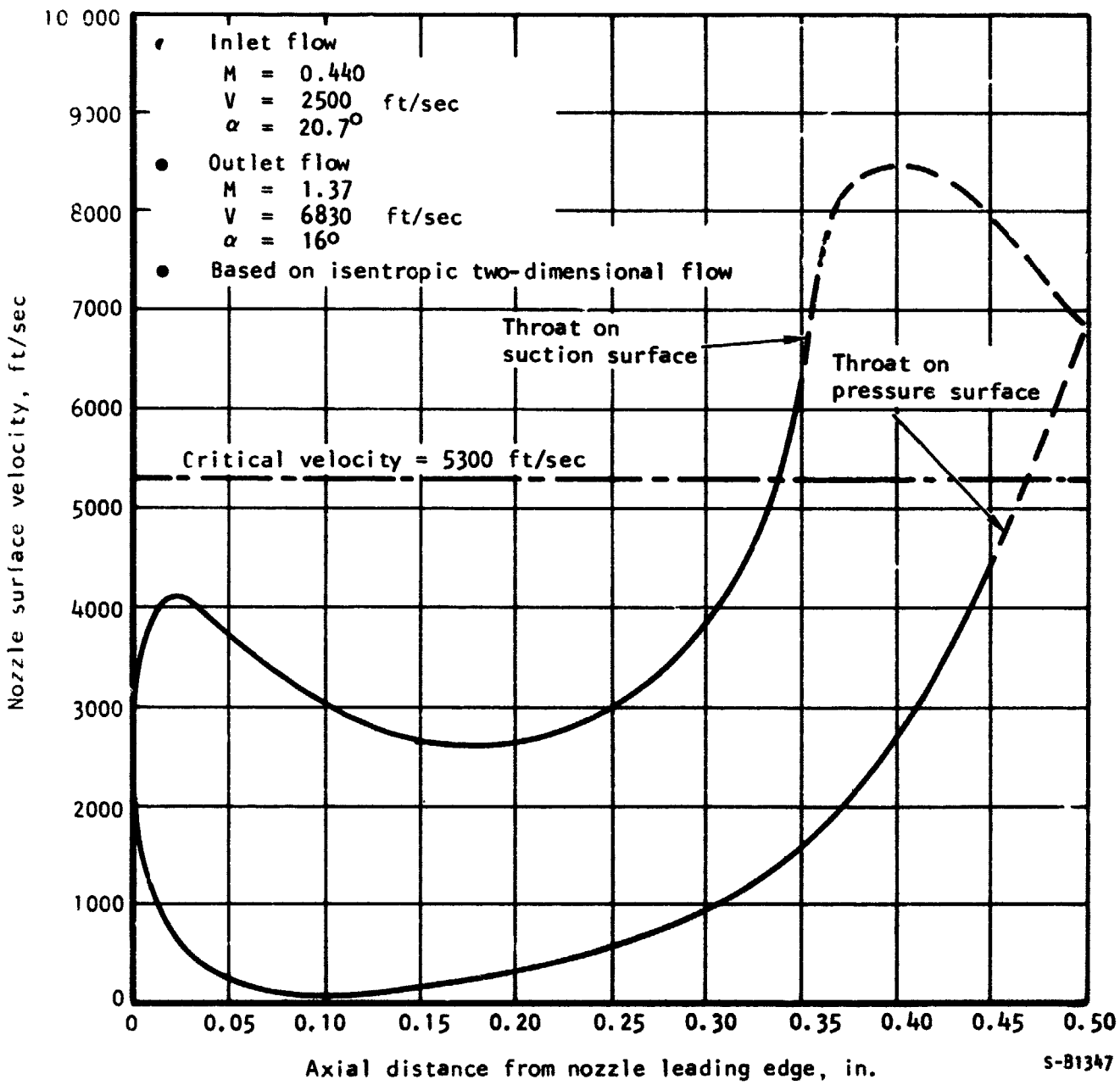

Figure 5-8.--NASA H_2-O_2 APU Turbine Second-Stage Nozzle Surface Velocities.

REDESIGNED TURBINE 1-16-73

INPUT DATA

AXIAL IMPULSE TURBINE

RPM	TTO	PTO	EXIT PRES	EXIT AREA	GAMMA	GAS CONST	RF-NOZ-EXIT	BF-NOZ-THRT
63000.0	1962.60	390.200	18.1500	8.0000	1.3570	455.850	.98000	1.00000

PUMPING LOSS COEFFICIENT = 1.4000 BLADE DISK FRICTION COEFFICIENT = .1000

THE REVISED VERSION OF THE PROGRAM IS USED.
ALL STAGES MAY HAVE SUBSONIC NOZZLES.

STAGE	NOZZLE TH AREA	NOZ EXIT AREA	NOZ INL ANGLE	NOZ EXT ANGLE	BLADE IN ANGLE	PITCH	ADMISSION	MIN H/D	NO. OF BLADES	TIP GAP	AX CHORD	BLADE HEIGHT	BLADE EXIT ANGLE
1	.1517	.2335	-.0000	16.00	23.00	5.566	.2785	.0457	85	.0100	.350	.2650	21.70
2	.6300	.6930	-.0000	16.00	23.00	5.631	.9670	.0550	85	.0100	.350	.3300	21.70

STAGE	KEX	ETAND	ETAK
1	.50000	.9216	.9596
2	.50000	.9216	.9596

OUTPUT DATA

RPM	MASS FLOW	PRES RATIO	EXIT PRES	OA AD HEAD	OA CO	OA U/CO	OA EFFIC	SHP	TORQUE	TORQ COEF
63000.00	.2404	21.4986	18.1500	1883506.6	11009.68	.13909	.53363	439.402	439.579	.95990

STAGE	AD HEAD	WHL SPD	CO	U/CO	NOZ EFF	ST EFF	HYD EFF	INC DECR	PUMP DECR	DF DECR	BDF DECR
1	1256559.5	1531.26	8992.0570	.1703	.9228	.4408	.4482	.0075	.0019	.0007	.0048
2	944775.1	1549.14	7797.0755	.1987	.9014	.4881	.4925	.0047	.0014	.0007	.0023

STAGE	MASS FLOW	MACH NO	REL MACH	VELOCITY	REL VEL	REL FLO ANG	NOZ IN PT	ROT IN PT	ROT EX PT	ROT EX PS
1	.2404	1.7025	1.4148	8637.8264	7178.31	19.3708	390.2000	329.7670	105.9649	67.5863
2	.2352	1.5468	1.2385	7402.5986	5928.87	20.1301	84.0667	70.0919	23.9954	18.1500

STAGE	IN TOTAL TEMP	IN REL TOT TEMP	NOZ EX ST TEMP	ROT EX TOT TEMP	DISK RN	PROF LOSS COEF	DISK LOSS COEF	TORQUE	TORQ COEF	ETAK
1	1962.6000	1753.9922	1293.8241	1642.9137	430257.45	.8271	.0005	242.2649	.6477	.9596
2	1642.9137	1465.9658	1151.4407	1376.7615	143439.01	.7941	.0007	197.3145	.6147	.9596

Figure 5-9.-- NASA H_2-O_2 APU Turbine Design Point
Printout from T-MAP Program.

The overall efficiency is shown in fig. 5-10 as a function of the velocity ratio (u/c_o) at several pressure ratios, and the overall efficiency as a function of overall pressure ratio at different back pressures is illustrated in fig. 5-11. The overall efficiency versus shaft power (at constant speed of 63,000 rpm) developed at several back-pressure values is given in fig. 5-12. All these computations assumed the gas composition indicated in table 5-1.

H_2-O_2 APU Turbine Mechanical Design

Mechanical design of the H_2-O_2 turbine included consideration of the turbine aerodynamics, thermal management, stress analysis, and metallurgical problems, all of which influenced the final configuration. Important parameters that influenced the final design include the need for an efficient two-stage, partial-admission impulse-turbine design, running with close tip clearance (0.010-in.); the use of hydrogen-rich working fluid; the need to avoid heat soak-back after shutdown; and the requirements of long-life, including many starts and stops. The overall cross section of the machine is shown in dwg. 581192.

Because of efficiency, the radial and axial location of first-stage turbine blading relative to the inlet nozzle is critical. Clearance between the blade tips and the stationary segments must be minimal at the hot design operating conditions. To predict these clearances, it is necessary to determine by means of a thermal model the hot temperature distribution at several specified conditions. The prediction of tip clearance is further subject to uncertainties because distortion may be present. Referring to fig. 5-13, the turbine housing that supports the seal segments around both wheels must reach back to the gearbox through the hot zone of the turbine exhaust torus. It is desirable to keep the structure supporting the hot structure uniform in temperature and as cool as possible to minimize distortions.

The first-stage turbine wheel is mounted to the second-stage wheel, and the two are attached to the shaft by four studs. Centering and power transmission is accomplished by curvic couplings, shown schematically in figs. 5-14 and 5-15. To maximize heat transfer between the two wheels, the conventional convex-to-concave curvic coupling configuration is used, while the second-stage, wheel-to-shaft attachment is done through convex-to-convex curvic couplings. The poorer heat transfer through the convex-to-convex coupling will minimize the heat flux into the shaft and the bearings. The four studs are loaded in tension to the design load of 3900 lb by a hydraulic loader that attaches to the portion of the stud extending beyond the nut. This extension is later cut off. Each nut is supported by the turbine wheel, thus preventing loading of the stud end caused by centrifugal force. Lands on the studs provide support for the stud in the wheel during rotation.

The spline coupling, bearing, and bearing spacer are held in place by a center tie bolt (see dwg. 581192) loaded in tension to about 10,000 lb, which stiffens the rotating assembly. The shaft effective diameter in bending is increased in this way to approximately that of the ball bearing inner race. The shaft stiffness increases roughly as the cube of the diameter.

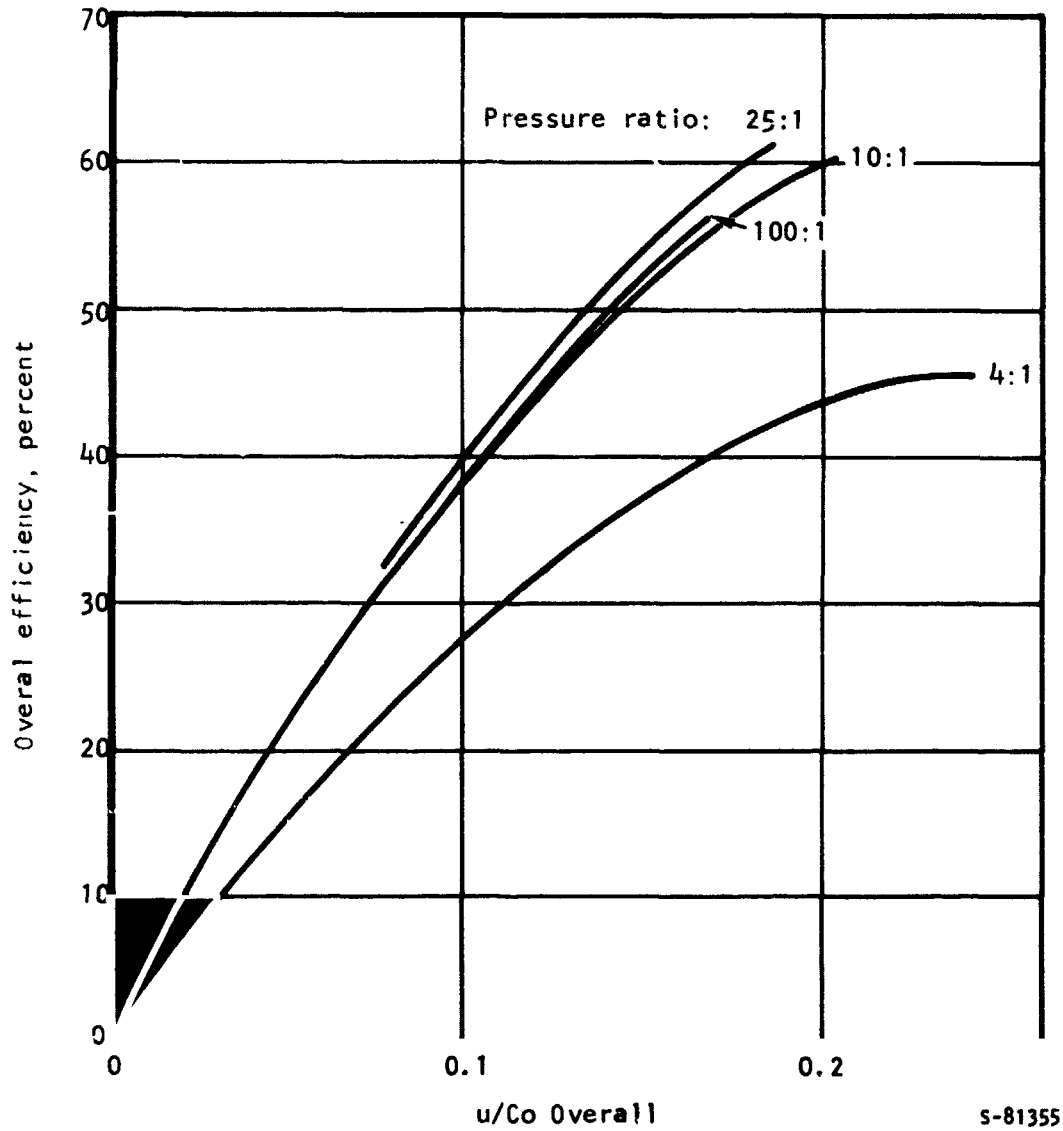

Figure 5-10.--Efficiency vs u/Co at Different Pressure Ratios.

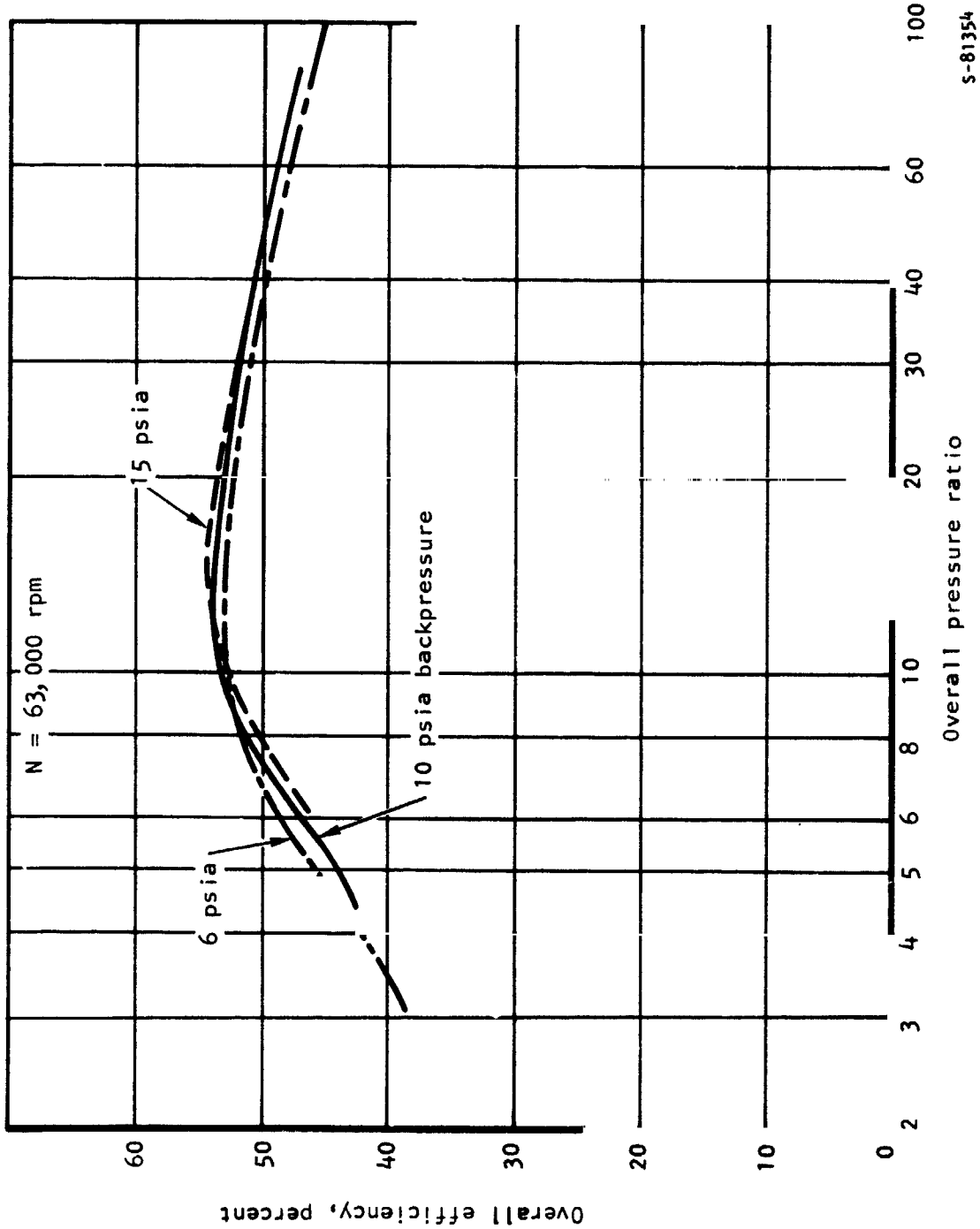

Figure 5-11.--Efficiency vs Pressure Ratio.

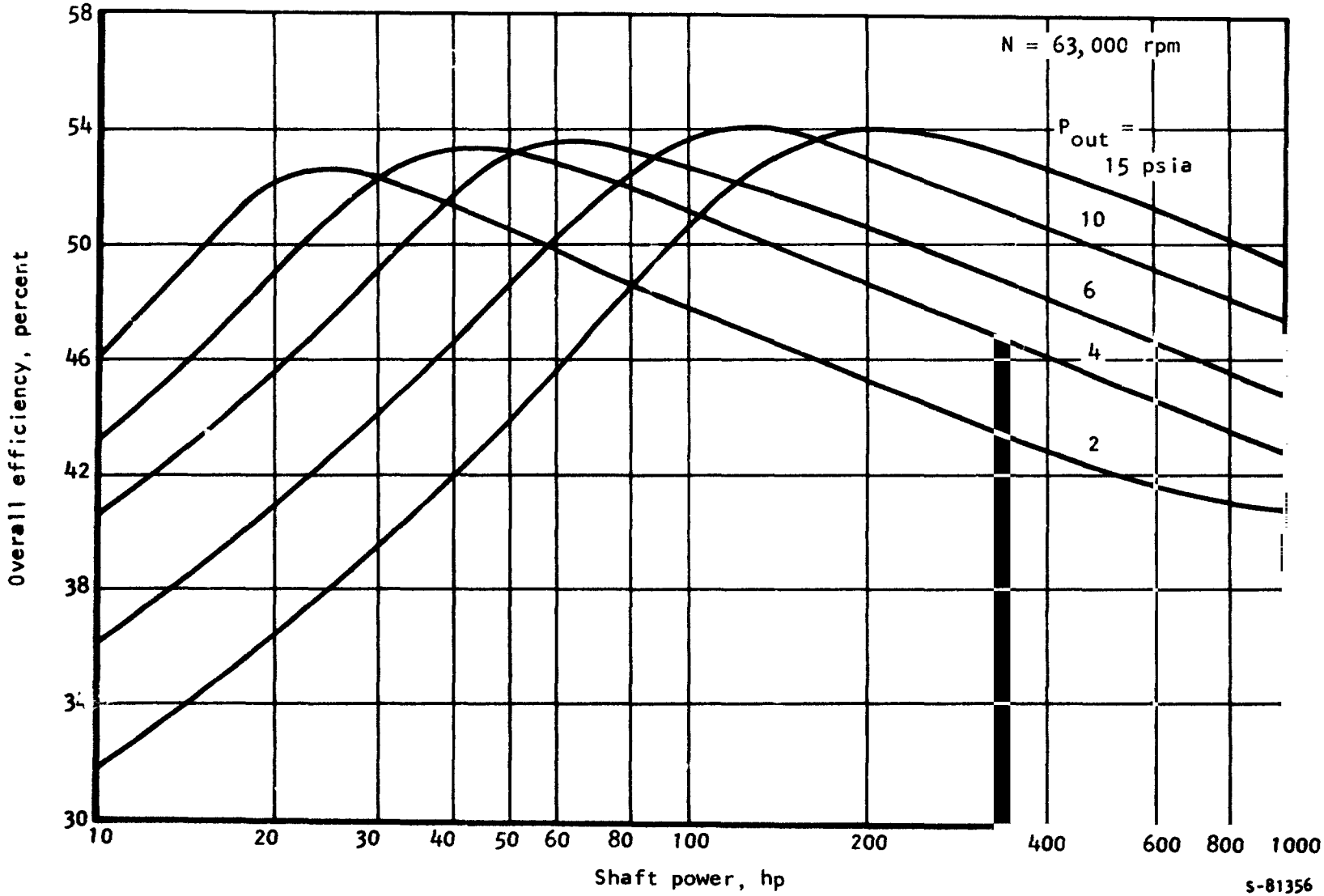

Figure 5-12.--Efficiency vs Developed Power.

FOLDOUT FRAME

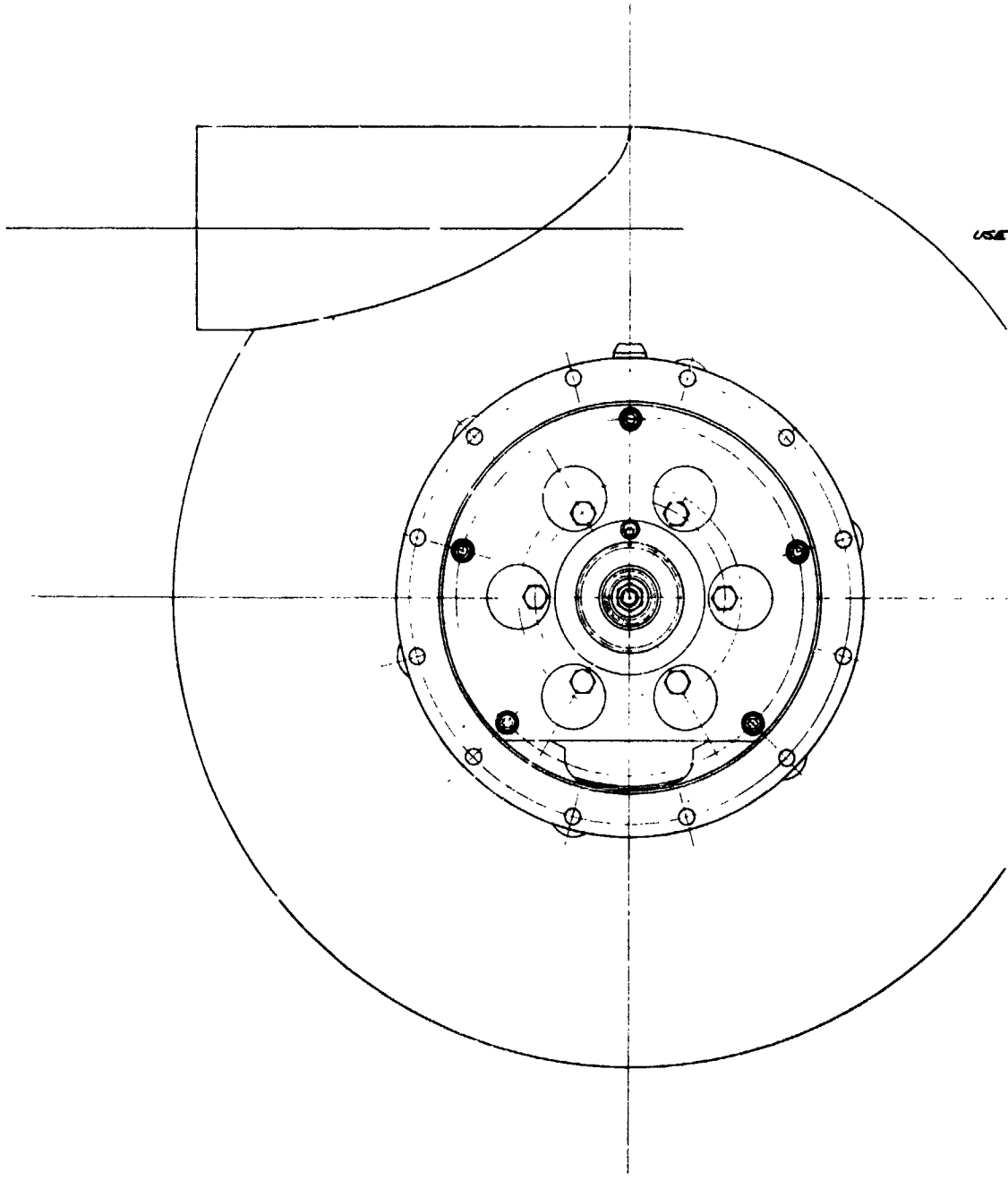

FOLDOUT FRAME

2

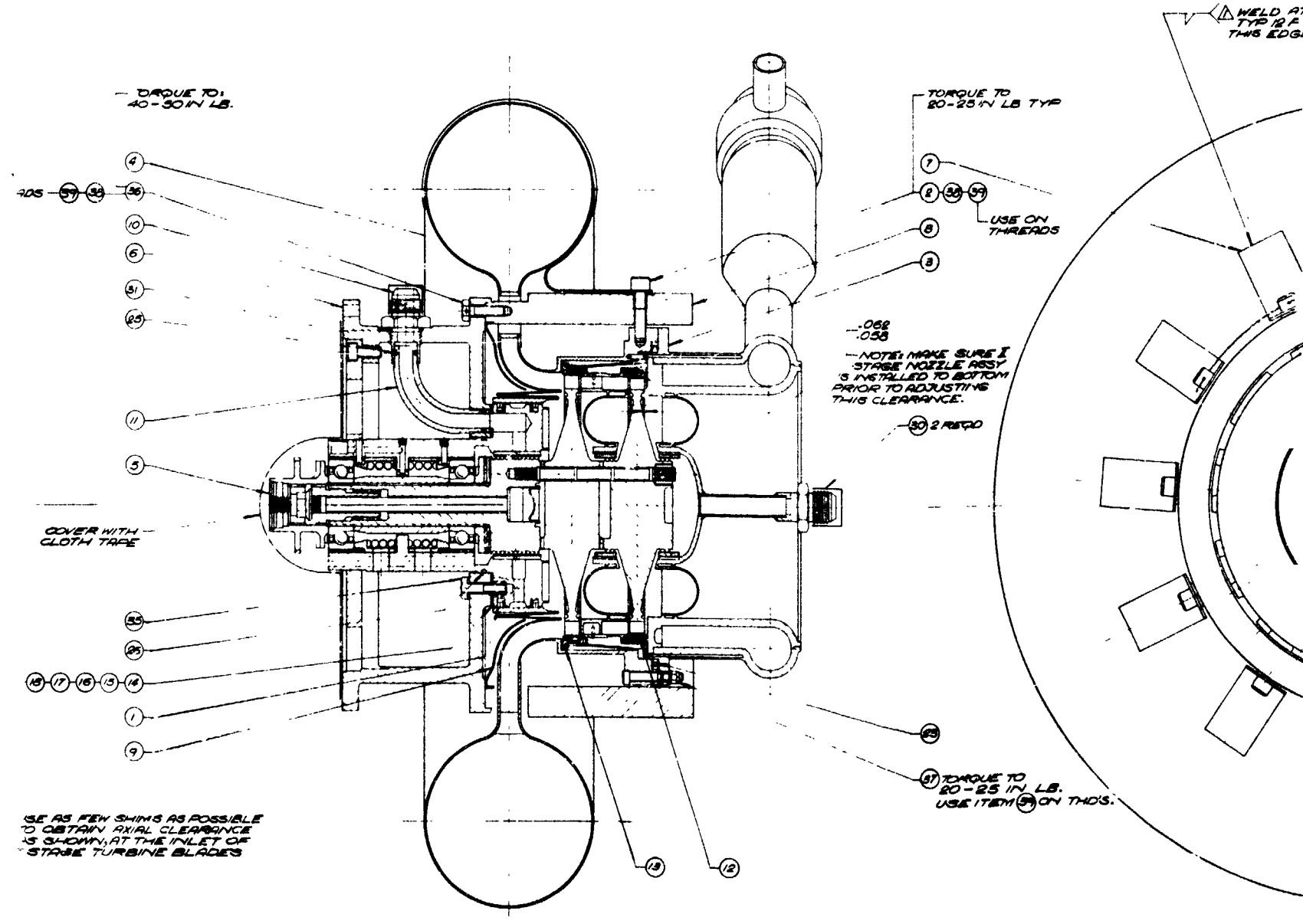

SECTION Z-Z

FOLDOUT FRAME 3

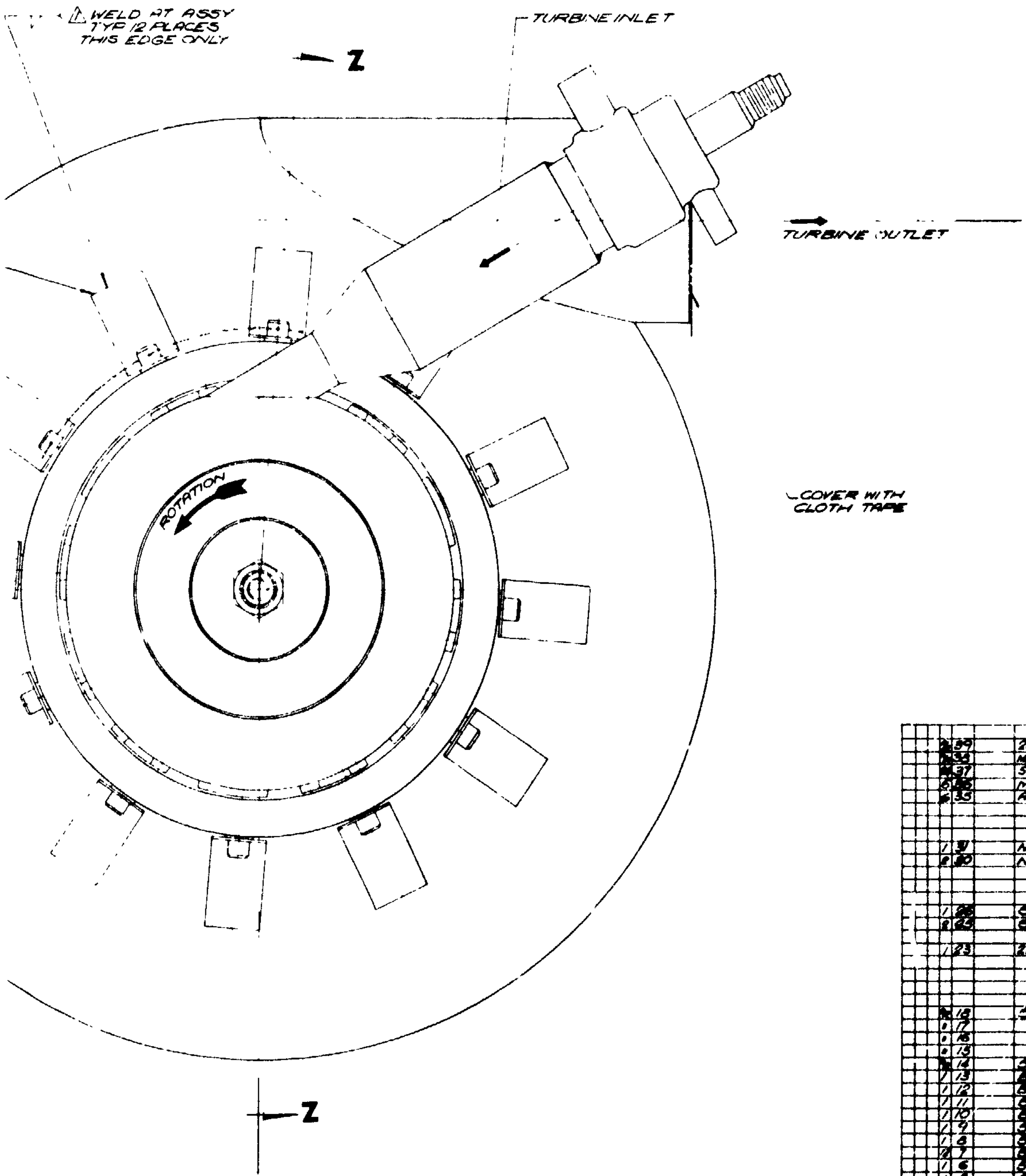

QTY REQD	ITEM NO.	PART OR IDENTIFYING NO.	NOMENCLATURE OR DESCRIPTION	NOTE
[illegible]	39	219-090-90XV	COMPOUND	
[illegible]	38	MS20995C[illegible]	LOCKWIRE	
[illegible]	37	523-121-9003	NUT (.190-32)	
6	36	MS9564-10	SCREW (.250-28)	
6	35	AS1805E7	SCREW ASSY (SELF SEALING REF)	3
1	31	NAS1593-8	PACKING	
2	30	MS50M-6B	CAP, PROTECTIVE	
1	26	890260041	PACKING	
2	25	890260018	PACKING	
1	23	220840R1300	SEAL (K SEAL REF)	2
[illegible]	18	581272-5	SHIM	
[illegible]	17	-4	"	
[illegible]	16	-3	"	
[illegible]	15	-2	"	
[illegible]	14	581272-1	SHIM	
1	13	B-109170	SEGMENT ASSY 3RD STAGE	1
1	12	B-109169	SEGMENT ASSY 1ST STAGE	1
1	11	581[illegible]-1	ELBOW	
1	10	581[illegible]-1	FITTING	
1	9	581[illegible]-1	SHIELD, HEAT	
1	8	581[illegible]-1	RING, CONTAINMENT	
[illegible]	7	581[illegible]-1	ARM ASSY, TORUS SUPPORT	
1	6	581[illegible]-1	HOUSING SUPPORT	
1	5	581[illegible]-1	ROTATING ASSY	
1	4	581[illegible]-1	TORUS & HOUSING ASSY T OUTLET	
1	3	[illegible]	[illegible] TORUS ASSY	
[illegible]	2	[illegible]	[illegible]	
[illegible]	1	[illegible]	[illegible] ASSY	

PARTS LIST

5. MANUFACTURED & SOLD BY: GOULD INC., CLEVITE ENGINE PARTS DIVISION CLEVELAND OHIO.
4. MANUFACTURED & SOLD BY: ABSCOA INDUSTRIES, INGLEWOOD CALIF.
3. MANUFACTURED & SOLD BY: HARRISON MFG. DIVISION 3020 EMPIRE AVE BURBANK CALIF.
2. VENDOR ITEM, SEE SOURCE CONTROL DRAWING.
1. WELD PER AIR SPEC. WB518.

NOTES UNLESS OTHERWISE SPECIFIED

AIRESEARCH MANUFACTURING COMPANY

POWER UNIT ASSEMBLY

J 70210 581192

APPLICATION: 581191-1 | 581164

SCALE 1/1

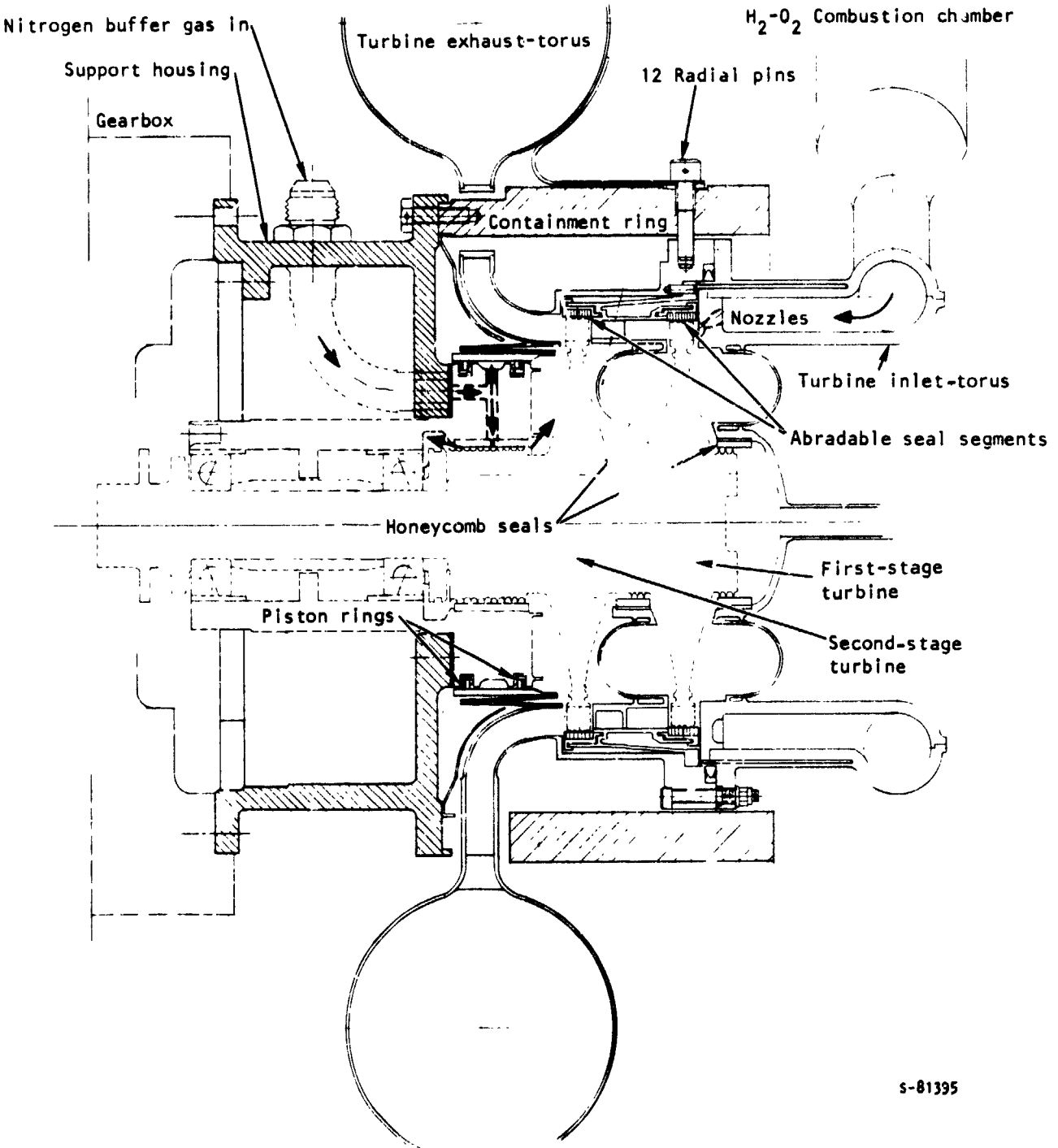

Figure 5-13.--Turbine Supporting Structure.

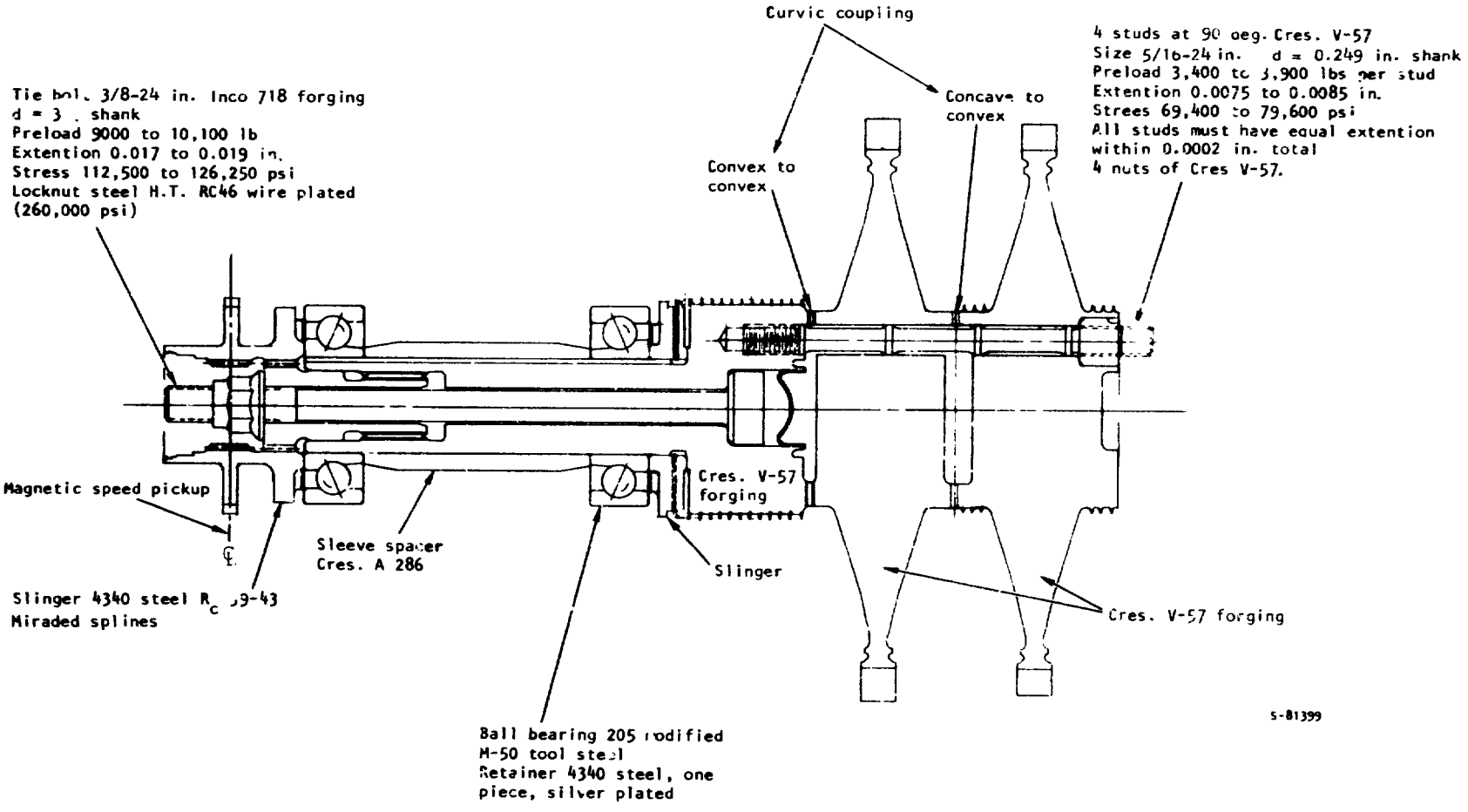

Figure 5-14 --Turbine Rotating Assembly

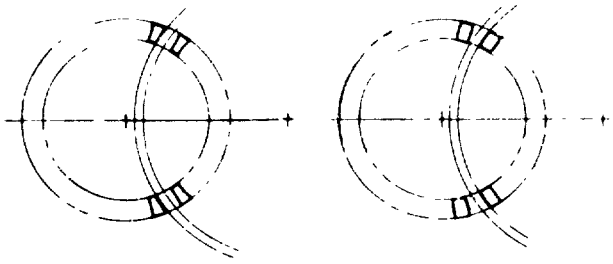

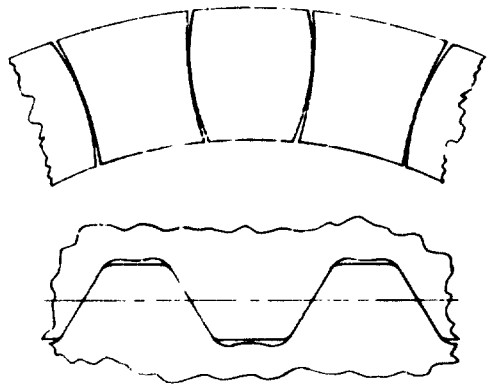

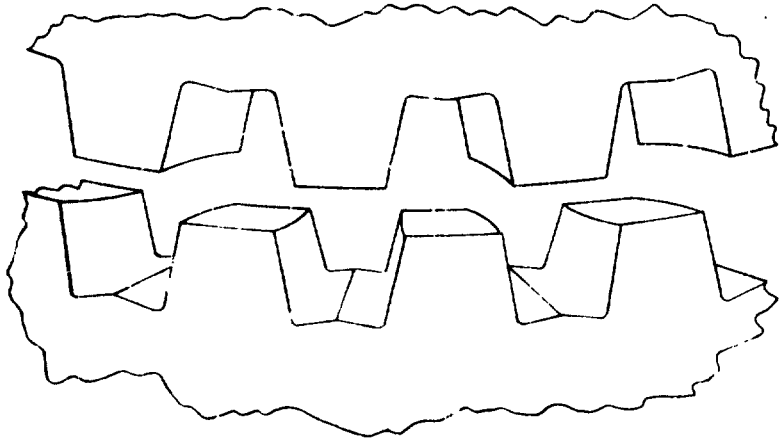

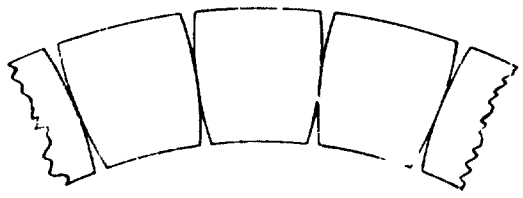

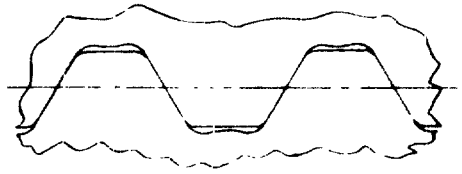

s-81397

Figure 5-15.--Curvic Couplings

The outside of the shaft is slotted for the full length of the bearing fit. Oil for ball bearing inner race cooling is pumped through these slots by a centrifugal slinger. Internal splines at the end of the shaft opposite the turbine wheels transmit the output torque to gearbox via a quill shaft.

The hydrogen rick working fluid may have a deleterious effect on all hot metallic parts. This limits the choice of materials available, and imposes additional restraints on the acceptable working stresses for turbine components.

The two turbine wheels, the four studs and nuts, and the shaft are made of CRES V-57 steel, a modified CRES A286. V-57 was selected because of its resistance to hydrogen embrittlement. The central tie-bolt material is INCO 718 stressed to about 126,000 psi. To protect it from the hydrogen environment, a cap is welded to the shaft end. Both ball bearings are made of M-50 tool steel and have a silver-plated 4340 steel separator.

Some additional features of the rotating assembly are shown in fig. 5-16. The bearing carrier is a rugged structure supporting the bearings and a stationary labyrinth seal on the turbine side. Resilient mounts are provided for both ball bearings (stiffness 60,000 lb/in.). These are secured with pins to prevent axial movement and rotation. Two springs and spring guides are used to provide a double bearing preload in the event of a thrust reversal. Oil is delivered to the bearings from two oil jets that are an integral part of the bearing carrier. Excess oil is carried away from the bearings to two slingers on the outboard of each bearing and by drain holes in the center of the bearing carrier. Early in the design of this machine, the use of carbon-face-type seals was considered to prevent oil from leaking into the turbine cavity. Because of development costs involved, it was decided to use a gas-pressurized labyrinth seal for the test hardware. Nitrogen buffer gas is introduced under pressure in the center of the labyrinth seal, and its flow in both directions prevents oil from leaking to the outside and hydrogen from entering the bearing cavity.

The turbine assembly is supported from the gearbox by a support housing (detail 6, in dwg. 581192), which is attached to the gearbox housing by a flange and 12 0.25-in.-dia bolts. The bearing carrier is bolted to the support housing by six 10/32-in. screws. Shims are provided between the bearing carrier and support housing to adjust the axial clearance between the first-stage turbine and nozzle. The support housing is bolted to the containment ring, which reaches through the holes in the turbine outlet torus by means of six lugs. Since the containment ring is cooler, it is used to provide support and guidance for the turbine housing. The hot turbine housing is supported from the containment ring by twelve radial pins. These pins permit radial growth of the turbine housing and at the same time maintain the concentricity of the hot turbine housing relative to the containment ring and the rotating assembly. Because the turbine housing expands and contracts with temperature, all connections between it and any cooler structure must have flexibility. During startup when the hot gases first begin to flow through the gas passages, an almost instantaneous heating and expansion of the structure in contact with the gas will occur. The lighter the cross-section of the component, the quicker will be its thermal response. The surrounding heavier

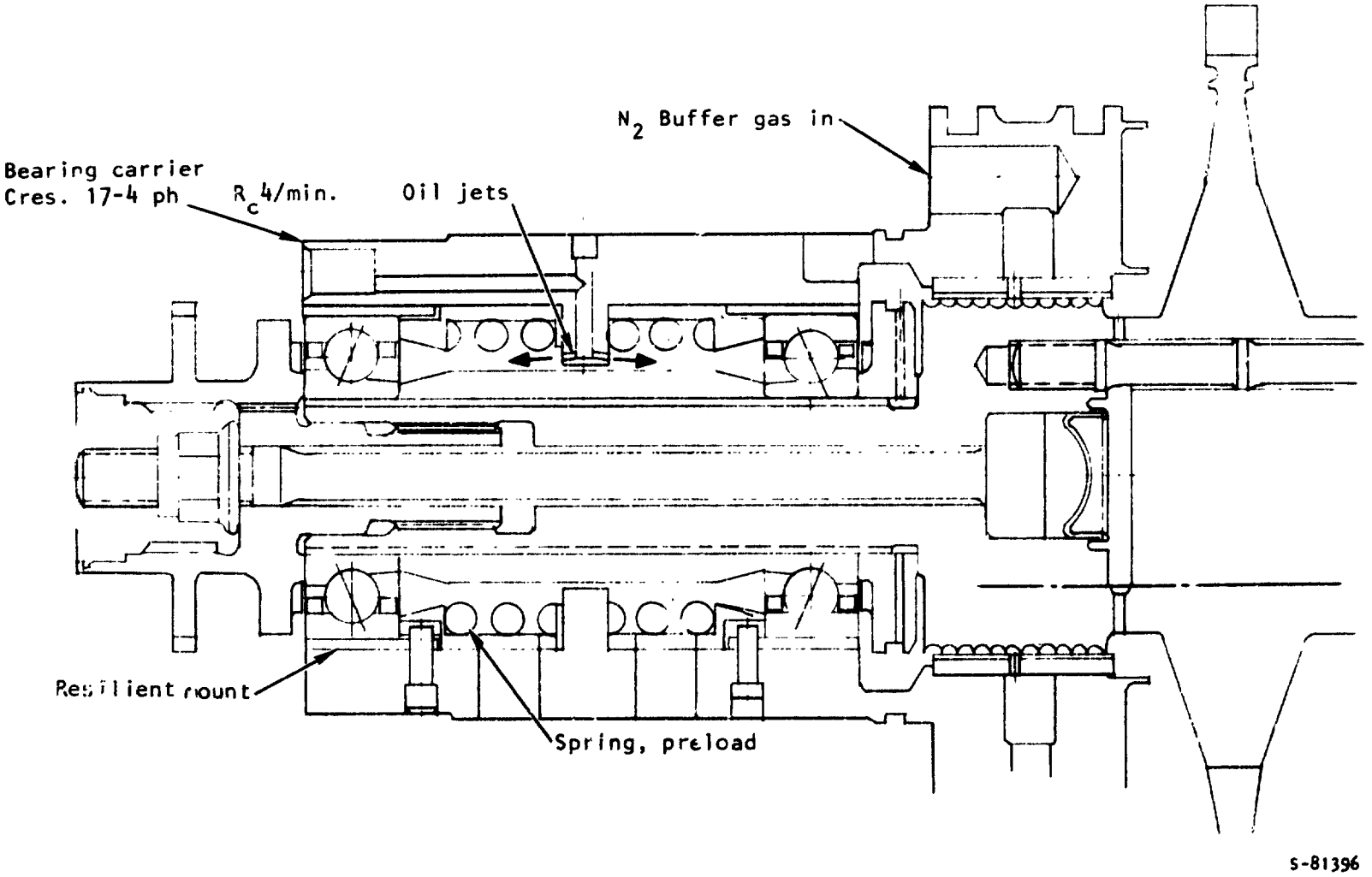

Figure 5-16.--Bearing Carrier

structure will not respond as fast, resulting in a relative movement between the two parts that must be accommodated. Flexible structures are used in a number of places, e.g., between the first-stage nozzle torus and the flange of turbine housing, to reduce the stresses between the hot and cold parts. This is mandatory for high fatigue life.

After shutdown, heat contained in the turbine wheels and hot static structure will soak back to the cooler gearbox. The rate of this heat transfer will affect the temperature of turbine seal and bearings. This temperature will first rise and then fall as the entire APU reaches a thermal equilibrium condition. The maximum bearing temperature attained is critical only if it exceeds the coking temperature of lubricating oil. Thermal cycling of hot portions of the turbine can lead to low cycle fatigue failures of the hot static structure. This imposed additional limitations on the maximum operating stress level of all components.

In addition to allowing for radial dimensional changes between parts, provision is made for their free axial growth. The radial pins in the containment ring establish the axial location of the inlet torus and leave the turbine outlet torus free to move. When this occurs leakage of exhaust products is prevented by a double piston ring expansion joint. The nitrogen buffer gas used for the labyrinth shaft seal is also directed into the space between the two piston rings. Since the nitrogen gas pressure is higher than the ambient and higher than hydrogen outlet pressure, nitrogen will flow outward in both directions, preventing leakage of hydrogen to the atmosphere.

The hydrogen/oxygen combustor is shown in the upper right corner of dwg. 581192. To prevent a localized hot area in the first-stage nozzle torus, the hot gas from the combustor is introduced tangentially downstream just beyond the last drilled nozzle. In this way, the hot gas must travel circumferentially almost 170-deg before entering the first nozzle, providing uniform heating of the nozzle torus. A similar feature is built into the second-stage nozzle assembly. The annulus between the inlet of the second-stage nozzle and the discharge of the first-stage turbine wheel permits circulation of hot gas.

Although great effort has been made to minimize distortions, the possibility of rubbing between the rotating and stationary parts exists. If this should occur, it should not be detrimental. Stationary segments installed over the turbine blade tips (segmented to provide for expansion) are fitted on the inner diameter with an abradable material that will wear readily if touched by the rotating turbine blades. In the same way, the three labyrinth seal stators will wear to establish a running clearance with the rotor. The stator of the shaft labyrinth is lined with bronze while the two turbine seals are made of 1/32 cell size stainless steel honeycomb.

The rotating assembly is built up as a separate cartridge that can be installed or removed from the turbine housing. Trapped between the two turbine wheels is the second-stage nozzle ring, which is supported for balancing from the bearing carrier by a special assembly fixture. This fixture prevents damage to the intermediate labyrinth seal. The rotating assembly is dynamically balanced outside of the turbine in a special balancing fixture.

Bearings

The ball bearings selected for the APU are 205-size angular contact type with relieved inner ring and outer land riding machined separator. The material is M-50 for the balls and rings and silver plated steel for the ball separator. The nominal DN number is 1.575×10^6. Computer analysis was carried out to design the bearing for the loads and speeds encountered during ground check, liftoff, reentry, horizontal flight, and landing. A B_{10} fatigue life (90 percent survival) of 1000 hr is forecast under the design vibration acceleration, and unbalance conditions. The bearings are lubricated by directed flow from an oil jet and cooled by the same lubricating oil and also by the oil flowing under the bearing bores through slots cut on the shaft.

Turbine Thermal Analysis

Introduction.--A series of computerized thermal analyses of the turbine assembly was performed for the configuration shown in fig. 5-17 just prior to the final design (fig. 5-18). The carbon face seal and thermal barriers were replaced by a nitrogen pressurized labyrinth seal to reduce development costs for the final test design. The thermal design configuration and the final design configuration are thermally conservatively similar. The purpose of the thermal design analyses was to support the mechanical design effort and verify thermal performance, acceptability, and reliability of the proposed turbine concept.

Analytical method.--A detailed thermal model (nodal network) simulating the above-mentioned turbine thermal design configuration was first constructed for use with the AiResearch thermal analyzer computer program (H0298) that is described in the following section. This model, consisting of over 200 nodes (temperature elements) and shown in fig. 5-19, was subjected to various boundary conditions corresponding to specified steady-state and transient operating/soakback and startup conditions. The ensuing computer runs gave the temperature results reported herein.

AiResearch thermal analyzer computer program (H0298) description.--To perform the detailed conduction, convection, radiation, and fluid stream heat transfer calculations, an analog of the thermal problem was constructed on the transient and steady-state thermal analyzer computer program (H0298) described below.

Transient heat transfer calculations are developed by the explicit finite difference method described by Dusinberre (ref. 5-1). This method is based on the transfer of heat along thermal resistance paths by virtue of a temperature difference between heat storage elements that absorb or release heat as a result of a temperature increase or decrease.

Steady-state heat transfer calculations are based on the conservation of energy under equilibrium conditions. This means that all the heat flowing into an element plus the heat generated within the element must equal the heat flowing out of the element. The resulting equations in a steady-state

FOLDOUT FRAME

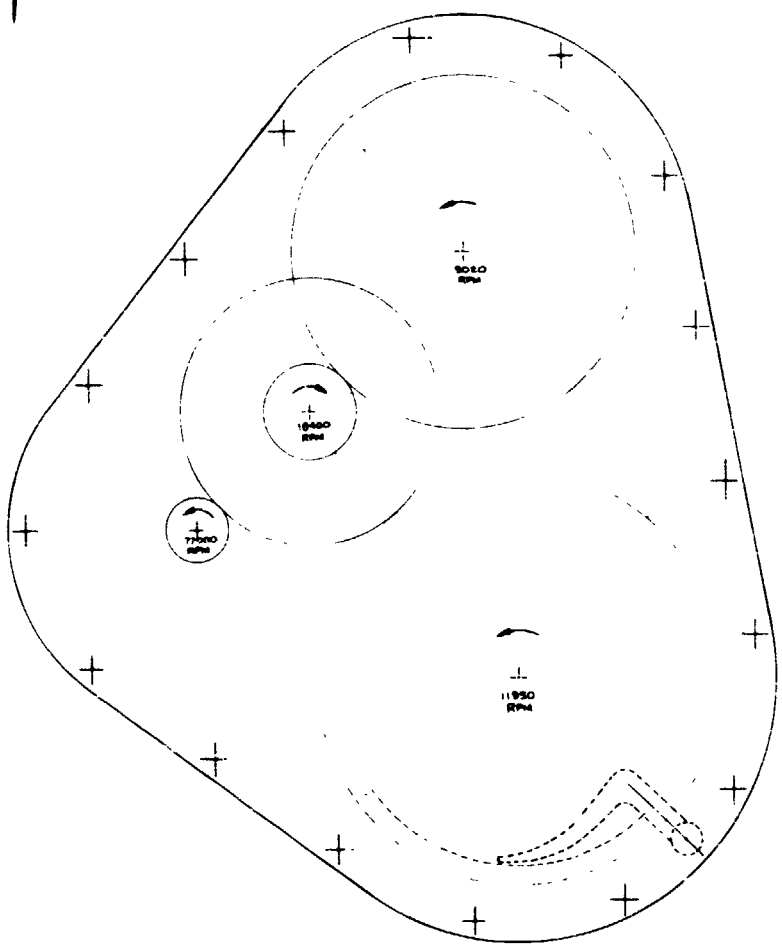

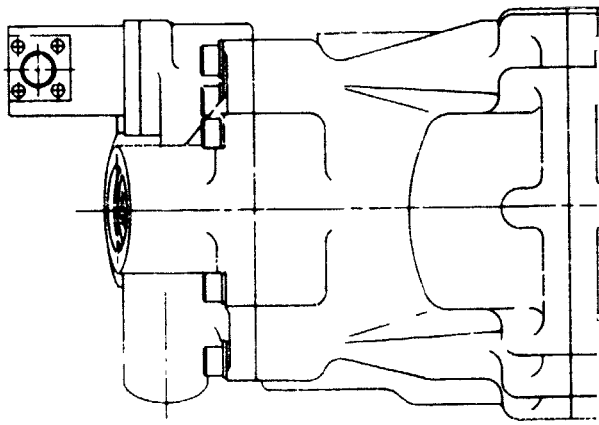

INSTALLATION OF OPTIONAL FUEL BOOST PUMP

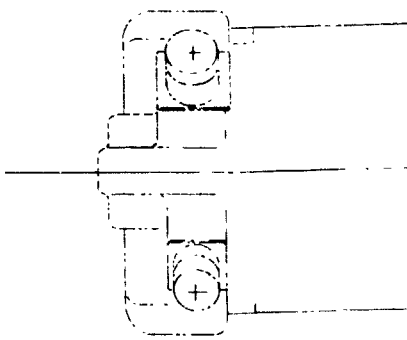

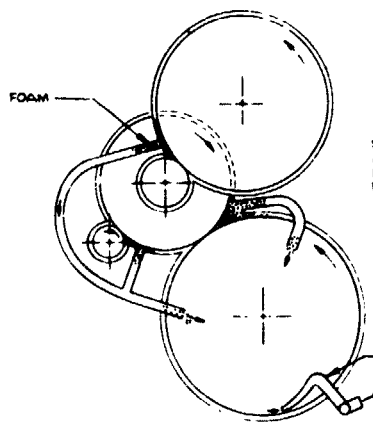

SCAVENGE PUMPS USING GEARS AS DRAG PUMPS. ALL FEED INTO LARGE GEAR WITH ROTATING SUMP

ZERO GRAVITY LUBRICATION

FOLDOUT FRAME 2

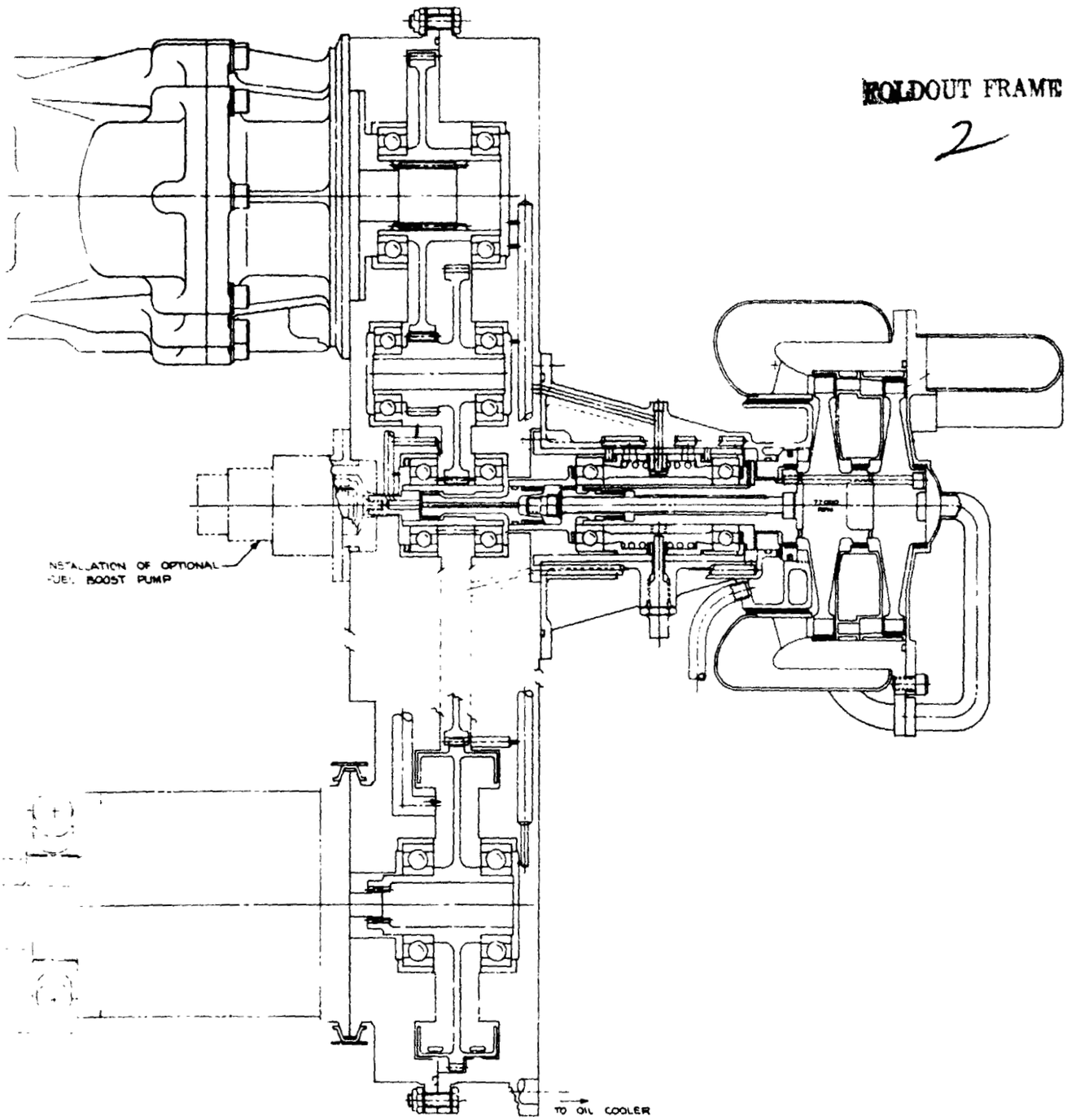

Figure 5-17.--Power Unit and Gearbox Cross-Section Used in Thermal Analysis.

FOLDOUT FRAME

/

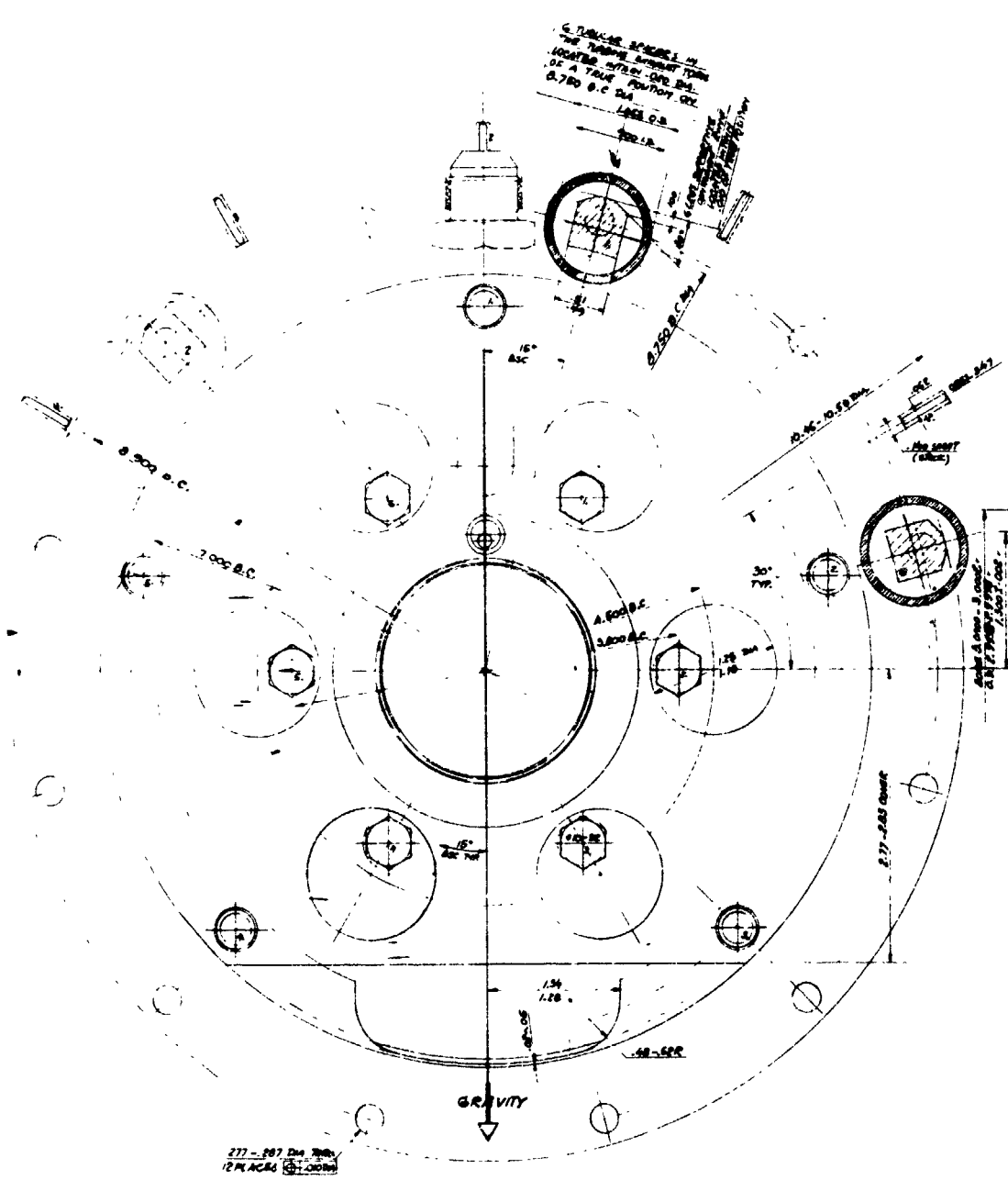

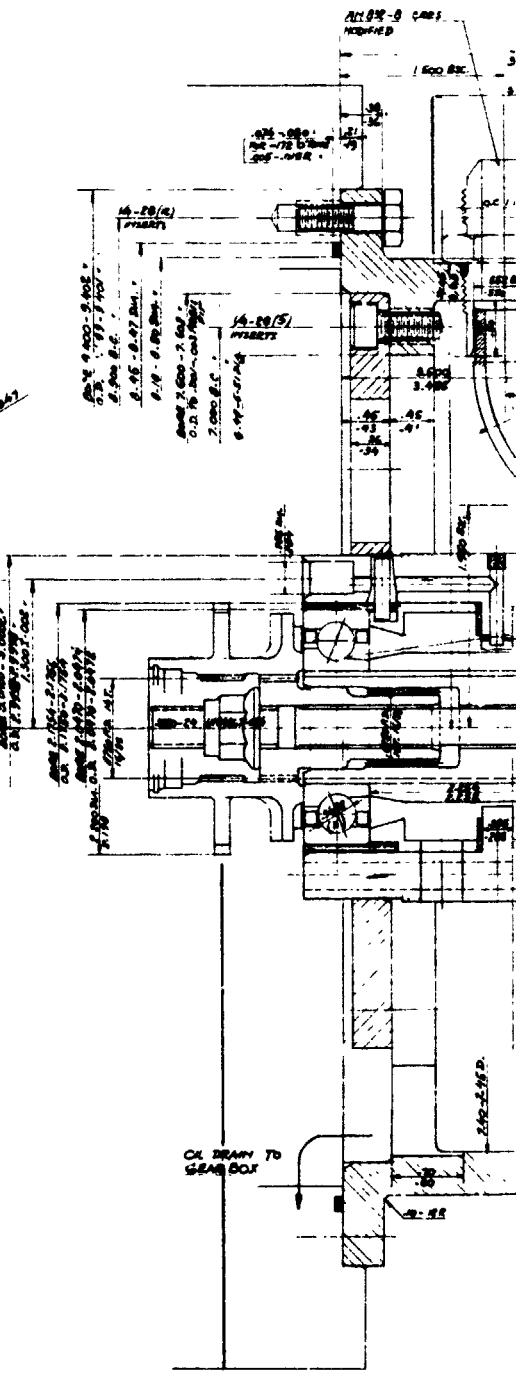

FOLDOUT FRAME

2

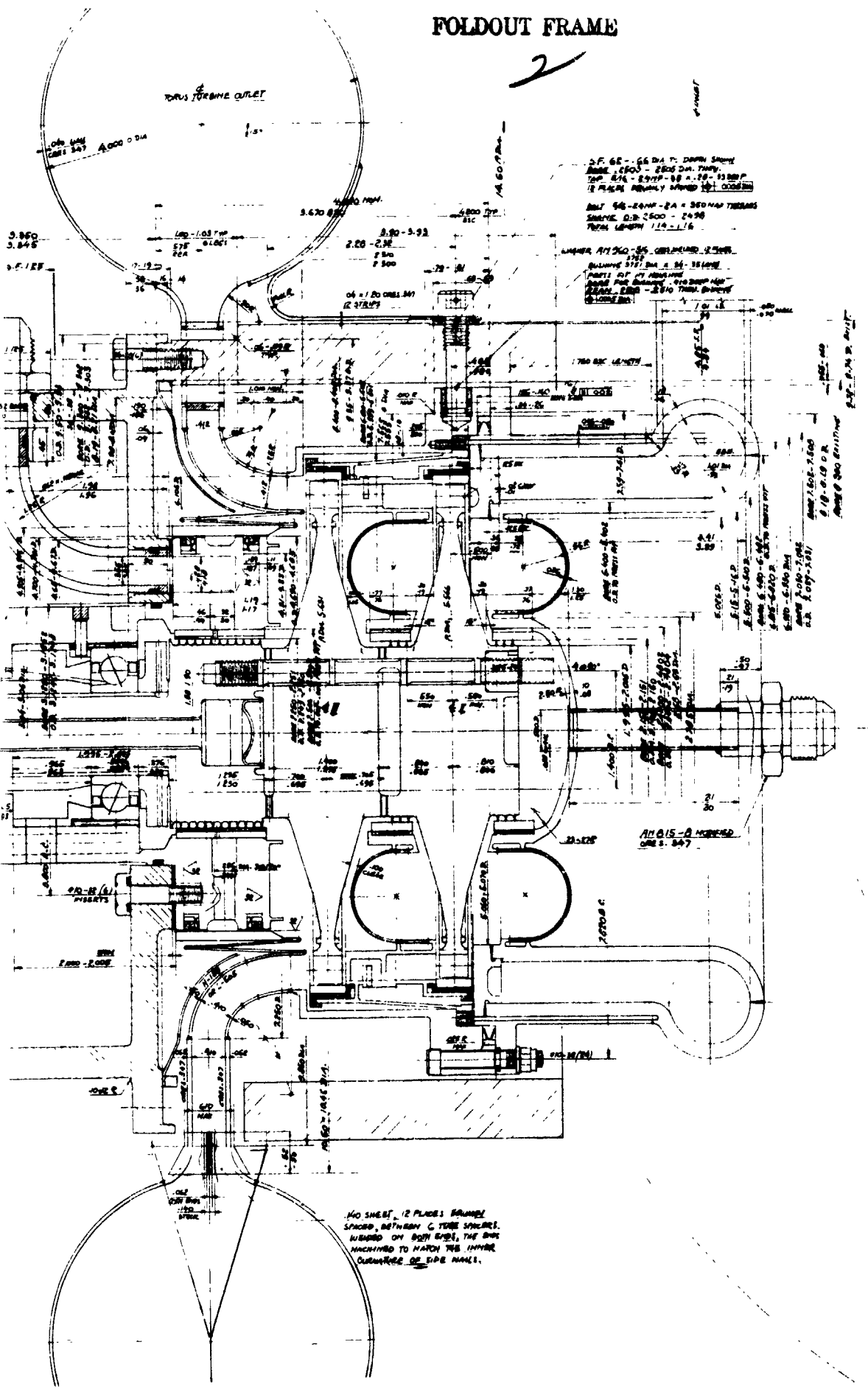

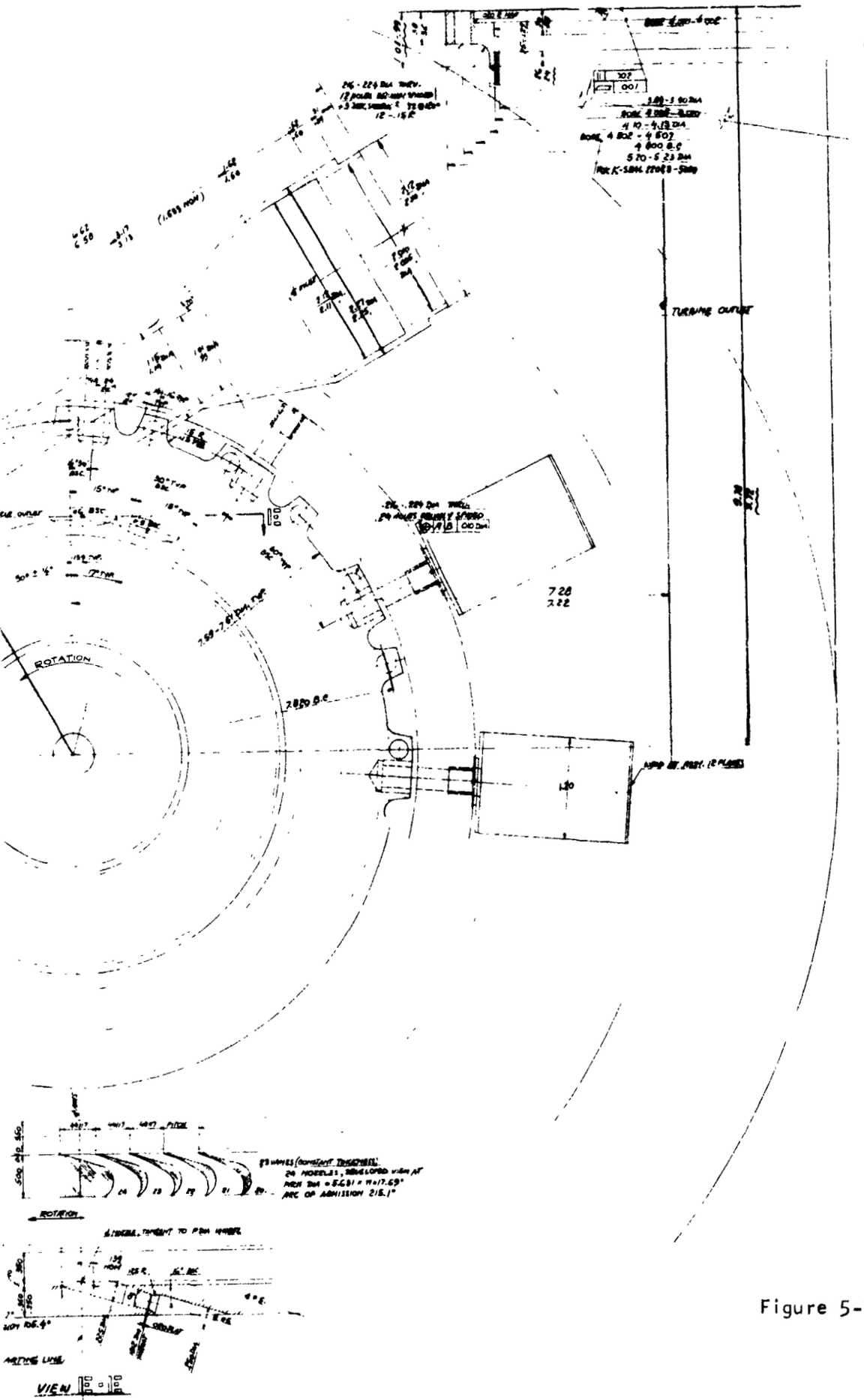

Figure 5-18.--Power Unit Space Shuttle APU Layout of Simplified Test Turbine.

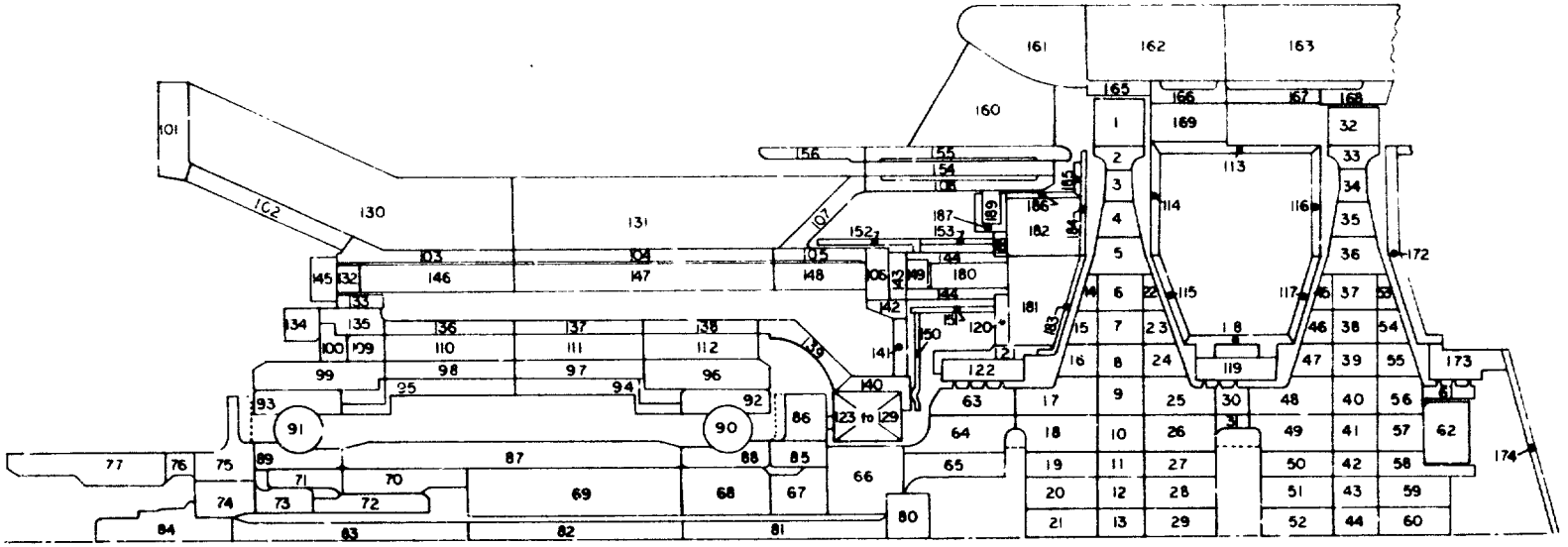

Figure 5-19.--Space Shuttle APU Turbine Assembly Thermal Model (Nodal Network).

solution may be reduced to a set of simultaneous linear equations. These equations may be solved by he iteration method, also known as the Gauss-Seidel method. The iteration or successive substitution method follows a fixed sequence of operations that (when repeated a sufficient number of times) will give a solution accurate within the limits of the model. In this method the temperature of each element is calculated as the weighted average of the temperatures of its neighbors plus the temperature rise due to heat generation. This process is repeated for each element in the problem, and new values of the thermal resistance between elements are calculated on the basis of the new temperatures where necessary. These new resistance and temperature values are used to calculate successive sets of values, and the process is repeated until the temperature change between successive substitutions is acceptably small and the heat flow into each element matches the heat flow out within 2 percent.

Heat transfer calculations may be input to fluid stream elements by conduction, convection, or radiation. Fluid stream heat transfer calculations have provision for preventing the outlet fluid temperature from overshooting the surrounding surface temperature, a thermodynamic impossiblity. The steady-state fluid stream calculations are based on thermal capacity rate calculations, while transient fluid stream calculations may be based on the thermal capacitance of each element moving in the fluid stream to simulate lag conditions.

Heat transfer to the turbine blades is evaluated using the relative total temperature (T_T) of the hot gas flowing over the turbine blades and the turbulent flow flat plate heat transfer coefficient calculated from eq. (5-1) below.

$$h_b = 0.0296 \frac{K_f}{L} \left[\frac{L V_b \rho_f}{\mu f} \right]^{0.8} P_{r_f}^{1/3} \qquad (5\text{-}1)$$

In eq. (5-1), the fluid properties are determined at Eckert's (ref. 5-2) reference temperature, as shown in eq. (5-2).

$$T_f = T_s + 0.5 (T_b - T_s) + 0.22 (T'_{adw} - T_s) \qquad (5\text{-}2)$$

where

$$T_s = T'_T - \frac{(V'_b)^2}{2 g_c J C_p} \qquad (5\text{-}3)$$

$$T'_{adw} = T_s + (P_{r_f})^{1/3} (T'_T - T_s) \qquad (5\text{-}4)$$

Heat transfer along the sides of the turbine disks is calculated considering disk pumping and windage friction. Disk pumping produces a recirculation flow of hot gas between the turbine disk and shroud, and the windage friction adds heat to this recirculation flow.

The heat transfer coefficients along the sides of the disk are calculated by the methods described by Richardson and Saunders (ref. 5-3). The laminar flow equation used for RE ≤ 200,000 is given as eq. (5-5).

$$h_d = 0.4\,(C_h)\,\frac{K_f}{R}\left[GRAS\cdot\left(\frac{\frac{2\pi}{60}R^2\,(RPM)\,\rho}{\mu}\right)^2\right]^{1/4}\left(\frac{P_r}{0.7}\right)^{1/3} \qquad (5\text{-}5)$$

The turbulent flow equation used for RE > 200,000 is given as eq. (5-6).

$$h_d = 0.0195\,(C_h)\,\frac{K_f}{R}\left[\frac{\frac{2\pi}{60}R^2\,(RPM)\,\rho}{\mu}\right]^{0.8}\left(\frac{P_r}{0.7}\right)^{1/3} \qquad (5\text{-}6)$$

If the value of H calculated from either falls below SKF (2)/DG, when DG is the gap spacing between the rotating disk and a static shroud, then the value of H = SKF(2)/DG. Windage friction is calculated from eqs. (5-7), (5-8), (5-9), and (5-10) for enclosed rotating disks, the applicable equation depending on the regime of flow.

Regime 1: When $RE \le 2.84\left(\frac{R}{DG}\right)^{2.21}$ and $RE < 1.58 \times 10^5$

$$q_{wind} = 7.58 \times 10^9\,\frac{\left(\frac{RPM}{1000}\right)^3\left(\frac{R}{5}\right)^5\frac{\rho}{32.2}}{RE\left(\frac{DG}{R}\right)} \qquad (5\text{-}7)$$

Regime 2: When $RE \ge 2.84\left(\frac{R}{DG}\right)^{2.21}$ and $RE < 1.58 \times 10^5$

$$q_{wind} = 4.48 \times 10^9\,\frac{\left(\frac{RPM}{1000}\right)^3\left(\frac{R}{5}\right)^5\left(\frac{\rho}{32.2}\right)\left(\frac{DG}{R}\right)^{0.1}}{RE^{0.5}} \qquad (5\text{-}8)$$

Regime 3: When $1.58 \times 10^5 \le RE < 1 \times 10^6$

$$q_{wind} = 0.1237 \times 10^9\,\frac{\left(\frac{RPM}{1000}\right)^3\left(\frac{R}{5}\right)^5\left(\frac{\rho}{32.2}\right)\left(\frac{DG}{R}\right)^{0.1}}{RE^{0.2}} \qquad (5\text{-}9)$$

Regime 4: When $RE > 1 \times 10^6$

$$q_{wind} = 0.627 \times 10^7 \left(\frac{RPM}{1000}\right)^3 \left(\frac{R}{5}\right)^5 \frac{\rho}{32.2} \qquad (5\text{-}10)$$

where

$$RE = \frac{\left(\frac{2\pi}{60}\right) R^2 \, (PPM)\, \rho}{\mu}$$

R = disk radius, ft

RPM = revolutions/min

ρ = density, lb/cu ft

μ = viscosity, lb/ft sec

DG = gap between rotating disk and static shroud, ft

q_{wind} = windage heating, watts

Heat transfer in the nozzles is calculated by the method given in Bartz (ref. 5-4). Conduction heat transfer throughout the turbine assembly considers the variation of thermal conductivity and specific heat of each material with temperature.

Thermal results.--A series of eight thermal analyses was performed on the thermal model shown in fig. 5-19. Four steady-state and four transient thermal analyses were performed. Six of the eight thermal analyses assumed Udimet 700 turbine disks with a turbine inlet temperature of 1600°F, while the remaining two cases assumed V-57 turbine disks and tie bolts with a 1500°F turbine inlet temperature.

The following steady-state and transient thermal analyses were performed:

Case 1: Sea-level, full-power, steady-state conditions with 1600°F TIT, 200°F oil, and Udimet 700 disks.

Case 2: Sea-level, idle, steady-state conditions with 1600°F TIT, 200°F oil, and Udimet 700 disks.

Case 3: Altitude, idle, steady-state conditions with 1600°F TIT, 200°F oil, and Udiment disks.

Case 4: A transient soakback analysis from altitude, idle conditions obtained from case 3.

Case 5: A 70°F start acceleration to sea-level idle conditions described in case 2 with 100°F oil.

Case 6: A 70°F start acceleration to sea-level, full-power conditions described in case 1 with 100°F oil.

Case 7: A 70°F start acceleration to sea-level, full-power conditions with 1500°F TIT, 100°F oil, and V-57 bolts and disks.

Case 8: Sea-level, full-power, steady-state conditions with 1500°F TIT, 100°F oil, and V-57 bolts and disks.

Labyrinth seal leakage, disk pumping, and oil flow.--In order to perform the thermal analysis of the turbine assembly, it was necessary to calculate the labyrinth seal leakage flow rate (1) from the first stage overboard, (2) between the first and second stages, and (3) from the second-stage overboard. The disk pumping flow rate and the cooling oil flow rates also were required. Table 5-3 lists the labyrinth seal leakage flow, the disk pumping flow, and the cooling oil flow for each of the conditions analyzed.

The labyrinth seal leakage flow was estimated using the technique given in Rossler (ref. 5-5). The disk pumping flow was estimated using Metzger (ref. 5-6).

Table 5-3

LABYRINTH SEAL LEAKAGE, DISK PUMPING, AND COOLING OIL FLOW

Labyrinth seal leakage				Disk pumping				Cooling oil	
				First stage		Second stage			
Case no.	No. 1, lb/hr	No. 2, lb/hr	No. 3, hr	Front, lb/hr	Aft, lb/hr	Front, lb/hr	Aft, lb/hr	Flow Rate, lb/min	Inlet temp., °F
1	25.316	26.236	3.984	13.02	23.37	0.0	6.762	8.013	200
2	2.82	2.821	4.782	4.976	5.327	0.0	4.682	8.013	200
3	3.31	3.391	0.4815	2.566	2.719	0.0	1.792	8.013	200
4	0.0	0.0	0.0	0.0	0.0	0.0	0.0	0.0	N/A
5	2.82	2.821	0.10	4.976	5.327	0.0	4.646	8.013	100
6	25.316	26.236	3.984	13.02	23.37	0.0	6.762	8.013	100
7	24.094	24.946	4.187	9.95	18.7	0.0	5.96	8.013	100
8	24.094	24.946	4.187	9.95	18.7	0.0	5.96	8.013	100

Steady-state results.--Temperature distributions for the four steady-state thermal analyses of the turbine assembly (including disks) during steady-state operations are shown in figs. 5-20 through 5-29.

Fig. 5-20 presents the thermal distribution of the turbine assembly for a turbine inlet temperature of 1600°F at sea-level full-power conditions. The analysis also assumes a 200°F oil inlet temperature and Udimet 700 disks. The temperatures were found to range from 203°F for the quill shaft to 1541°F for the first-stage nozzle assembly. The first-stage blade was found to be 1353°F and the second-stage blade 1026°F. The disk temperatures varied from 1272° to 1333°F for the first stage and 1100° to 1046°F for the second stage. Note that the rim of the second-stage disk is slightly cooler than the bore of the disk. This is due to axial conduction into the bearing sump.

Fig. 5-21 presents the thermal distribution of the turbine assembly for a turbine inlet temperature of 1600°F at sea-level idle power conditions. An oil inlet temperature of 200°F was assumed, as were Udimet 700 disks. The temperatures were found to vary from 202°F for the quill shaft to 1485°F for the first-stage nozzle assembly. The first-stage blade was 1366°F with a first-stage disk ranging from 1287°F at the bore to 1372°F at the rim. The second-stage blade was 1201°F with a disk temperature range of 1185°F at the bore to 1203°F at the rim.

Fig. 5-22 presents the thermal distribution of the turbine assembly for a turbine inlet temperature of 1600°F at altitude, idle power conditions. An oil inlet temperature of 200°F was assumed, as were Udimet 700 disks. The temperatures varied from 201°F for the quill shaft to 1440°F for the first-stage nozzle assembly. The first-stage blade was 1354°F with a first-stage disk ranging from 1259°F at the bore to 1337°F at the rim. The second-stage blade was 1055°F with a disk ranging from 1108°F at the bore to 1069°F at the rim. Again, the effects of axial conduction into the sump are evident since the second-stage disk rim temperature is lower than the bore temperature.

Fig. 5-23 presents the thermal distribution of the turbine assembly for a turbine inlet temperature of 1500°F at sea-level, full-power conditions. An oil inlet temperature of 100°F and V-57 bolts and disks were assumed. The temperatures were found to vary from 107°F for the quill shaft to 1447°F for the first-stage nozzle assembly. The first-stage blade was 1282°F with a first-stage disk ranging from 1207°F at the bore to 1264°F at the rim. The second-stage blade was found to be 991°F with a disk temperature range of 1049°F at the bore to 1008°F at the rim. Again, the effects of axial conduction on the second-stage disk temperatures are noticeable.

Startup transient results.--Startup transient thermal results were obtained primarily to determine the turbine disk temperature gradients and resulting thermal stresses that occur during such extreme transient conditions. Two types of transient thermal results are presented. The first is a thermal distribution of the entire turbine at a specific time into the transient, and the second is a family of curves for both the first- and second-stage turbine disks showing the temperature history of the various disks as a function of time and disk radius.

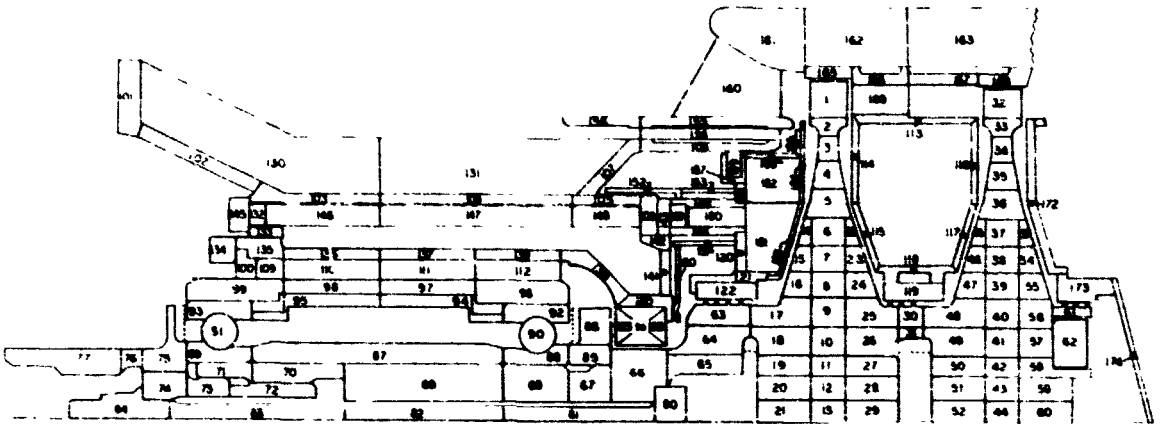

Node	Temp (°F)	Node	Temp (°F)	Node	Temp (°F)	Node	Temp (°F)	Node	Temp (°F)
1	1026	41	1276	81	357	121	910	[illegible]	1028
2	1046	42	1276	82	333	122	912	162	1105
3	1064	43	1275	83	230	123*	692	163	1161
4	1080	44	1272	84	223	124*	731	164*	1124
5	1084	45	1279	85	445	125*	794	165	1164
6	1092	46	1273	86	510	126*	977	166	1206
7	1095	47	1267	87	227	127*	N/A	167	1224
8	1097	48	1258	88	333	128*	610	168	1526
9	1100	49	1256	89	285	129*	548	169	1220
10	1100	50	1254	90	345	130	276	170*	1123
11	1100	51	1254	91	305	131	427	171*	1541
12	1100	52	1253	92	332	132	262	172	1302
13	1100	53	1297	93	295	133	256	173	1275
14	1074	54	1295	94	276	134	250	174	1220
15	1072	55	1294	95	262	135	252	175**	N/S
16	1070	56	1293	96	282	136	253	176**	N/S
17	1064	57	1289	97	267	137	464	177**	N/S
18	1063	58	1289	98	258	138	307	178**	N/S
19	1054	59	1288	99	266	139	402	179**	N/S
20	1066	60	1287	100	256	140	537	180	731
21	1068	61	1331	101	250	141	636	181	915
22	1112	62	1304	102	248	142	666	182	895
23	1118	63	874	103	284	143	679	183	933
24	1125	64	861	104	414	144	729	184	938
25	1139	65	848	105	677	145	252	185	929
26	1138	66	589	106	676	146	281	186	896
27	1134	67	437	107	709	147	416	187	839
28	1132	68	313	108	853	148	652	188	829
29	1131	69	234	109	257	149	698	189	844
30	1164	70	217	110	256	150	759	190**	N/S
31	1179	71	242	111	264	151	788		
32	1353	72	220	112	282	152	721		
33	1353	73	231	113	1223	153	774		
34	1312	74	229	114	1191	154	874		
35	1300	75	236	115	1206	155	894		
36	1293	76	229	116	1238	156	883		
37	1289	77	214	117	1232	157*	250		
38	1284	78*	205	118	1222	158*	894		
39	1281	79*	203	119	1223	159*	864		
40	1278	80	602	120	889	160	981		

* Not shown

** Gas nodes

N/S (Not Shown)

N/A (Not Applicable)

All temperatures are in °F

Figure 5-20.--Space Shuttle APU Turbine Assembly Temperature Distribution for Case 1.

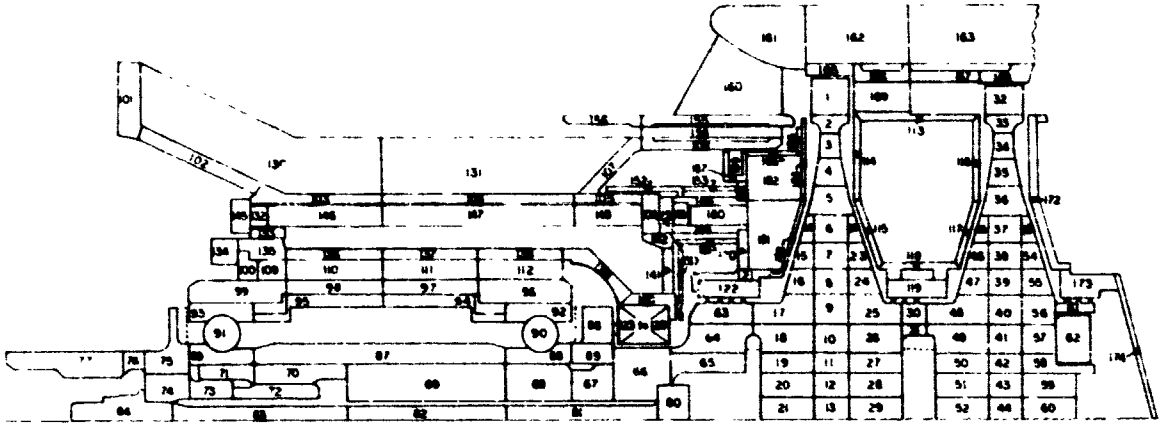

Node	Temp (°F)	Node	Temp (°F)	Node	Temp (°F)	Node	Temp (°F)	Node	Temp (°F)
1	1201	41	1292	81	361	121	1038	161	1156
2	1203	42	1289	82	335	122	1001	162	1177
3	1204	43	1289	83	228	123*	673	163	1196
4	1205	44	1287	84	221	124*	742	164*	1146
5	1206	45	1302	85	447	125*	803	165	1200
6	1203	46	1297	86	511	126*	984	166	1232
7	1202	47	1293	87	226	127*	N/A	167	1245
8	1199	48	1287	88	323	128*	628	168	1455
9	1196	49	1285	89	277	129*	560	169	1252
10	1192	50	1283	90	332	130	278	170*	1139
11	1188	51	1282	91	295	131	436	171*	1485
12	1186	52	1282	92	321	132	261	172	1273
13	1185	53	1309	93	286	133	254	173	1250
14	1198	54	1306	94	269	134	248	174	1199
15	1194	55	1302	95	257	135	250	175**	N/S
16	1188	56	1299	96	278	136	251	176**	N/S
17	1176	57	1294	97	263	137	267	177**	N/S
18	1166	58	1291	98	254	138	307	178**	N/S
19	1160	59	1290	99	260	139	408	179**	N/S
20	1160	60	1289	100	253	140	547	180	764
21	1160	61	1287	101	250	141	651	181	1084
22	1209	62	1286	102	248	142	685	182	1044
23	1210	63	912	103	285	143	699	183	1143
24	1211	64	899	104	421	144	760	184	1053
25	1215	65	886	105	698	145	252	185	1128
26	1212	66	603	106	696	146	281	186	1048
27	1208	67	442	107	742	147	423	187	907
28	1205	68	311	108	942	148	671	188	888
29	1204	69	234	109	253	149	724	189	920
30	1236	70	216	110	252	150	760	190**	N/S
31	1234	71	238	111	262	151	820		
32	1366	72	223	112	279	152	737		
33	1352	73	229	113	1255	153	803		
34	1337	74	227	114	1239	154	983		
35	1322	75	233	115	1245	155	1020		
36	1314	76	227	116	1278	156	1020		
37	1307	77	213	117	1271	157*	250		
38	1302	78*	205	118	1261	158*	1033		
39	1299	79*	202	119	1262	159*	935		
40	1295	80	848	120	998	160	1181		

* Not shown

** Gas nodes

N/S (Not Shown)

N/A (Not Applicable)

All temperatures are in °F

Figure 5-21.--Space Shuttle APU Turbine Assembly Temperature Distribution for Case 2.

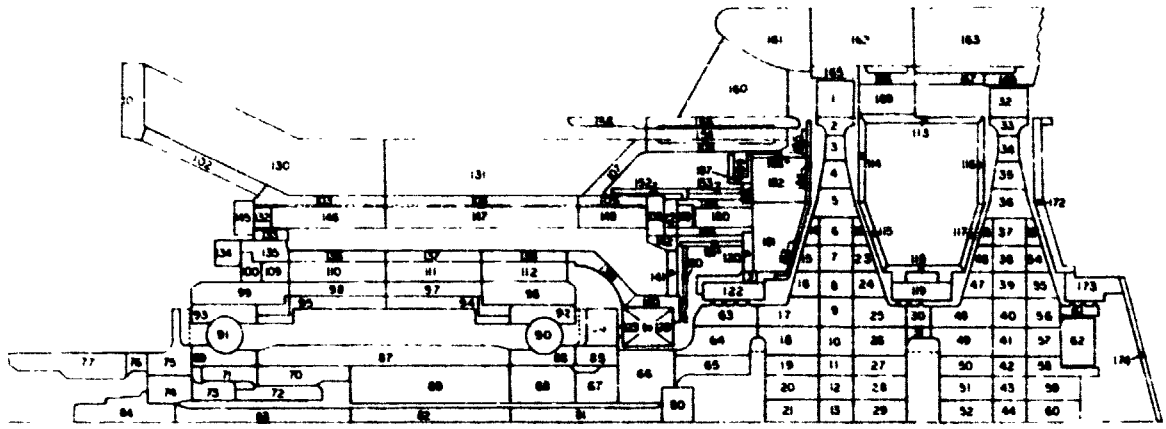

Node	Temp (°F)	Node	Temp (°F)	Node	Temp (°F)	Node	Temp (°F)	Node	Temp (°F)
1	1055	41	1266	81	342	121	885	161	1053
2	1069	42	1262	82	319	122	875	162	1100
3	1079	43	1260	83	226	123*	705	163	1147
4	1090	44	1259	84	219	124*	1539	164*	1103
5	1097	45	1283	85	456	125*	1558	165	1121
6	1 31	46	1277	86	558	126*	1592	166	1194
7	1104	47	1271	87	222	127*	N/A	167	1218
8	1109	48	1264	88	318	128*	398	168	1409
9	1111	49	1259	89	274	129*	382	169	1223
10	1111	50	1256	90	327	130	246	170*	1099
11	1109	51	1254	91	292	131	371	171*	1440
12	1108	52	1253	92	314	132	249	172	1253
13	1108	53	1288	93	282	133	244	173	1222
14	1086	54	1283	94	259	134	240	174	114[illegible]
15	1087	55	1278	95	250	135	241	175**	N/S
16	1090	56	1273	96	266	136	239	176**	N/S
17	1086	57	1266	97	252	137	248	177**	N/S
18	1082	58	1262	98	246	138	269	178**	N/S
19	1081	59	1261	99	255	139	319	179**	N/S
20	1081	60	1260	100	246	140	379	180	530
21	1082	61	1279	101	250	141	414	181	901
22	1116	62	1244	102	246	142	431	182	875
23	1123	63	801	103	267	143	439	183	931
24	1129	64	792	104	360	144	525	184	941
25	1142	65	781	105	482	145	244	185	929
26	1139	66	542	106	444	146	258	186	876
27	1135	67	426	107	548	147	346	187	791
28	1133	68	304	108	726	148	444	188	785
29	1131	69	225	109	246	149	486	189	768
30	1175	70	213	110	244	150	596	190**	N/S
31	1172	71	214	111	250	151	729		
32	1354	72	221	112	262	152	769		
33	1337	73	226	113	1230	153	778		
34	1321	74	225	114	1181	154	824		
35	1305	75	230	115	1199	155	880		
36	1296	76	224	116	1260	156	879		
37	1287	77	211	117	1253	157*	250		
38	1281	78*	204	118	1232	158*	849		
39	1276	79*	201	119	1234	159*	809		
40	1270	80	726	120	858	160	1039		

* Not shown

** Gas nodes

N/S (Not Shown)

N/A (Not Applicable)

All temperatures are in °F

Figure 5-22.--Space Shuttle APU Turbine Assembly Temperature Distribution for Case 3.

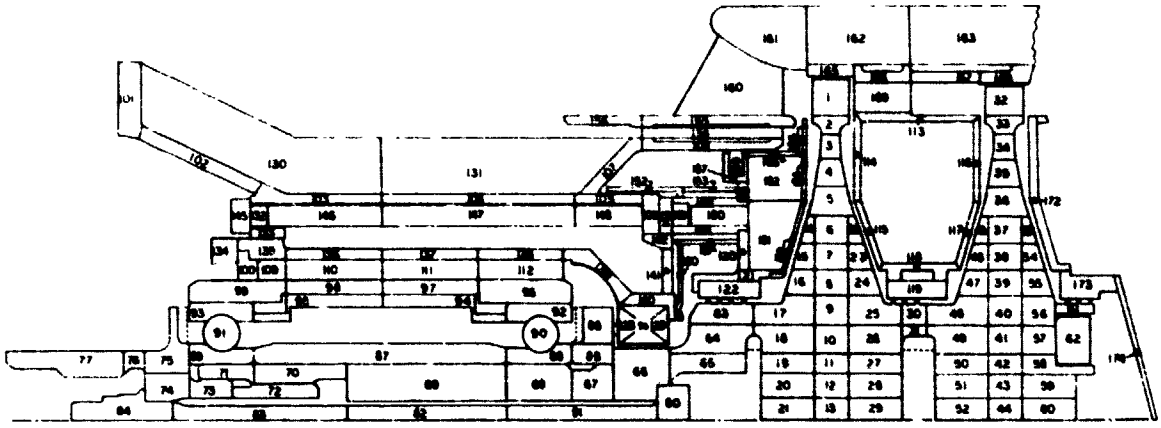

Node	Temp (°F)	Node	Temp (°F)	Node	Temp (°F)	Node	Temp (°F)	Node	Temp (°F)
1	991	41	1210	81	261	121	880	161	928
2	1008	42	1209	82	237	122	821	162	1003
3	1022	43	1208	83	127	123*	583	163	1060
4	1036	44	1207	84	119	124*	654	164*	1038
5	1042	45	1215	85	347	125*	716	165	1088
6	1046	46	1210	86	415	126*	903	166	1140
7	1048	47	1204	87	125	127*	N/A	167	1155
8	1049	48	1197	88	219	128*	544	168	1435
9	1050	49	1193	89	175	129*	478	169	1159
10	1048	50	1193	90	227	130	210	170*	1042
11	1049	51	1192	91	193	131	389	171*	1447
12	1049	52	1192	92	215	132	170	172	1234
13	1049	53	1230	93	183	133	155	173	1209
14	1032	54	1227	94	160	134	143	174	1158
15	1029	55	1226	95	150	135	148	175**	N/S
16	1027	56	1225	96	167	136	145	176**	N/S
17	1021	57	1220	97	153	137	158	177**	N/S
18	1020	58	1220	98	146	138	199	178**	N/S
19	1020	59	1220	99	154	139	317	179**	N/S
20	1022	60	1219	100	148	140	467	180	691
21	1023	61	1261	101	163	141	582	181	885
22	1061	62	1233	102	165	142	613	182	866
23	1067	63	842	103	211	143	633	183	904
24	1072	64	827	104	371	144	688	184	909
25	1084	65	811	105	641	145	159	185	900
26	1082	66	513	106	632	146	191	186	869
27	1079	67	344	107	684	147	345	187	811
28	1077	68	210	108	839	148	609	188	800
29	1075	69	133	109	147	149	656	189	821
30	1123	70	115	110	144	150	717	190**	N/S
31	1119	71	137	111	151	151	752		
32	1282	72	122	112	167	152	684		
33	1264	73	128	113	1162	153	739		
34	1247	74	126	114	1135	154	864		
35	1234	75	132	115	1148	155	888		
36	1228	76	126	116	1176	156	889		
37	1223	77	113	117	1171	157*	163		
38	1219	78*	107	118	1162	158*	891		
39	1216	79*	107	119	1163	159*	878		
40	1213	80	769	120	858	160	907		

* Not shown

** Gas nodes

N/S (Not Shown)

N/A (Not Applicable)

All temperatures are in °F

Figure 5-23.--Space Shuttle APU Turbine Assembly Temperature Distribution for Case 8.

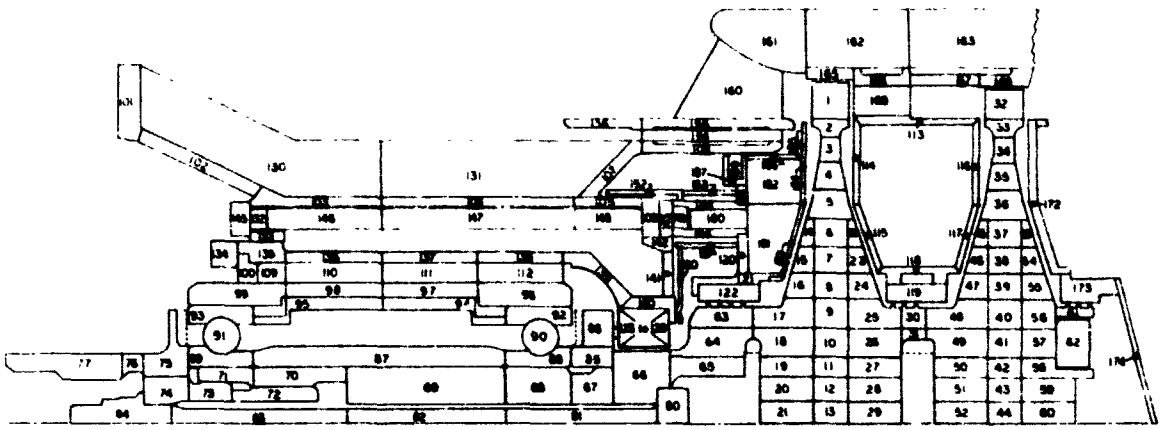

Node	Temp (°F)	Node	Temp (°F)	Node	Temp (°F)	Node	Temp (°F)	Node	Temp (°F)
1	1053	41	270	81	118	121	493	161	283
2	799	42	226	82	117	122	376	162	290
3	639	43	201	83	91	123*	259	163	359
4	469	44	189	84	100	124*	310	164*	202
5	372	45	558	85	219	125*	402	165	592
6	305	46	484	86	325	126*	674	166	878
7	260	47	414	87	97	127*	N/A	167	820
8	232	48	353	88	140	128*	96	168	1297
9	203	49	270	89	128	129*	85	169	1030
10	174	50	217	90	137	130	71	170*	235
11	149	51	186	91	132	131	71	171*	1389
12	131	52	171	92	134	132	82	172	947
13	123	53	558	93	128	133	86	173	922
14	335	54	496	94	95	134	93	174	802
15	297	55	444	95	94	135	91	175**	N/S
16	271	56	401	96	101	136	94	176**	N/S
17	230	57	312	97	94	137	95	177**	N/S
18	181	58	267	98	94	138	93	178**	N/S
19	149	59	256	99	103	139	89	179**	N/S
20	130	60	246	100	98	140	85	180	82
21	121	61	959	101	71	141	86	181	111
22	303	62	370	102	90	142	85	182	100
23	266	63	209	103	75	143	84	183	824
24	252	64	186	104	71	144	104	184	782
25	251	65	178	105	78	145	85	185	702
26	211	66	185	106	80	146	75	186	423
27	170	67	169	107	81	147	71	187	169
28	147	68	128	108	134	148	76	188	153
29	136	69	101	109	98	149	88	189	144
30	457	70	99	110	95	150	131	190**	N/S
31	404	71	111	111	95	151	160		
32	1287	72	95	112	100	152	90		
33	1104	73	100	113	1008	153	115		
34	961	74	101	114	545	154	227		
35	749	75	103	115	505	155	342		
36	629	76	101	116	918	156	360		
37	529	77	98	117	922	157*	70		
38	452	78*	97	118	700	158*	432		
39	388	79*	98	119	769	159*	400		
40	329	80	137	120	387	160	524		

* Not shown.

** See nodes

N/S (Not Shown)

N/A (Not Applicable)

All temperatures are in °F

Figure 5-24.--Space Shuttle APU Turbine Assembly Temperature Distribution for Case 5 at Startup, t = 40 sec.

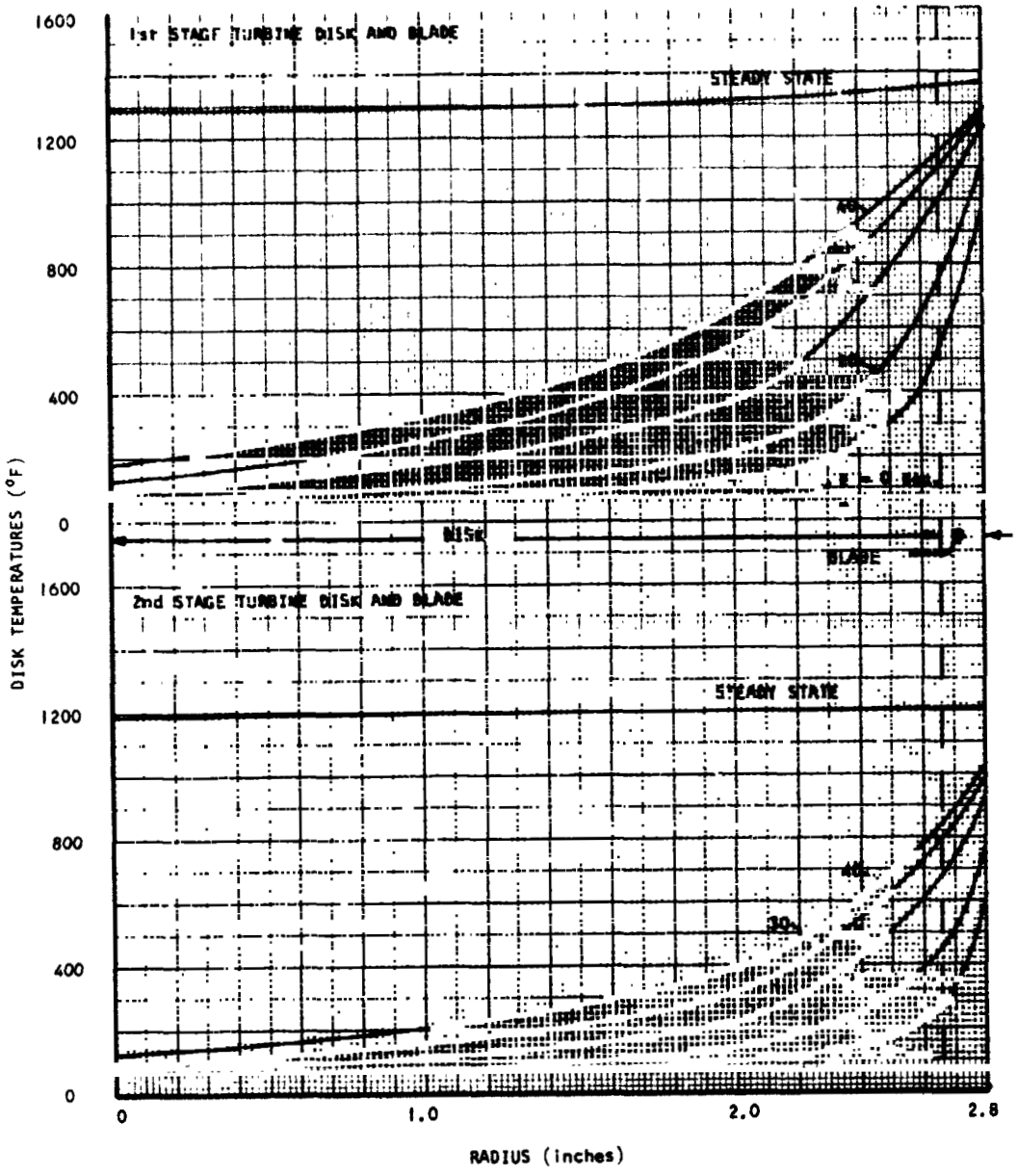

Figure 5-25.--First- and Second-Stage Disk Temperature Distributions During Startup Transient to Steady-State Operations (Cases 5 and 2).

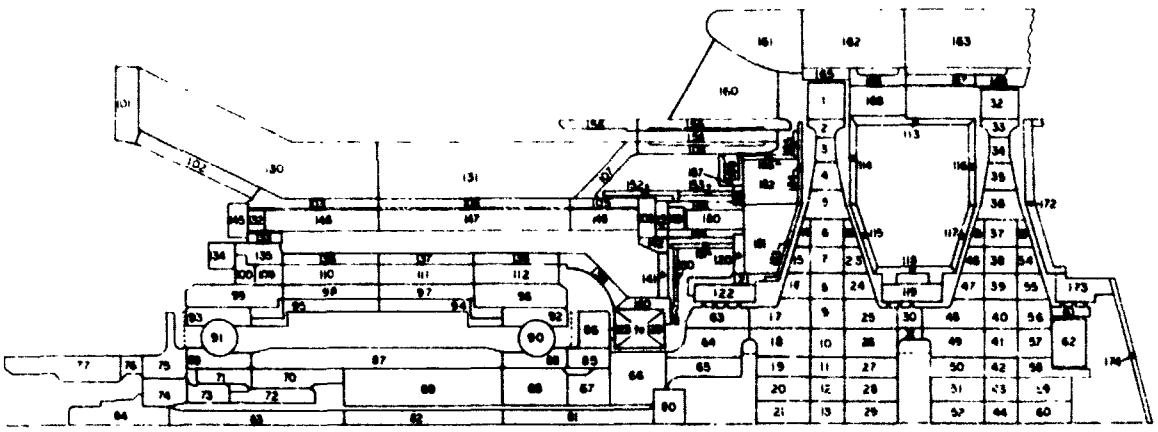

Node	Temp (°F)	Node	Temp (°F)	Node	Temp (°F)	Node	Temp (°F)	Node	Temp (°F)
1	1006	41	459	81	129	121	598	161	437
2	897	42	395	82	126	122	612	162	445
3	798	43	355	83	91	123*	286	163	499
4	665	44	335	84	100	124*	329	164*	257
5	572	45	879	85	229	125*	420	165	895
6	483	46	777	86	330	126*	687	166	1112
7	415	47	685	87	97	127*	N/A	167	1096
8	361	48	609	88	141	128*	149	168	1482
9	310	49	472	89	128	129*	110	169	1194
10	262	50	382	90	138	130	71	170*	284
11	223	51	329	91	132	131	72	171*	1505
12	196	52	303	92	134	132	82	172	1189
13	182	53	895	93	128	133	86	173	1136
14	486	54	789	94	95	134	93	174	1027
15	417	55	704	95	94	135	92	175**	N/S
16	359	56	626	96	101	136	95	176**	N/S
17	291	57	515	97	94	137	96	177**	N/S
18	239	58	476	98	95	138	97	178**	N/S
19	201	59	461	99	104	139	98	179**	N/S
20	177	60	443	100	98	140	110	180	95
21	165	61	1196	101	71	141	123	181	110
22	531	62	577	102	80	142	118	182	98
23	478	63	500	103	73	143	115	183	747
24	438	64	434	104	72	144	147	184	656
25	430	65	398	105	106	145	86	185	597
26	355	66	231	106	105	146	75	186	390
27	286	67	186	107	119	147	71	187	257
28	247	68	132	108	210	148	87	188	229
29	228	69	103	109	99	149	113	189	207
30	722	70	99	110	95	150	323	190**	N/S
31	629	71	111	111	95	151	277		
32	1345	72	95	112	100	152	161		
33	1267	73	100	113	1193	153	204		
34	1185	74	101	114	964	154	356		
35	1083	75	103	115	990	155	530		
36	975	76	101	116	1171	156	590		
37	857	77	98	117	1101	157*	70		
38	745	78*	97	118	1039	158*	655		
39	644	79*	98	119	1081	159*	612		
40	549	80	230	120	487	160	702		

* Not shown

** Gas nodes

N/S (Not Shown)

N/A (Not Applicable)

All temperatures are in °F

Figure 5-26.--Space Shuttle APU Turbine Assembly Temperature Distribution for Case 6 of Startup, t = 40 sec.

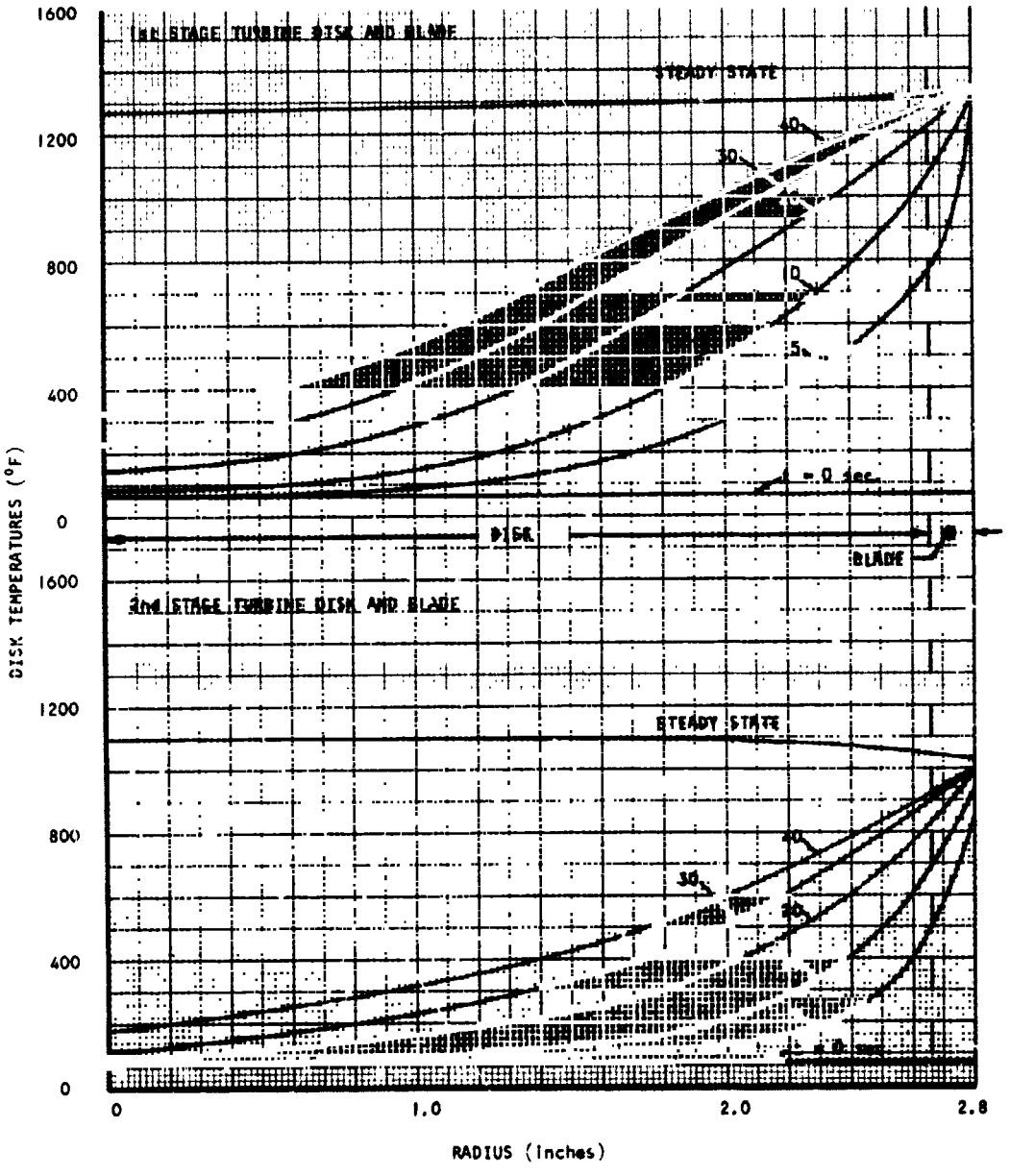

Figure 5-27.--First- and Second-Stage Disk Temperature Distributions During Startup Transient to Steady-State Operations (Cases 6 and 1).

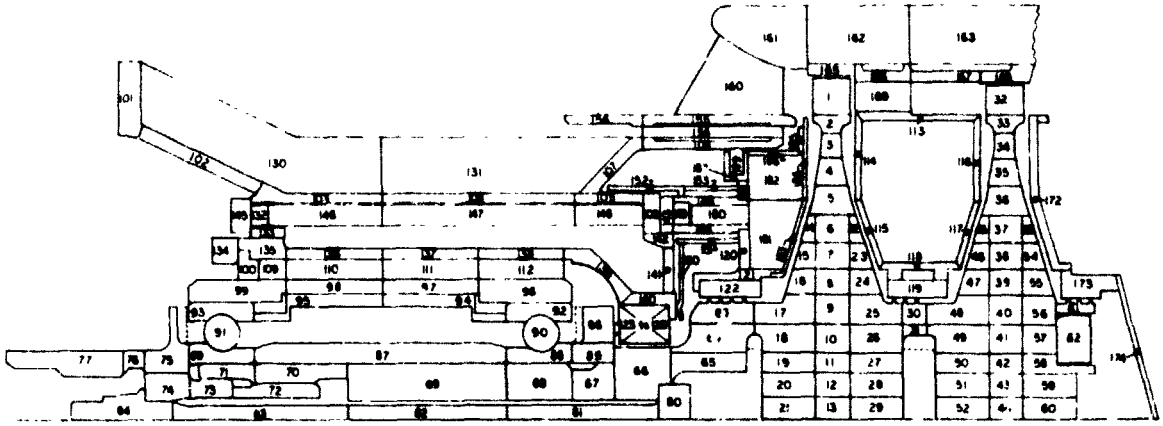

Node	Temp (°F)	Node	Temp (°F)	Node	Temp (°F)	Node	Temp (°F)	Node	Temp (°F)
1	977	41	496	81	128	121	574	161	761
2	892	42	433	82	124	122	588	162	595
3	811	43	392	83	91	123*	285	163	568
4	699	44	372	84	100	124*	332	164*	284
5	616	45	871	85	229	125*	423	165	976
6	553	46	784	86	332	126*	689	166	1078
7	463	47	701	87	97	127*	N/A	167	1056
8	403	48	627	88	141	128*	144	168	1400
9	346	49	500	89	128	129*	109	169	1140
10	290	50	415	90	138	130	71	170*	298
11	248	51	363	91	132	131	72	171*	1415
12	219	52	336	92	134	132	82	172	1149
13	204	53	884	93	128	133	86	173	1080
14	532	54	795	94	96	134	93	174	978
15	461	55	722	95	94	135	91	175**	N/S
16	398	56	653	96	100	136	94	176**	N/S
17	323	57	563	97	94	137	95	177**	N/S
18	266	58	504	98	94	138	97	178**	N/S
19	224	59	489	99	103	139	97	179**	N/S
20	198	60	472	100	98	140	109	180	96
21	184	61	1137	101	71	141	123	181	107
22	574	62	598	102	79	142	118	182	97
23	520	63	485	103	73	143	115	183	724
24	474	64	418	104	72	144	148	184	646
25	458	65	386	105	109	145	85	185	595
26	381	66	228	106	106	146	75	186	401
27	313	67	185	107	135	147	71	187	257
28	272	68	132	108	342	148	87	188	244
29	252	69	102	109	98	149	114	189	258
30	714	70	99	110	95	150	319	190**	N/S
31	636	71	111	111	95	151	274		
32	1275	72	95	112	100	152	163		
33	1206	73	100	113	1137	153	208		
34	1134	74	101	114	917	154	575		
35	1042	75	103	115	941	155	803		
36	955	76	101	116	1110	156	875		
37	858	77	98	117	1045	157*	70		
38	765	78*	97	118	980	158*	885		
39	673	79*	98	119	1023	159*	856		
40	586	80	228	120	468	160	882		

* Not shown

** Gas nodes

N/S (Not Shown)

N/A (Not Applicable)

All temperatures are in °F

Figure 5-28.--Space Shuttle APU Turbine Assembly Temperature Distribution for Case 7 at Startup, t = 40 sec.

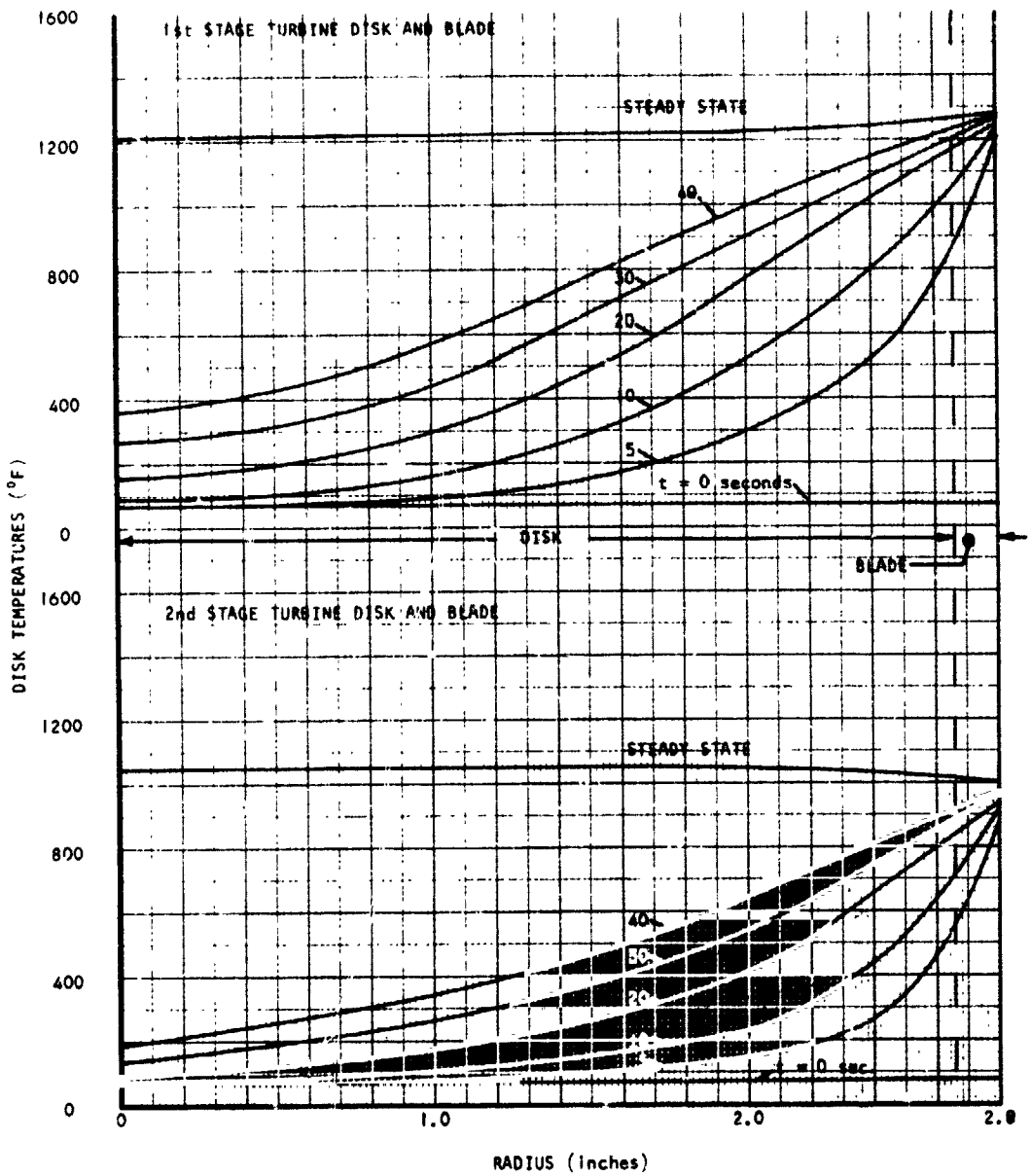

Figure 5-29.--First- and Second-Stage Disk Temperature Distributions During Startup Transient to Steady-State Operations (Cases 7 and 8).

Figs. 5-24 and 5-25 present the thermal distribution at t = 40 sec and the temperature history vs radius for the first- and second-stage disks. These results are based on an initial (starting) uniform turbine assembly temperature of 70°F, in addition to the same boundary conditions previously stated for the sea-level, idle, steady-state results. This, of course, assumes that the boundary conditions remain reasonably constant throughout the startup transient from initial conditions to sea level idle. As expected, the results indicate large turbine disk temperature gradients immediately after startup initiation, particularly for the first-stage disk. These gradients are gradually reduced until they are at their minimum when steady state is achieved. The steady-state condition corresponds to case 2.

Figs. 5-26 and 5-27 present the transient thermal results from a 70°F start to sea-level, full-power conditions with a turbine inlet temperature of 1600°F. The thermal results are similar to the previous case. The steady-state condition corresponds to case 1.

Figs. 5-28 and 5-29 present the transient thermal results for the 1500°F turbine inlet temperature condition with V-57 bolts and disks from a 70°F start to sea-level full power. The steady-state condition corresponds to case 8. Again, the thermal results are similar to the previous two cases.

Shutdown transient results.--Figs. 5-24 and 5-25 present the thermal results of a soakback thermal analysis from an altitude, idle, 1600°F turbine inlet temperature condition. The soakback transient thermal analysis was obtained primarily to determine the maximum (hot-end) turbine bearing and stagnant oil temperatures that occur during shutdown thermal soakback following normal altitude, idle, steady-state operation. During steady-state operation, there is no problem with the bearing and oil temperatures since active thermal control is provided by oil flow through the bearings and shaft; however, after shutdown, oil flow stops, and there is no longer any thermal control (unless it is provided by other means). The large amount of energy stored in the turbine disks during steady-state operation (at much higher temperatures) now slowly conducts (soaks back) to the shaft, bearings, and other low-temperature surroundings until an equilibrium conduction eventually is achieved. During this time the bearing and oil temperatures continue to increase until this condition is reached. Thus, it is obvious that the maximum bearing and oil temperatures during shutdown soakback are primarily dependent on two factors: (1) the thermal energy level of the turbine disks as determined by the turbine inlet temperature during steady-state operation, and (2) the thermal capacity (ability to absorb heat) of the materials surrounding the disks, especially in the area of the bearings.

Fig. 5-30 presents the temperature distribution of the turbine assembly during a soakback from altitude idle at t = 80 sec. Fig. 5-31 presents temperature histories of various parts and components of the turbine during soakback. These include the first-stage disk, the second-stage disk, the turbine shroud, the face seal support, the face seal rotor, the turbine end bearing, and the gear end bearing. The results indicate that no danger of oil coking during soakback exists for this turbine design.

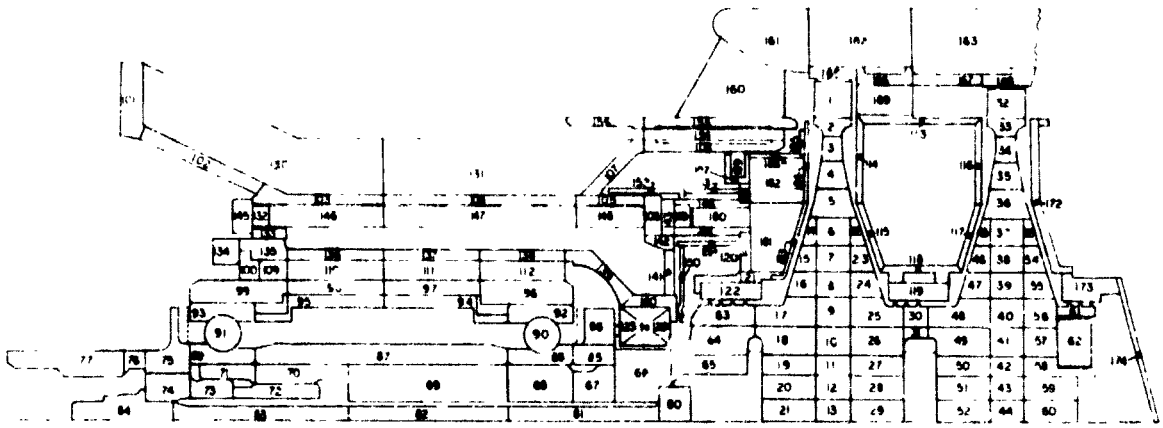

Node	Temp (°F)	Node	Temp (°F)	Node	Temp (°F)	Node	Temp (°F)	Node	Temp (°F
1	1083	41	1253	81	491	121	886	161	1048
2	1082	42	1253	82	338	122	881	162	1077
3	1083	43	1253	83	268	123*	630	163	1089
4	1085	44	1254	84	242	124*	1018	164*	1057
5	1088	45	1254	85	514	125*	979	165	1080
6	1092	46	1255	86	538	126*	903	166	1114
7	1096	47	1255	87	259	127*	636	16	1099
8	1100	48	1254	88	377	128*	413	168	1110
9	1103	49	1253	89	254	129*	403	169	1137
10	1105	50	1252	90	324	130	257	170*	1041
11	1107	51	1252	91	262	131	360	171*	1056
12	1108	52	1251	92	301	132	260	172	1047
13	1108	53	1251	93	261	133	259	173	1046
14	1090	54	1251	94	275	134	259	174	1058
15	1093	55	1249	95	260	135	259	175**	N/S
16	1096	56	1247	96	289	136	264	176**	N/S
17	1098	57	1248	97	274	137	260	177**	N/S
18	1100	58	1249	98	261	138	310	178**	N/S
19	1102	59	1249	99	260	139	364	179**	N/S
20	1103	60	1248	100	260	140	404	180	557
21	1103	61	1200	101	250	141	428	181	899
22	1035	62	1230	102	247	142	441	182	876
23	1099	63	759	103	263	143	447	183	926
24	1105	64	754	104	351	144	531	184	947
25	1111	65	765	105	481	145	263	185	934
26	1113	66	575	106	430	146	270	186	879
27	1114	67	502	107	543	147	348	187	791
28	1114	68	406	108	523	148	451	188	786
29	1114	69	270	109	260	149	494	189	767
30	1122	70	256	110	262	150	604	190**	N/S
31	1125	71	252	111	275	151	732	* Not shown	
32	1240	72	248	112	292	152	769	** Gas nodes	
33	1247	73	245	113	1149	153	778	N/S (Not Shown)	
34	1249	74	242	114	1150	154	815	N/A (Not Applicable)	
35	1251	75	24	115	1166	155	862	All temperatures are in °F	
36	1253	76	38	116	1208	156	858		
37	1255	77	228	117	1209	157*	250		
38	1255	78*	224	118	1192	158*	816		
39	1254	79*	213	119	1192	159*	767		
40	1253	80	570	120	859	160	1060		

Figure 5-30.-- Space Shuttle APU Turbine Assembly Temperature Distribution for Case 4 at Shutdown, t = 80 sec.

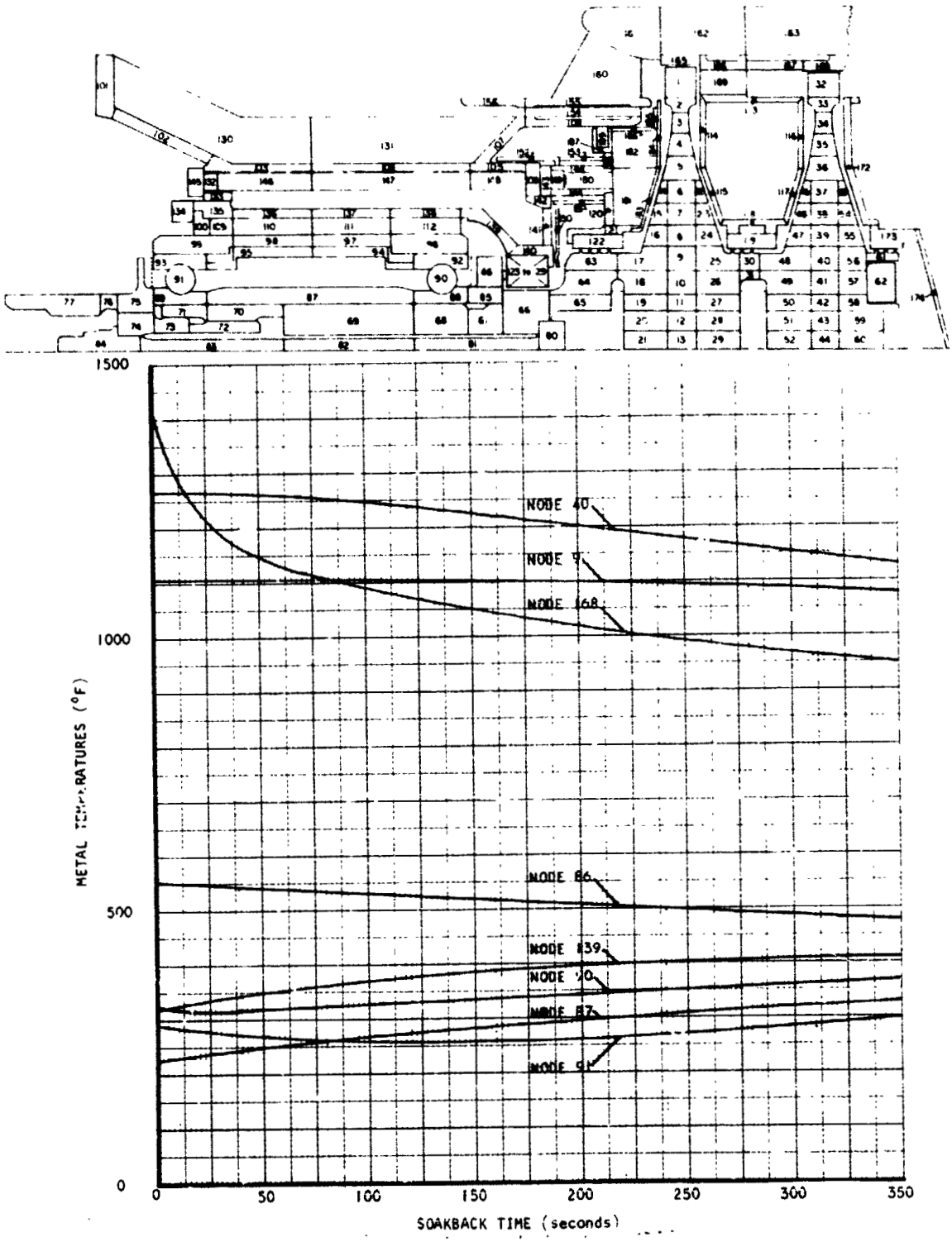

Figure 5-31.--Temperature Histories of Selected Components During Soakback from Altitude Idle (Cases 3 and 4).

Stress and Dynamics

In the analysis of the structural integrity of the H_2O_2 APU for the operating environment described below particular attention was paid to the dynamic and thermal aspects of the design. The APU rotor is designed for 2000 stop-start duty cycles and 1000 hr of operation. In the life calculations, it was assumed that the worst operating condition was the only mode of operation for the full 1000 hr and 2000 duty cycles. Other pertinent design criteria are listed in table 5-4. The design loading conditions listed in table 5-5 were formulated with NASA-Lewis approval from several sources of published data and specifications for the Space Shuttle program. All loads are assumed to be applied to the APU rotor simultaneously and to act continuously through the operation.

TABLE 5-5

LOAD CONDITIONS

Type of loading	Magnitude
Acceleration	± 4 g
Gyroscopic	3.5 rad/sec
Vibration	± 5 g
Unbalance	0.02 gm-in. (each wheel)

Turbine wheel stress analysis.--For turbine wheel disc stresses, the radial and tangential components of the combined centrifugal and thermal stresses on the first-stage turbine wheel disc from transient to steady-state condition are shown in figs. 5-32 through 5-35. Temperature distribution in the disc is presented in fig. 5-36 for the 1500°F TIT, sea-level, full-power operating condition at a turbine speed of 63,000 rpm. The combined stresses on the second-stage turbine wheel are shown in figs. 5-37 and 5-38, and fig. 5-39 indicates its temperature distribution in the disc for the same operating condition as the first-stage wheel. In both steady-state and transient stress distributions, the discontinuity in stress at midradius is due to the influence of the curvic coupling platform.

The disc rims of the first- and second-stage wheels experience compressive tangential stresses during startup due to high thermal gradients from the disc tip to the center of the wheel (as shown in figs. 5-32, 5-33, 5-34, and 5-37). The maximum elastic compressive tangential stress at the disc rims is shown in fig. 5-40 as 110 ksi at 9 sec and 76 ksi at 18 sec after startup for the first- and second-stage wheels, respectively. The radial tip growth of the first-stage turbine wheel during transient to steady-state operation is shown in fig. 5-41.

TABLE 5-4

PERTINENT DESIGN CRITERIA

Component	Parameter	Design criteria
Turbine wheel	Overspeed (hot run)	Design overspeed to be 1.35 x 63,000 rpm = 85,000 rpm
		Average stress in the turbine disc to be less than 80 percent of the ultimate strength
	Disc radial growth	Total creep strain that turbine disc experiences at the end of 1000 hr to be approximately 0.2 percent
	Operational life	Combined effect of creep and fatigue to be considered
		Uses a cumulative damage theory; a 0.5 percent creep strain is considered to be failure strain
Turbine wheel bolt and central tie-bolt	Design environment	Simultaneous application of acceleration, vibration, gyroscopic, thermal, centrifugal, and wheel unbalance loads
	Operational life	Fatigue and relaxation to be considered
	Assembly lockup	No looseness permitted under the combined loadings
Static structure	Design environment	Design only for ground operation
		Thermal and pressure loads to be considered
Rotor dynamics	Critical speed	Critical speeds to be excluded from the operating speed range
Containment structure	Wheel burst	Design to contain all wheel fragments at burst
Material	Properties	Use available minimum properties in the strength calculation

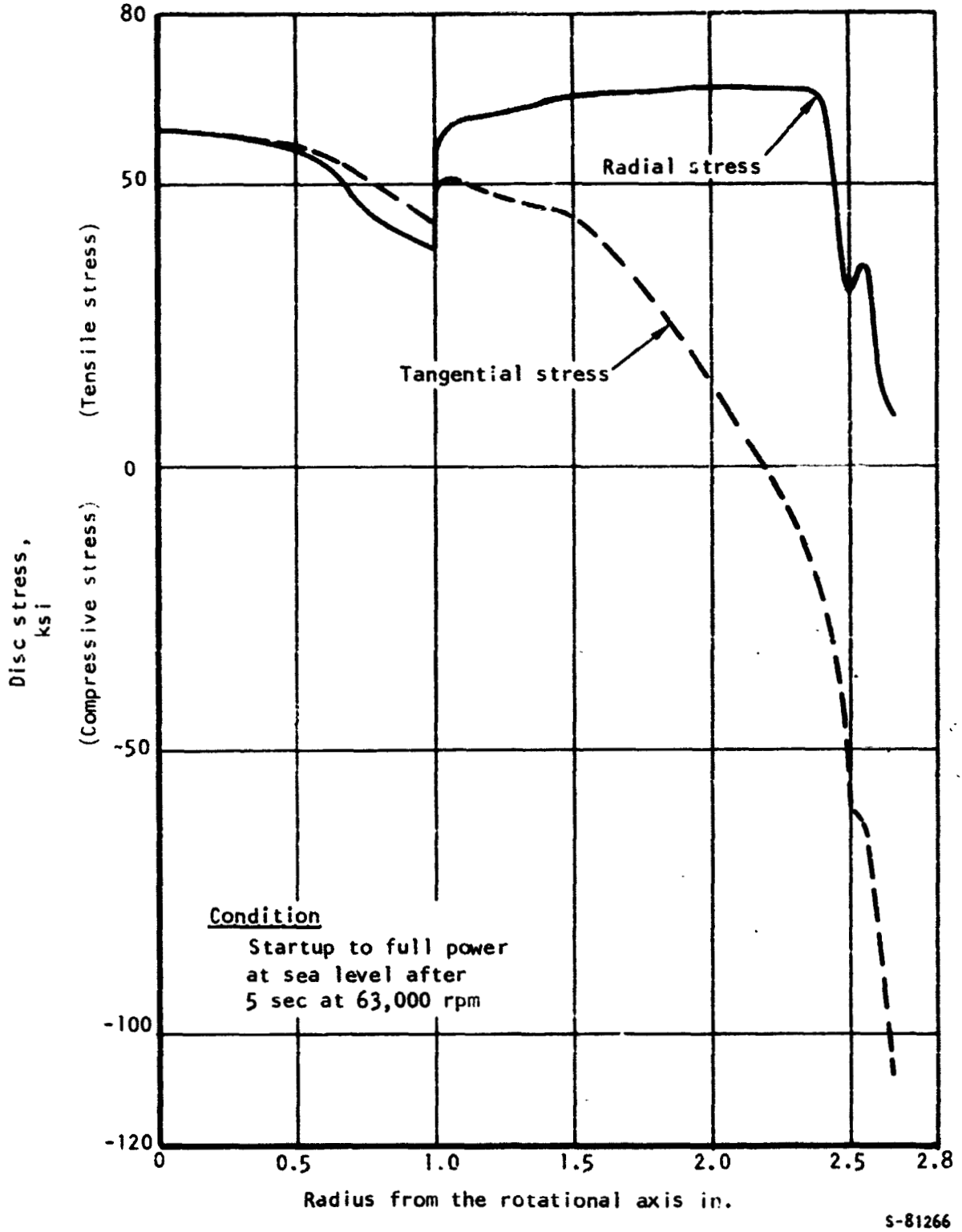

Figure 5-32.--First-Stage Turbine Wheel Disk Stress vs Radius.

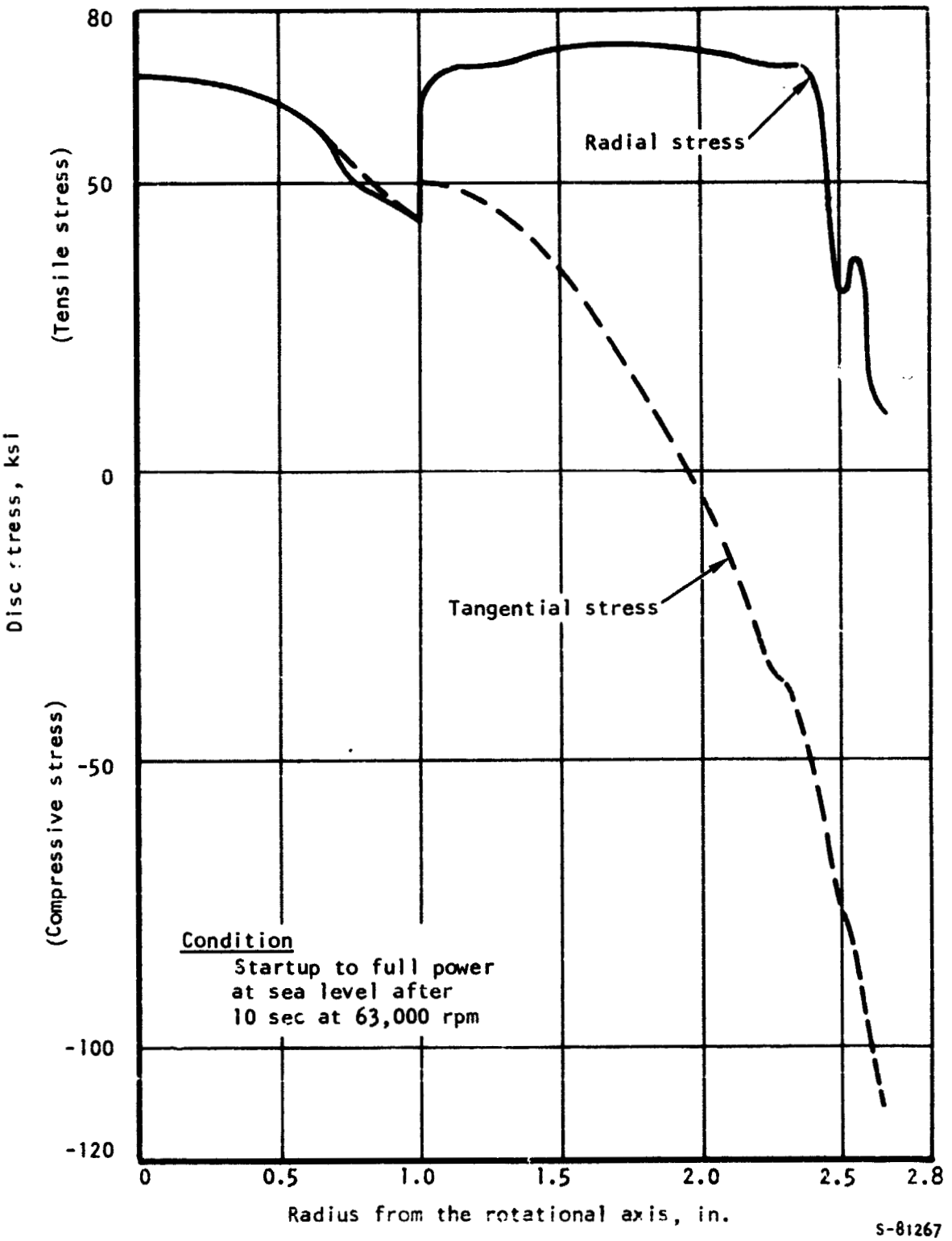

Figure 5-33.--First-Stage Turbine Wheel Disk Stress vs Radius.

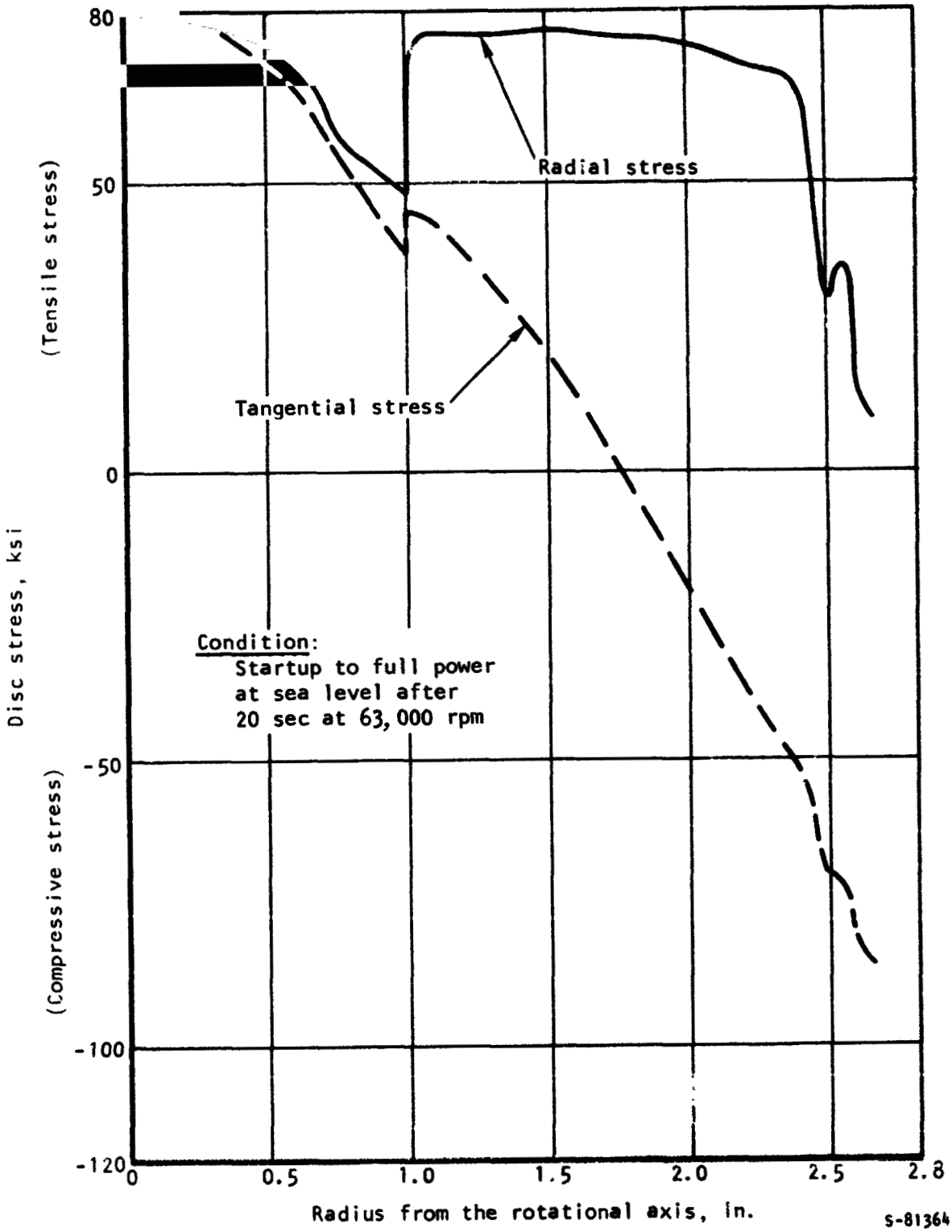

Figure 5-34.--First-Stage Turbine Wheel Disk Stress vs Radius.

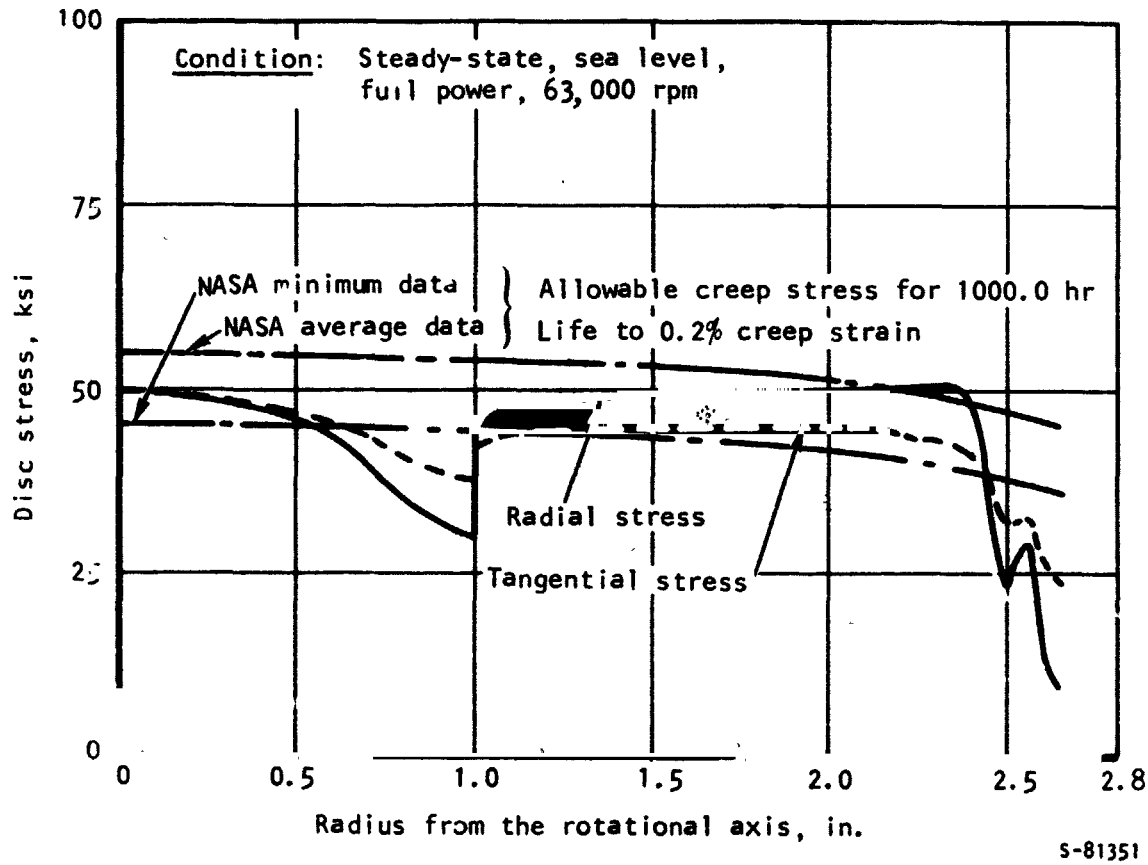

Figure 5-35.--First-Stage Turbine Wheel Disk Stress vs Radius.

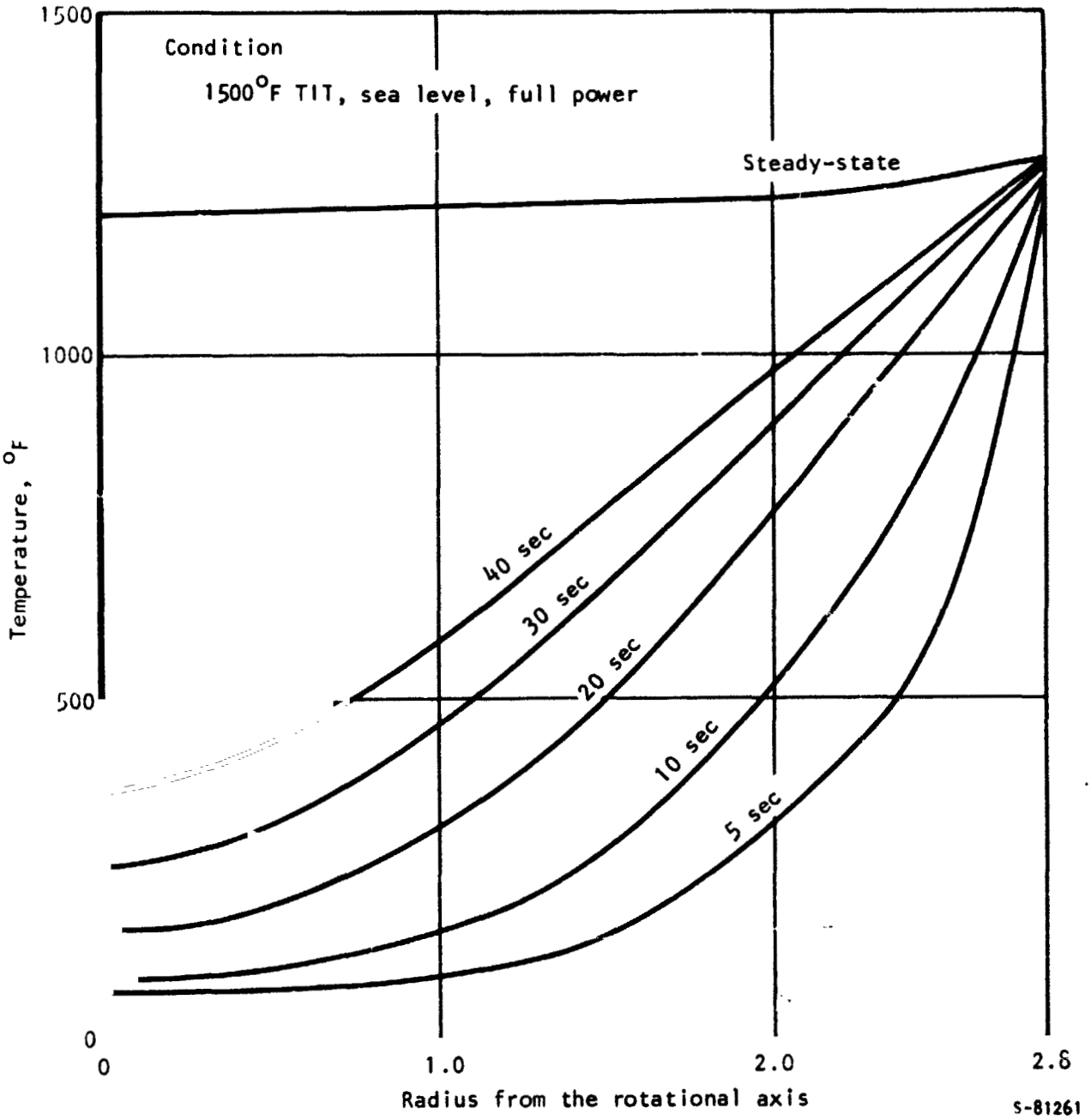

Figure 5-36.--First-Stage Turbine Wheel Temperature vs Radius.

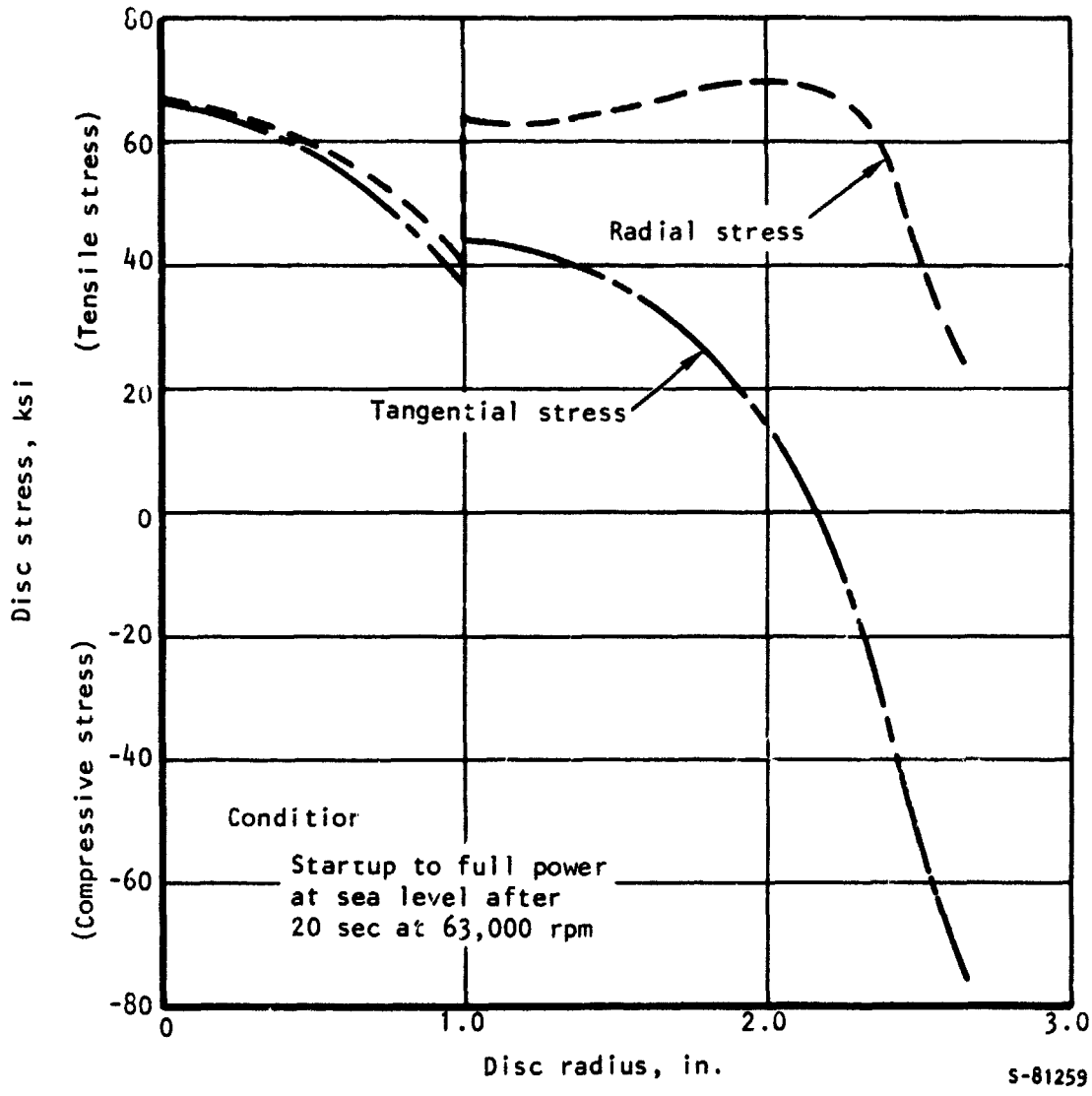

Figure 5-37.--Second-Stage Turbine Wheel Disk Stress vs Radius.

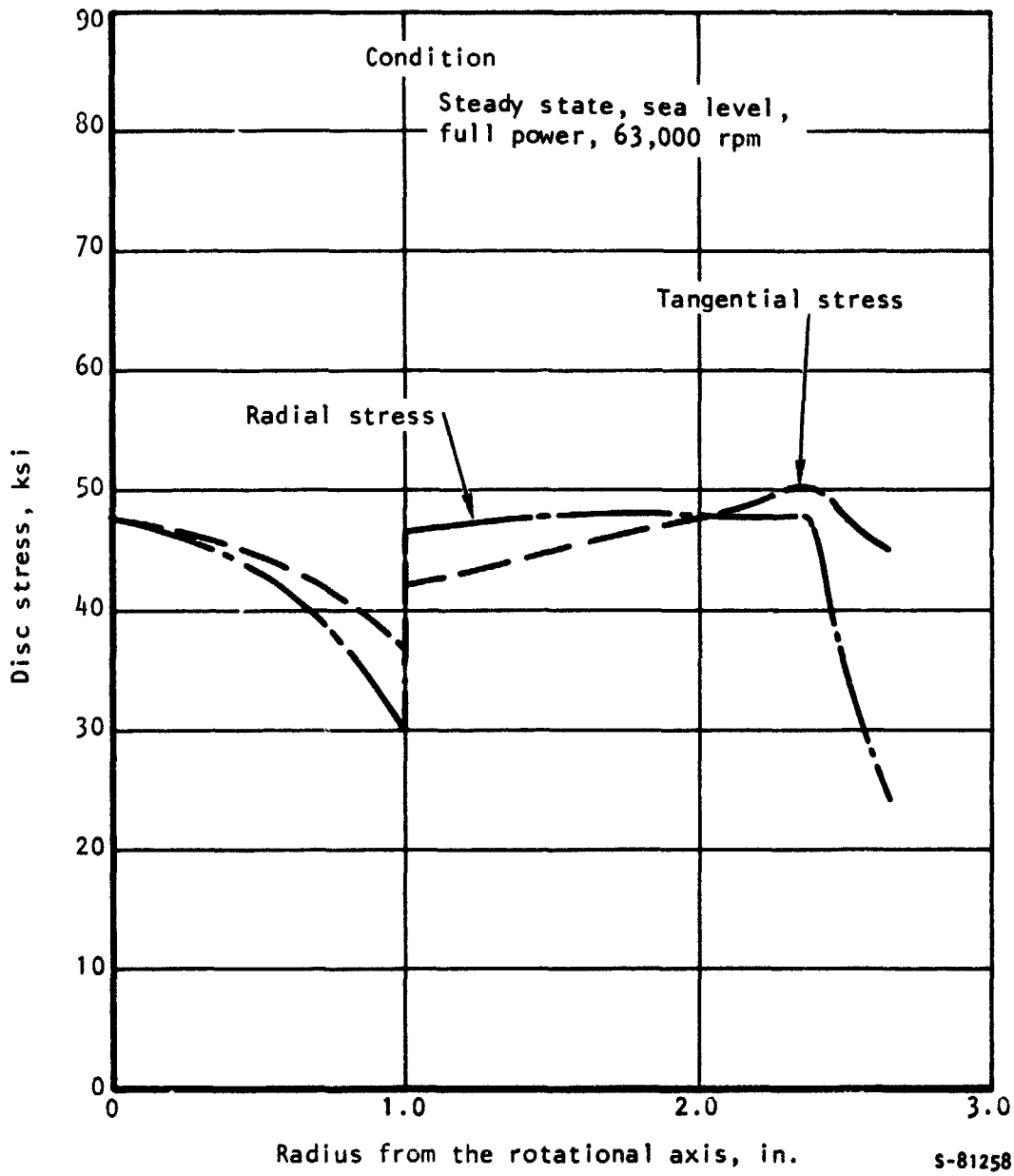

Figure 5-38.--Second-Stage Turbine Wheel Disk Stress vs Radius.

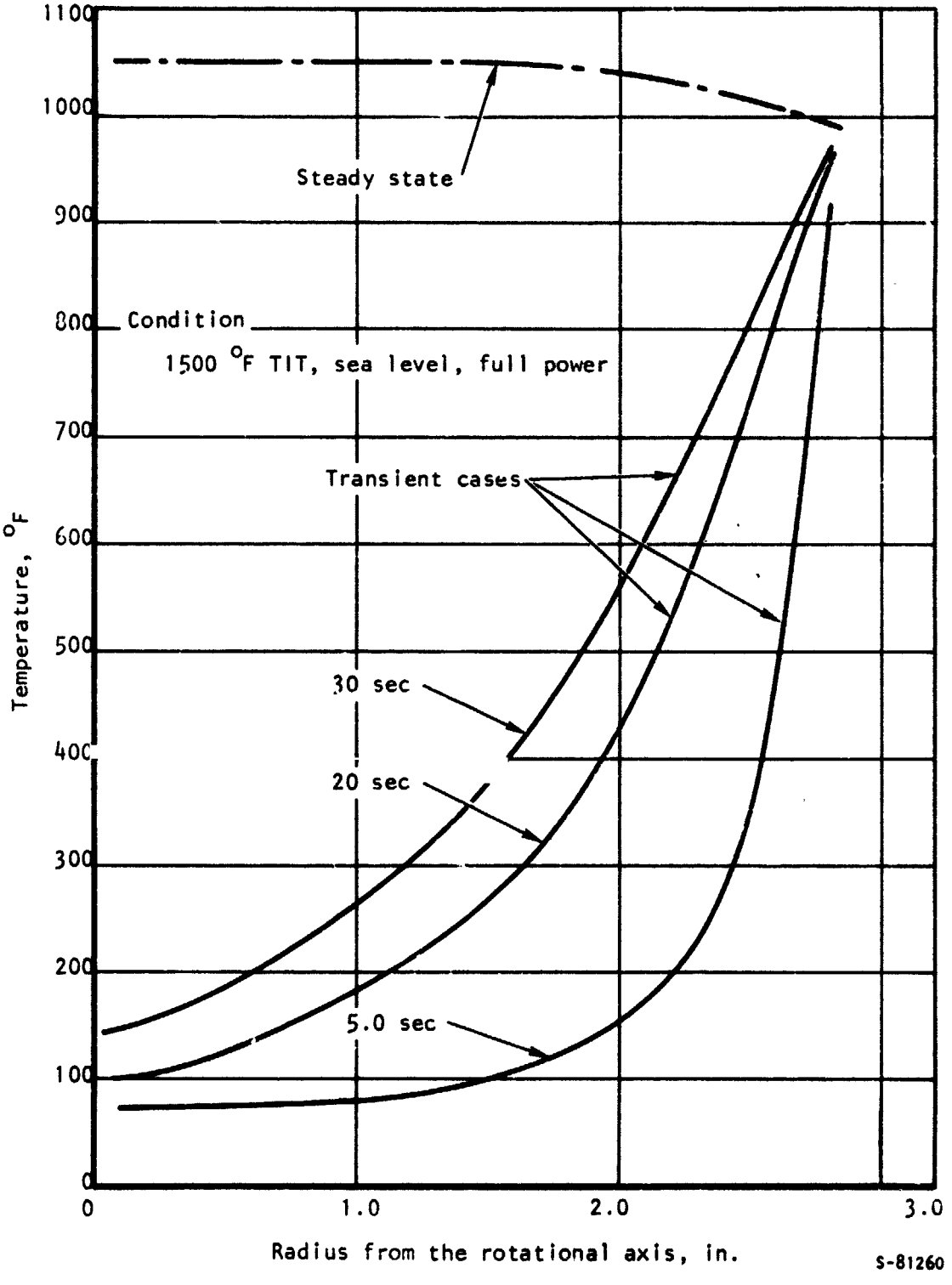

Figure 5-39.--Second-Stage Turbine Wheel Temperature vs Radius.

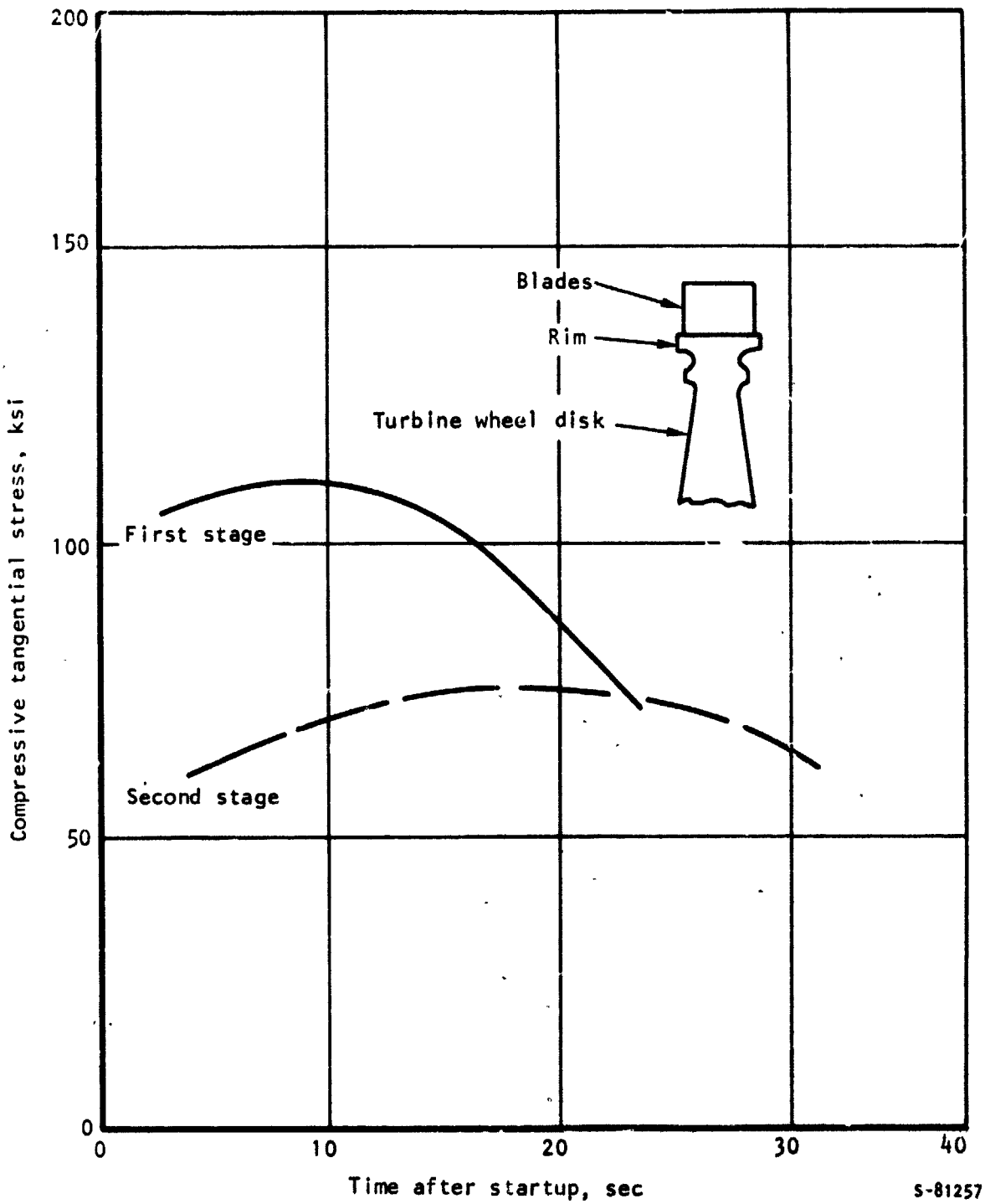

Figure 5-40.--Turbine Wheel Rim Transient Compressive Elastic Stresses.

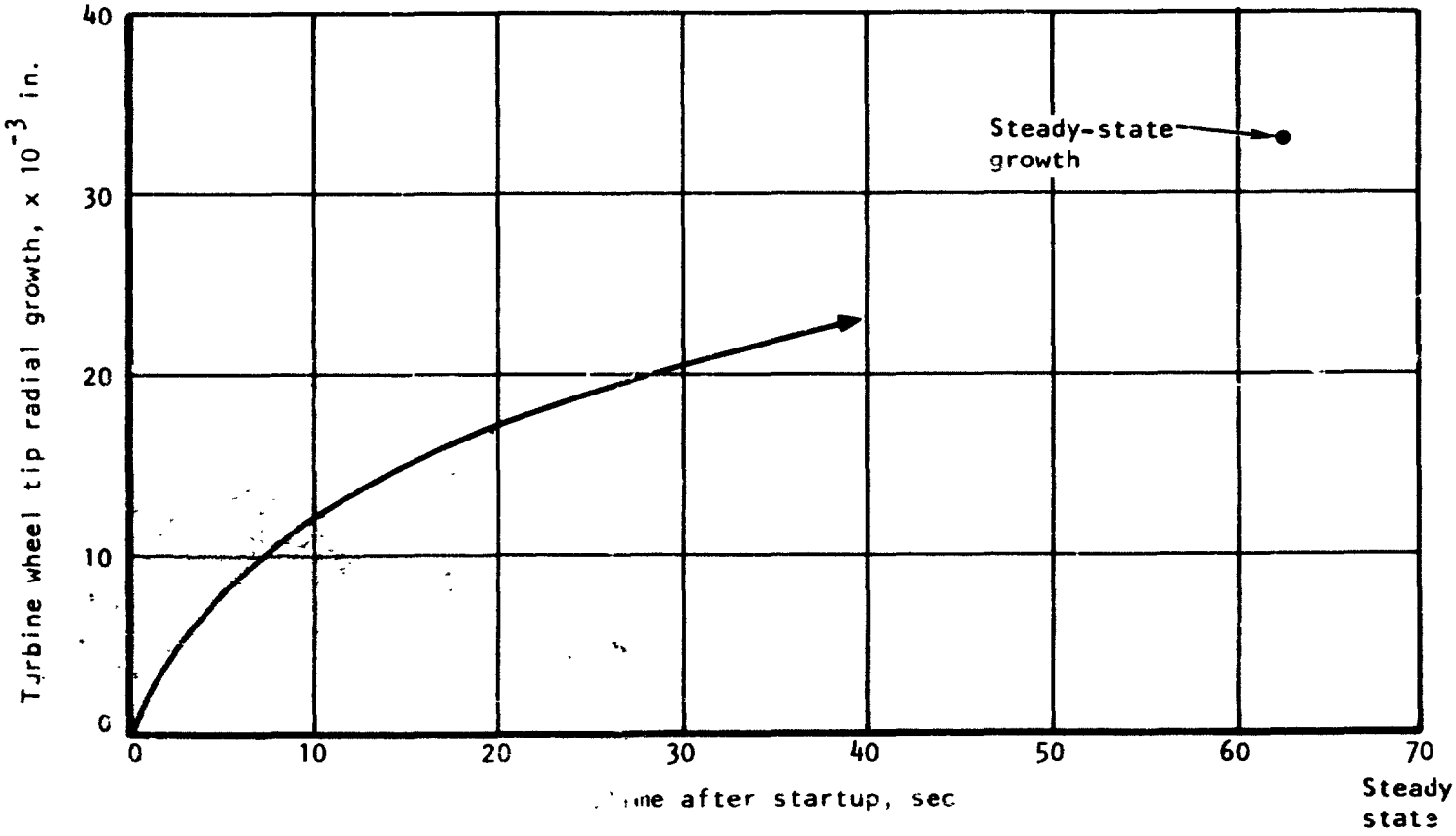

Figure 5-41.--First-Stage Turbine Wheel Transient Wheel Tip Radial Growth.

For turbine wheel operational life, the criteria investigated include fatigue, creep, and the combined effect of fatigue and creep. The analysis is centered on the bolt-hole region of the wheel and the disc rim, where theoretical stress concentration factors of 2.1 and 1.2 exist at the bolt hole and the rim, respectively.

Fatigue cycles to failure were determined by the AiResearch computer program, which uses the Wetzel-Morrow elastic-plastic method in combination with the Manson-Hirschberg universal slopes technique for predicting life. Scatter factors of 10 for high cycle fatigue and 3 for low cycle fatigue are applied to the calculated cycles to failure. Further, the 0.5 percent creep strain is considered a conservative rupture strain for determining the combined effect of fatigue and creep. The creep data for an austenitic alloy V-57, grade E (as obtained from NASA-Lewis) are shown in figs. 5-42 and 5-43.

The combined effect of fatigue and creep is based on the following cumulative damage theory:

$$\Sigma \frac{n}{N} + \frac{t}{C} = 1.0$$

where n = number of required stop-start duty cycles

N = cycles to failure

t = required operating hours

C = time to creep 0.5 percent strain

In the analysis, it is assumed that two stop-start duty cycles per 1-hr operation will occur. Since the first-stage turbine wheel is more critical than the second-stage wheel in terms of stress and thermal distribution, the analysis is conducted only for the first-stage wheel.

The result of the stop-start duty cycles at turbine bolt hole is shown in fig. 5-44. The effect of overspeed (to prestress the bolt hole) to 82,000 rpm prior to the first duty cycle is included in the analysis. At the design turbine speed of 63,000 rpm, the steady-state stress level during operation at the bolt hole, which is located 0.75 in. from the rotational axis, is 42.0 ksi (see fig. 5-35). This stress level at the wheel metal temperature of 1215°F determines the stop-start duty cycles of the wheel at the bolt hole. Assuming that the stress fluctuates from 0 to 42.0 to 0 ksi, the cycles to failure are 77,500 cycles. A typical computer output is shown in table 5-6. As shown in fig. 5-45, the time to creep 0.5 percent strain at 1215°F is approximately 10,000 hr.

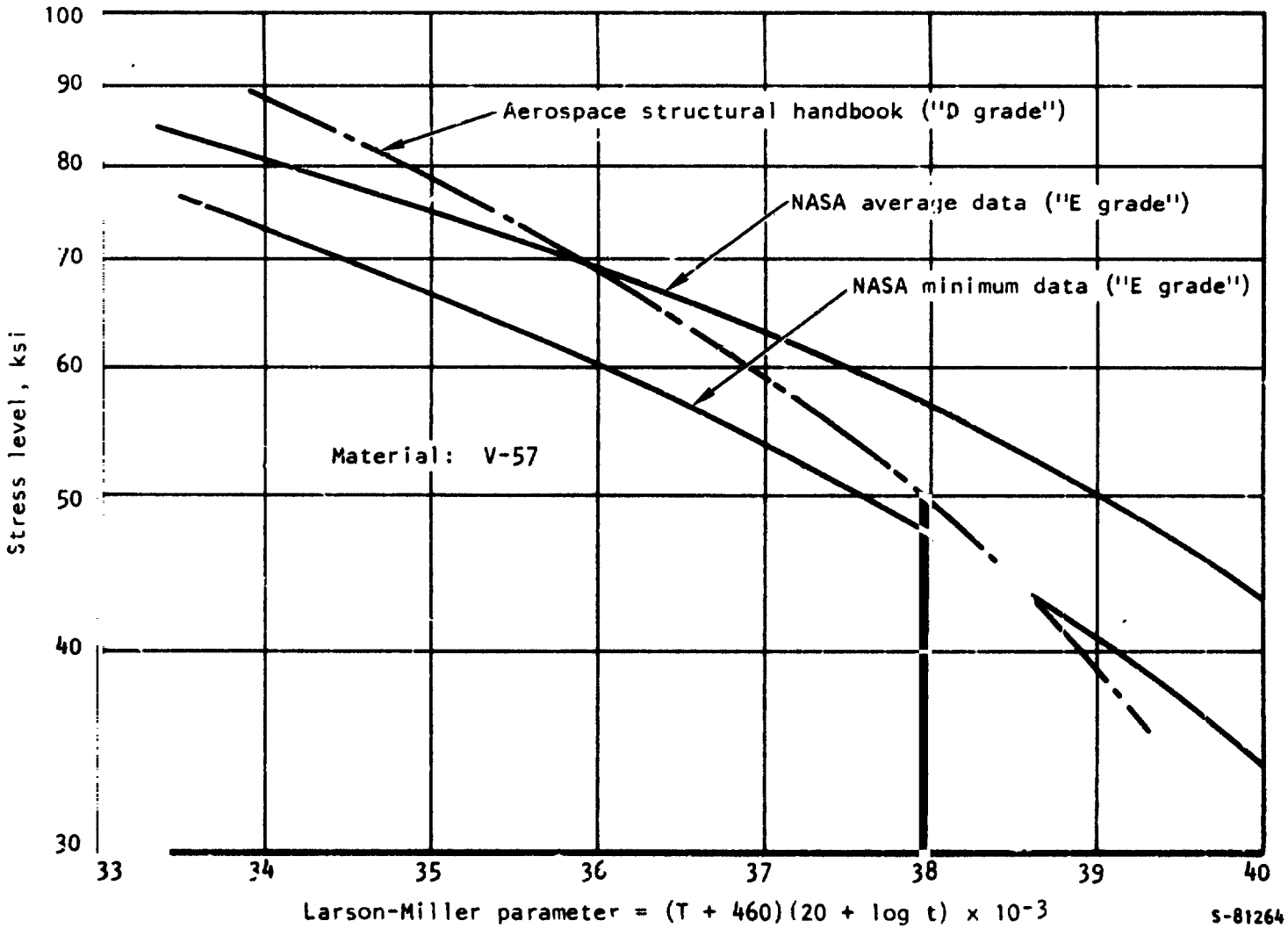

Figure 5-42.--Stress Level versus Larson-Miller Parameter for 0.2 Percent Creep Strain.

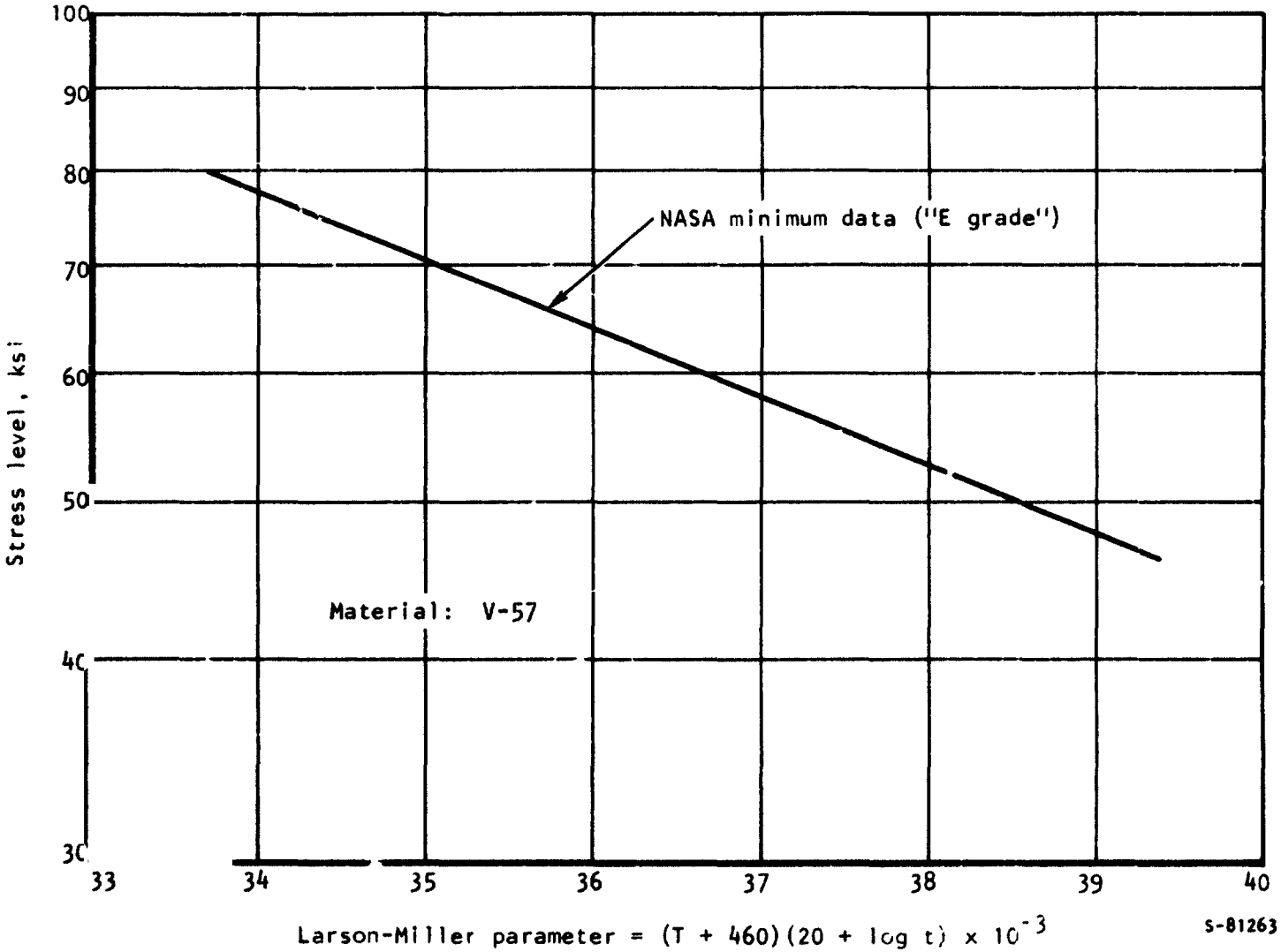

Figure 5-43.--Stress Level versus Larson-Miller Parameter for 0.5 Percent Creep Strain.

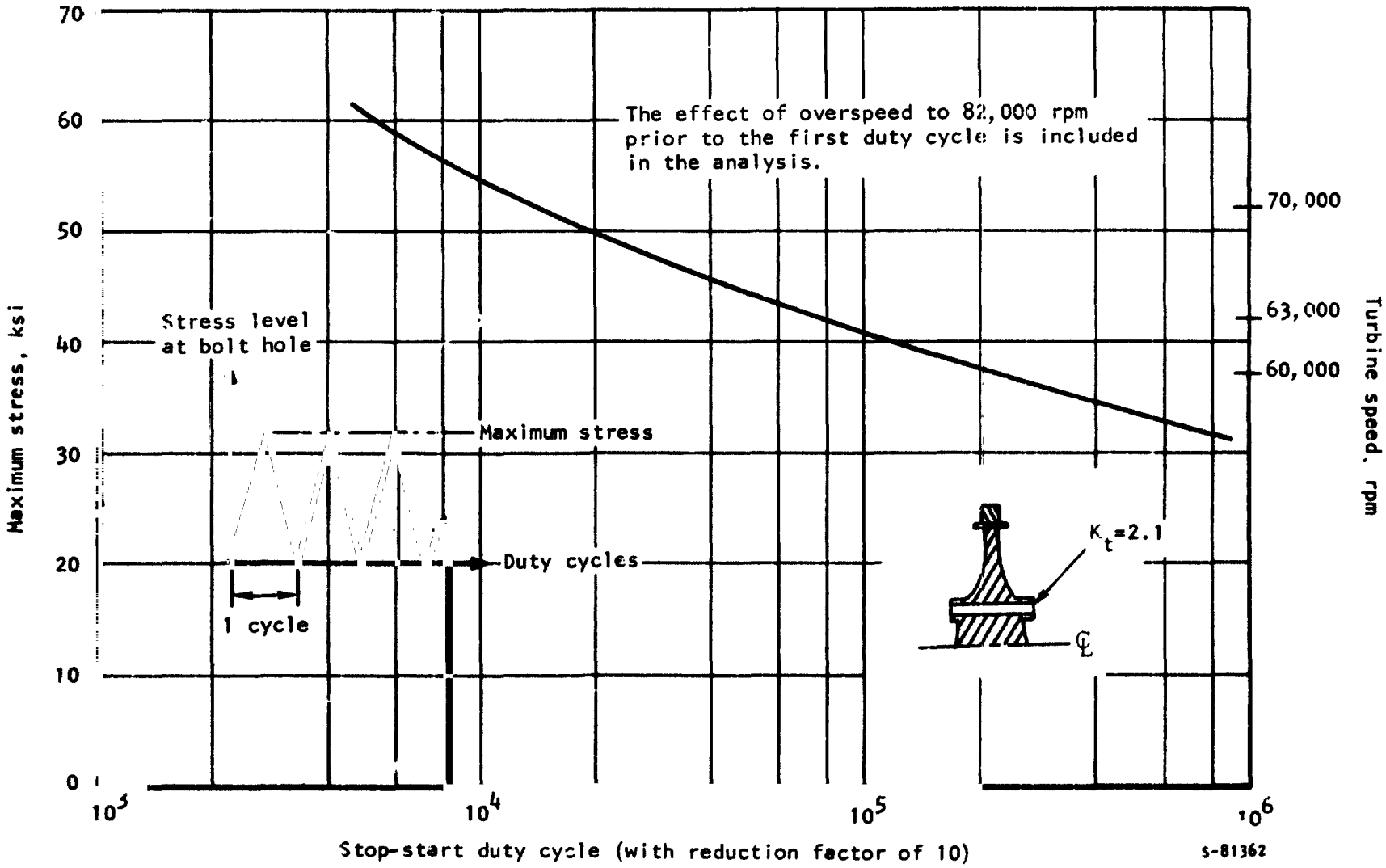

Figure 5-44.--First-Stage Turbine Wheel Duty Cycle at Turbine Bolt Hole (K_t = 2.1) at 1215°F.

TABLE 5-6

SPACE SHUTTLE APU FIRST STAGE TURBINE WHEEL BOLT HOLE FATIGUE ANALYSIS

STRESS CONCENTRATION FACTOR = 2.10
STRAIN CYCLING HARDENING EXPONENT .150
ULTIMATE TENSILE STRESS = 125000.
FAILURE TRUE STRESS = 167000.
FAILURE TRUE STRAIN = .287700

CYCLE	APPLIED ENGRG. NOMINAL STRESS (PSI)	TRUE STRESS THIS CYCLE (PSI)	TRUE STRAIN THIS CYCLE (IN/IN)	TRUE STRESS TOTAL (PSI)	TRUE STRAIN TOTAL (IN/IN)
1	.710000+05	.105531+06	.948901-02	.105531+06	.948901-02
2	.710000+05	.149365+06	.670428-02	-.438341+05	.278473-02
3	.420000+05	.873575+05	.401129-02	.435234+05	.679602-02
4	.420000+05	.873216+05	.401294-02	-.437982+05	.278308-02
5	.420000+05	.873541+05	.401144-02	.435559+05	.679452-02
6	.420000+05	.873249+05	.401279-02	-.437690+05	.278174-02
7	.420000+05	.873508+05	.401160-02	.435819+05	.679333-02
8	.420000+05	.873273+05	.401263-02	-.437464+05	.278070-02
9	.420000+05	.873402+05	.401172-02	.436018+05	.679242-02
10	.420000+05	.873309+05	.401251-02	-.437291+05	.277991-02

THE DIFFERENCE BET' 2 SUCCEFDING HYPERBOLAS IS LESS THAN 1 MICRO IN/IN

TOTAL STRAIN = .401251-02 IN/IN

LIFE OF UNIT AT ABOVE DELTA STRAIN = .775526+06 CYCLES
---.------ LIFE IS DETERMINED BY MANSON-HALFORD EQUATION.

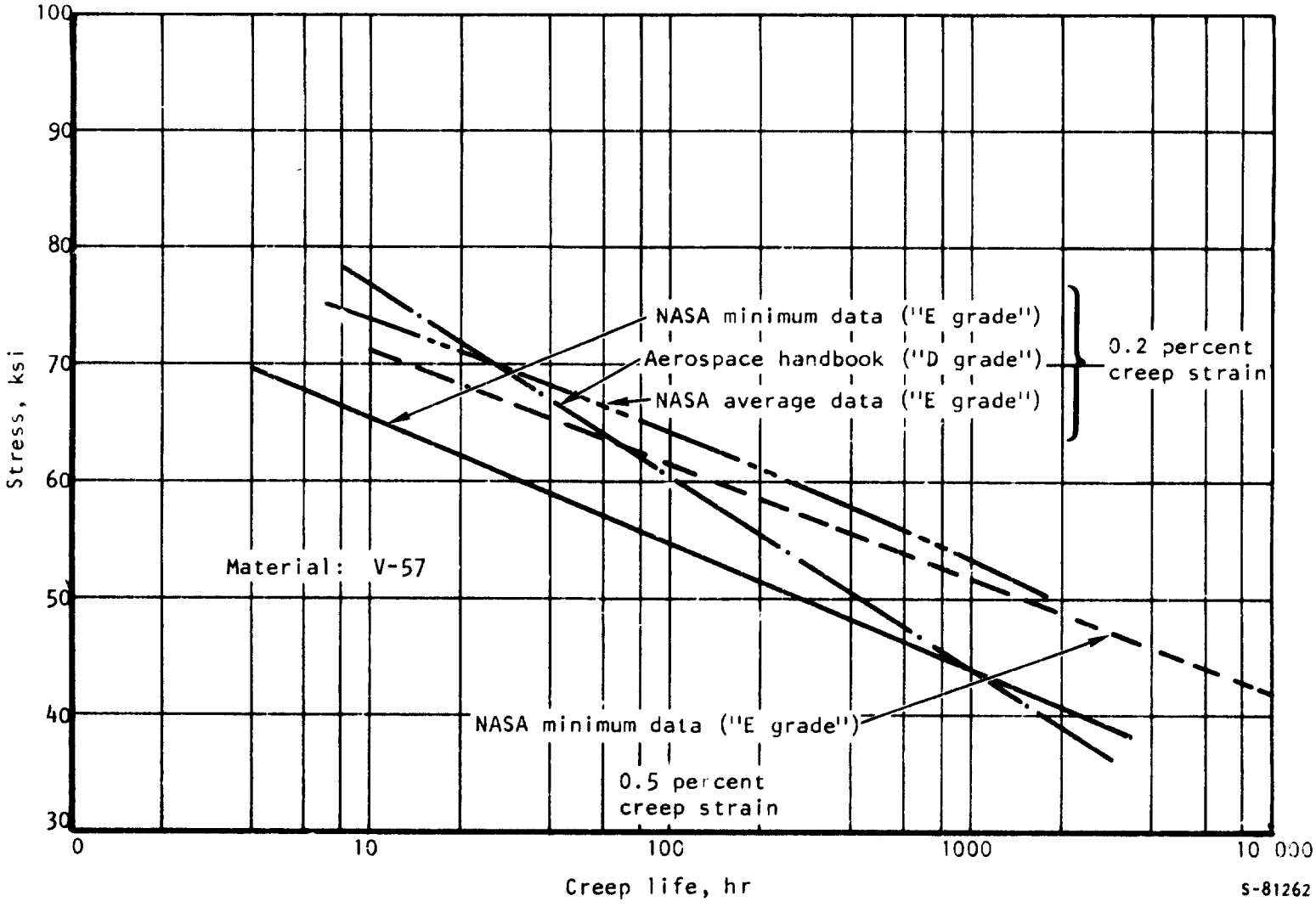

Figure 5-45.--Stress versus Time for 0.2 Percent and 0.5 Percent Creep Strain at 1215°F.

Combined fatigue and creep effects for the wheel at the bolt hole as a function of speed is given in fig. 5-46. The total operational life of the wheel at the bolt hole is 7900 hr and 15,800 duty cycles.

The operational life of the disc rim of the first-stage turbine wheel is controlled by fatigue. The creep damage to the rim is negligible because the stress level during the steady-state operation is low (see fig. 5-35). The result of the stop-start duty cycles at the disc rim is presented in table 5-7; (fatigue only) the operational life is 3210 hr and 6420 duty cycles, (combined fatigue and creep).

The total creep strain experienced by the first-stage turbine wheel during 1000 hr of operation will be approximately 0.2 percent strain (see fig. 5-26); the permanent radial growth of the wheel is 0.00583 in. at the end of 1000 hr operation.

Critical speed analysis.--A critical speed analysis of the rotating assembly was performed using an AiResearch critical speed analysis computer program. The analytical model and the critical speeds as a function of bearing resilient mount spring rate are shown in fig. 5-47. The resilient mount bearing stiffness is 60,000 lb/in. for both bearings. Shown in fig. 5-48 are the radial deflections at the first-stage turbine wheel with a maximum out-of balance tolerance of 0.02 gm-in. with no damping in the bearings.

Past experience has shown that traversing balanced rigid body modes will not produce any problems. As shown in figs. 5-47 and 5-48, the operating speed range is well clear of both rigid body and flexible modes.

Containment analysis:--The containment structural analysis was conducted to determine the geometrical requirements for the containmert structure for safely containing the turbine wheel fragments from a burst wheel. The design is intended to prevent the following two types of failure:

(1) Piercing--The thickness that prevents piercing the containment ring is selected on a basis that permits deformation up to the point of cracking the armor.

(2) Hoop burst--The quantity of ring material and its configuration is selected on a basis such that the total translational fragment energy in a wheel is absorbed by plastic deformation of the armor. The volume of the material selected is such that a tensile hoop failure of the armor is prevented.

AiResearch conducted numerous whirl-pit wheel burst tests using a variety of containments, wheel materials, and shapes. Based on the test data with theoretical interpretation, an empirical formula was developed to design a safe containment structure. The subject containment ring is designed to operate at the metal temperature of 500°F and will contain a quad-hub burst (because of four turbine bolt holes) of the wheel at the turbine speed of 113,400 rpm. The containment material is a maraging steel 18 Ni-250.

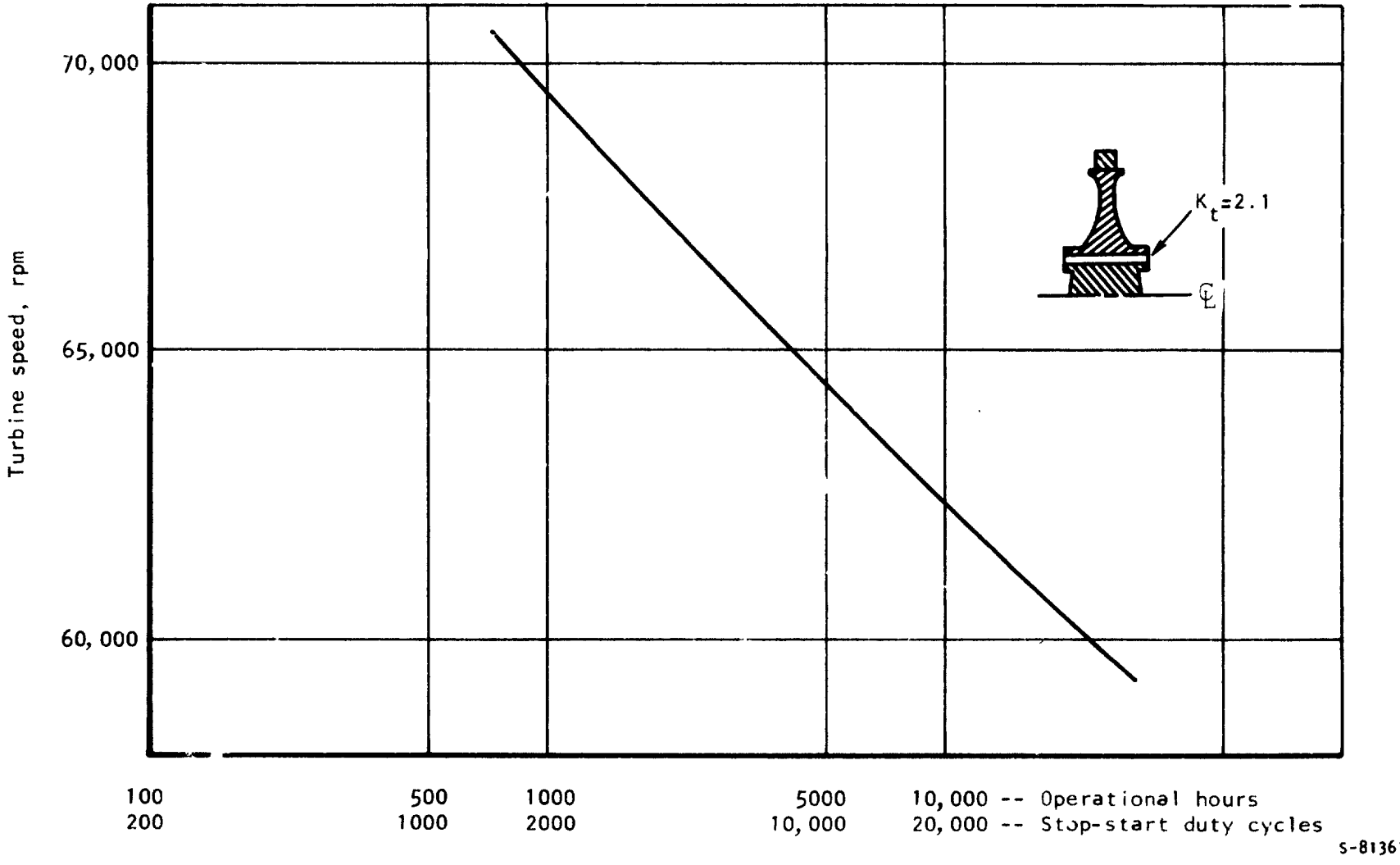

Figure 5-46.--First-Stage Turbine Wheel Operational Life vs Turbine Speed at Turbine Bolt Hole.

TABLE 5-7

SPACE SHUTTLE APU FIRST STAGE TURBINE WHEEL RIM FATIGUE ANALYSIS

STRESS CONCENTRATION FACTOR = 1.20
STRAIN CYCLING HARDENING EXPONENT .150
ULTIMATE TENSILE STRESS = 125000.
FAILURE TRUE STRESS = 167000.
FAILURE TRUE STRAIN = .287700

CYCLE	APPLIED ENGRG. NOMINAL STRESS (PSI)	TRUE STRESS THIS CYCLE (PSI)	TRUE STRAIN THIS CYCLE (IN/IN)	TRUE STRESS TOTAL (PSI)	TRUE STRAIN TOTAL (IN/IN)
1	.406000+05	.490175+05	.218127-02	.490175+05	.218127-02
2	.150600+06	.154146+06	.954394-02	-.105128+06	-.736267-02
3	.134000+06	.157675+06	.738678-02	.525472+05	.241090-04
4	.134000+06	.125078+06	.931189-02	-.725309+05	-.928778-02
5	.134000+06	.140093+06	.831384-02	.675624+05	-.973938-03
6	.134000+06	.136507+06	.853229-02	-.689442+05	-.950622-02
7	.134000+06	.137527+06	.846899-02	.685825+05	-.103723-02
8	.134000+06	.137260+06	.848547-02	-.686772+05	-.952270-02
9	.134000+06	.137330+06	.848114-02	.686527+05	-.104156-02
10	.134000+06	.137311+06	.848230-02	-.686584+05	-.952386-02
11	.134000+06	.137316+06	.848199-02	.686576+05	-.104187-02
12	.134000+06	.137315+06	.848205-02	-.686574+05	-.952392-02

THE DIFFERENCE BETWEEN 2 SUCCEEDING HYPERBOLAS IS LESS THAN 1 MICRO IN/IN

TOTAL STRAIN = .848205-02 IN/IN

LIFE OF UNIT AT ABOVE DELTA STRAIN = .965250+04 CYCLES
---------- LIFE IS DETERMINED BY MANSON-HALFORD EQUATION.

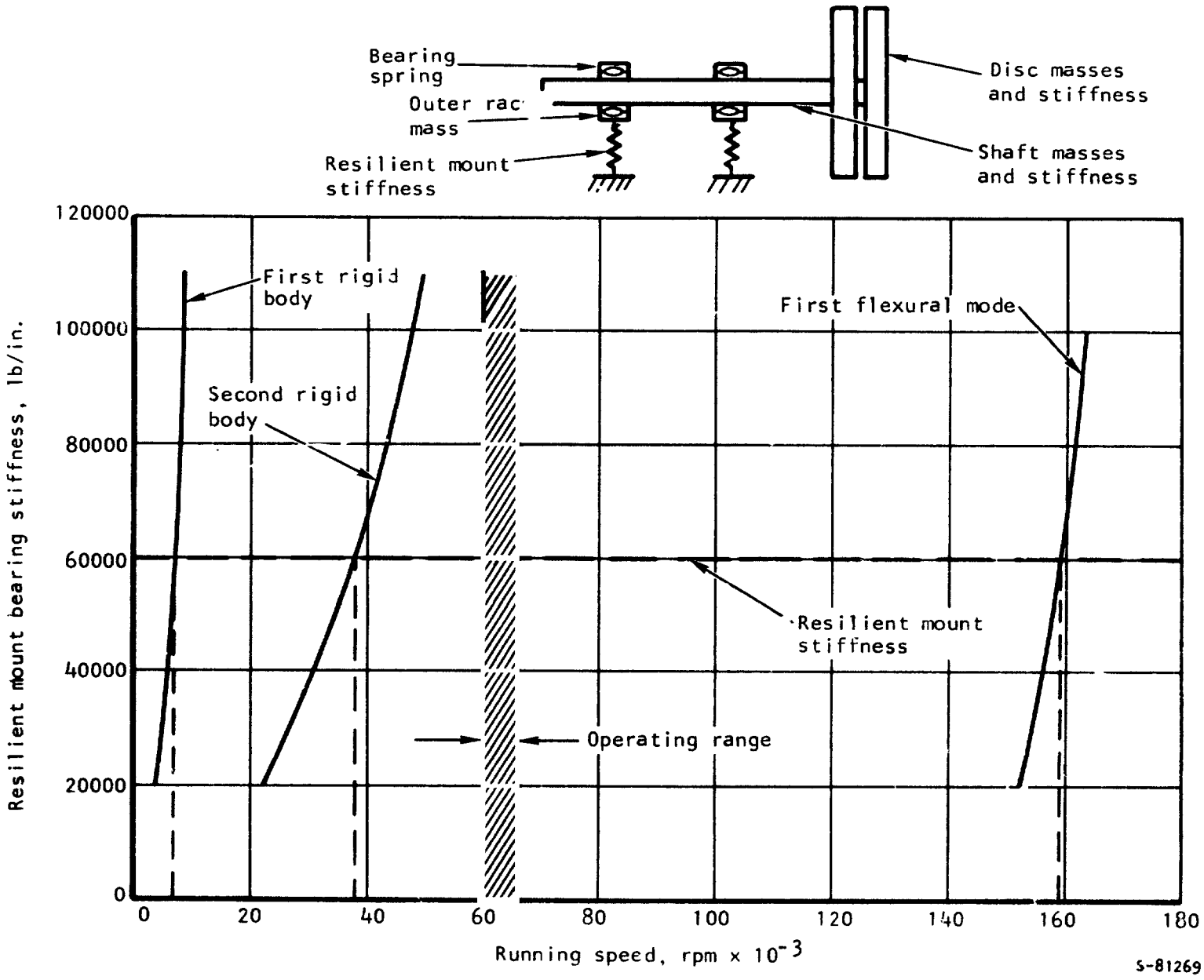

Figure 5-47.--Resilient Mount Bearing Stiffness vs Running Speed.

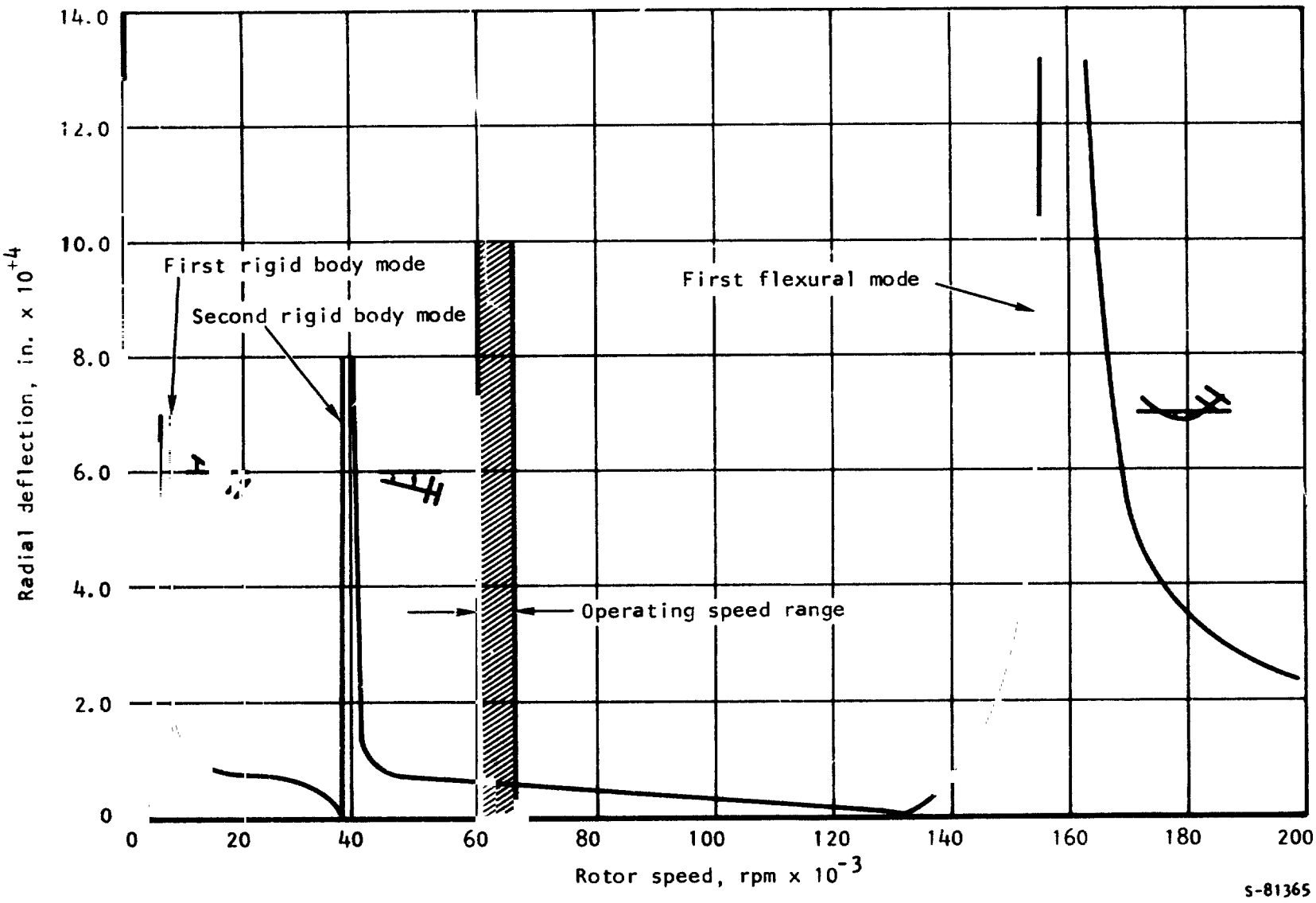

Figure 5-48.--First-Stage Wheel Radial Deflection vs Rotor Speed (Wheel Imbalance = 0.02 gm-in.).

Turbine wheel bolt analysis: The turbine wheel bolts used in assembling the first- and second-stage wheels to the rotor shaft are designed to take simultaneous loads from acceleration, vibration, gyroscopic, thermal, centrifugal, and wheel unbalance imposed on the two wheels during the APU operation. The pertinent design loads are listed in table 5-5.

The bolt preload is carefully determined so that no separation between the wheels and the rotor shaft occurs during the APU operation under the combined loads. Furthermore, the stress level at bolt operating temperature should be low enough such that only a negligible amount of bolt relaxation will result in 1000 hr of operation. An appreciable amount of relaxation will result in loss of preload and allow wheel separation from the rotor shaft under external loads. The bolt preload also must overcome axial disc shrinkage of the wheels due to centrifugal-thermal loads and relative thermal expansion of wheels and bolts.

Bolt material is an austenitic alloy V-57, which is the same as that used for the turbine wheels and thus minimizes the bolt preload required to overcome differential thermal expansion between bolt and wheel. The material exhibits good relaxation resistance and fatigue properties at operating temperature.

The required preload for room temperature assembly is 3443 to 3880 lb, and the nominal bolt stress levels are 71.30 and 80.0 ksi, respectively. At an operating speed of 63,000 rpm and operating temperature of 1100°F, the wheel bolt preload stress level becomes 26.1 to 33.0 ksi. This reduction in stress level is due primarily to the axial wheel shrinkage and the relative bolt-to-wheel expansion. As shown in fig. 5-49, bolt relaxation in 1000 hr is negligible at 1100°F and a stress level of 33.0 ksi. The stop-start duty cycle capability of the bolt at the thread root is 2500 cycles, with a reduction factor of 10 on the calculated 25,000 cycles.

Central tie bolt analysis: The central tie bolt used to assemble all the rotating assembly stacks (e.g., ball bearings, oil slingers, and a bearing spacer) as one rigid rotor is designed to take simultaneous loads from acceleration, vibration, gyroscopic, thermal, centrifugal, and wheel unbalance imposed on the two-stage wheels and on the rotor shaft during the APU operation. The pertinent design loads are listed in table 5-5. Based on the design criterion that no looseness is permitted in the rotating assembly during the APU operation, the bolt preload was determined so that no separation of the rotating assembly stacks occurs when subjected to various enternal loading conditions. Since the temperature of the compression stack is lower than that of the tie bolt during operation, a bolt consisting of Inconel 718 AMS 5662 was selected because its thermal coefficient of expansion is lower than that of the compression stack, and also it has good fatigue properties.

The required assembly preloads are 8970 to 10,140 lb, and the nominal bolt stresses are 112.3 and 127.0 ksi, respectively. Similarly, the steady-state operating stress levels in the bolt are 62.4 to 76.3 ksi. The stop-start duty cycles of the tie bolt at bolt head is approximately 10,000 cycles at the metal temperature of 850°F, with a reduction factor of 10 on the calculated cycles of 100,000 cycles. Creep was not critical because the stress and temperature levels are relatively moderate for Inconel 718.

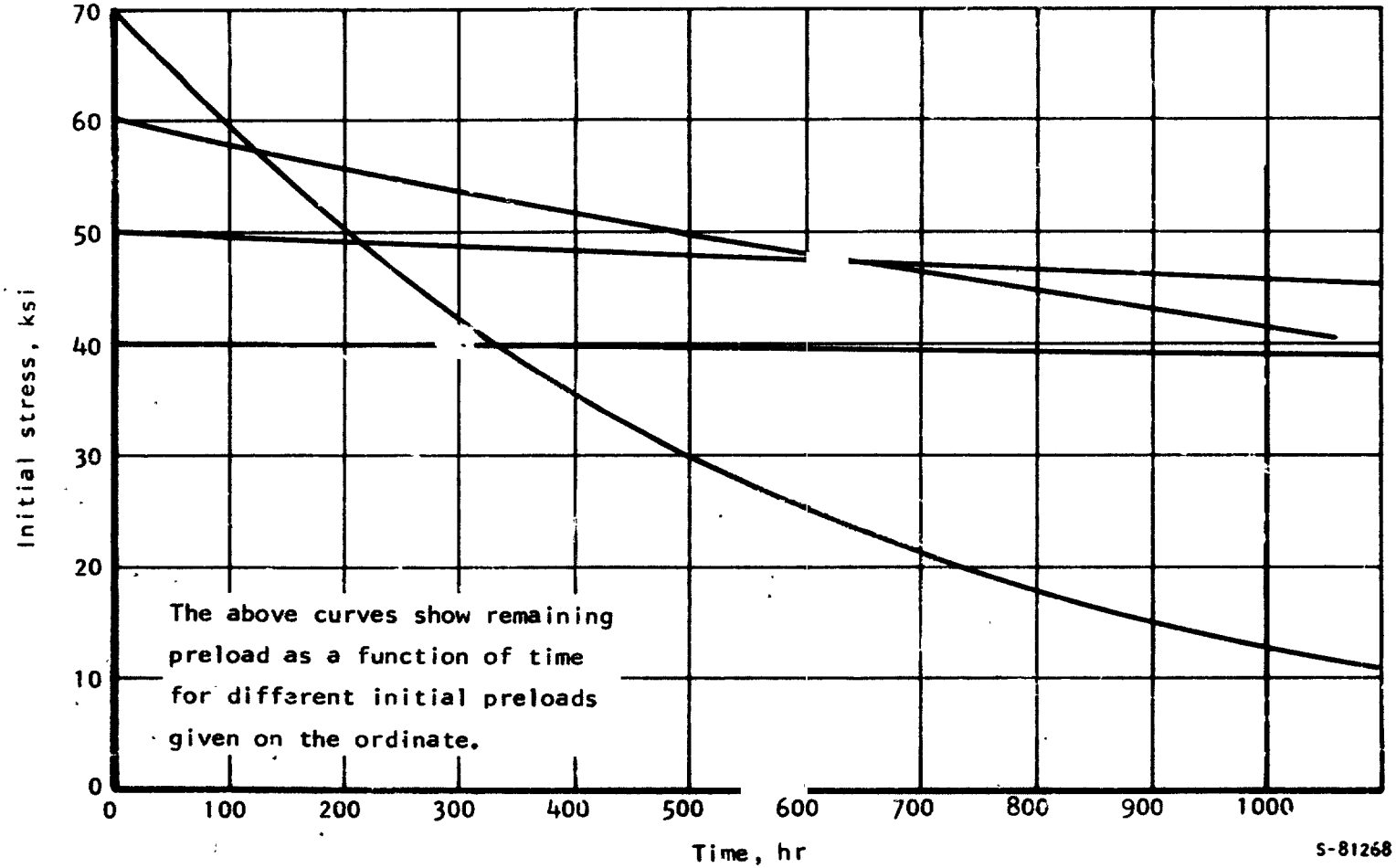

Figure 5-49.--Relaxation Stress vs Time for V-57 at 1100°F.

Static structure analysis: Critical areas of the static structure have been designed for 300 hr of ground testing. The thermal levels for this condition are 1500° and 1600°F TIT. Temperature gradients and operating pressures used in the analysis are listed in table 5-8. Structural items 1 through 6 (as defined in fig. 5-50) are considered to be critical, and detailed analyses were performed and adequate margins of safety established. Particular areas such as the inlet manifold flexible joint and the first- and second-stage seals (items 2, 3, and 4) have high transient temperature gradients during the startup phase of the operation; therefore, special attention was given to the load induced by the thermal differential deflection between the element and connecting structures.

A typical structural computer model is shown in fig. 5-51. This model is used for the stress analysis conducted for the first-stage seal (PN 581221-1.) The basic structural member incorporated in the computer program is a circular ring element having a triangular cross-sectional area. Each element is assumed to be isotropic, but temperatures, modulus of elasticity, and thermal coefficients of expansion are specified at each nodal point of the structural model. The pressures are assumed to be constant across each element surface and the temperatures are specified at each nodal point. Displacements for each nodal point and stresses (including the Von Mises effective stresses for each triangular element) are a computer output. Maximum stresses existing in items 1 through 6 and margins of safety for possible failure modes considered in the analysis are briefly summarized in table 5-8.

Gearbox Design

The preliminary design of the gearbox for the reference system is entirely different from the detail design of test system gearbox. A major consideration was fabrication cost of the test unit. Both designs are described below.

Zero-gravity-gearbox design.--This gearbox is a flight-type lightweight design incorporating zero-gravity (0-g) lubrication features and three power output pads, two for hydraulic pumps and a third for an alternator. It incorporates a carrier-gas lubricant scavenge system. Fig. 5-52 shows the gearbox design, which involves a nitrogen recirculating fan, gas passages to scavenge lubricant from the turbine carrier and alternator, and the centrifugal separator design to handle the carrier gas return flow.

Design requirements: The gearbox has the following design requirements:

Output pad for electrical alternator (12,000 rpm)

Output pads for hydraulic pumps (6000 rpm)

Means of circulating oil through the gearbox and the rotating assembly

Input pad for the rotating assembly (70,000 rpm)

Structural support for the entire turbine power unit

TABLE 5-8

STRESS AND SAFETY MARGIN SUMMARY

Operating loads						
Item*	Structural members	Material	Pressure level	Temperature gradient	Maximum stress	Margin of safety
1	Inlet manifold	Haynes 188	500 psig	1500°F uniform	10.9 ksi	Creep 0.95 percent strain at the end of 300 hr.
2	Inlet manifold flexible joint	Haynes 188	53 psig	800° to 1500°F	8.78 ksi at 1500°F	High. Creep 0.7 percent strain at the end of 300 hr.
3	First-stage seal	Haynes 188	53 psig	1250° to 1500°F	22.0 ksi at 1250°F	Stress level is well within the acceptable stress level. Three sigma minimum rupture stress at 1250°F in 300 hr is 43 ksi.
4	Second-stage seal	Haynes 188	66 psig	1250° to 1265°F	12.3 ksi at 1265°F	
5	Outlet manifold	Type 347 stainless steel	12.95 psi external pressure	1200°F uniform	External collapsing pressure = 59.5 psi	High. 4.5 for collapsing pressure.
6	Outlet manifold flexible joint	L-605	12.95 psi external pressure	500° to 1150°F	1.84 ksi at 1150°F	High. No creep problem because of low stress level.

NOTE: *Refer to fig. 4-50.

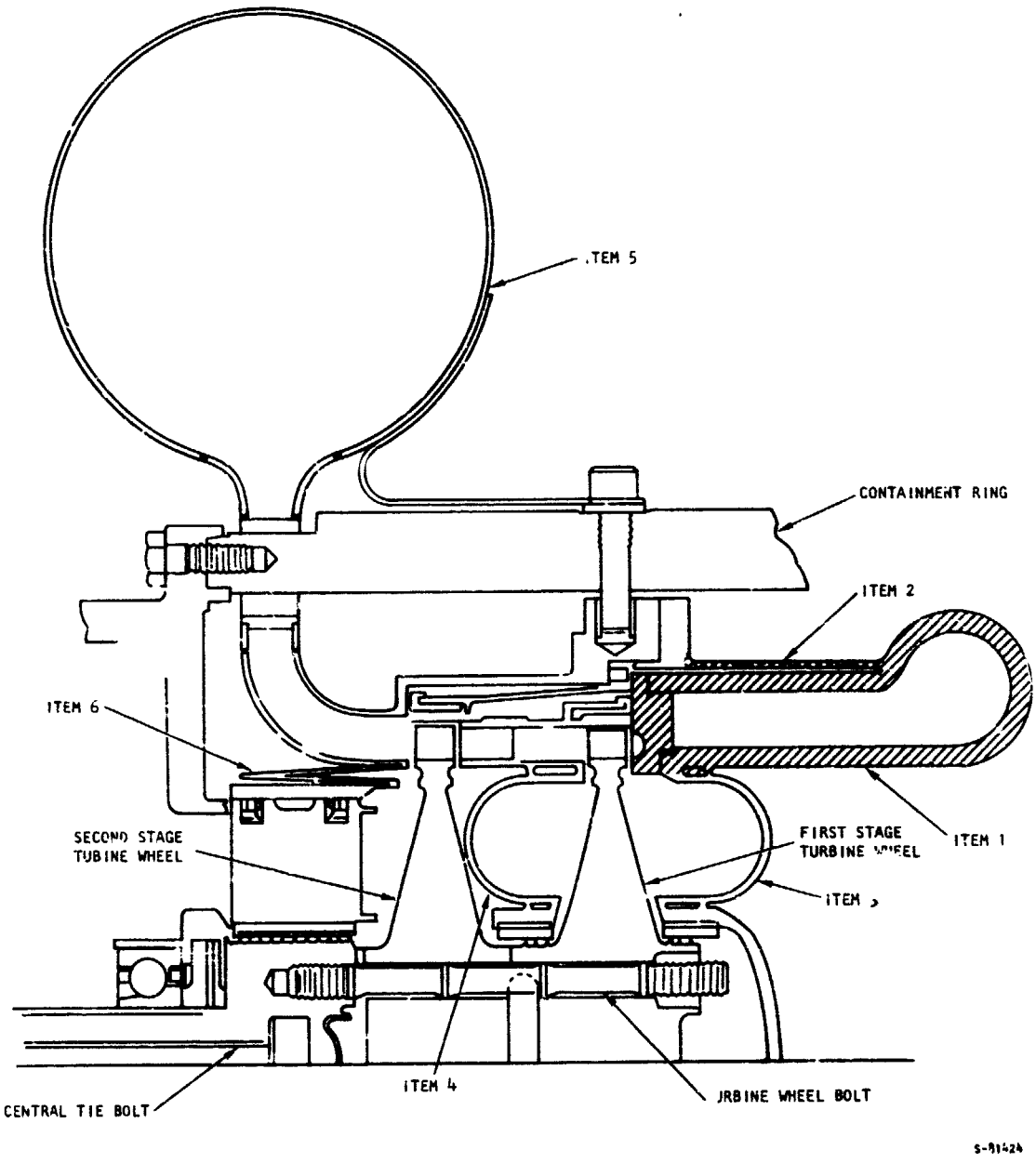

Figure 5-50.--Structural Item Definition.

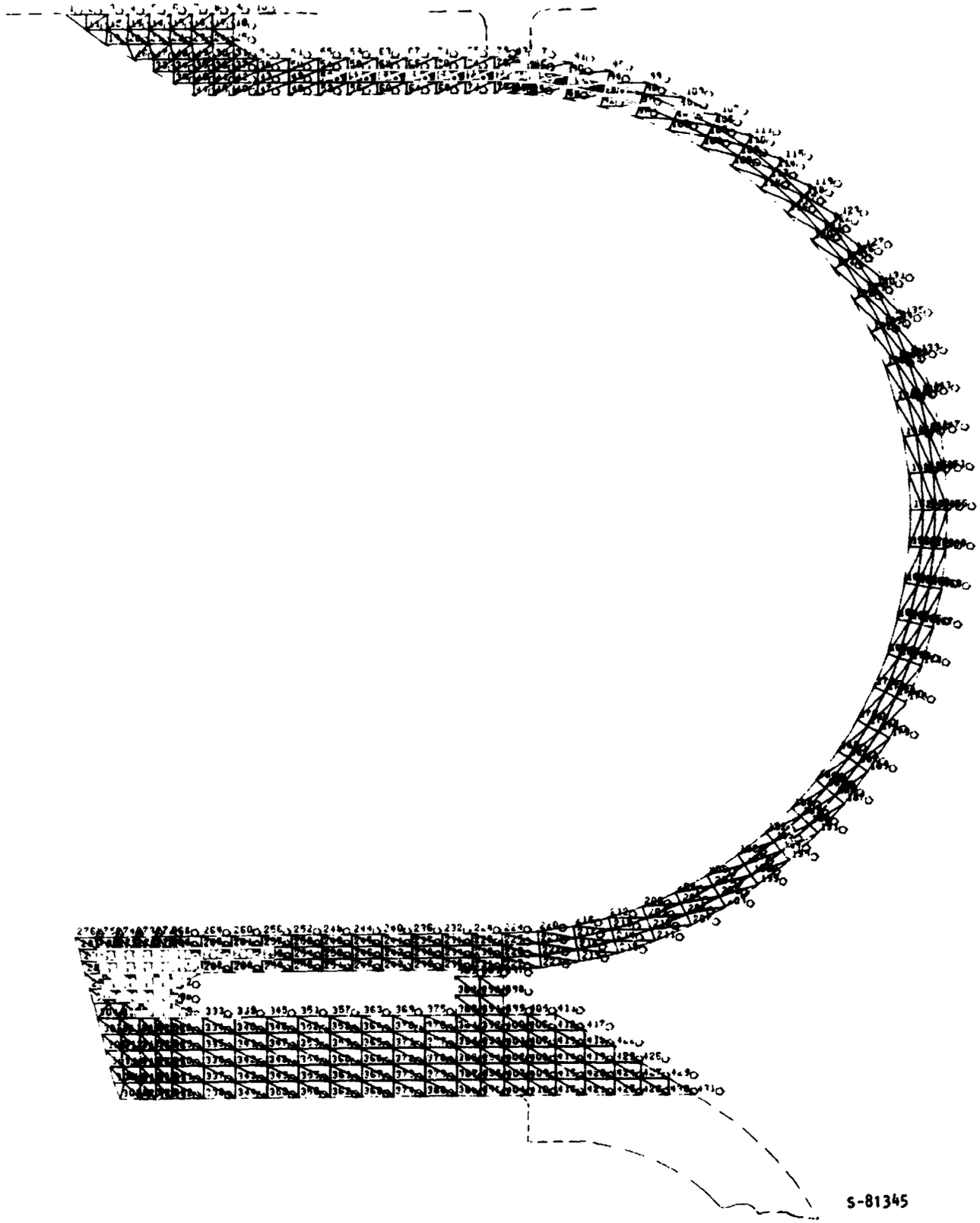

Figure 5-51.--Shuttle Seals Torus (First-Stage Seal (Item 3, Fig. 5-50) Triangular Element Computer Model).

FOLDOUT FRAME

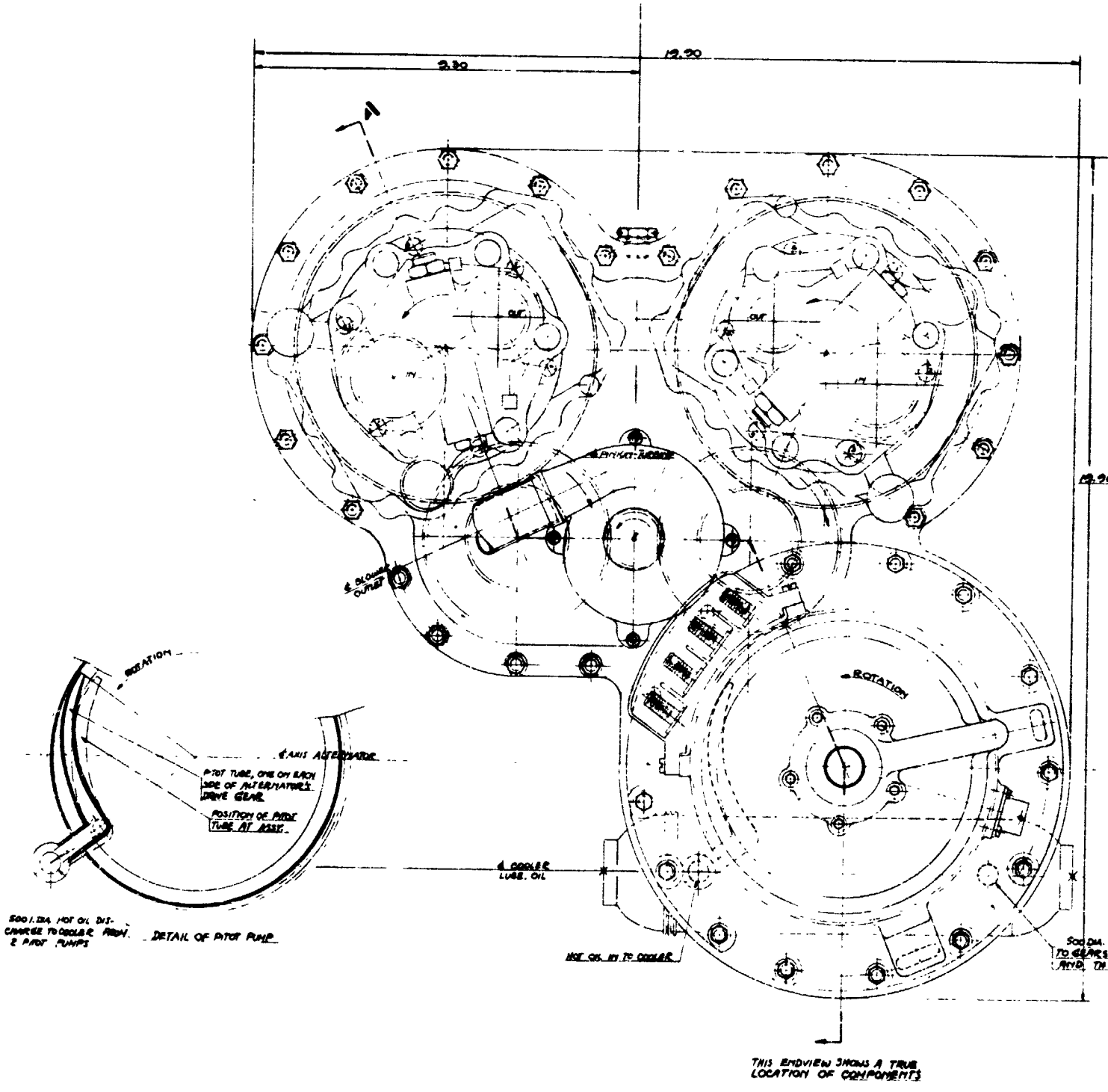

FOLDOUT FRAME

2

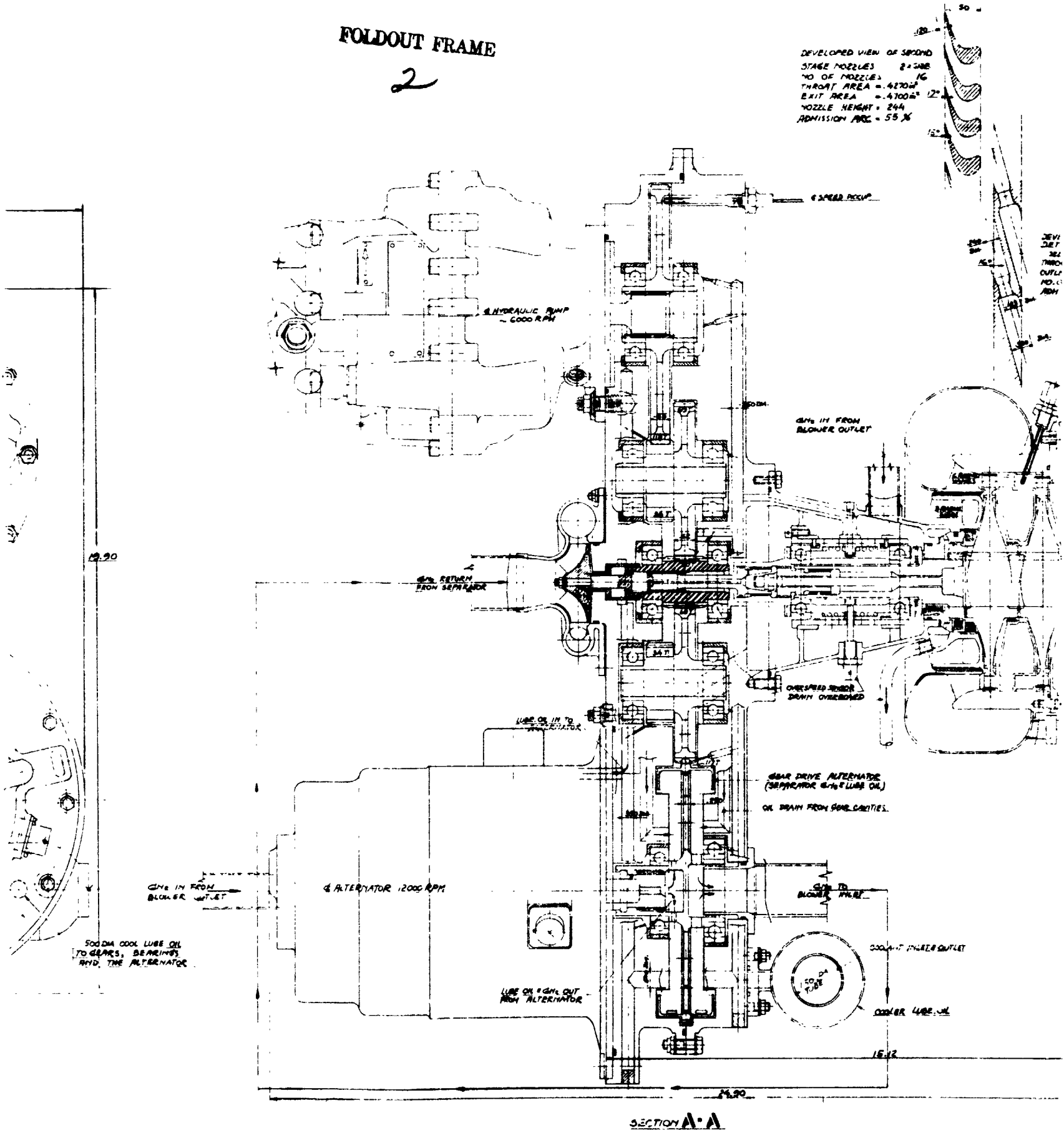

SECTION A-A

FOLDOUT FRAME

3

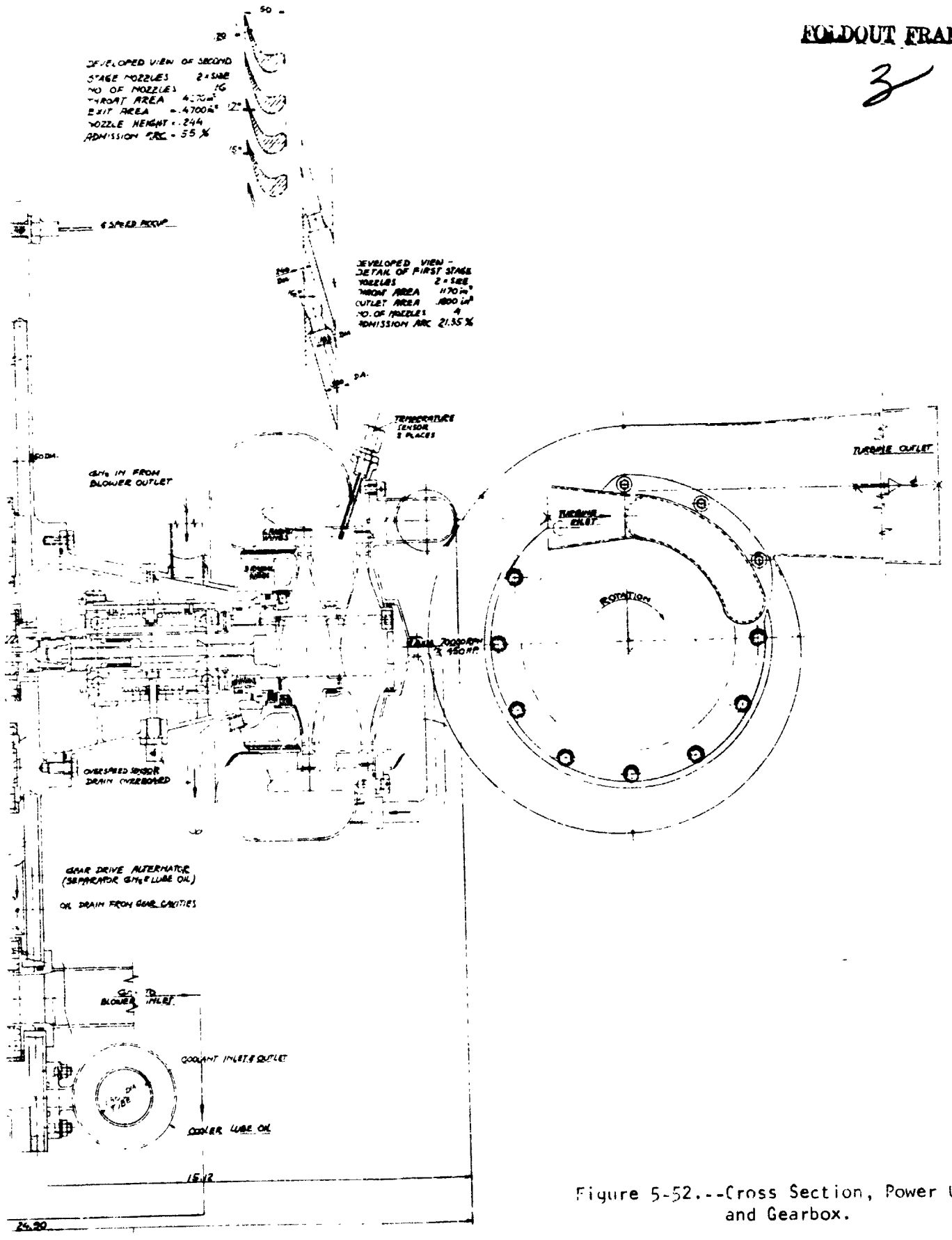

Figure 5-52.--Cross Section, Power Unit, and Gearbox.

The gearbox was sized to accommodate the following typical components:

Abex Model AP 27V-1 variable-delivery hydraulic pumps

Westinghouse Part No. 4QN60F alternator

Description: The gearbox shown in fig. 5-52 is a straight spur gear configuration with a single mesh reduction to the alternator and a double mesh reduction to each of the hydraulic pumps. This arrangement results in the minimum number of gears and a lightweight, close coupled, rigid housing assembly. Gear size and proportions have been computer designed and are based on a 20-deg tooth pressure angle. The tooth loading on the high-speed pinion and the pinion bearing load are the most critical parts of the entire assembly. AiResearch experience in similar designs indicates that conservative design values should be used in such cases, particularly where the pinion is driving a pulsating load such as a multicylinder, high-pressure pump. Accordingly, the pinion tooth Hertz stresses have been limited to 150 ksi.

Input drive to the gearbox is provided by a quill shaft connecting the turbine shaft and gearbox input shaft. Use of a quill shaft permits considerable freedom in the choice of the bearing mount flexibility and also minimizes the effects of alignment variances and torque pulsations.

The gearbox housing consists of a lightweight assembly of two halves, each of cast, ribbed construction. Housing material is 355 aluminum alloy. The requirements for lightweight, high rigidity, and minimum internal free volume for the oil are satisfied by this design.

The gearbox lubrication system is designed for operation in a zero-g as well as one-g environment. The concept used for circulating the oil mist through the gears and bearings is based on the NASA-sponsored technology developed in the Brayton cycle program. Some modifications have been made, however, to ensure that the oil mist is carried throughout the more complex gearbox.

The operation of the system is shown schematically in fig. 5-53. The oil and nitrogen gas are separated in the gearbox using the alternator gear as a centrifugal separator. The oil is then collected in the gear scoops and fed through the lubrication heat exchanger into two passages that distribute the oil to the alternator, bearings, and gear interfaces. The nitrogen gas is separated and fed out through the gear shaft into a nitrogen gas blower that distributes the gas through two passages, one to the alternator and one to the turbine bearing housing. The nitrogen mixture from the turbine housing and the alternator then enters the gearbox. Each of the four gears that drive the two pumps must be designed to collect the oil-foam mixture and direct the mixture to the alternator gear inner disk. This is achieved by minimizing the clearance volume around the gears and locating the baffling so that each gear will operate as a drag pump.

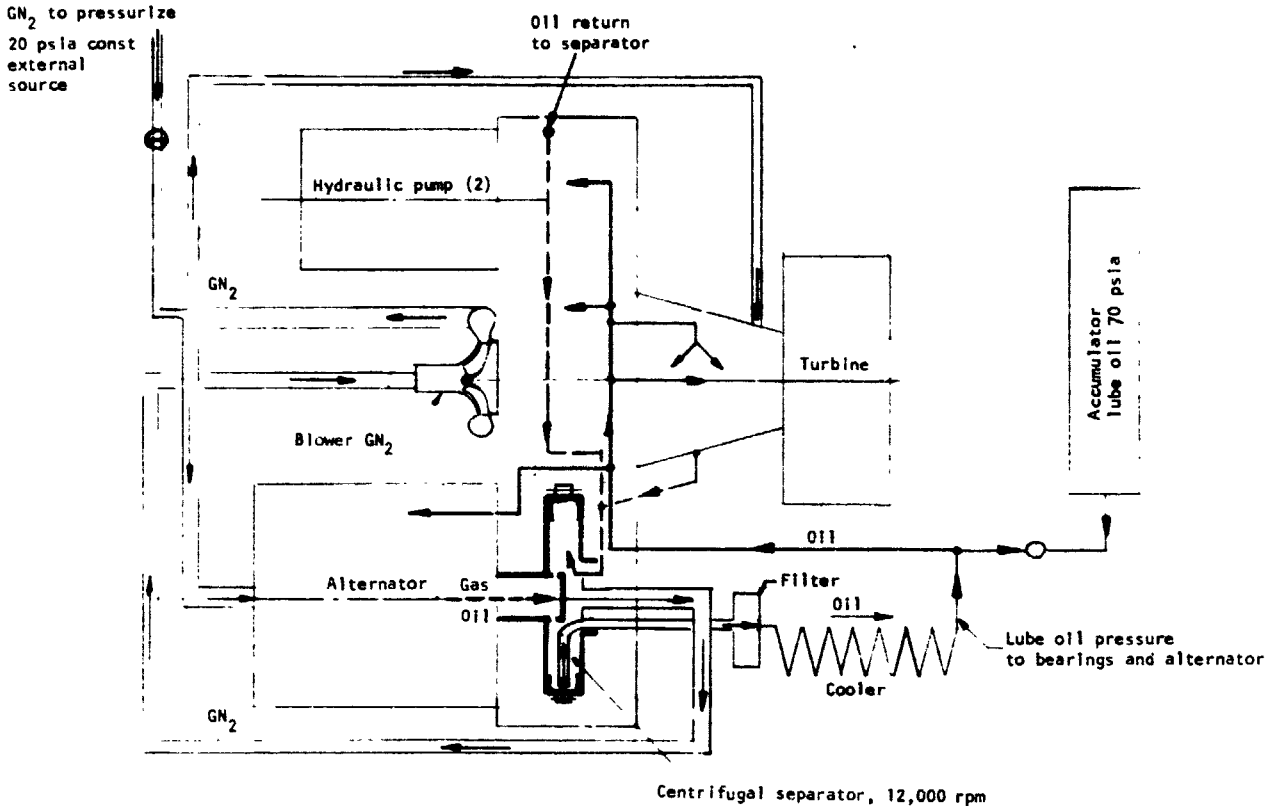

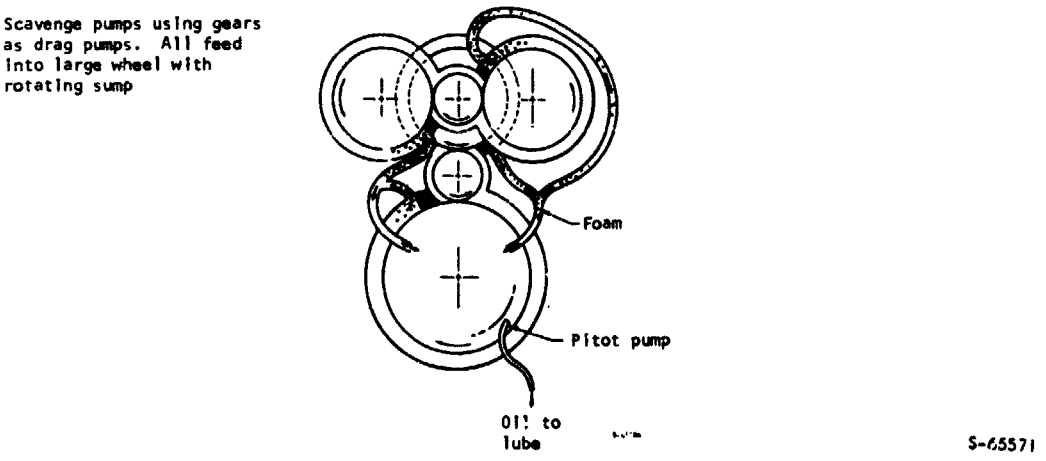

Figure 5-53.--Zero Gravity Lubrication.

Test system gearbox.--The test system gearbox will use many existing components. The starting point for the gear train design was the planetary gearbox manufactured for the Lockheed SST-ECS compressor, which was designed and tested to operate at comparable input speeds and horsepower. Two speeds were given: a turbine speed of 63,000 rpm and a hydraulic pump speed of 5000 rpm. In addition, the size of the two ABEX hydraulic pumps dictated the center spacing of the two output gears. The input horsepower from the turbine was given as 400. These basic parameters established the gearbox shown in the general cross section of dwg. 581193 and the gear train shown in fig. 5-54.

The first-stage speed reduction comprises an 18-tooth pinion, three 54-tooth planet gears with carrier, and a 126-tooth ring gear. This combination provides a reduction of 7:1, or an output speed of 9000 rpm. The carrier supporting the planet gears is nonrotating. An arrangement of a cluster of three planets around the pinion reduces the load on the pinion gear teeth, and the radial loads on the pinion bearings. This is critical when pinion speeds of approximately 63,000 rpm are considered. The pinion is supported by two ball bearings, preloaded in one direction by a coil spring. A quill shaft transmits the torque from the turbine to internal splines in the pinion. The torque from the pinion is divided between three planet gears that rotate on bushings about fixed pins in the carrier. The planet gears also engage the ring gear, made somewhat flexible by its small radial thickness and its external spline connection to the ring gear hub. Flexibility of the ring gear will compensate for inaccuracies in the gear system, assuring more equal load sharing between the three planet gears.

The ring gear hub is pinned to the 9000-rpm pinion and held axially by a locknut on the end of the shaft. Torque from this gear is split equally between the two mating gears, and the speed is reduced to an output rmp of 5000 by the tooth ratio of 55:95. By placing of the two output gears symmetrically about the pinion, the load on the pinion bearings becomes negligible. The two shaft of the output gears are provided with internal splines for coupling to two ABEX hydraulic pumps.

As shown in fig. 5-54, the housing for the gearbox is made of two slabs of aluminum joined together on the vertical face. All bearings are installed in steel bushings that are bolted and shrunk in the aluminum housing and line-bored in place. The steel planet carrier is attached to the turbine side aluminum housing, and becomes the basis for the location of the other bearings. It carries the high-speed planet bearings and provides support for one of the 9000-rpm pinion bearings.

The gearbox and the turbine are lubricated by an external oil supply distributed to the gears and bearings as shown in fig. 5-55. Oil to the high-speed turbine bearings is supplied from the gearbox and enters the turbine bearing carrier via a coupling tube. In the turbine bearing carrier, one jet lubricates each bearing, and the oil is returned to the sump by means of an oil slinger. Oil for cooling the turbine bearings enters the tube shown at the

FOLDOUT FRAME

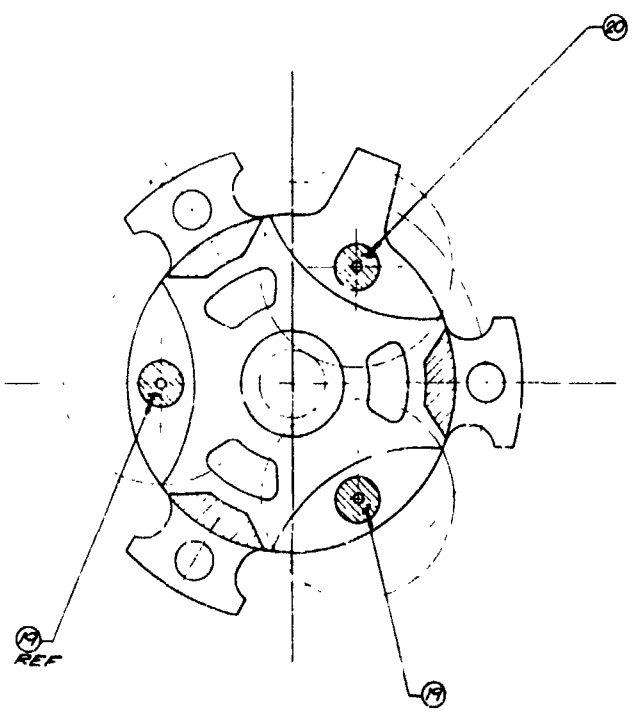

SECTION Z-Z

FOLDOUT FRAME

2

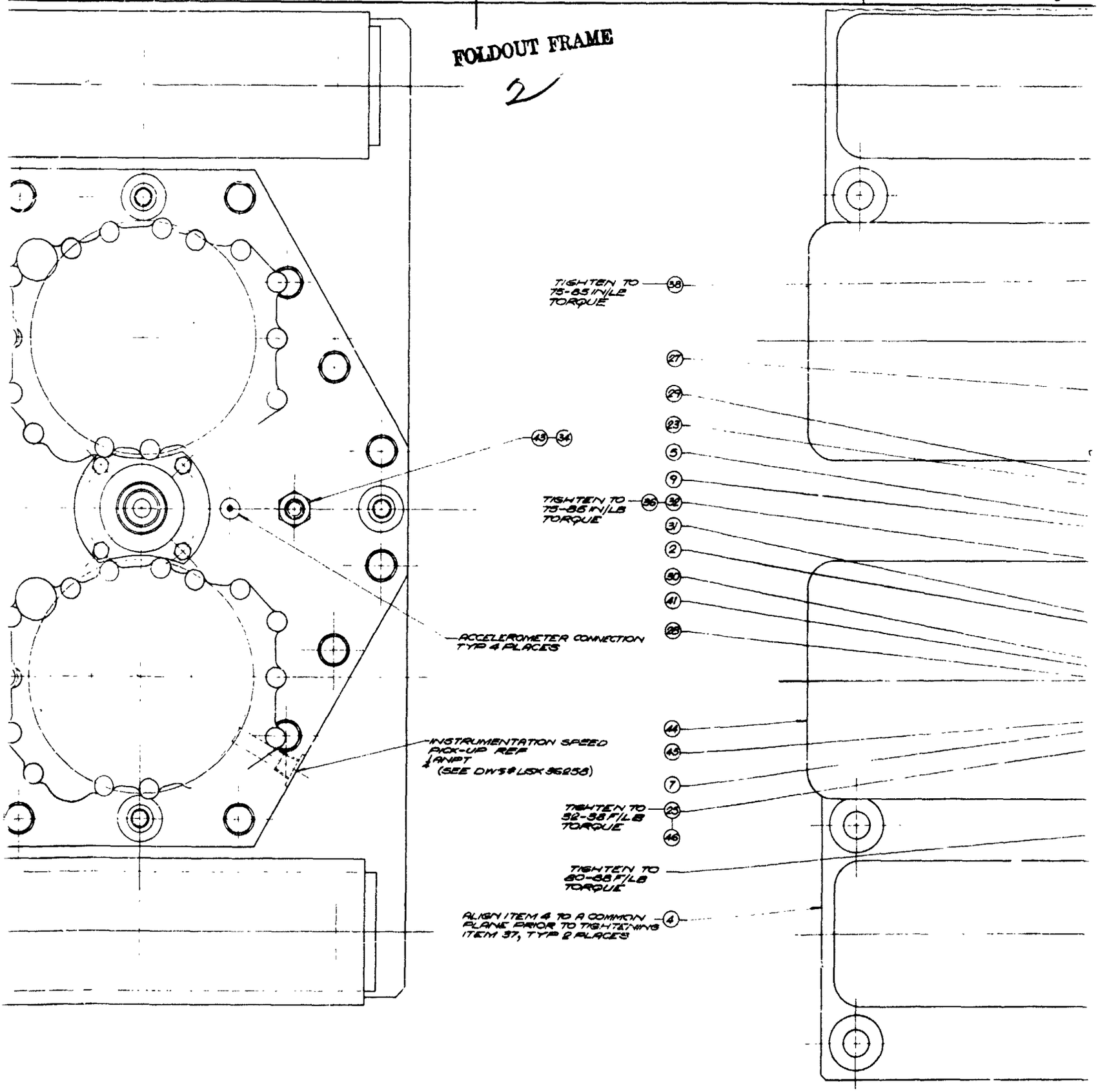

FOLDOUT FRAME 3

	REVISIONS		
ZONE / LTR	DESCRIPTION	DATE	APPROVED

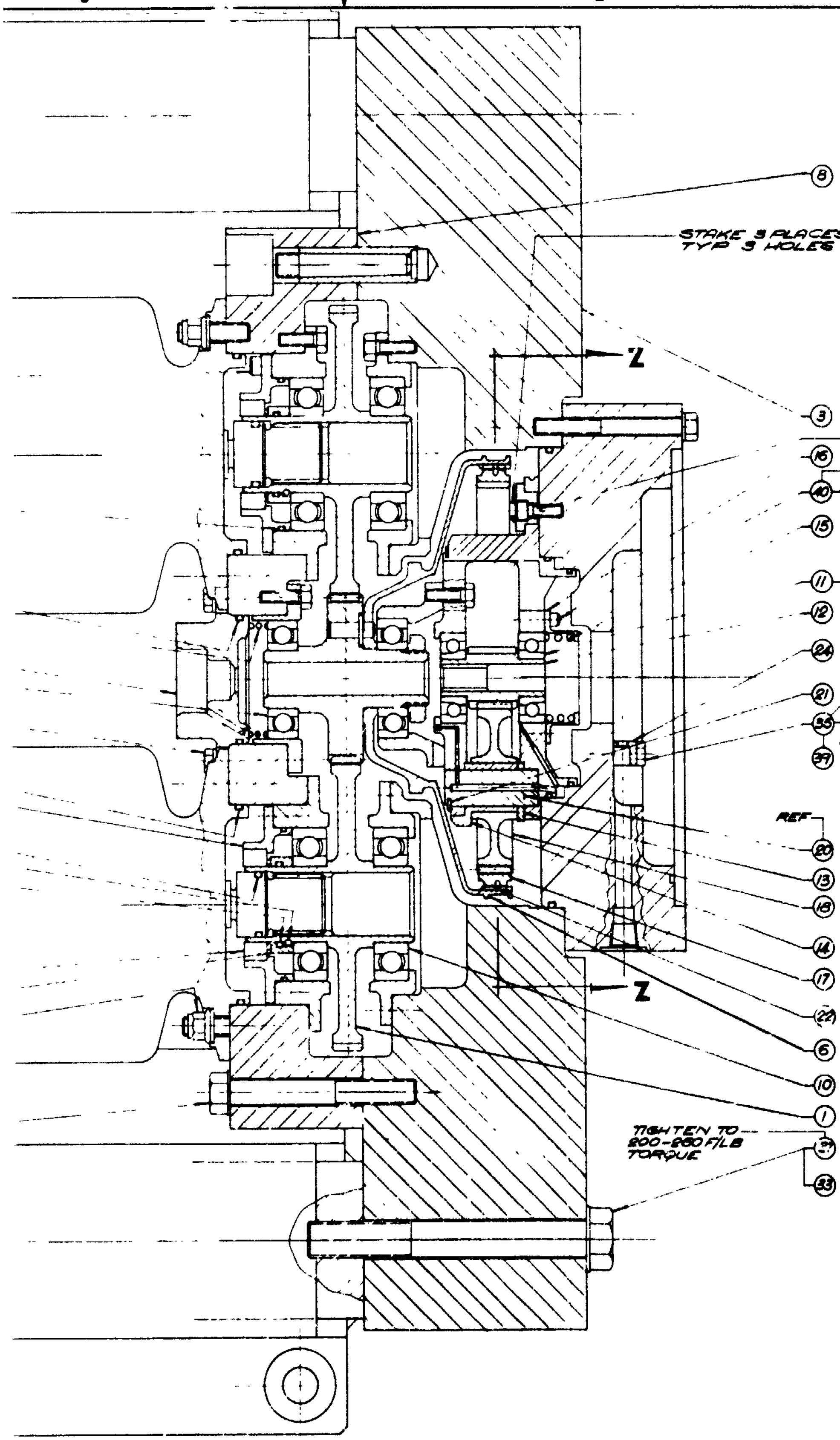

QTY REQD	ITEM NO.	PART NO.	NOMENCLATURE OR DESCRIPTION		ZONE
8	46	AN960C816	WASHER		4B
8	45	63-162-C3	SEAL, OIL	3	4B
2	44	65041	PUMP-HYDRAULIC MODEL APITV	2	4B
1	43	AN815-4	UNION		4C
2	41	MS19060-435	.125 DIA STL. BALL		4B
8	40	MS24673-2	SCREW #10-32		4C
[illegible]	39	[illegible]	[illegible]		4C
[illegible]	38	[illegible]	[illegible] (...-3A)		4D
[illegible]	37	[illegible]	[illegible] (...-16UNJF-3A)		4B
[illegible]	36	MS9490-12	BOLT ([illegible] UNJF-3A)		4C
[illegible]	35	MS9490-12	BOLT (.250-28 UNJF-3A)		4C
1	34	NAS1596-6	PACKING		4C
[illegible]	33	AN960C416	WASHER		4B
[illegible]	32	[illegible]	WASHER		4C
[illegible]	31	[illegible]	PACKING		4C
[illegible]	30	[illegible]	PACKING		4B
1	29	[illegible]	PACKING		4C
[illegible]	28	NAS1593-129	PACKING		4B
[illegible]	27	NAS1593-041	PACKING		4C
[illegible]	25	[illegible]-3006	NUT		4B
1	24	[illegible]-1	SUPPORT		4C
1	23	681173-1	SPRING, COMPRESSION		4C
1	22	681381-1	RING, RETAINER		4B
1	21	681256-1	RING, RETAINER		[illegible]
1	20	681210-3	PIN		[illegible]
[illegible]	19	681210-1	PIN		[illegible]
[illegible]	18	681226-1	GEAR, PLANET		[illegible]
1	17	681225-1	GEAR, RING		[illegible]
1	16	681184-1	RETAINER, [illegible]		[illegible]
1	15	681181-1	[illegible]		[illegible]
[illegible]	14	681184-1	[illegible]		[illegible]
[illegible]	13	681172-[illegible]	[illegible]		[illegible]
1	12	681172-1	GEAR, PINION		[illegible]
[illegible]	11	681007-1	BEARING, [illegible]		[illegible]
[illegible]	10	[illegible]	[illegible], BALL		[illegible]
1	9	[illegible]7-1	BEARING, BALL		[illegible]
1	8	[illegible]	[illegible]		[illegible]
[illegible]	7	[illegible]	[illegible]		[illegible]
1	6	581230-1	DRIVE ASSY		[illegible]
1	5	[illegible]247-1	HOUSING, OIL NOZZLE		[illegible]
[illegible]	4	[illegible]-1	BRACKET ASSY		[illegible]
1	3	[illegible]-1	CASE ASSY		4C
[illegible]	2	[illegible]	[illegible], OIL SEAL		4C
[illegible]	1	[illegible]	[illegible]		[illegible]

PARTS LIST

AIRESEARCH MANUFACTURING COMPANY

GEAR BOX & HYD. PUMP ASSY. ASSY

J 70210 581193

SCALE 1/1

3. APPLY LOCKWIRE PER MS33540

2 PUMP, HYDRAULIC-VENDOR ITEM MAY BE PURCHASED FROM ABEX CORPORATION AEROSPACE DIV 3151W 5TH ST OXNARD CALIF 93030.

1 "GITS" OIL SEAL-VENDOR ITEM MAY BE PURCHASED FROM GECO SALES CORPORATION 2261 FEDERAL AVE LOS ANGELES CALIF 90064.

NOTES: UNLESS OTHERWISE SPECIFIED

APPLICATION

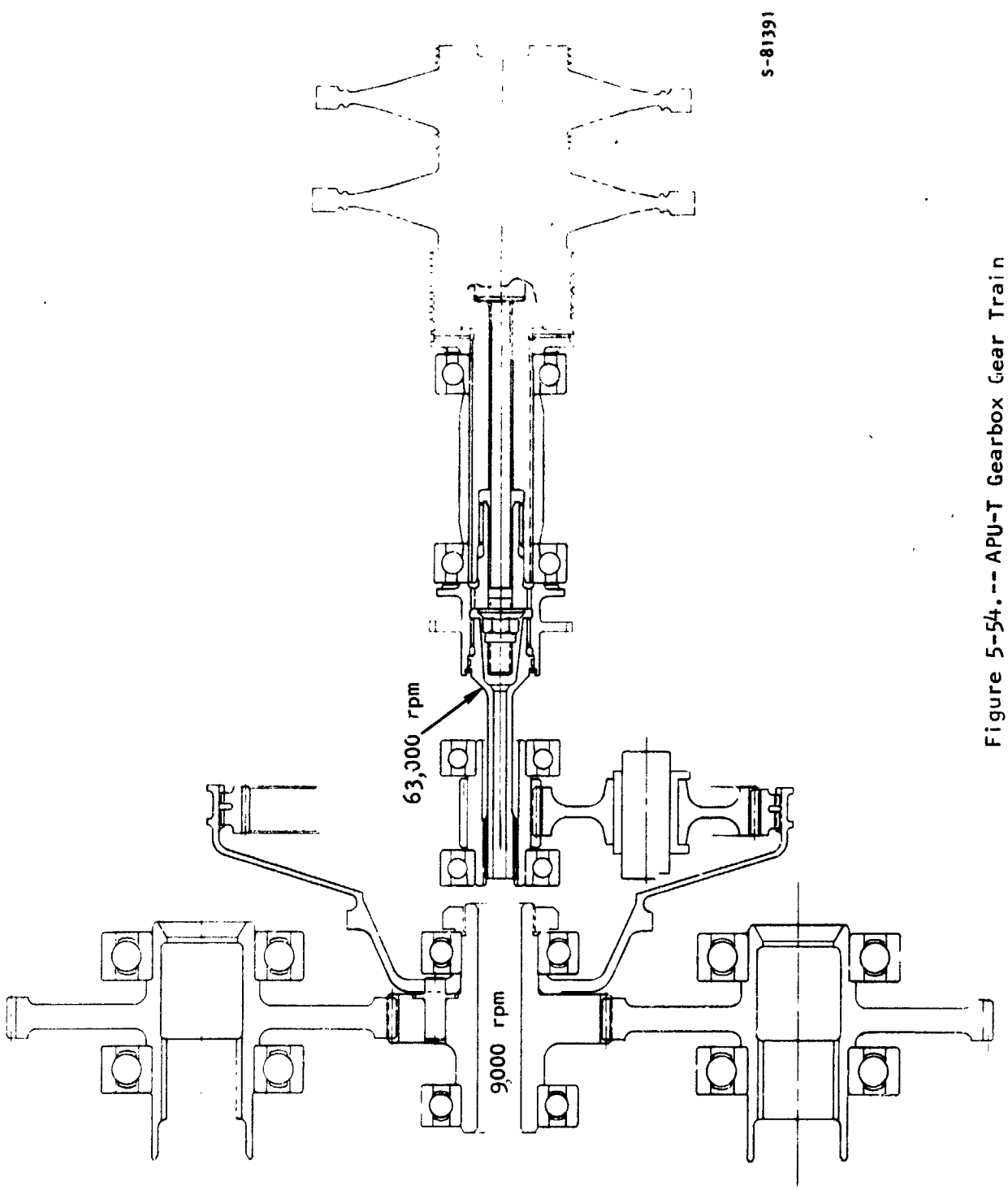

Figure 5-54.-- APU-T Gearbox Gear Train

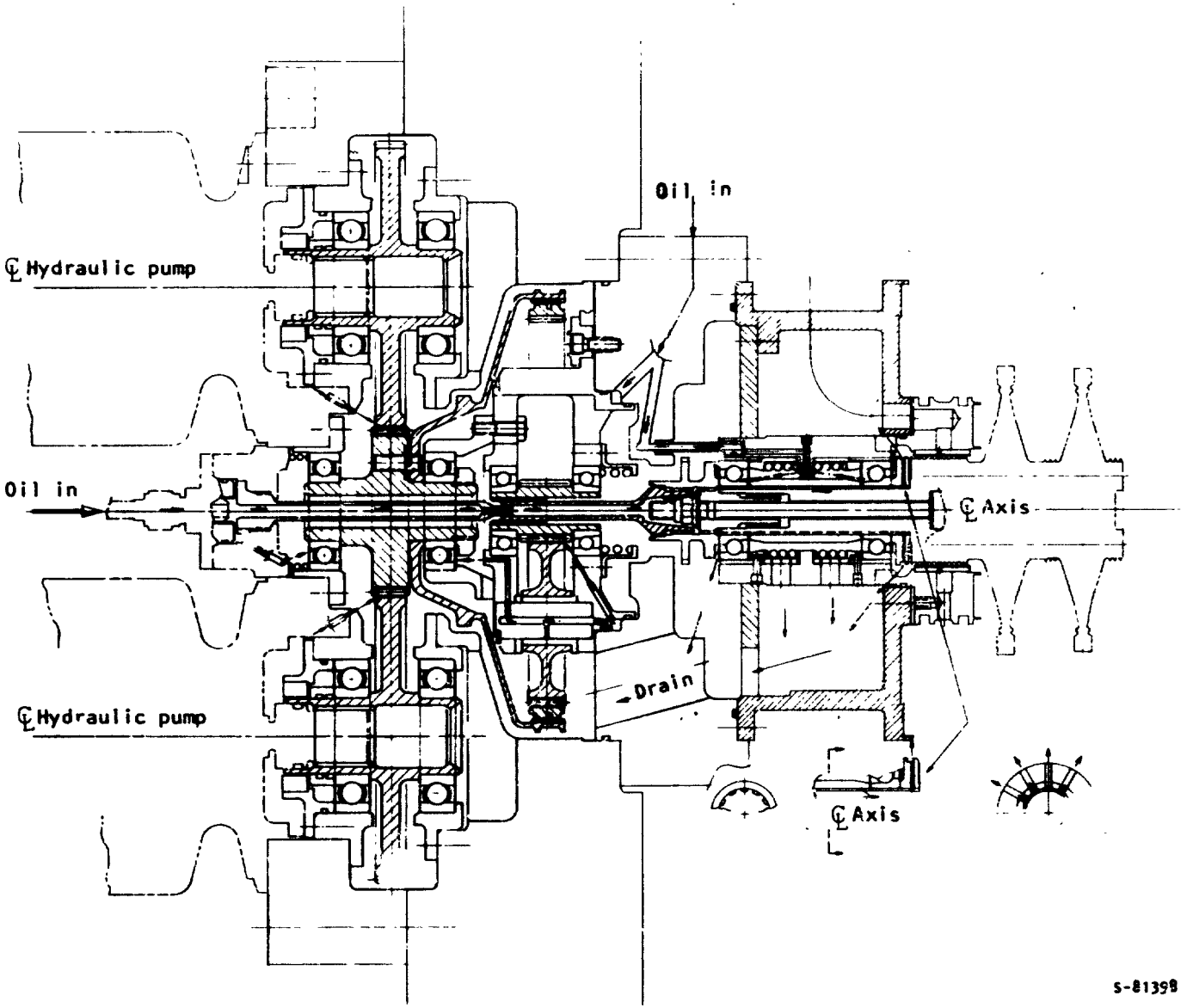

Figure 5-55.--APU-T Gearbox Lubrication

left of fig. 5-55, flows through the tube shown at the left, and flows through the tube inside the 9000-rpm hollow pinion shaft to the high-speed pinion, where it jets into the hollow quill shaft. From the quill shaft, the oil enters the turbine shaft and flows through axial grooves under the two ball bearings and ball bearing spacer to the slinger, where it is pumped out and into the pump. Oil-jets within the gearbox are provided for lubricating the 63,000-rpm pinion, the 9000-rpm gear, and the two bearings supporting this gear. The rest of the bearing and gears are splash lubricated. The planet bushings are lubricated by internal passages in the planet carrier that feed oil to the three stationary pins.

The two ABEX hydraulic pumps are attached at the gearbox using standard accessory pads. To prevent oil from leaking into the pad cavity, each shaft is fitted with a carbon-face-type seal.

References

5-1. Dusinberre, G.M., Heat Transfer Calculations by Finite Differences, International Textbook Company, Scranton, Pennsylvania, 1961.

5-2. Eckert, E.R.G., Transactions of the ASME, Vol. 78, 1956, p. 1273.

5-3. Richardson, P.D., and O.A. Saunders, "Studies of Flow and Heat Transfer Associated with a Rotating Disc," Journal Mechanical Engineering Science, Vol. 5, No. 4, 1963.

5-4. Bartz, D.R., "A Simple Equation for Rapid Estimation of Rocket Nozzle Convective Heat Transfer Coefficient," Jet Propulsion, January, 1957.

5-5. Rossler, W.V., Leakage through Labyrinth Seals, AiResearch Mfg. Co., Report No. K-403-R, January 19, 1961.

5-6. Metzger, D.E., Turbine Rotor Cooling Studies: Part II - Heat Transfer and Pumping on a Plane Disk with Stationary Shroud - Effects of Shroud Size and Placement, Mech. Engr. Dept., Arizona State University, Tempe, Arizona, Technical Report No. ME-696, December 1969.

SECTION 6

COMBUSTOR DESIGN AND DEVELOPMENT

SECTION 6

COMBUSTION DESIGN AND DEVELOPMENT

Combustor Design

The hydrogen-oxygen combustor was designed to provide efficient combustion of fuel-rich gaseous hydrogen-oxygen mixtures. Additional requirements included:

(1) Good mixing within a short distance

(2) Wall temperatures compatible with common high-temperature structural materials

(3) Operation over a turndown ratio of at least 10:1

(4) Operation over an oxidizer-to-fuel ratio range of 0.4 to 0.9

(5) Reliable ignition at startup without a requirement for sequencing the propellant flows

(6) Capability of immediate relight in the event of flameout

The combustor designed for the APU-T, illustrated in fig. 6-1, meets all these requirements.

Fig. 6-2, a cross-sectional view of the combustor, illustrates most of the design features. The principal characteristics of the combustor are listed in table 6-1.

Oxygen is fed into an annular manifold in the head of the combustor surrounding the spark plug cavity; then it is metered through eight nozzles arranged in a circle in the injector head and that discharge parallel to the combustor axis. A ninth oxygen passage, leading from the oxygen manifold to the spark plug cavity, is described later as part of the ignition system.

Hydrogen is fed into a larger annular manifold in the combustor head just downstream of the oxygen manifold. From here, approximately 40 percent of the flow is directed into the cooling jacket (described later) and the reamining 60 percent passes through the eight annular openings that surround the oxygen jets. Thus, the combustor burner has eight annular hydrogen-oxygen jets with the hydrogen on the outside. The oxygen is completely consumed before it can come in contact with any hot metal parts.

The combusted gas mixture resulting from the main burner has a mixed temperature of approximately 2650°R, which is too high to be allowed to come into contact with uncooled walls. Therefore, the combustion chamber is surrounded by a copper liner that has an extended heat transfer surface of expanded metal fins brazed on its OD (fig. 6-1). The previously mentioned cooling hydrogen

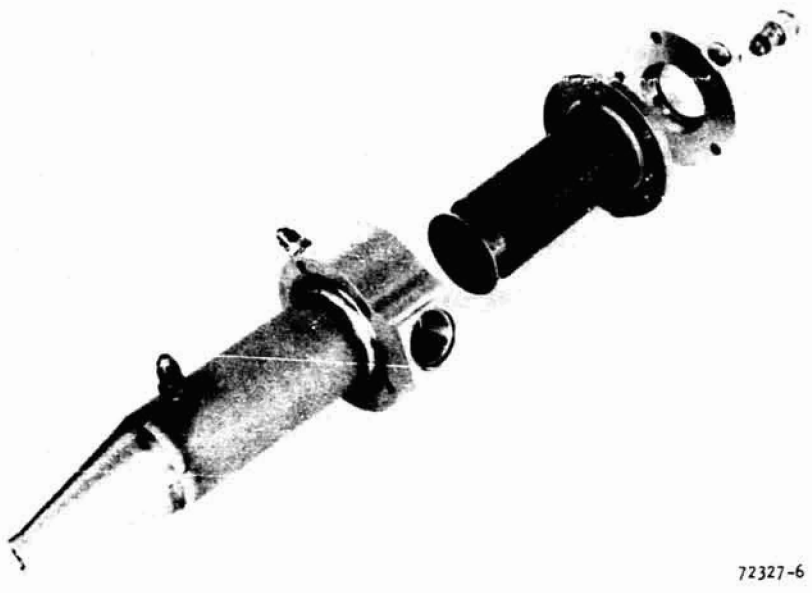

Figure 6-1.-- Hydrogen-Oxygen Combustor (Prototype Test Unit).

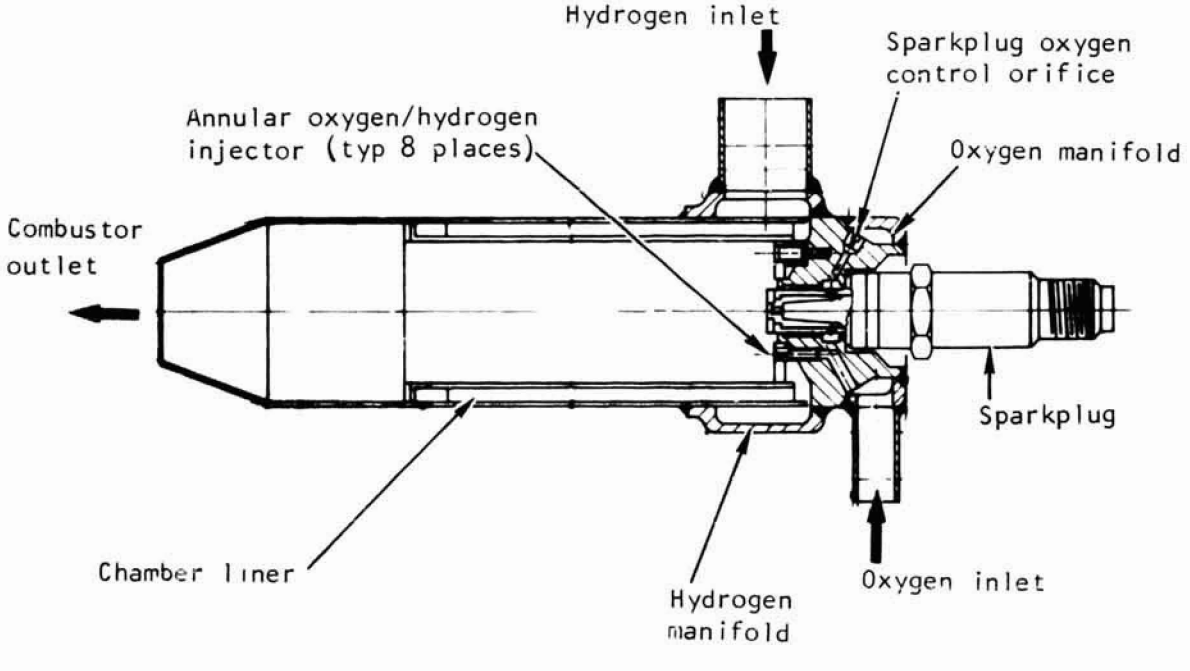

Figure 6-2.-- Sectional View of the APU-T Hydrogen-Oxygen Combustor.

TABLE 6-1

COMBUSTOR DESIGN SUMMARY

Combustor characteristics	Value	Notes	Combustor characteristics	Value	Notes
Chamber length, in.	5.50		Main burner (continued)		
Chamber diameter, in.	1.460		Theoretical mixture temperature, ^{o}R	2650	
Length-to-diameter-ratio	3.77		Injector bolt circle, in.	0.860	
Rated flow, lb/sec	.204	Velocities, etc. calculated using $600^{o}R$ inlet temperature	Injector location, D_i/D_c	.59	
Hydrogen, lb/sec	.116		Velocity "unlit", ft/sec	~70	
Oxygen, lb/sec	.088		Velocity upstream of flame, ft/sec	60.4	
Oxidizer-to-fuel-ratio, lb/lb	.76		Velocity after flame, ft/sec	195	
Spark plug			Wall cooling		
Location		Coaxial	Type		Annulus, finned
O_2 flow, lb/sec	.008		Quantity	1	
Control orifice diameter, in.	.045		Diameter, in.	n/a	
Control orifice area, sq in.	.0017		Passage area, sq in.	~0.5	
Control orifice velocity, ft/sec	335		Surface area, sq in.	>100	
Spark gap, in.	.015		Surface area ratio, S/Sc	>5.5	Hot/cool
Spark gap area, sq in.	.0083		Hydrogen velocity, ft/sec	103	
Spark gap velocity, ft/sec	71		Secondary injection		
Spark volts, volts	17,000		Number of holes	16	
Spark frequency, sparks/sec	120		Hole diameter, in.	.055	
Spark energy, millijoules	5		Hole area, sq in.	.038	
Main burner			H_2 velocity, ft/sec	[b]1380+	
Injector type		Shower head	Hole direction		Radial
Number of injectors	[a]8		Injector/cooling H_2, percent/percent	60/40	
O_2 injector diameter, in.	.052		Temperature after mixing, ^{o}R	1960	
O_2 injector area, $in.^2$	.0169		Operational range		Design point for this analysis
O_2 injector flow, lb/sec	.080		O_2 inlet temperature, ^{o}R	300-1000	R - 600 AIR - 600
O_2 injector velocity, ft/sec	335		H_2 inlet temperature, ^{o}R	500-1300	R - 600 AIR - 600
O_2 injector velocity head, psi	24.0		O_2 inlet pressure, psi	50-500	R - 410 AIR - 410
H_2 injector diameter, in.	.157		H_2 inlet pressure, psi	50-500	R - 410 AIR - 410
H_2 injector area, $in.^2$	.057		Materials		
H_2 injector flow, lb/sec	.0695		O_2 injector	CRES	
H_2 injector velocity, ft/sec	1380		Injector plate	Copper	
H_2 injector velocity head, psi	26.6		Body	CRES 347	
O/F at injector, lb/lb	1.15		Cooling sleeve	Copper	
O/F including spark plug, lb/lb	1.25		Tail pipe	CRES 347	

NOTES:

[a] In effect, there are nine injectors including the spark plug.

[b] Velocities, etc., based on $600^{o}R$ hydrogen. Actually hydrogen temperature will increase as it passes through wall cooling passages.

flows past these fins and maintains an allowable wall temperature on the copper liner. After the cooling hydrogen is passed through the fins, it is injected into the combusted gas stream to provide additional mixing and further cooling.

Ignition is obtained from a spark plug in which oxygen gas is fed into the annulus between the electrode insulator and the spark plug body. This oxygen then passes through the spark gap and out into the combustor. As the oxygen passes through the spark, some oxygen molecules are heated to a very high temperature and immediately come into contact with hydrogen molecules in the combustion chamber. This causes the oxygen jet issuing from the spark plug to ignite and form a pilot light for the remaining jets in the combustor. There are no special provisions to feed hydrogen to the area of ignition, as inherently there is sufficient hydrogen in the region because of the hydrogen-rich atmosphere in the combustion chamber. This type of ignition system will work under steady-state flow conditions in the combustor and does not require any special transient control of either of the propellant gases.

This type of combustor is inherently capable of operation over wide pressure and/or oxidizer-to-fuel ratio ranges. The combustion zones are identical in principle to the common gas burner jet except that the oxidizer is the inner jet in this combustor. The length of the jet increases as the oxidizer-to-fuel ratio range is increased, just as a gas stove jet increases when the gas (inner jet) flow is increased. Chamber pressure has no effect upon the length of the jet, so combustor operation essentially is independent of chamber pressure throughout the desired region of operation.

The combustor is made entirely of type 347 corrosion-resistant steel except for the copper liner assembly. The prototype test unit, illustrated in fig. 6-1, was built in several pieces and bolted together to facilitate examination, modification, and assembly. This unit is to be reworked as shown in fig. 6-2 and welded or brazed together so the combustor body and manifold are a one-piece assembly.

Combustor Test Results

The combustor was tested in accordance with the combustor test plan except as noted herein. The only hardware modification required during the entire test program was to reduce the spark gap from 0.035 to 0.015 in. to obtain a spark at the higher operational pressures (200 to 300 psia before ignition). The combustor met all design performance requirements.

Nozzle flow coefficient.--The flow coefficient of the combustor nozzle was determined by flowing hydrogen gas through the combustor and calibrating it against the NASA-supplied venturi PN V6 (0.2725 x 0.0680). The experimentally determined flow coefficient of 0.993 was used in subsequent data analyses.

Injector pressure drops.--The injector pressure drops were measured and found to meet the design objectives. Also, the flow split between the hydrogen injectors and the cooling jacket was found to be 35 percent through the cooling jacket. The design objective was 40 percent, but since the liner temperature remained less than 900°F, this coolant flow rate was considered to be sufficient.

Operational envelope.--The combustor was ignited and performance tested over a range that exceeded the specified operational envelope of the test plan, as shown in fig. 6-3. The three test plan curves represent 1.5, 5.0, and 15.0 lb/min total propellant flow rates.

Light-off limits.--The combustor originally was fitted with a spark plug with 0.035-in. electrode gap. Using this plug, it was found that the combustor failed to ignite at unlit chamber pressures in excess of 240 psia. A review of Pashen's Law, which describes the relationship between the breakdown potential of a spark gap as a function of the pressure-distance multiple, indicated that a gap of 0.035 in. was indeed too great. Therefore, a spark plug with a 0.015-in. gap was used during the March 13, 1973 tests, and successful ignition was achieved under all conditions attempted. A summary of these conditions is presented in fig. 6-3, which shows successful ignition at points completely surrounding the APU operational envelope. The typical design points plotted in fig. 6-3, were taken from a compilation of system computer runs made on December 7, 1972 to describe the operation of the presently defined APU.

Characteristic velocity (C*).--The characteristic velocity as determined by the test data is shown in fig. 6-4. Characteristic velocity was determined by the equation:

$$C^* = \frac{P A_t g}{w}$$

$$A_t = A_g f_{TR}$$

where: A_g = geometric area of throat, sq in.

f_{TR} = influence factor correcting for change in throat area caused by metal temperature change during firing

This is plotted against a background curve of theoretical C* provided by NASA for propellant inlet temperature of 530°R.

C* efficiency.--The C* efficiency, calculated from test data is shown in figs. 6-5 and 6-6. In fig. 6-5, C* efficiency is plotted as a function of oxidizer-to-fuel ratio and in fig. 6-6 as a function of chamber pressure. Neither parameter appears to have an appreciable effect upon the chamber performance.

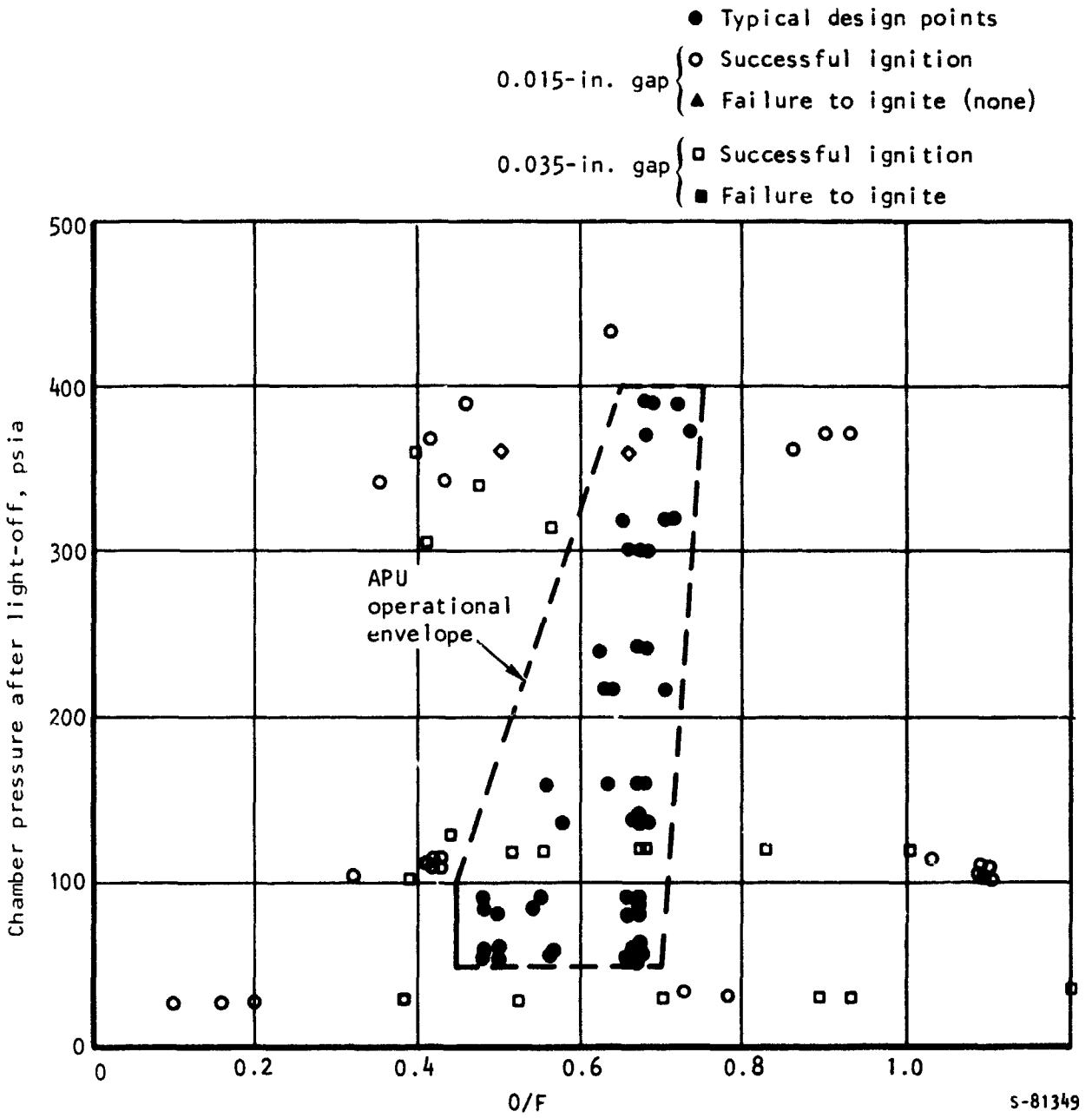

17,000 volts, 50 sparks/sec, 5 millijoules/spark, 0.015-in gap
test data 3-13-73

Figure 6-3.--Summary of Test Points.

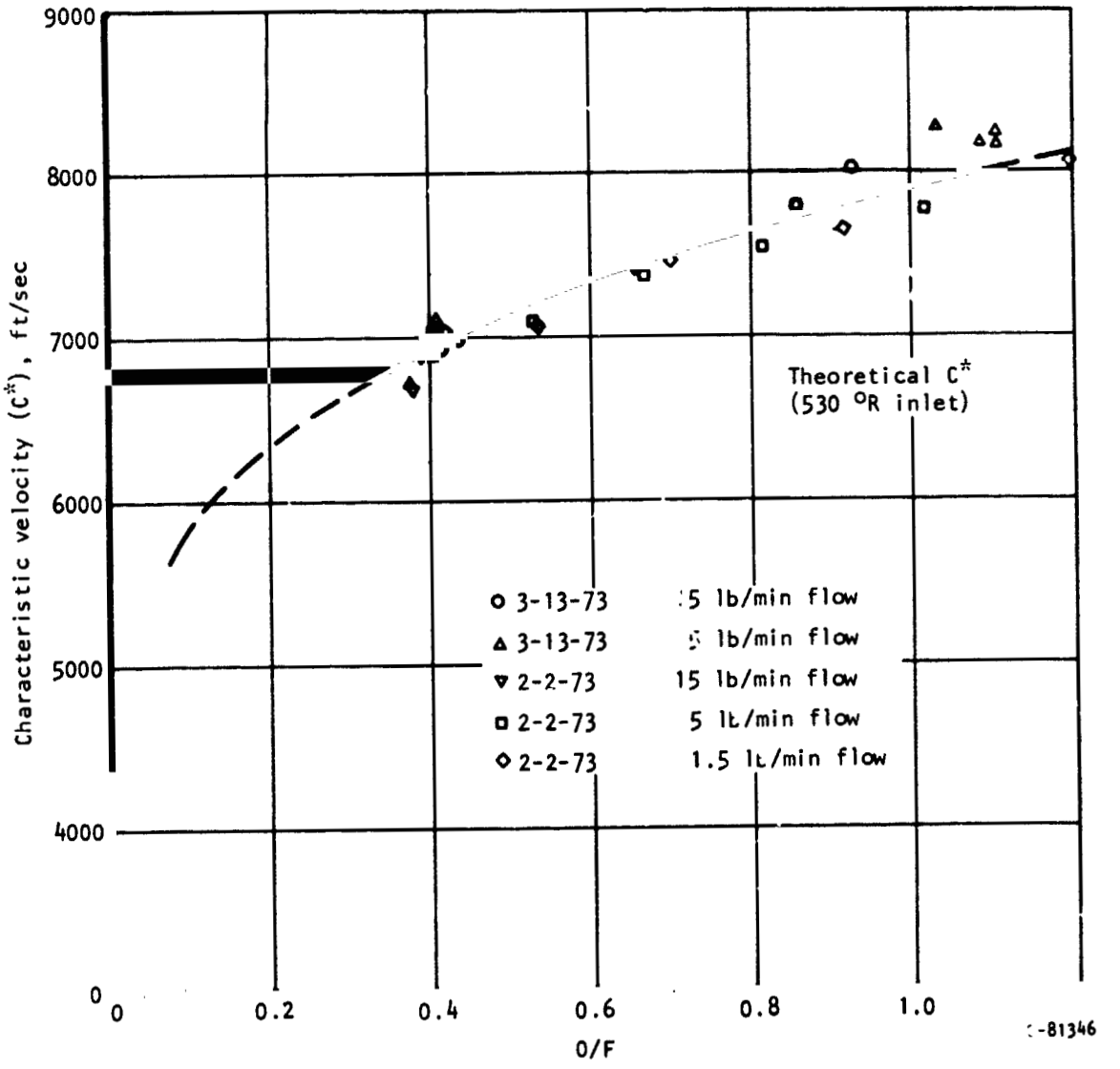

Figure 6-4.--Characteristic Velocity.

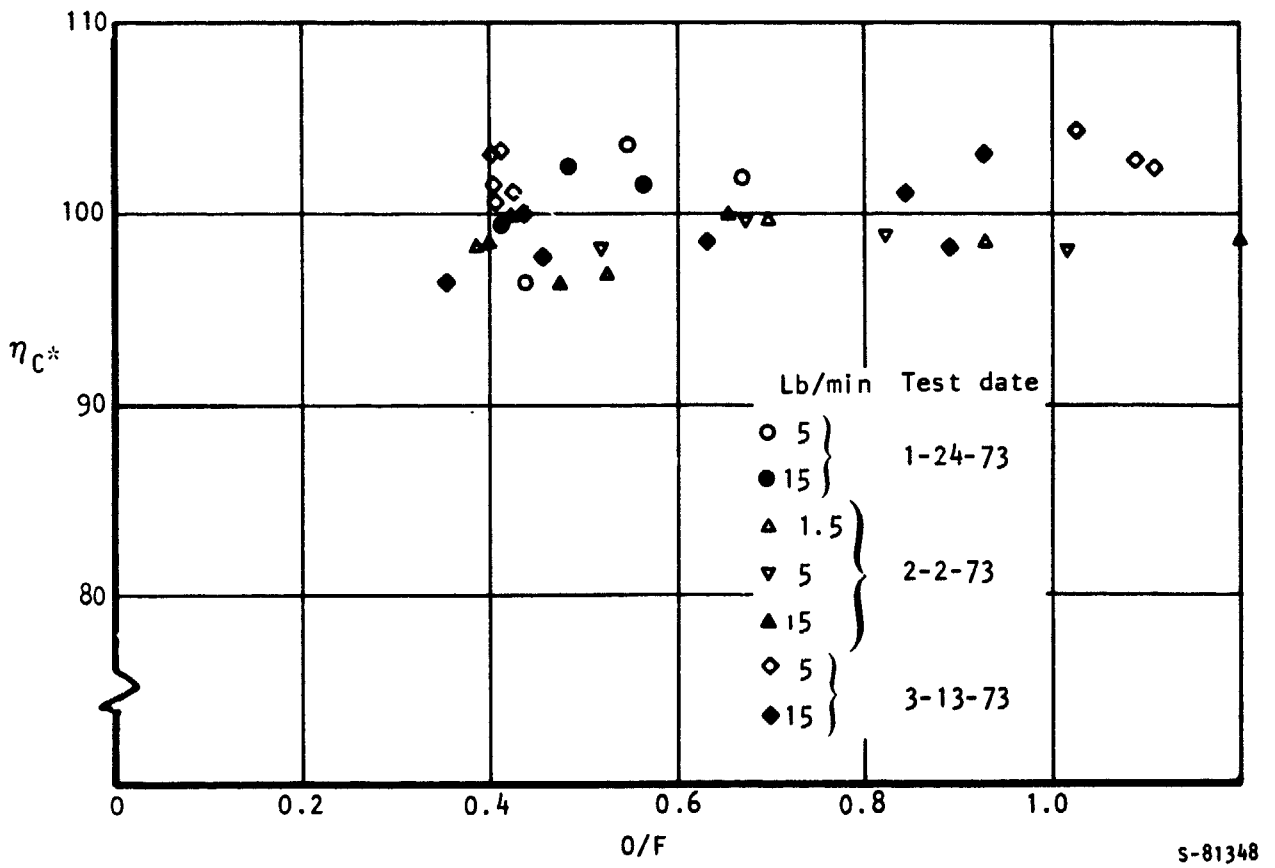

Figure 6-5.--Combustion Efficiency as a Function of Oxidizer/Fuel.

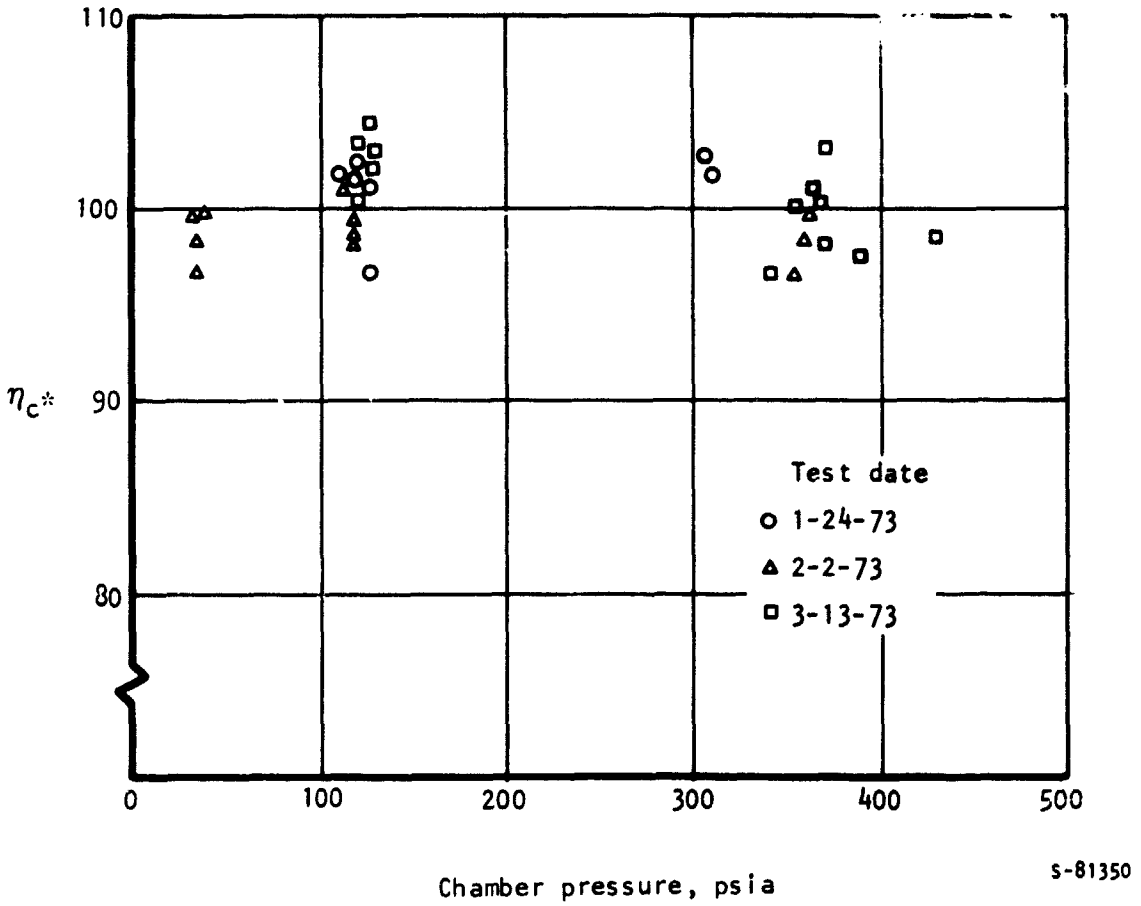

Figure 6-6.--Combustion Efficiency as a Function of Pressure.

C* efficiency.--The C* efficiency, calculated from test data, is shown in figs. 6-5 and 6-6. In fig. 6-5, C* efficiency is plotted as a function of oxidizer-to-fuel ratio and in fig. 6-6 as a function of chamber pressure. Neither parameter appears to have an appreciable effect upon the chamber performance.

Chamber wall temperature.--During all runs the combustor nozzle metal temperatures were recorded. After each run prior to March 13, 1973, the uninsulated portion of the combustor wall was observed and the heat-induced discolorations indicated uniform heating of the wall downstream of the copper liner. The near-the-wall thermocouple of the temperature profile tests indicated no hot zones throughout the five locations of rotation. The tip of the copper liner was coated with Tempilaq® paint during the February 2, 1973 test sequence and observations of the color pattern on several occasions during the test sequence indicated uniform heating and a maximum liner temperature greater than 770°R and less than 900°F. This includes operation with the average temperature of 1903°F (the average of the four gas stream temperature profile thermocouples).

Gas stream temperature profile.--The gas stream profile was mapped by means of four thermocouples located 4.25 in. downstream of the injectors. During the test sequence the injector head and copper liner were rotated through five circumferential positions to provide for twenty temperature data points under each test condition. These results showed that the combustor and cooling gases were well mixed by this point.

SECTION 7

SYSTEM HEAT EXCHANGERS

SECTION 7

SYSTEM HEAT EXCHANGERS

The heat exchanger specifications resulting from the preliminary design system analysis are presented below. The regenerator and preheater are identical. The hydraulic and lube oil coolers are also identical.

Specification

SSAPU Lubricating and Hydraulic Oil Cooler

FUNCTION 5-1-73

This heat exchanger is utilized in two different applications in the SSAPU propellant conditioning system. The use of one heat exchanger for two different applications was dictated by economic considerations. The lubricating and hydraulic oils are cooled in order to maintain acceptable gearbox and hydraulic pump temperatures. The heat sink is hydrogen which has been conditioned to an acceptable temperature level by the preheater and the regenerator.

DESIGN POINT

Table 7-1 lists the heat transfer design point for the lube/hydraulic cooler design shown on drawing L-198787. The design point was established by system analysis, and represents a hydraulic oil operating condition. This design is adequate for all lubricating and hydraulic oil operating points.

TABLE 7-1

LUBE/HYDRAULIC COOLER HEAT TRANSFER DESIGN POINT

	Cold Side	Hot Side
Fluid	Hydrogen	MIL-H-83282
Flow rate, lb/min	1.026	52
Inlet temperature, ^{o}R	400	775
Outlet temperature, ^{o}R	757.6	733
Inlet pressure, psia	600	200
Core pressure drop, psi	0.098	1.70
Effectiveness	0.953	0.112
Duct diameter, in.	1.0	1.0
Total Heat Transferred, Btu/min	1282	

DESCRIPTION

The lube/hydraulic cooler is a tube and shell multipass crossflow heat exchanger. In both configurations, the overall flow direction is counterflow. The heat exchanger, as shown on drawing L-198787, has the following core geometry.

Number of tubes	120
Tube diameter	0.125 in. OD
Tube wall thickness	0.008 in.
Tube designation	
Inside	DMP08
Outside	SLI25025

The hydrogen inside the tubes makes a single pass through the heat exchanger, and the shell side fluid flows across the tube bundle four times.

PERFORMANCE

Figure 7-1 presents the hydrogen pressure drop of the heat exchanger and Figure 7-2 presents the same information for the oil side. These pressure drops do not account for inlet and outlet manifold losses, and are thus representative of core and internal turning losses only. Manifold losses are accounted for in the system program as a portion of the ducting losses. Figures 7-3 and 7-4 present the heat transfer conductance for the hydrogen and oil sides respectively. The system program evaluates these conductances as a function of flow, corrects them for temperature and pressure dependent variations in physical properties, and then combines the corrected conductances on the two sides into an overall heat transfer conductance for the heat exchanger at the particular operating point. This overall heat transfer conductance, and the ratio of the weight flow-specific heat products uniquely determine the performance of the heat exchanger. When used as the lube oil cooler the system program also corrects the oil side values to account for the different oil.

DISCUSSION

The AiResearch thermal analyzer program has been utilized to examine in detail the operating conditions of the lube/hydraulic cooler. Two nodal models were utilized, each with a total of 198 nodes; one model was employed for the lube oil configuration, and the other for the hydraulic application. Steady state operating conditions 14 and 15B were examined and the results verified the performance and pressure drop predicted by the system computer program from Figures 7-1 thru 7-4. The results of the thermal analyzer study were also utilized to define the structural requirements of the heat exchanger, and to ensure that no local temperatures occur that would lead to congealing of the oil.

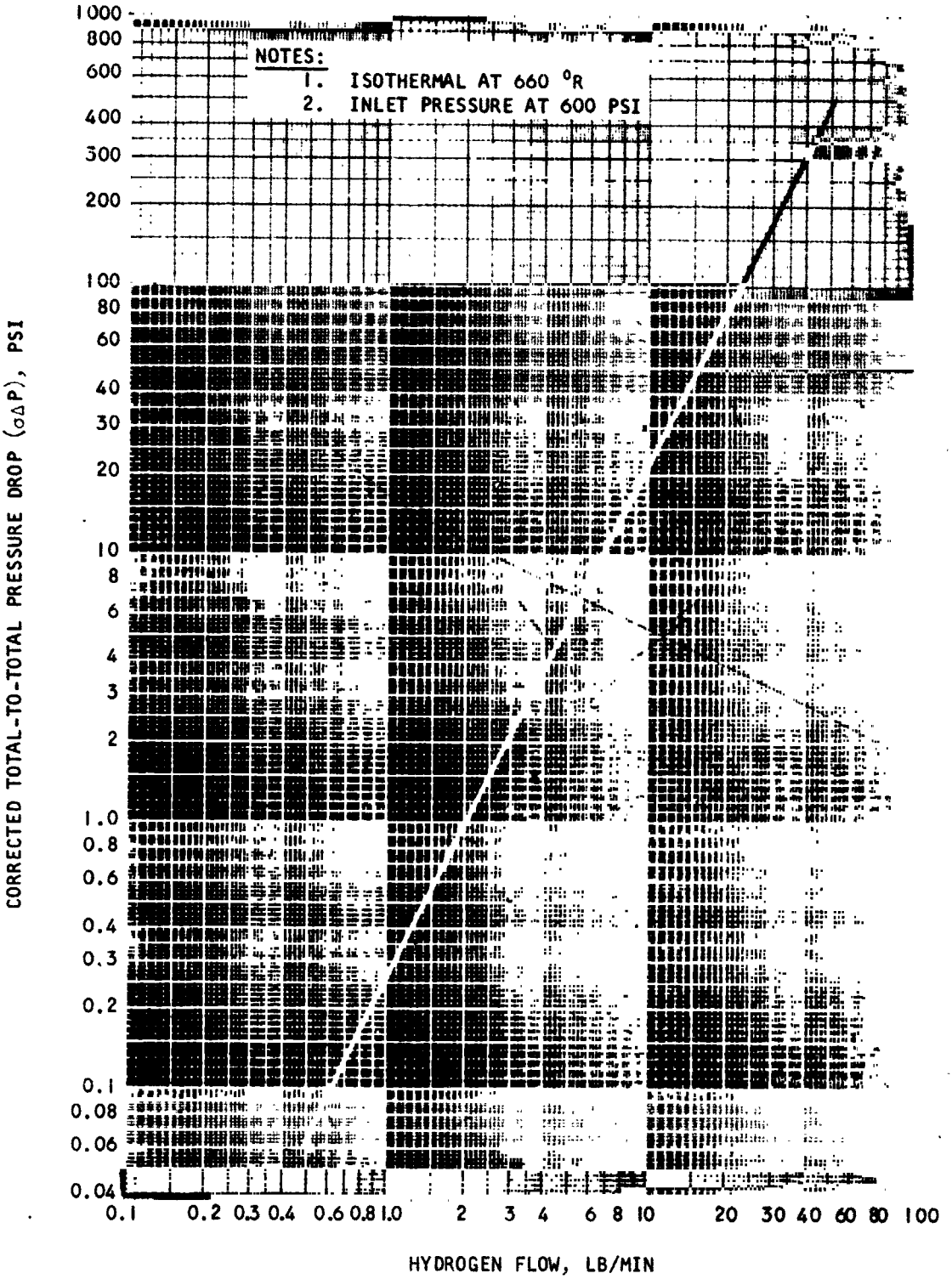

Figure 7-1. Hydrogen Pressure Drop, SSAPU Lubricating and Hydraulic Oil Cooler

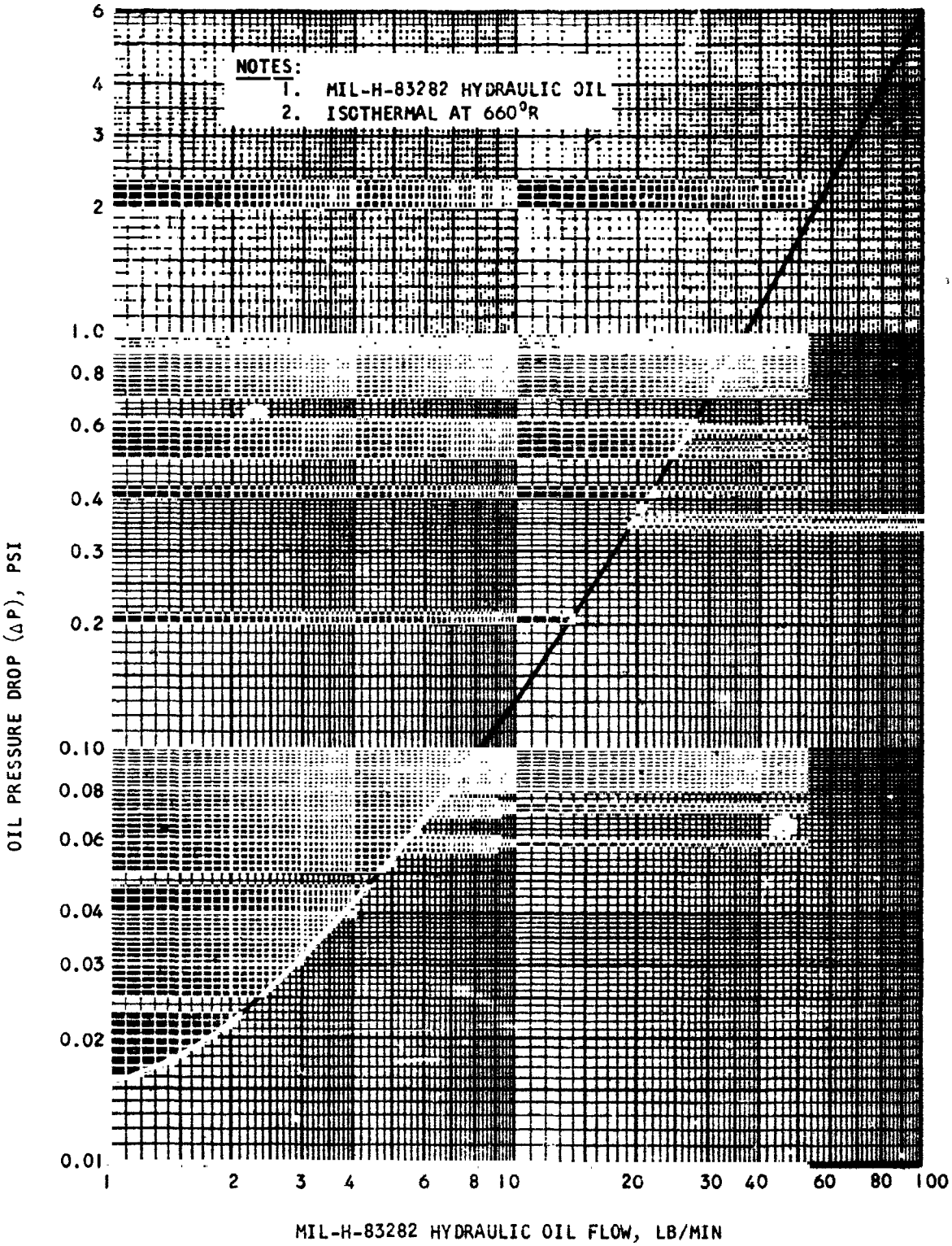

Figure 7-2. Oil Pressure Drop, SSAPU Lubricating and Hydraulic Oil Cooler

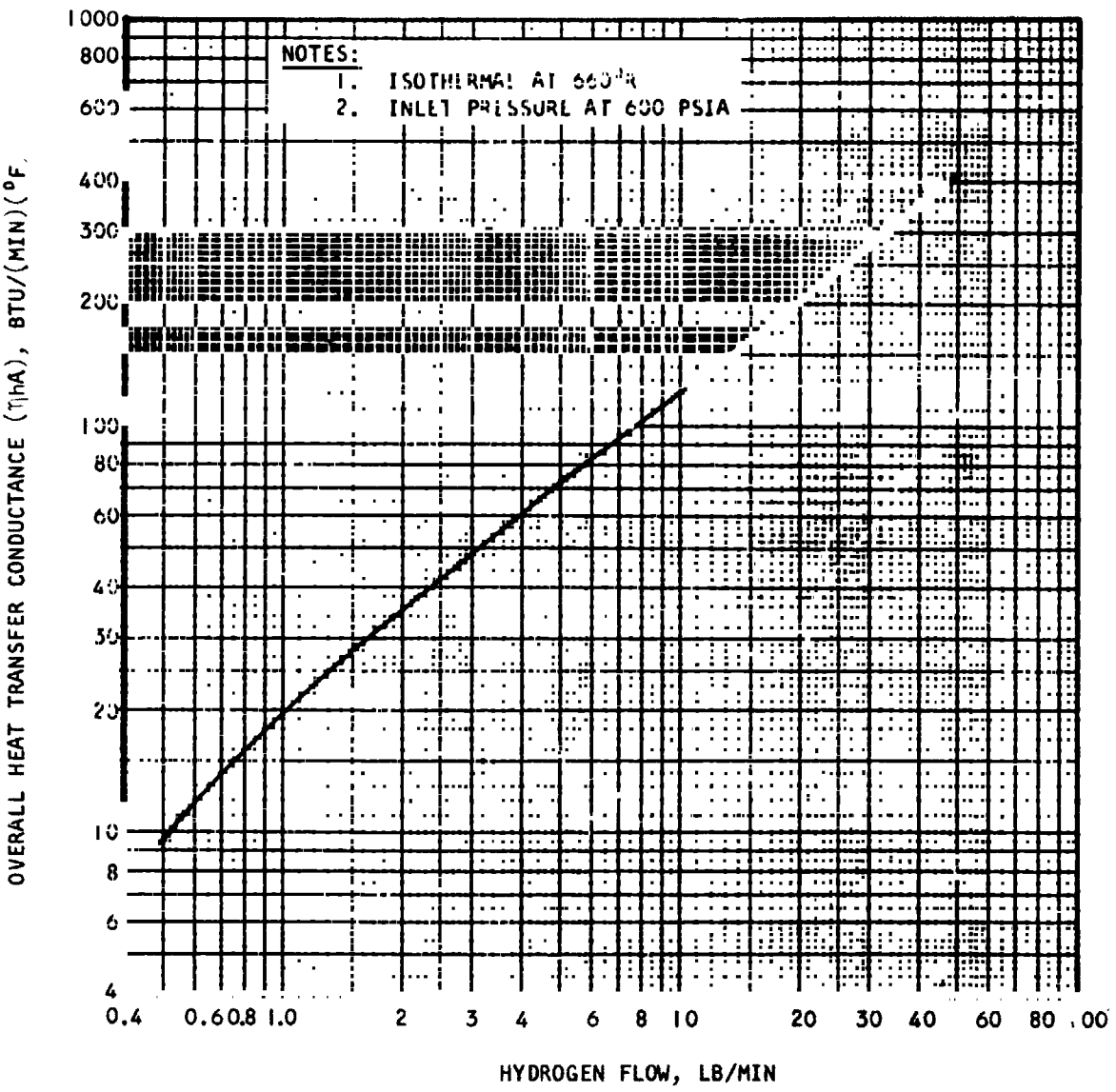

Figure 7-3. Hydrogen Heat Transfer Conductance, SSAPU Lubricating and Hydraulic Oil Cooler

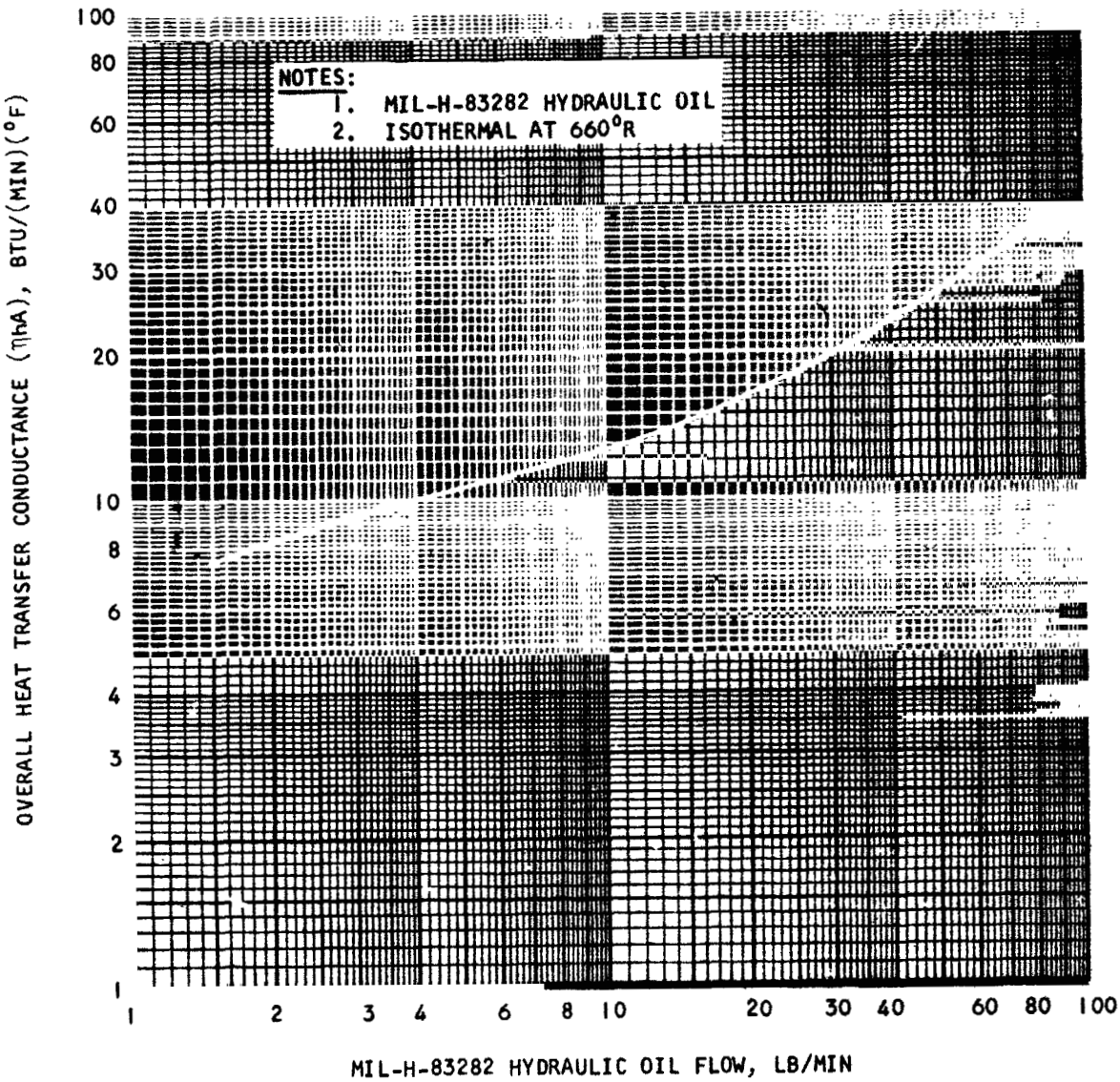

Figure 7-4. Oil Heat Transfer Conductance, SSAPU Lubricating and Hydraulic Oil Cooler

Although the heat transfer design point is defined by a hydraulic oil operating condition, the most severe structural environment occurs when the heat exchanger is operated as the lube oil cooler. Although operating points exist with higher hot fluid inlet temperatures than Condition 14, temperature level alone is not the determining factor of stress level. The combination of flow, temperature, and matrix temperatures for lube oil cooler operation at Condition 14 indicate the worst thermal stress condition, and thus the unit, which has been stressed to these levels, will be adequate at all other operating points. The structural design point is listed in **Table 7-2.**

TABLE 7-2

LUBE/HYDRAULIC COOLER STRUCTURAL REQUIREMENTS

Life: 1000 Start Stop Cycles
Material: 347 Stainless Steel
Operating Conditions:

	Hot Side	Cold Side
Fluid	MIL-L-23699	Hydrogen
Flow rate, lb/min	28.5	8.331
Inlet temperature, ^{0}R	611.1	469.7
Outlet temperature, ^{0}R	518.1	509.0
Inlet pressure, psia	200	600

SPECIFICATION

SSAPU REGENERATOR AND PREHEATER

FUNCTION

This heat exchanger is utilized in two different applications in the SSAPU propellant conditioning system. The use of one heat exchanger for two different applications was dictated by economic considerations. The preheater warms the cryogenic hydrogen to an acceptable temperature level such that, after passing through the regenerator, the hydrogen represents an acceptable temperature heat sink for the hydraulic oil. The heat source for the preheater is hot hydrogen from the recuperator. The regenerator cools the hydrogen after it has absorbed the hydraulic heat load, so that it is at a suitable temperature level to cool the lube oil. The heat sink in the regenerator is the hydrogen outlet from the preheater.

DESIGN POINT

Table 7-3 lists the heat transfer design point for the preheater/regenerator design shown on drawing L-198786. The design point was established by system analysis, and represents a regenerator operating condition. This design is adequate for all preheater and regenerator operating points.

TABLE 7-3

PREHEATER/REGENERATOR HEAT TRANSFER DESIGN POINT

	Cold Side	Hot Side
Fluid	Hydrogen	Hydrogen
Flow rate, lb/min	1.026	1.026
Inlet temperature, ^{o}R	88	755
Outlet temperature, ^{o}R	400	420
Inlet pressure, psia	600	600
Core pressure drop, psi	0.0756	0.0867
Effectiveness	0.468	0.502
Duct diameter, in.	1.0	1.0
Total Heat Transferred, Btu/min	1237	

DESCRIPTION

The preheater/regenerator is a tube and shell multipass crossflow heat exchanger. In the preheater configuration, the overall flow direction is counterflow, whereas in the regenerator application, the unit is operated in parallel flow. The heat exchanger, as shown on drawing L-198786, has the following core geometry.

Number of tubes	83
Tube diameter	0.125 in. OD
Tube wall thickness	0.008 in.
Tube designation	
Inside	DMP08
Outside	125108

The hydrogen inside the tubes makes a single pass through the heat exchanger, and the shell side hydrogen flows across the tube bundle six times. One header plate is fixed, and the other incorporates a sliding joing which eliminates thermal expansion problems.

PERFORMANCE

Figure 7-5 presents the hydrogen pressure drop of both sides of the heat exchanger. These pressure drops do not account for inlet and outlet manifold losses, and are thus representative of core and internal turning losses only. Manifold losses are accounted for in the system program as a portion of the ducting losses. **Figure 7-6 presents the heat transfer conductance for hydrogen** flowing on the two sides of the heat exchanger. The system program evaluates these conductances as a function of flow, corrects them for temperature and pressure dependent variations in physical properties, and then combines the corrected conductances on the two sides into an overall heat transfer conductance for the heat exchanger at the particular operating point. This overall heat transfer conductance, the ratio of the weight flow-specific heat products, and the flow configuration (parallel or counter) uniquely determine the performance of the heat exchanger.

DISCUSSION

The AiResearch thermal analyzer program has been utilized to examine in detail the operating conditions of the preheater/regenerator. Two nodal models were utilized, each with a total of 232 nodes; one model was employed for the preheater (counterflow) configuration, and the other for the regenerator (parallel flow) application. Steady state operating conditions 14 and 15B were examined and the results verified the performance and pressure drop predicted by the system computer program from **Figures 7-5 and 7-6. The results of** the thermal analyzer study were also utilized to define the structural requirements of the heat exchanger.

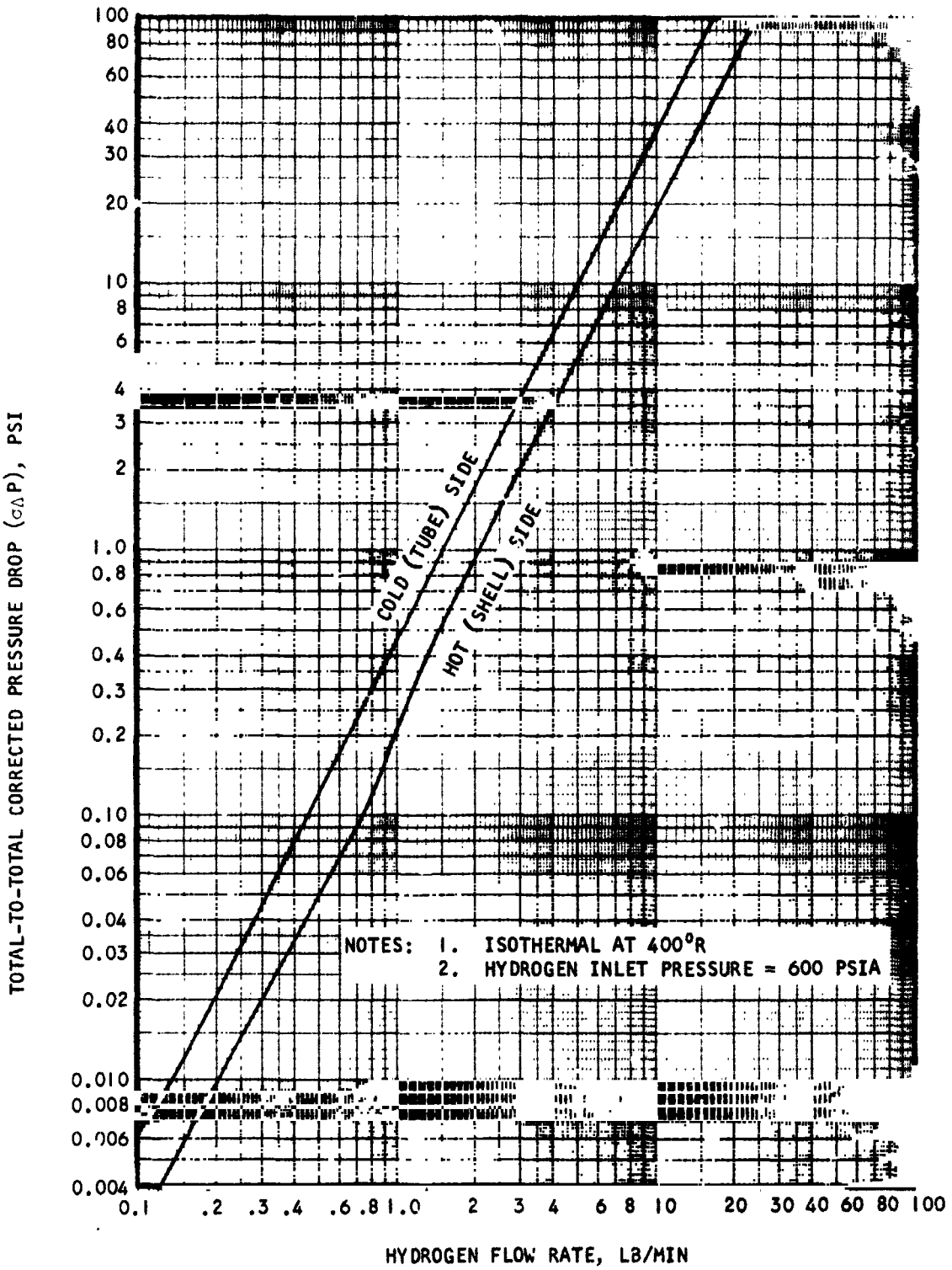

Figure 7-5. Pressure Drop of SSAPU Preheater/Regenerator

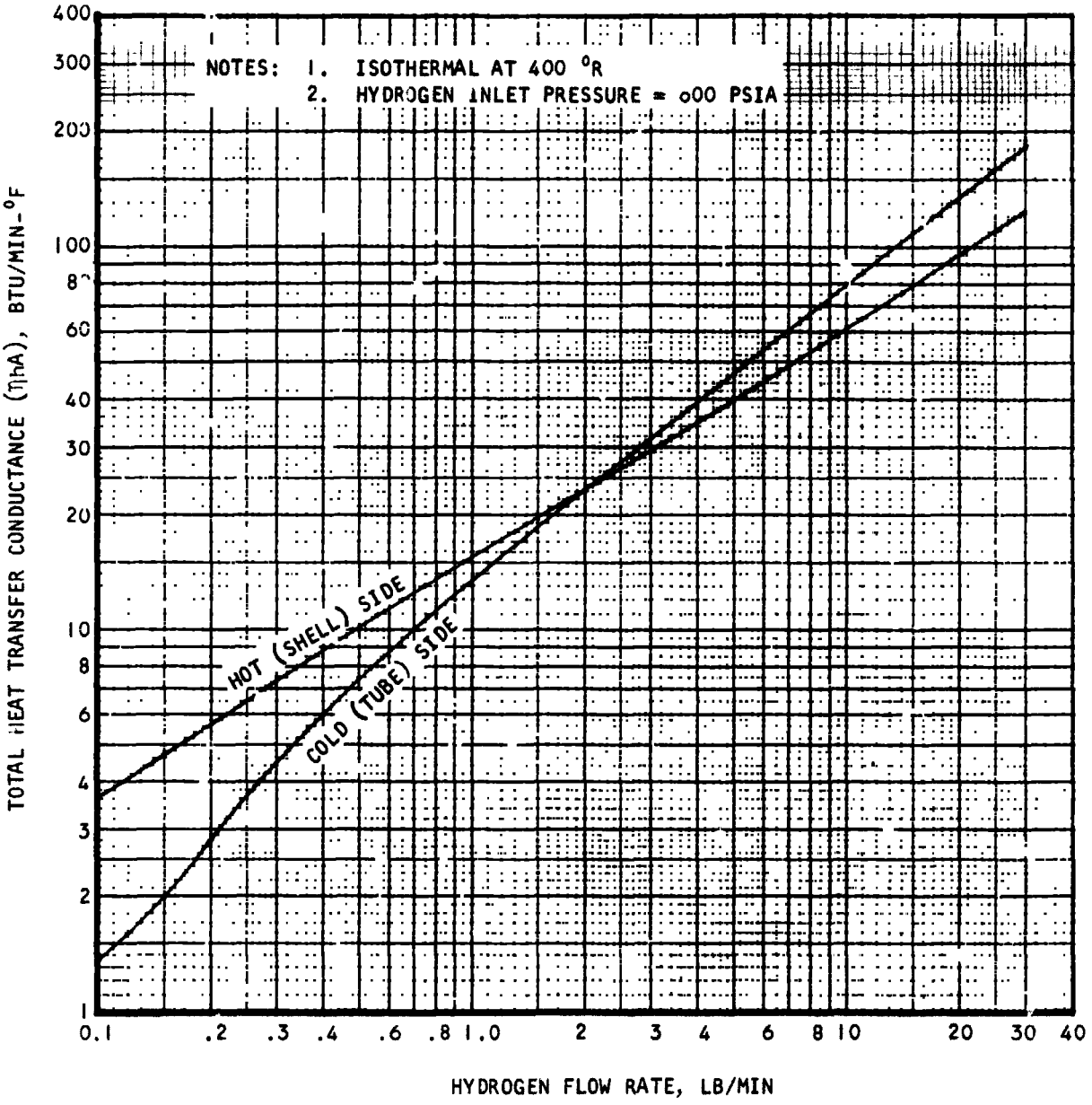

Figure 7-6. Heat Transfer Conductance of SSAPU Preheater/Regenerator

Although the heat transfer design point is defined by a regenerator operating condition, the most severe structural environments occur when the heat exchanger is operated as the preheater. In defining the structural operating conditions, no-bypass operating points were not considered. Although bypass operating points exist with higher hot fluid inlet temperatures than Condition 14, temperature level alone is not the determining factor of stress level. The combination of flow, temperature, and matrix temperatures for preheater operation at Condition 14 indicate the worst condition, and thus the unit, which has been stressed to these levels, will be adequate at all other operating points. The structural design point is listed in Table 7-4.

TABLE 7-4

PREHEATER/REGENERATOR STRUCTURAL REQUIREMENTS

Life: 1000 Start Stop Cycles
Material: 347 Stainless Steel
Operating Conditions:

	Hot Side	Cold Side
Fluid	Hydrogen	Hydrogen
Flow rate, lb/min	7.693	8.331
Inlet temperature, ^{o}R	1152	55
Outlet temperature, ^{o}R	679	426
Inlet pressure, psia	600	600

SPECIFICATION

SSAPU TEMPERATURE EQUALIZER

FUNCTION 5-1-73

The hydrogen-oxygen temperature equalizer functions to bring the temperature of the two propellant flows to nearly the same level at the inlet to the propellant flow control valves. This component tends to reduce the turndown ratio required for the reference APU system and may thereby facilitate system controllability. A vented buffer zone is provided between the hydrogen and oxygen passages, thus precluding mixing of the two fluids in the unlikely event of a leak in one of the fluid passages.

DESIGN POINT

Table 7-5 lists the heat transfer design point for the temperature equalizer design shown on drawing 159580. The design point was established by system analysis, and the resulting design is adequate for operating conditions.

TABLE 7-5

TEMPERATURE EQUALIZER HEAT TRANSFER DESIGN POINT

	Cold Side	Hot Side
Fluid	Oxygen	Hydrogen
Flow rate, lb/min	6.034	8.422
Inlet temperature, ^{o}R	300	707.9
Outlet temperature, ^{o}R	661.6	688.6
Inlet pressure, psia	674.6	507.4
Core pressure drop, psi	1.50	8.16
Duct diameter, in.	0.5	1.0
Total Heat Transferred, Btu/min	569	

The structural design point is listed in Table 7-6. This condition represents the worst case combination of pressures and temperatures. The equalizer has been designed to withstand the conditions of Table 7-6.

DESCRIPTION

The temperature equalizer is an annular plate fin heat exchanger. Three concentric finned passages are provided. The inner passage carries the oxygen, and the outer the hydrogen. The middle passage separates the two fluids and

TABLE 7-6

TEMPERATURE EQUALIZER STRUCTURAL DESIGN POINT

Life	1000 start stop cycles
Material	347 stainless steel
Hydrogen side operating pressure	700 psig
Hydrogen side proof pressure	1050 psig
Oxygen side operating pressure	900 psig
Oxygen side proof pressure	1350 psig
Hydrogen inlet temperature	700 - 1100°R
Oxygen inlet temperature	275 - 560°R
Hydrogen outlet temperature	680 - 1100°R
Oxygen outlet temperature	650 - 1100°R

is vented, thus providing a buffer zone between the two highly reactive fluids. The fin designation in the three passages is listed below:

Oxygen fin	28R-0.100-0.1(0)-.006
Buffer fin	28R-0.040-0.1(0)-.006
Hydrogen fin	12R-0.125-0.5(0)-.006

The heat exchanger is constructed of stainless steel, with the exception of the heat transfer fins, which are formed from copper. This fin material was selected from thermal performance optimization considerations.

PERFORMANCE

Figure 7-7 presents the pressure drop characteristic of both sides of the heat exchanger. Figure 7-8 presents the corresponding heat transfer conductances. The buffer passage conduction resistance has been combined with the oxygen conductance. These curves represent the performance and pressure drop utilized by the system performance program.

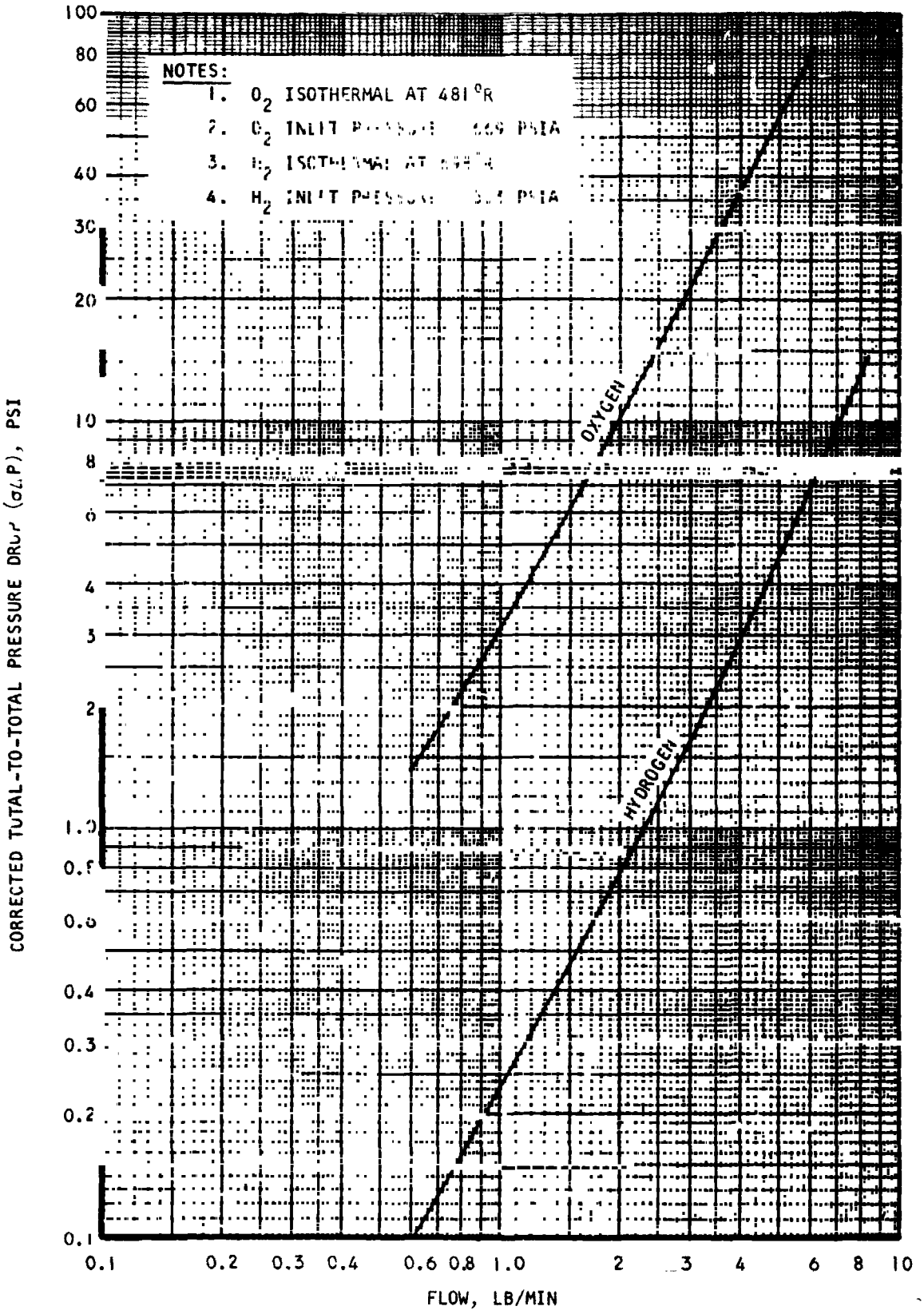

Figure 7-7. Isothermal Pressure Drop, SSAPU Temperature Equalizer

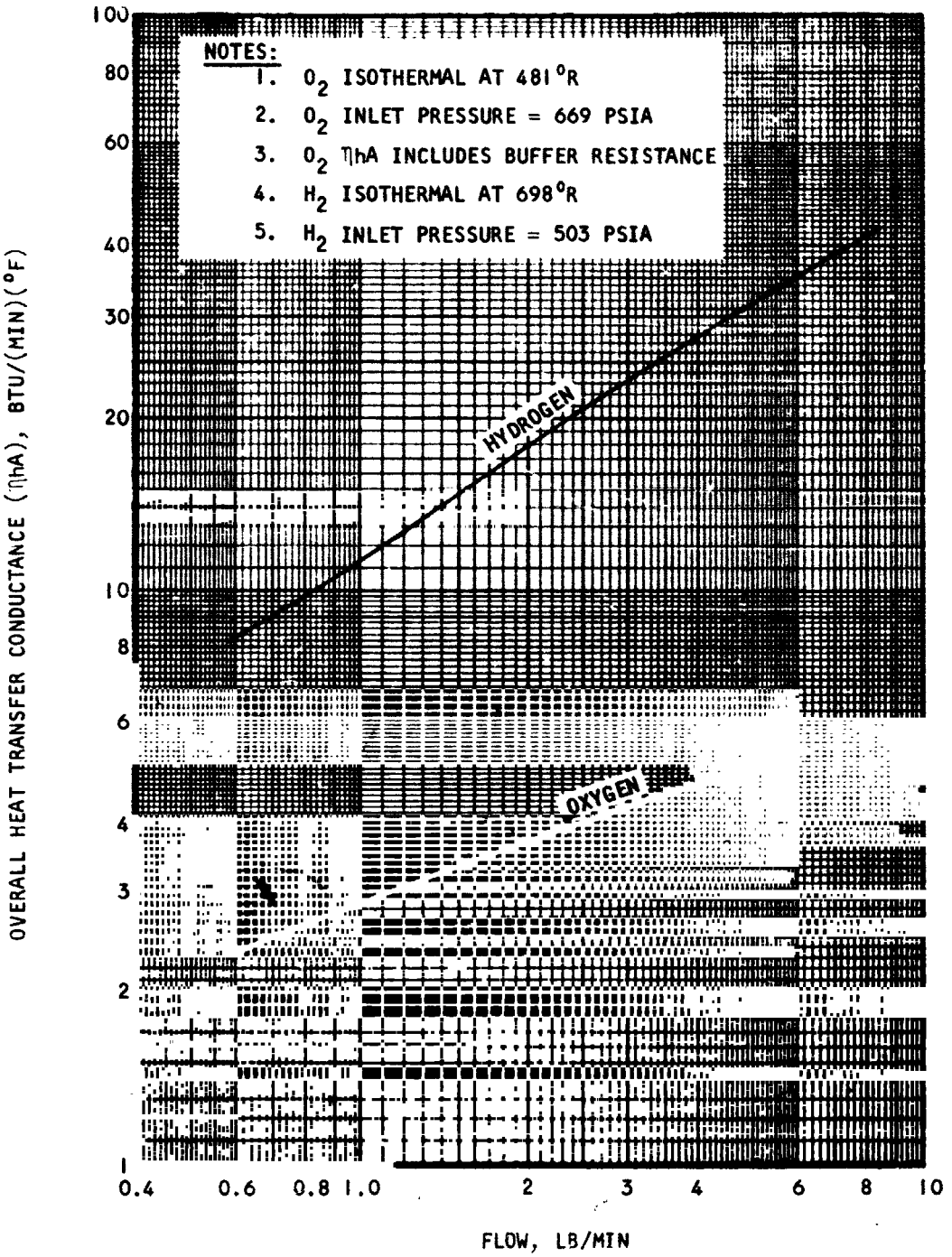

Figure 7-3. Heat Transfer Conductance, APU Temperature Equalizer

PRELIMINARY SPECIFICATION

SSAPU RECUPERATOR

FUNCTION

This heat exchanger operates with hydrogen on the cold side and turbine exhaust gas on the hot side. It serves to provide sufficient heat input into the cycle for propellant thermal conditioning and to improve cycle thermal efficiency by recovering waste heat from the turbine exhaust.

DESIGN REQUIREMENTS

Table 7-7 lists the design point for the heat exchanger design shown in Drawing No. L-198783. This design point was established by system analysis, and the resulting design is adequate for all operating points.

TABLE 7-7

RECUPERATOR DESIGN POINT

	Cold Side	Hot Side
Fluid	Hydrogen	Hydrogen-Steam (60-40 by Mass)
Flow rate, lb/min	8.43	14.67
Inlet temperature, ^{0}R	503	1366
Outlet temperature, ^{0}R	1122	785*
Inlet pressure, psia	600	16.8
Core pressure drop, psi	1.8	1.86
Effectiveness	0.717	0.673
Duct diameter, in.	1.0	4.0
Total heat transferred, Btu/min	18,059	

* Minimum allowable outlet temperature = $700^{0}R$

DESCRIPTION

The recuperator is a box and U-tube design, as shown in Drawing No. L-198783, with the following core geometry:

Number of tubes	768
Tube diameter	0.125 in. OD
Tube wall thickness	0.010 in.
Tube designation	
Inside	DMP 08
Outside	150100

The exhaust gas from the turbine flows in a single pass through the shell side of the heat exchanger. This minimizes the pressure drop in the exhaust gas stream. The hydrogen flows in cross counterflow through the tubes of the unit. This flow arrangement allows the box structure to be lightly pressure-loaded by the exaust gas and the high pressure hydrogen is contained within the tubes of the heat exchanger.

PERFORMANCE

Figures 7-9 and 7-10 present the corrected pressure drop of the exhaust products and hydrogen side, respectively. These pressure drops do not account for inlet and outlet manifold losses, and are thus representative of core loss only. Manifold losses are accounted for in the system program as a portion of the ducting losses. **Figures 7-11 and 7-12 present the heat transfer conductance** for the exhaust gas and hydrogen sides of the heat exchanger, respectively as a function of flow. The system program evaluates these conductances as a function of flow, corrects them for temperature and pressure dependent variations in physical properties, and then combines the conductances on the two sides into an overall heat transfer conductance for the recuperator at the particular operating point. This overall heat transfer conductance and the ratio of the weight flow-specific heat products uniquely determine the performance of the heat exchanger.

DISCUSSION

The AiResearch thermal analyzer program has been utilized to examine in detail the operating conditions of the recuperator. A nodal model utilizing 144 metal and fluid nodes was used. The steady state operating conditions examined were numbers 14 and 158. In addition, the start transient was examined. The results of these studies verified the performance and pressure drop predicted by the system computer program from **Figures 7-9 through 7-12. The** results of the thermal analyzer study were also utilized to define the structural requirements of the heat exchanger.

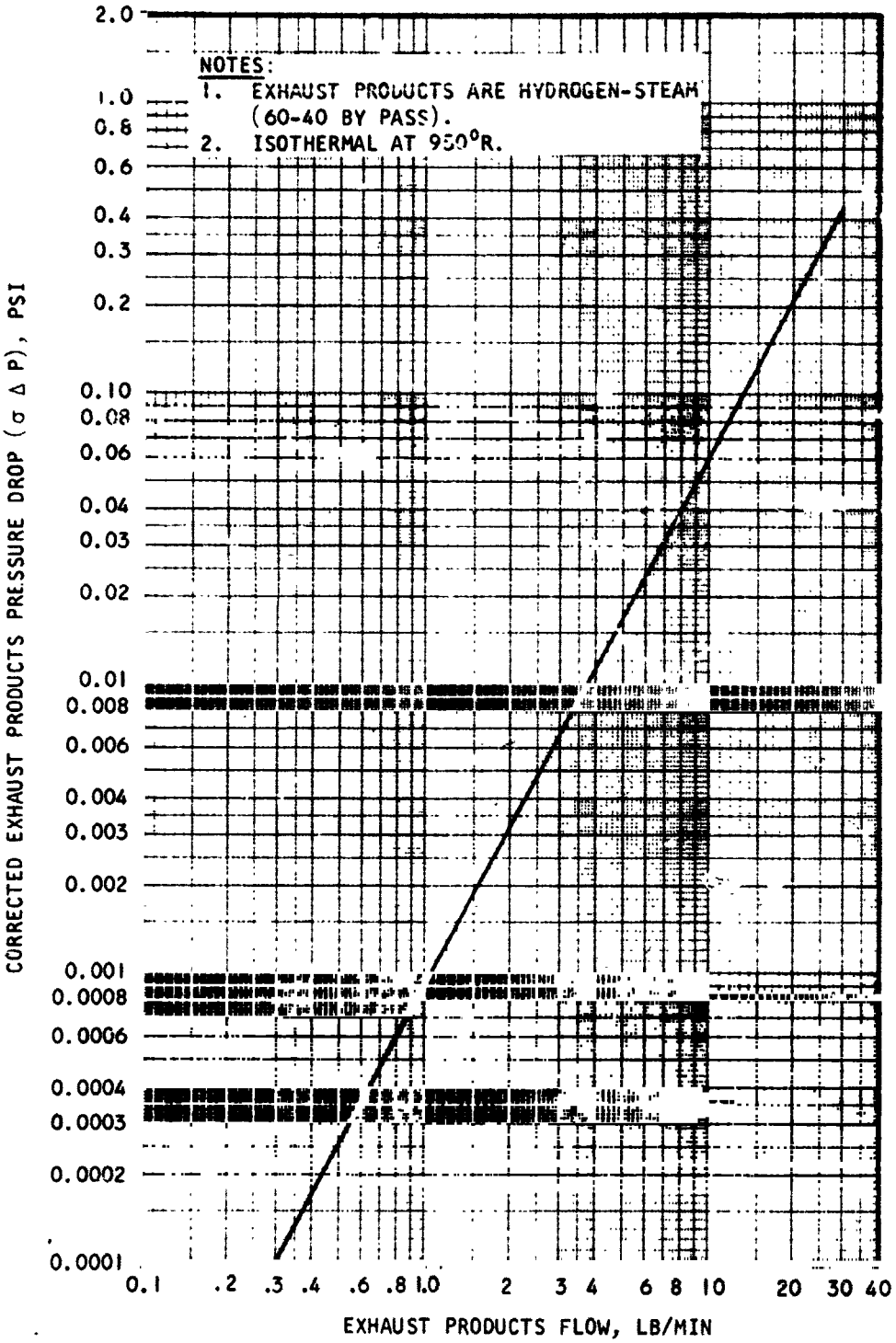

Figure 7-9. Exhaust Products Pressure Drop of Recuperator

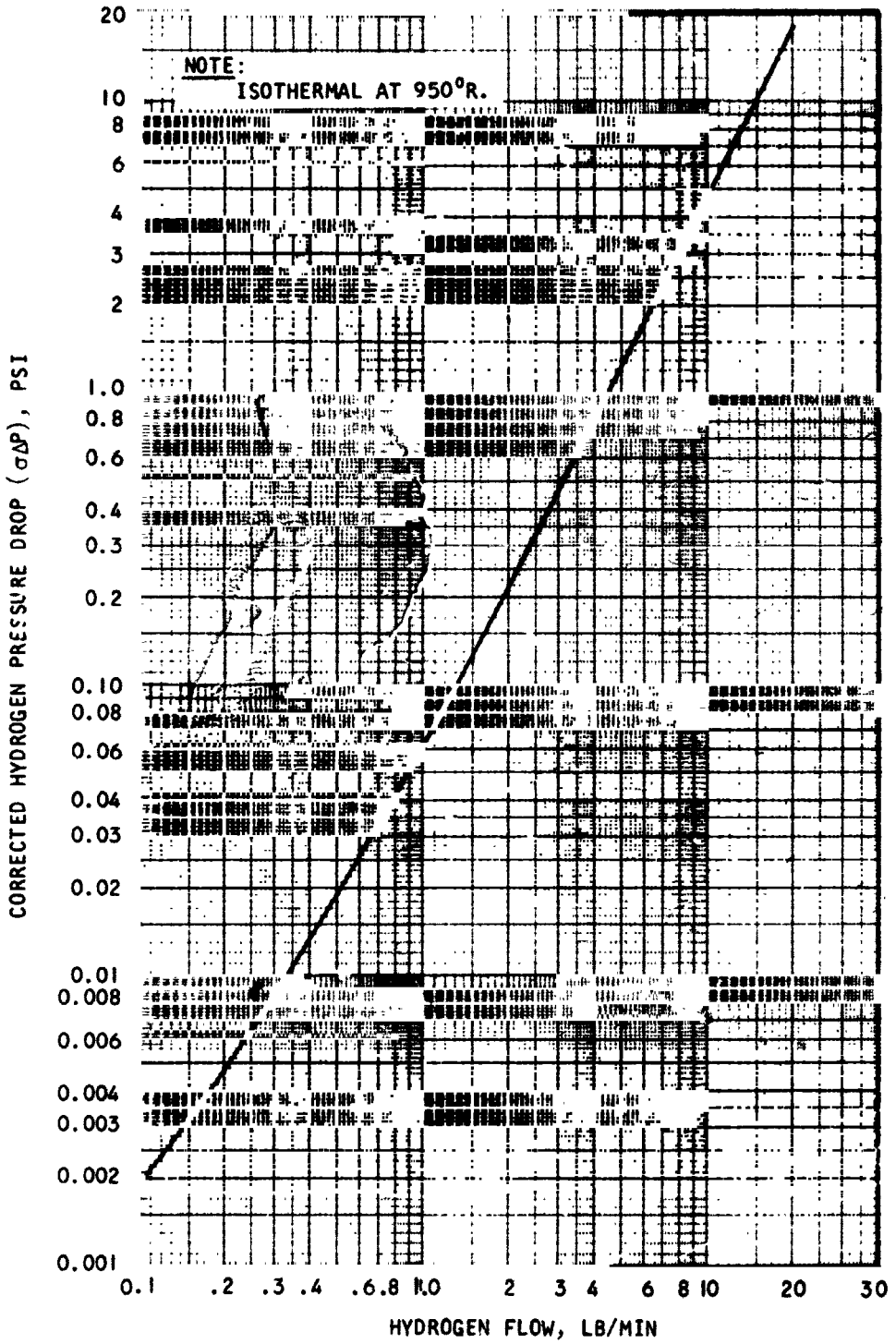

Figure 7-10. Hydrogen Pressure Drop of Recuperator

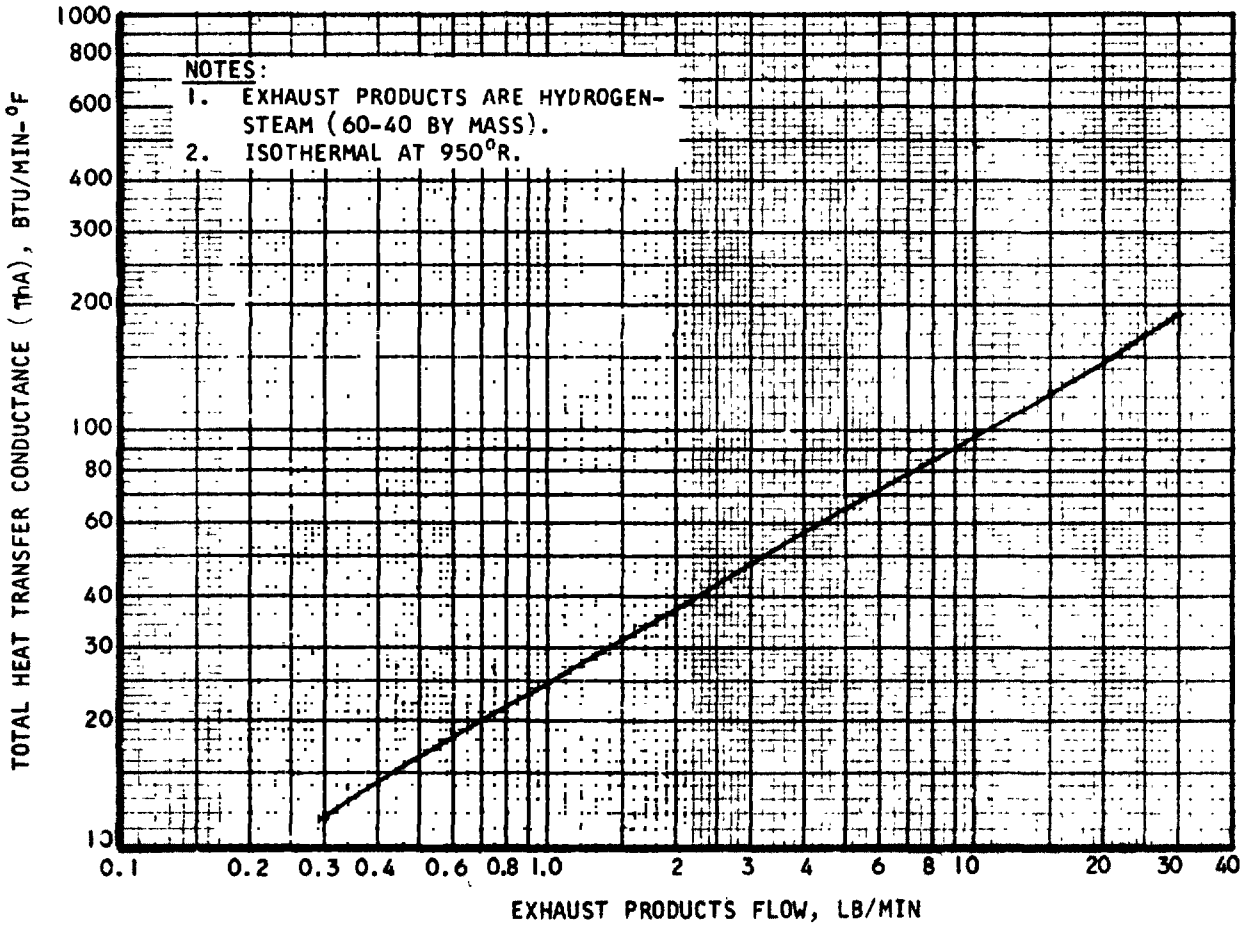

Figure 7-11. Exhaust Products Heat Transfer Conductance of Recuperator

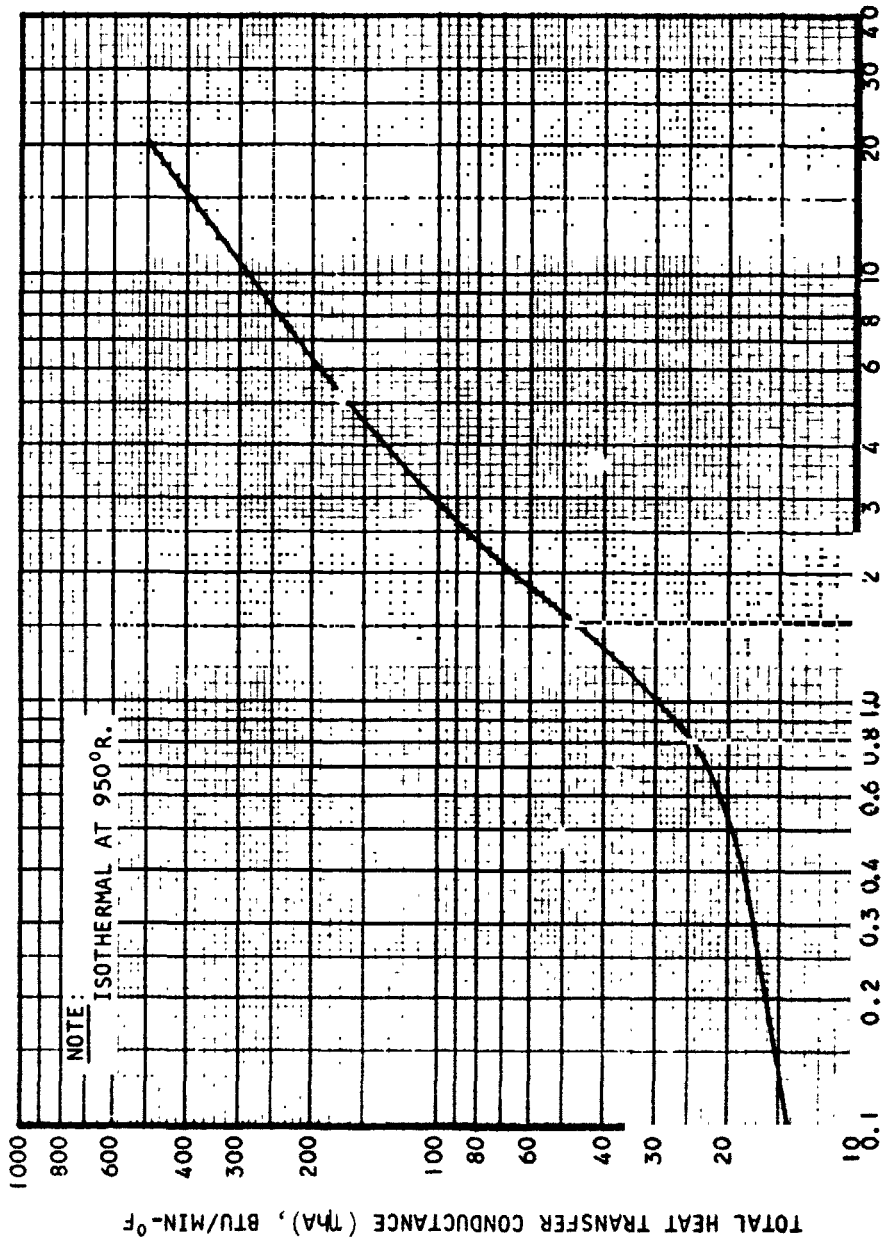

Figure 7-12. Hydrogen Heat Transfer Conductance of Recuperator

The nodal model indicates that all metal temperatures are above 700°R at condition 15B, and thus no water will be condensed from the exhaust products. At condition 14, approximately 12 percent of the matrix is below 700°R, and thus some condensation will occur. This condition will not impose operating penalties, and cannot cause freezeup on shutdown. The condensation occurs at the exit face of the core, and only over one-third of the tube length. The water condensed will be immediately carried downstream, and thus cannot fill the core. In addition, this operating condition represents sea level full power. In the unlikely event of shutdown from full power, the residual water will not be exposed to the hard vacuum of space and the attendant flash freezing.

Thus the recuperator preliminary design presented here is adequate in all respects for the intended application.

Test System Heat Exchangers

This section summarizes the analyses performed to assure adequate performance and structural integrity for the six heat exchangers contained in the system. Each of two of the heat exchangers is utilized in two separate locations in the system, which was made possible by similarity of requirements. All heat exchangers were designed to conform to the specification presented in this section.

System design iterations.--The heat exchangers described in this section represent the result of many design iterations. To define individual requirements, system operation must be investigated over a wide range of operating parameters. Representative heat exchangers are designed and the performance calculated. The performance characteristics are then input to the APU system program, and many operating conditions are investigated.

As system operating points that cause undesirable conditions are identified, scaling factors may be utilized to modify the calculated heat exchanger performance. This procedure results in a new set of heat exchanger requirements. The heat exchangers are redesigned, the performance over a wide range of conditions calculated, and new inputs prepared for the system program.

Design procedure.--The design of the heat exchangers is performed with the aid of standard computer programs. The allowable fluid pressure drops and the heat transfer required form the basis for the problem statement. The fluid flow rates and temperatures and pressures are also required conditions.

The heat transfer and pressure loss characteristics of the many heat exchanger surfaces available at AiResearch have been accumulated over may years of testing. These data have been complied and are stored in computer data banks.

Based on the input conditions, the design computer programs determine the heat exchanger required to satisfy the single operating point. During this design process, many solutions to the single-point operating condition are calculated. Each solution represents one combination of the many heat transfer surfaces available, allowing the most attractive to be selected.

Once a particular heat exchanger has been selected for a given application, its performance over the full range of operating parameters is required. Another type of computer program, performance prediction, is utilized to generate the required information.

In the performance prediction computer programs, the geometry of the heat exchanger and the pertinent characteristics of the surfaces are input. Fluid flow rates and temperature levels may be varied over any range desired. The performance at each operating condition specified is calculated and the resulting performance map is utilized as input to the APU system program.

The next step in the design procedure occurs after the heat exchanger is determined acceptable for all system operating conditions. Thermal analyzer programs are utilized to investigate local phenomena in the heat exchanger core, such as congealing of oil, condensation of water from the exhaust products, and the effects of flow maldistribution. In addition, local temperature levels and profiles used to determine thermal stress levels. At this stage in the design process, a layout drawing is prepared.

A detailed stress analysis of the heat exchanger as depicted on the layout drawing is preformed. The conditions investigated include proof and burst pressure, pressure cycling, flow-induced vibrations, and both steady-state and transient cyclic thermal stresses. The heat exchanger is modified as necessary to withstand all imposed loading.

Upon completion of the above design procedures and approval following a design review, the heat exchanger detail drawings are made.

Lube oil hydraulic oil cooler.--The test system lube/hydraulic oil cooler is shown in dwg. 159550. In this tube-and-shell, four-pass, cross-counterflow heat exchanger, the hydrogen flows inside the tubes, and the oil flows across the tube bundle four times in an overall counterflow direction. The unit is of all-stainless-steel brazed and welded construction. Since the unit does not experience the high temperature gradients of some of the remaining heat exchangers, it is a more conventional design. This type of construction is typical of many oil cooling heat exchangers manufactured by AiResearch.

The hydrogen flows inside the tubes for pressure containment reasons, and the lower pressure oils flow in the shell side. The tubes are periodically ring-dimpled for turbulence promotion, and are arranged in a staggered pattern with respect to oil flow direction.

The lube/hydraulic oil cooler was modeled in detail in the thermal analyzer computer program. The nodal model employed is presented in fig. 7-13. The steady-state metal temperatures for two operating conditions are presented in tables 7-8 and 7-9. The solutions presented in table 7-8 indicate the conditions that exist when lube oil is the hot fluid. Table 7-9 presents the corresponding information when the heat exchanger is utilized to cool hydraulic fluid. The inlet conditions, flow and temperature, are taken from the input of the APU system computer program. In addition to providing the metal temperature information, the steady-state solutions indicate that fluid outlet temperatures are in agreement with the system program. Thus, the detailed model for the thermal analyzer has verified the performance predictions of the other computer programs utilized.

The lube/hydraulic oil cooler was structurally analyzed for pressure test, tube variation, and pressure-thermal cycle life requirements. The design shown in dwg. 159550 was found satisfactory for the structural loads encountered in the lube oil and hydraulic oil cooling applications. A summary of stresses, margins of safety, and cyclic life fraction summation are given in table 7-10.

FOLDOUT FRAME

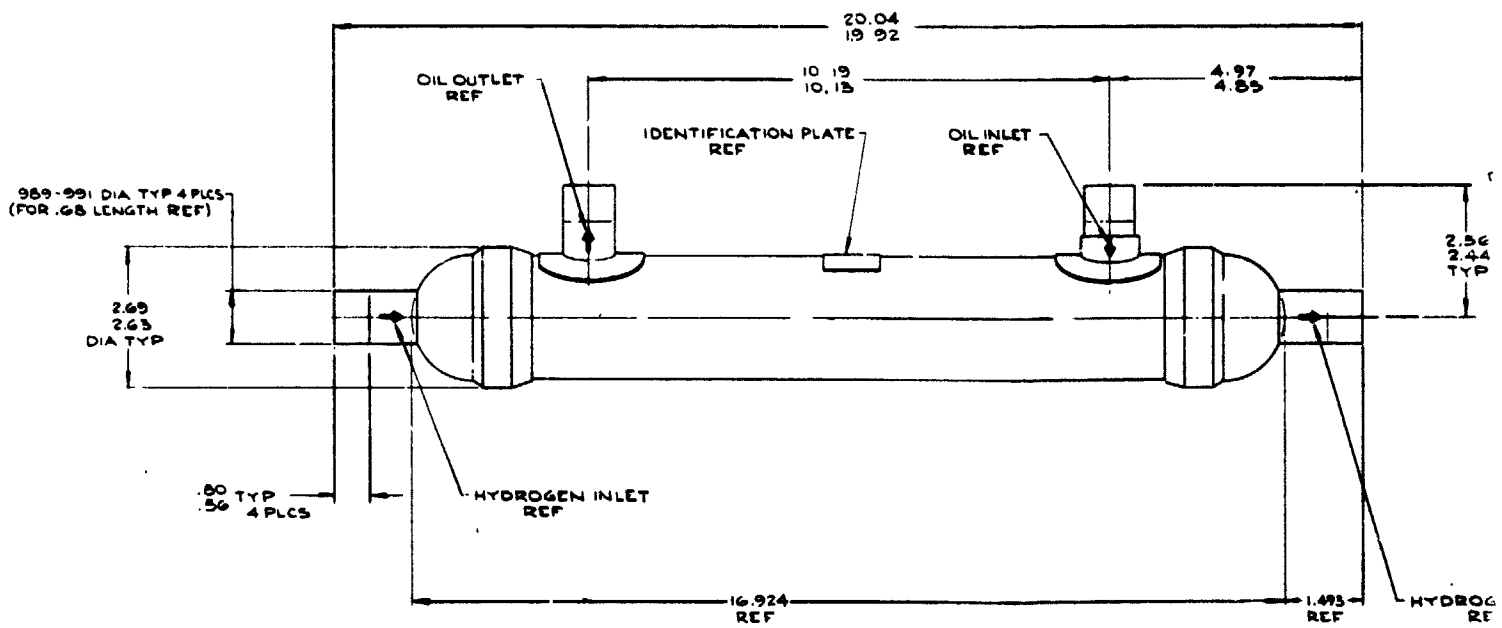

3. THIS UNIT IS DESIGNED TO WITHSTAND 500 PSIG PROOF ON THE OIL SIDE AND 1050 PSIG PROOF ON THE HYDROGEN SIDE @ 72°F
2. ALL OPENINGS ARE PROVIDE WITH SHIPPING COVERS REMOVE ONLY AT TIME OF INSTALLATION.
1. DIMENSIONS SHOWN ARE FOR INSTALLATION PURPOSES ONLY.

FOLDOUT FRAME 2

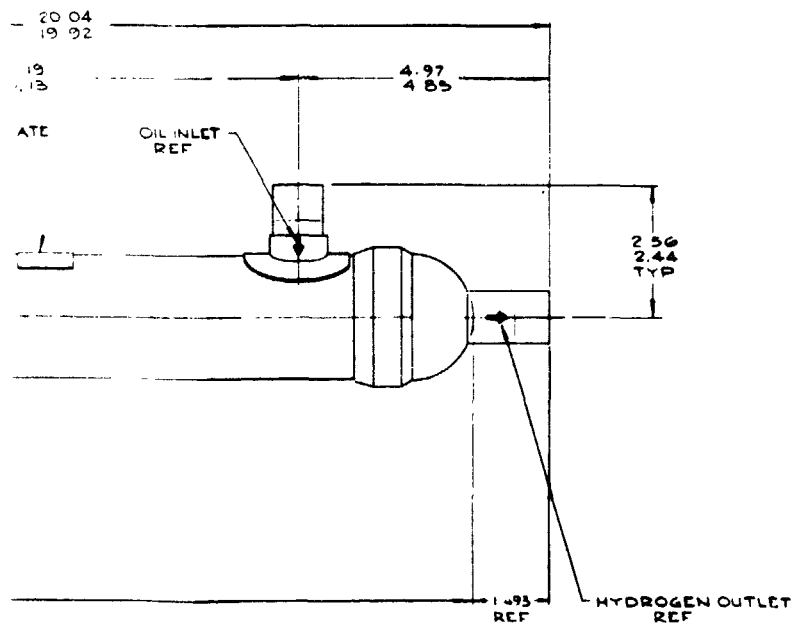

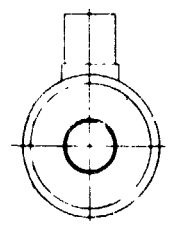

THIS UNIT IS DESIGNED TO WITHSTAND 300 PSIG PROOF ON THE OIL SIDE AND 1050 PSIG PROOF ON THE HYDROGEN SIDE @ 72° F

ALL OPENINGS ARE PROVIDE WITH SHIPPING COVERS REMOVE ONLY AT TIME OF INSTALLATION

DIMENSIONS SHOWN ARE FOR INSTALLATION PURPOSES ONLY.

PART NO.	ASSY NO.	CALC WEIGHT	REMARKS
159550-1-1	159551-1		

COOLER OUTLINE, OIL, LUBE/HYDRAULIC

E | 70210 | 159550

FINAL APPLICATION

7-27/7-28

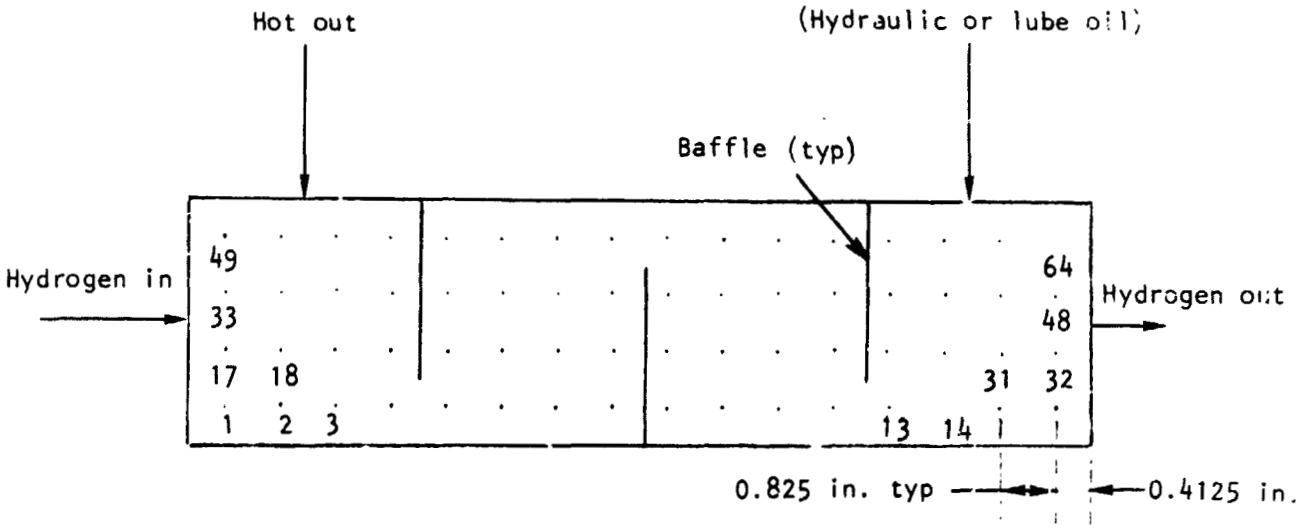

Notes: 1. Node numbers listed; refer to matrix

2. Oil and hydrogen streams have a corresponding number of nodes

3. Oil is mixed between passes

S-81256

Figure 7-13.--Lube Oil and Hydraulic Fluid Coolers Nodal Model.

TABLE 7-8

LUBE OIL COOLER METAL NODE STEADY-STATE SOLUTION

Condition 14		Condition 15B	
NODE NO.	TEMP.	NODE NO.	TEMP.
1	480.81	1	540.46
2	482.80	2	562.21
3	484.77	3	581.27
4	486.70	4	597.26
5	488.10	5	612.24
6	491.09	6	625.97
7	493.05	7	638.23
8	494.97	8	649.03
9	500.54	9	673.63
10	503.10	10	683.34
11	505.61	11	691.40
12	508.09	12	698.42
13	511.34	13	704.81
14	513.93	14	710.44
15	516.48	15	715.50
16	518.98	16	719.88
17	480.17	17	534.10
18	482.04	18	555.56
19	483.91	19	574.64
20	485.73	20	591.66
21	489.24	21	613.20
22	491.54	22	627.34
23	493.58	23	639.95
24	495.42	24	650.98
25	499.91	25	670.84
26	502.34	26	680.50
27	504.76	27	686.62
28	507.12	28	695.75
29	511.70	29	705.13
30	514.45	30	711.15
31	517.15	31	716.53
32	519.79	32	720.78
33	479.71	33	529.12
34	481.51	34	550.21
35	483.28	35	569.38
36	485.01	36	585.83
37	489.42	37	614.61
38	491.64	38	629.32
39	493.62	39	642.23
40	495.47	40	653.42
41	499.39	41	668.48
42	501.72	42	678.05
43	504.01	43	686.19
44	506.24	44	693.38
45	512.15	45	705.96
46	515.05	46	712.13
47	517.91	47	717.40
48	520.69	48	721.94
49	478.89	49	524.89
50	480.54	50	546.09
51	482.16	51	564.28
52	483.76	52	580.77
53	489.31	53	616.80
54	491.63	54	631.90
55	493.92	55	645.03
56	496.17	56	656.31
57	498.62	57	666.55
58	500.83	58	675.99
59	503.03	59	684.24
60	505.18	60	691.29
61	512.37	61	707.22
62	515.44	62	713.50
63	518.46	63	718.81
64	521.41	64	723.28

Fluid conditions

Condition 14: Maximum power, sea level, 550°R bulk temperature of hydraulic fluid

Hot flow, lb/min	28.5
T in, °R	611
T out, °R	532
Cold flow, lb/min	8.33
T in, °R	470
T out, °R	508

Condition 15B: Idle power, altitude

Hot flow, lb/min	28.5
T in, °R	744
T out, °R	663
Cold flow, lb/min	1.17
T in, °R	422
T out, °R	706

Note: See fig. 7-13 for node locations.

TABLE 7-9

HYDRAULIC FLUID COOLER METAL NODE STEADY-STATE SOLUTION

Condition 14		Condition 15B	
NODE NO.	TEMP.	NODE NO.	TEMP.
1	474.98	1	604.07
2	477.56	2	622.24
3	480.06	3	638.75
4	482.48	4	652.94
5	485.24	5	665.05
6	487.65	6	676.44
7	490.00	7	685.99
8	492.30	8	693.93
9	497.70	9	707.84
10	500.41	10	713.51
11	503.04	11	717.73
12	505.59	12	721.31
13	508.49	13	724.14
14	511.02	14	726.79
15	513.47	15	728.95
16	515.83	16	730.71
17	474.56	17	597.96
18	477.06	18	616.96
19	479.50	19	634.03
20	481.86	20	648.79
21	485.41	21	666.50
22	487.90	22	677.86
23	490.32	23	687.55
24	492.69	24	695.23
25	497.19	25	706.57
26	499.81	26	712.16
27	502.36	27	716.70
28	504.84	28	720.39
29	508.69	29	724.43
30	511.30	30	727.09
31	513.83	31	729.24
32	516.27	32	730.99
33	474.17	33	591.98
34	476.58	34	611.69
35	478.95	35	629.29
36	481.26	36	644.57
37	485.59	37	668.08
38	488.16	38	679.39
39	490.66	39	686.80
40	493.10	40	696.57
41	496.76	41	705.35
42	499.50	42	711.05
43	501.78	43	715.70
44	504.19	44	719.50
45	508.92	45	724.76
46	511.61	46	727.42
47	514.22	47	729.56
48	516.73	48	731.29
49	473.76	49	586.29
50	476.11	50	606.66
51	478.42	51	624.66
52	480.66	52	640.40
53	485.80	53	669.85
54	488.45	54	681.06
55	491.03	55	690.36
56	493.54	56	697.99
57	496.36	57	704.22
58	498.83	58	709.99
59	501.23	59	714.74
60	503.57	60	718.64
61	509.22	61	725.14
62	512.01	62	727.78
63	514.68	63	729.90
64	517.29	64	731.60

Fluid conditions

Condition 14: Maximum power, sea level, 550°R bulk temperature of hydraulic fluid

Hot flow, lb/min	57
T in, °R	596
T out, °R	539
Cold flow, lb/min	8.33
T in, °R	460
T out, °R	505

Condition 15B: Idle power, altitude

Hot flow, lb/min	57
T in, °R	738
T out, °R	698
Cold flow, lb/min	1.17
T in, °R	397
T out, °R	735

Note: See fig. 7-13 for node locations.

TABLE 7-10

SUMMARY OF LUBE/HYDRAULIC OIL COOLER STRESSES

Part names and numbers	Design condition	Stress, ksi	Allowables, ksi	M.S. or Σ n/N**
Tubes at dimples	Proof pressure, 900 psi	38.7	32.0 typical at 150°F	-0.172*
	Vibratory	2.4		
	Pressure-thermal cycling (1000)	29.8		0.50
Header plate	Proof pressure, 900 psi	32.5	32.0	-0.015
	Pressure-thermal cycling (1000)	36.1		0.0003 $\Sigma\eta$ /N
Head manifold	Proof pressure, 900 psi	26.8	32.0	0.196
	Pressure thermal cycling (1000)	30.2		~0.00
Housing case	Proof pressure, 300 psi	10.8	32.0	1.97

*See discussion on page 7-2.

**The cyclic life fraction summation is an application of Miner's rule, where n is the required number of cycles at a given applied load and N is the expected cyclic life at this load.

The oil cooler structural design is controlled by the proof pressure requirement of 300 psig on the oil side and 900 psig on the hydrogen side. AiResearch computer program X0560 (used for analysis of shell-and-tube heat exchangers) was used to determine the pressure stresses. The analysis was based on pressure test of each heat exchanger flow circuit with the other circuit unpressurized. Results of the analysis show that the material yield strength is slightly exceeded at the center of the header plates and at the dimples adjacent to the header plates in tubes closest to the shell. These stresses are very localized and are considered acceptable. The header plate cyclic life fraction is very low and indicates a high margin of safety. The tube dimple stress of 38.7 ksi resulted from application of a stress concentration factor of 2.5, which was used for the dimple throughout the analysis and is appropriate for fatigue and cycle life calculations. However, the use of this factor in the proof pressure stress is conservative, and on the basis of experience, the tubes are considered structurally satisfactory.

Calculated fatigue damage resulting from 1000 pressure-thermal cycles and vibratory loading indicates a high margin of safety for the oil cooler. Acoustic noise and tube vibration levels for this unit are low.

Recuperator.--The recuperator, shown in dwg. 159560, is a tubular two-pass, cross-counterflow design of all stainless steel brazed and welded construction. The hot-fluid, turbine exhaust products flow across the tubes once to minimize pressure drop, and the hydrogen makes two passes through the tubes. Due to the large pressure and temperature differentials between the two fluids, a U-tube design was selected to minimize thermal stresses.

The tubes are dimpled periodically in the straight heat transfer sections to promote turbulence in the hydrogen. The U-bends are not dimpled. With this arrangement, the majority of the pressure drop occurs in the dimpled sections, and the unequal flow lengths in the U bends do not adversely affect flow distribution. The tubes are arranged in a staggered pattern with respect to exhaust gas flow so that there is direct impingement on every tube, thus maximizing the heat transfer coefficient. Five sound suppression baffles installed in the unit to eliminate acoustic noise caused by vortex shedding from the individual tubes.

Since the recuperator experiences the most severe high-temperature thermal environment of any heat exchangers in the system, the thermal analyzer computer program was utilized to investigate both steady-state and transient operating conditions. The model utilized is presented in fig. 7-14. In addition to the nodes, this model also utilized sections. The average temperature of each section and the section-to-section temperature differences are of prime interest in the U-tube design. These values dictate the differential thermal expansion, and thus the bending stresses. The results list section temperatures in addition to the node temperatures at the end of each section.

Table 7-11 presents the metal matrix temperatures for two steady-state operating conditions. These conditions represent the extremes of operation, full power and idle.

The sea level maximum power condition indicates that the metal temperatures in approximately 6 percent of the core are such that condensation of water may occur. This is not considered a serious condition because condensation will occur only at the exhaust products exit face, and any water will be carried out of the unit. In addition, if a sudden shutdown were to occur, there would be no freezing because the remaining water is exposed to 14.7 psia.

A worst-case start transient was also investigated. The transient conditions and metal temperatures are presented in table 7-12. The transient conditions assumed constitute the most severe environment in that instantaneous attainment of flow and temperature are assumed at zero time. The gas outlet temperatures during the transient are plotted in fig. 7-15. The sudden temperature change at 0.8 sec is caused by the exhaust products flow rate change. This characteristic has been essentially duplicated by the APU system computer program.

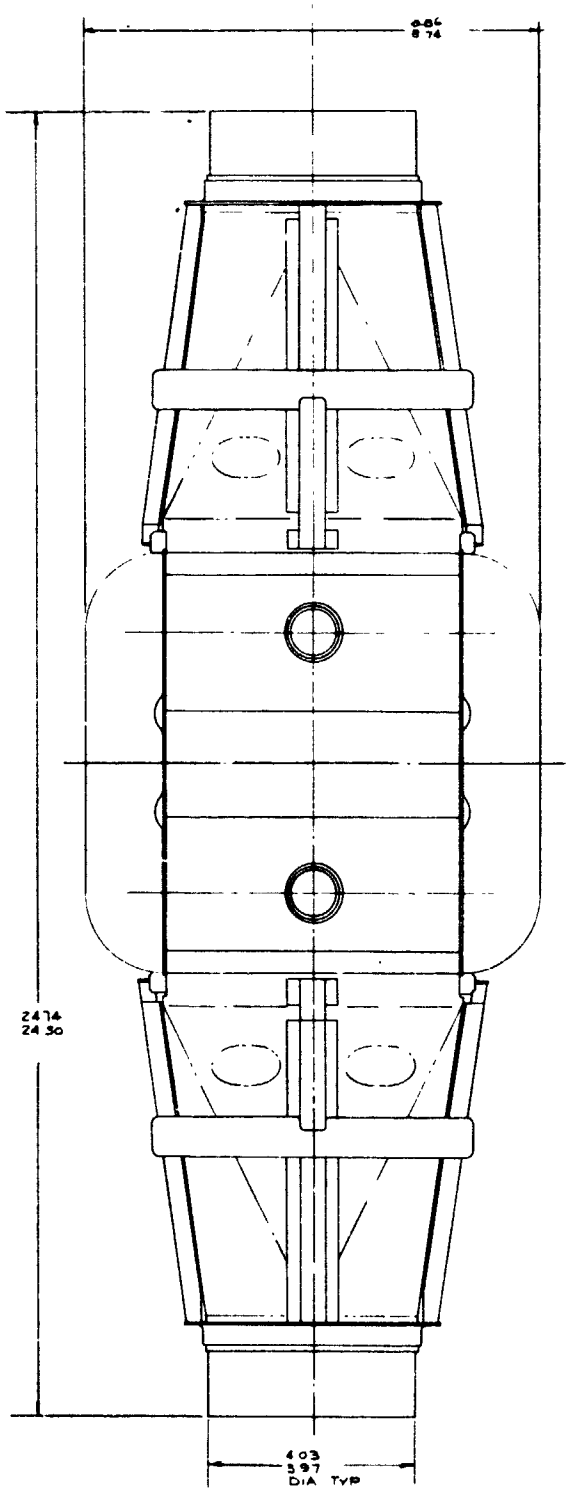

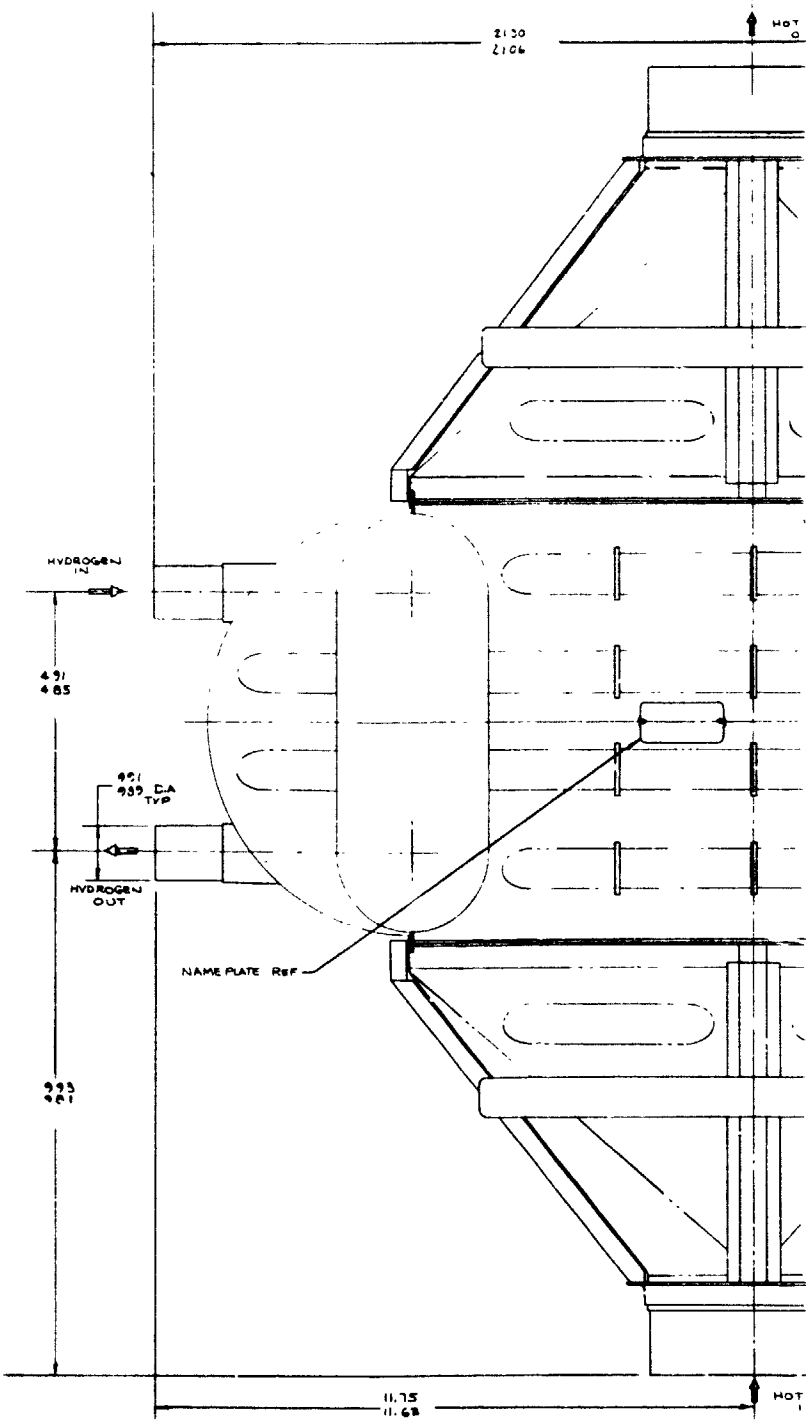

4 UNIT HAS BEEN HELIUM LEAK CHECKED FOR MAX LEAKAGE OF LESS THAN 1×10^{-6} CC/SECOND
3 UNIT DESIGNED TO WITHSTAND THE FOLLOWING CONDITIONS:
COLD SIDE - 600 PSIG MAX OPERATING AT 1050°F MAX,
900 PSIG PROOF - 1530 PSIG BURST
HOT SIDE - 187 PSIG EXTERNAL AT 1100°F MAX INTERNAL
2 SHIPPING CLOSURES ARE PROVIDED FOR ALL OPENINGS
REMOVE ONLY AT TIME OF INSTALLATION
1 ALL DIMENSIONS ARE FOR INSTALLATION PURPOSES ONLY.

NOTED UNLESS OTHERWISE SPECIFIED

FOLDOUT FRAME

1

FOLDOUT FRAME 2

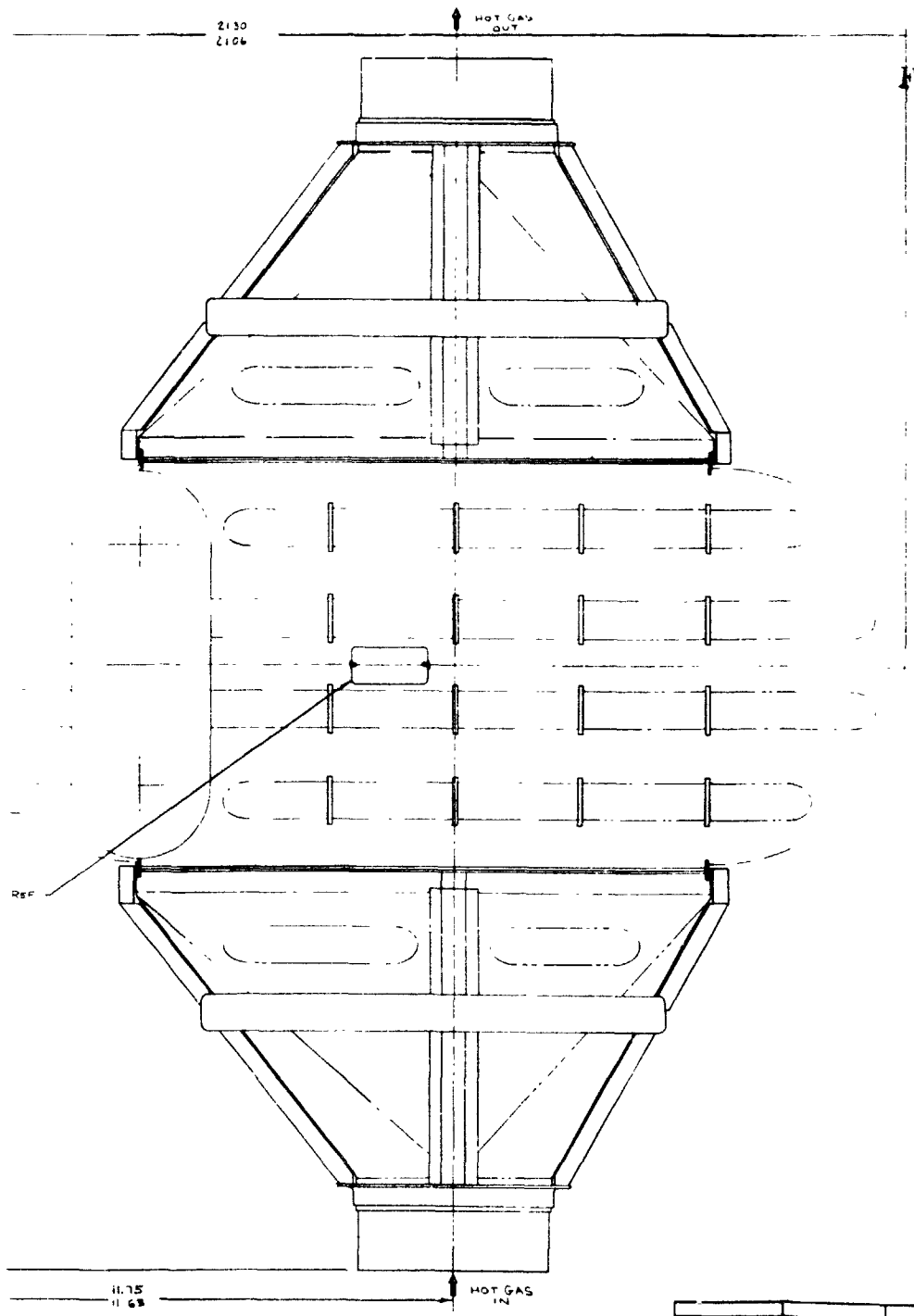

REVISIONS

4 UNIT HAS BEEN HELIUM LEAK CHECKED FOR MAX LEAKAGE OF LESS THAN 1×10^{-6} CC/SECOND

3 UNIT DESIGNED TO WITHSTAND THE FOLLOWING CONDITIONS:
COLD SIDE - 600 PSIG MAX OPERATING AT 1050°F MAX,
900 PSIG PROOF - 1500 PSIG BURST
HOT SIDE - 187 PSIG EXTERNAL AT 1100°F MAX INTERNAL

2 SHIPPING CLOSURES ARE PROVIDED FOR ALL OPENINGS
REMOVE ONLY AT TIME OF INSTALLATION

1 ALL DIMENSIONS ARE FOR INSTALLATION PURPOSES ONLY

NOTED UNLESS OTHERWISE SPECIFIED

159560-1-1	159561-1	
PART NO	ASSY NO	REMARKS

PARTS LIST

HEA. EXCHANGER OUTLINE, RECUPERATOR

SIZE	CODE IDENT NO	DWG NO
E	70210	159560

SCALE 1/1 SHEET 1 OF 1

APPLICATION (1) FINAL

7-35/7-36

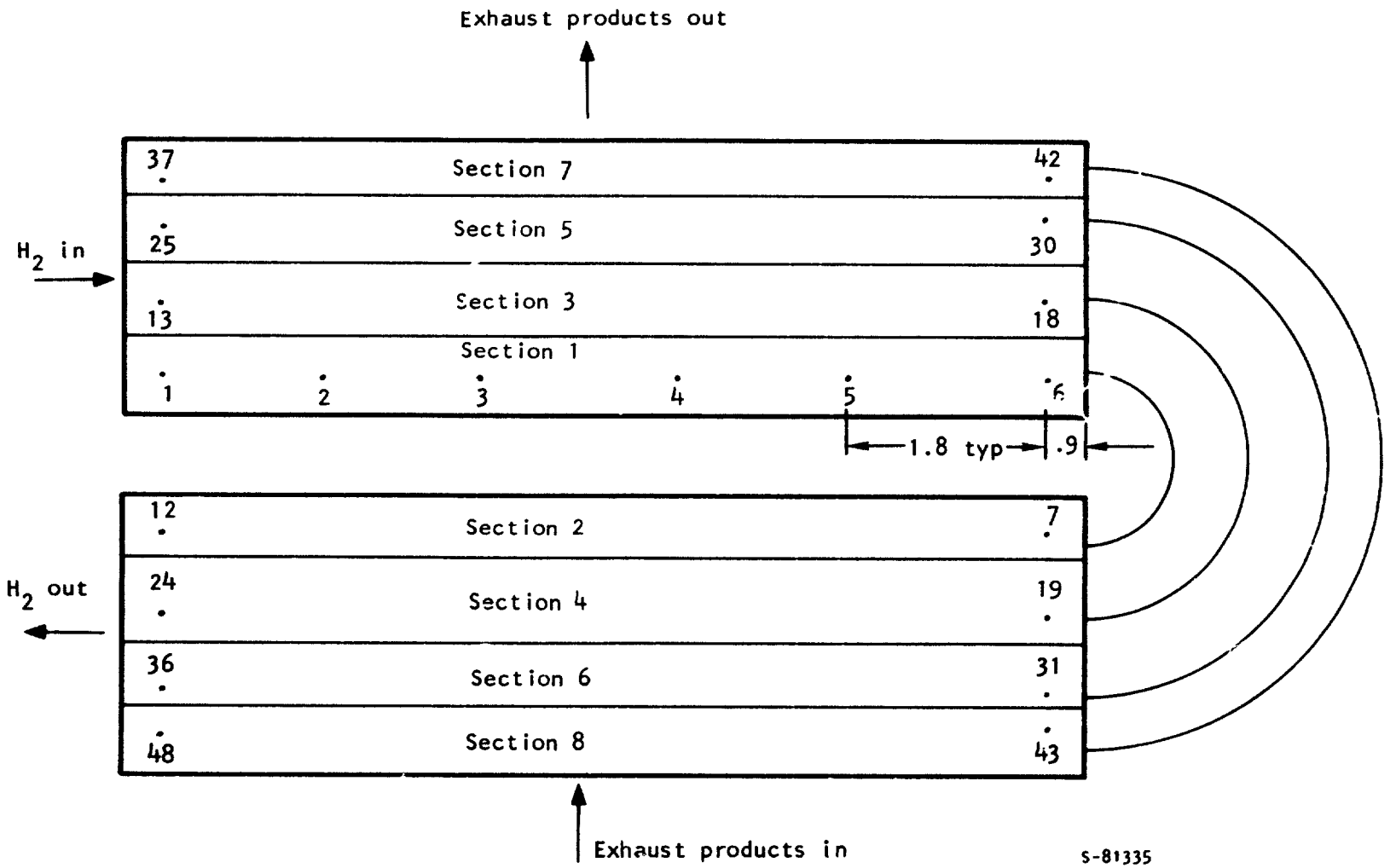

Figure 7-14.--Recuperator Nodal Model.

TABLE 7-11

RECUPERATOR STEADY-STATE
THERMAL ANALYZER SOLUTIONS

Section	Temperature, °R	
	Condition 14	Condition 15
1	866	1324
2	1031	1373
3	798	1283
4	1047	1374
5	743	1243
6	1083	1374
7	699	1204
8	1141	1375

Notes:

- All temperatures are metal temperatures in °R.
- Temperatures for sections are average values.
- Temperatures for nodes pertain to the node point
- Condition 14:

  Maximum power
  Sea level
  550°R hydraulic fluid
- Condition 15B

  Idle power
  Altitude
  750°R hydraulic fluid

Node	Temperature, °R	
	Condition 14	Condition 15
42	779	1353
30	824	1362
18	873	1367
6	925	1369
7	951	1368
19	940	1368
31	952	1368
43	996	1370
37	604	934
25	641	998
13	692	1080
1	767	1187
12	1111	1377
24	1146	1377
36	1194	1377
48	1254	1377
H_2 flow, lb/min	8.33	0.293
H_2 temp in., °R	509	707
H_2 temp out, °R	1145	1377
Exhaust products flow, lb/min	14.3	1.95
Exhaust products temp in	1384	1377
Exhaust products temp out	783	1215

TABLE 7-12

METAL TEMPERATURES FOR RECUPERATOR START TRANSIENT

Section	Time, sec										
	0.1	0.2	0.4	0.6	0.8	1.0	1.2	1.4	1.6	1.8	2.0
1	550	576	628	686	740	777	785	793	801	808	816
2	550	593	678	767	845	892	902	911	919	928	936
3	550	566	601	644	686	716	721	726	732	737	742
4	550	623	741	845	922	967	975	983	992	1000	1008
5	550	559	586	615	647	671	675	679	682	686	690
6	550	676	847	964	1035	1073	1081	1091	1100	1109	1118
7	550	556	572	595	620	638	641	644	646	649	651
8	550	773	1022	1137	1185	1210	1227	1243	1256	1267	1276
Node											
42	550	556	573	599	629	652	658	664	670	676	681
30	550	559	586	620	659	686	694	701	708	715	722
18	550	566	604	651	698	731	739	747	755	763	770
6	550	576	633	694	751	787	794	801	808	815	822
7	550	593	666	731	787	822	825	829	833	838	843
19	550	623	710	771	815	847	846	847	850	853	857
31	550	676	791	850	883	910	908	909	912	915	919
43	550	773	932	983	1002	1025	1036	1046	1054	1061	1066
37	550	556	568	583	598	609	606	604	602	601	600
25	550	559	578	599	619	635	632	629	628	627	673
13	550	566	593	622	651	674	671	670	670	671	673
1	550	576	616	658	698	731	734	739	745	750	756
12	550	593	683	788	888	950	966	981	996	1009	1023
24	550	623	756	890	1000	674	1077	1093	1108	1121	1134
36	550	676	875	1036	1145	1198	1214	1229	1243	1256	1268
48	550	773	1069	1237	1319	1351	1367	1381	1394	1406	1415

Conditions of start transient-unit soaked at 550°R

Cold inlet temperature constant at 550°R

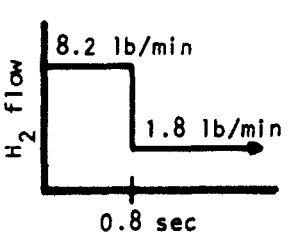

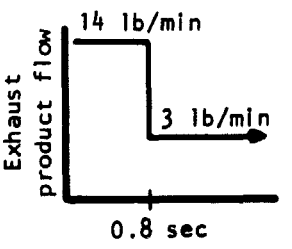

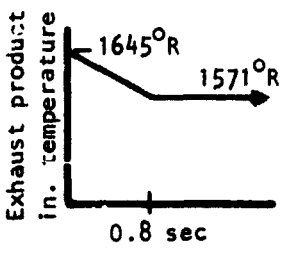

S-81270

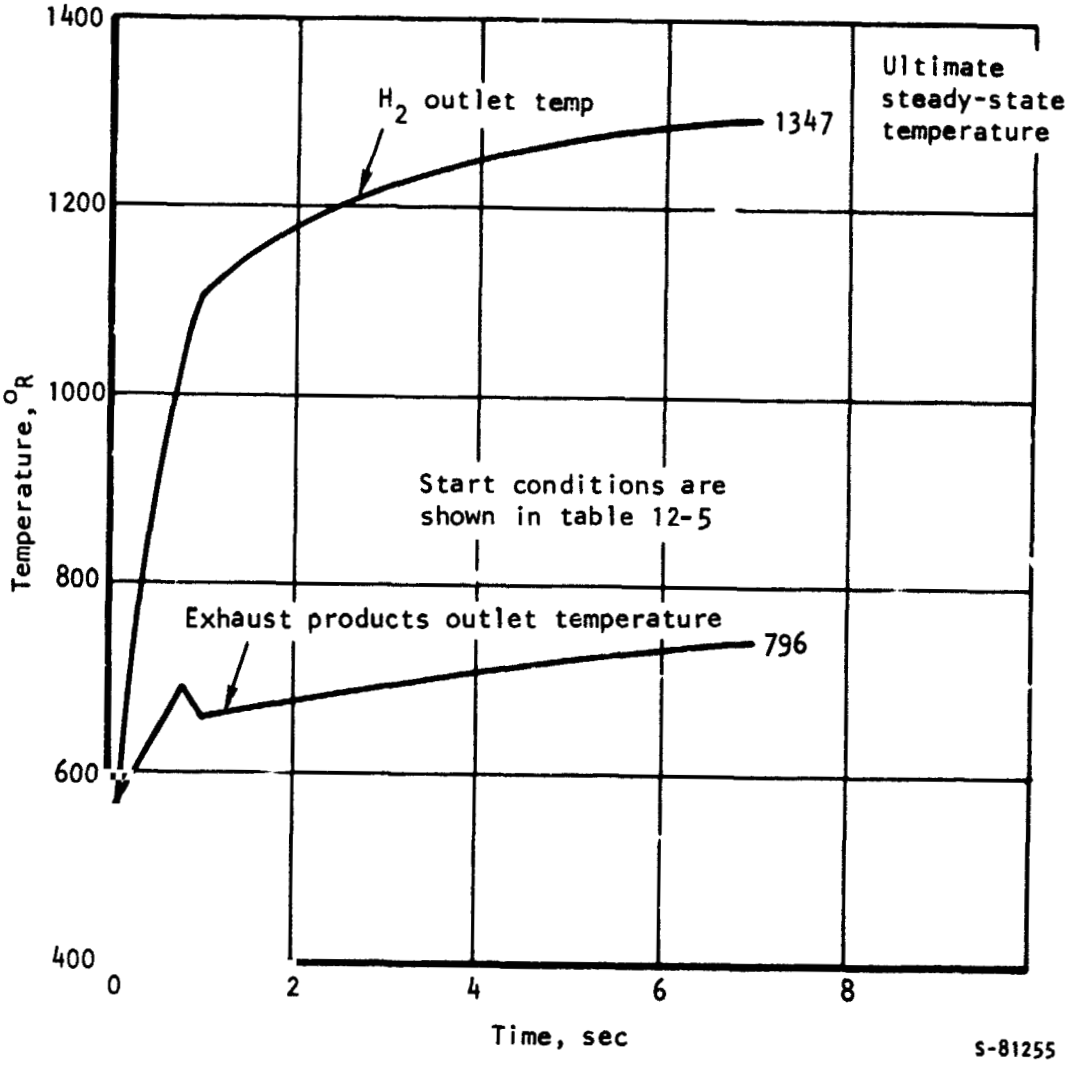

Figure 7-15.--Recuperator Start Transient.

The recuperator was analyzed for loads imposed by temperature, pressure, and acoustic vibration of the tubes. Preliminary designs and subsequent analysis led to the structural configuration of dwg. 159560, which meets the specified operational and test requirements. Each of the heat exchanger flow circuits was analyzed for the proof pressure at the maximum temperature condition. Calculated stresses and margins of safety are summarized in table 7-13.

A minimum U-tube bend radius of 1.50 in. was established to achieve a thermal stress level of 17.0 ksi at the first dimple, which is 0.75 in. away from the supporting plate adjacent to the bend. The analysis indicates that the cantilevered U-bend portions of the tubes may require lateral support for flight use to reduce vibration response.

Structural design of the hydrogen manifold region of the heat exchanger was dictated by pressure containment and thermal deformation. The cylindrical inlet and outlet manifolds are used to obtain acceptable pressure and thermal stresses. Direct attachment between manifolds was avoided, and attachment of the manifolds to the shell is by centrally located welds that allow for longitudinal thermal expansion. The shell structure surrounding the manifolds has the flexibility necessary to accommodate the required thermal deformation. Reduced stresses around the hydrogen inlet and outlet duct penetrations of the shell are obtained by the use of doublers.

Four beads on the side plates in the direction of the tubes are necessary. These beads are tied into the tube support plates to provide a structure that will withstand external collapsing pressure loads. The side plates fit closely to hydrogen manifolds, but are not attached to avoid thermal loads.

Bidirectional reinforcement of the combustion product ducts also was required to resist external pressure and buckling.

The entering combustion products are near sonic velocity and cause noise and vibration excitation of the tubes. Vortex shedding frequency is estimated as high as 67,000 Hz. This excites transverse vibration of the gas column and presents an acoustic noise problem. To eliminate it completely, 16 baffles (almost one per tube row) would be required. Five baffles are installed in the present design to suppress the audible noise. At least three times as many supporting plates are needed to eliminate tube vibration. With five supporting plates, the tubes vibrate in the fundamental mode under operating conditions with a 1.0 ksi bending stress at 210 g's. This corresponds to a small, acceptable displacement.

Preheater/Regenerator.--The preheater/regenerator, as shown in dwg. 159570, is of tube-and-shell, all-stainless-steel, brazed-and-welded construction. The large temperature differences between the tube and shell sides necessitated special provisions for thermal growth. Therefore, a bellows assembly has been incorporated in the unit. The colder hydrogen flows inside of the tube in both applications. The warmer hydrogen makes six passes across the tube bundle. The overall flow direction is cross-counterflow for the preheater and cross-parallel for the regenerator.

TABLE 7-13

SUMMARY OF STRESSES

Part names and numbers	Design conditions	Stresses, ksi	Allowable σ, or life N	M. S.
U-tubes	Proof pressure, 900 psig	11.50	20.00(1100°F)	0.74
	Thermal stress	17.00		
	Vibratory stress	8.69		<0.30*
Head pan assembly	Proof pressure, 900 psig	17.71	21.50(800°F)	1.214
	Thermal stress	10.15	N high**	
Side plate assembly	Proof, 14.7 psi external	10.91	20.0(1100°F)	0.83
	Thermal stress	4.28	N high**	
Return cap	Proof, 14.7 psi external	2.46	21.5(800°F)	High
Combustion product ducts	Proof, 14.7 psi external	11.20	20.0(1100°F)	0.79

*From the Modified Goodman diagram
**N = Allowable number of cycles at the given condition

PART NO.	A PORT	B PORT
159570-1-1	OUT	IN
159570-2-1	IN	OUT

FOLDOUT FRAME

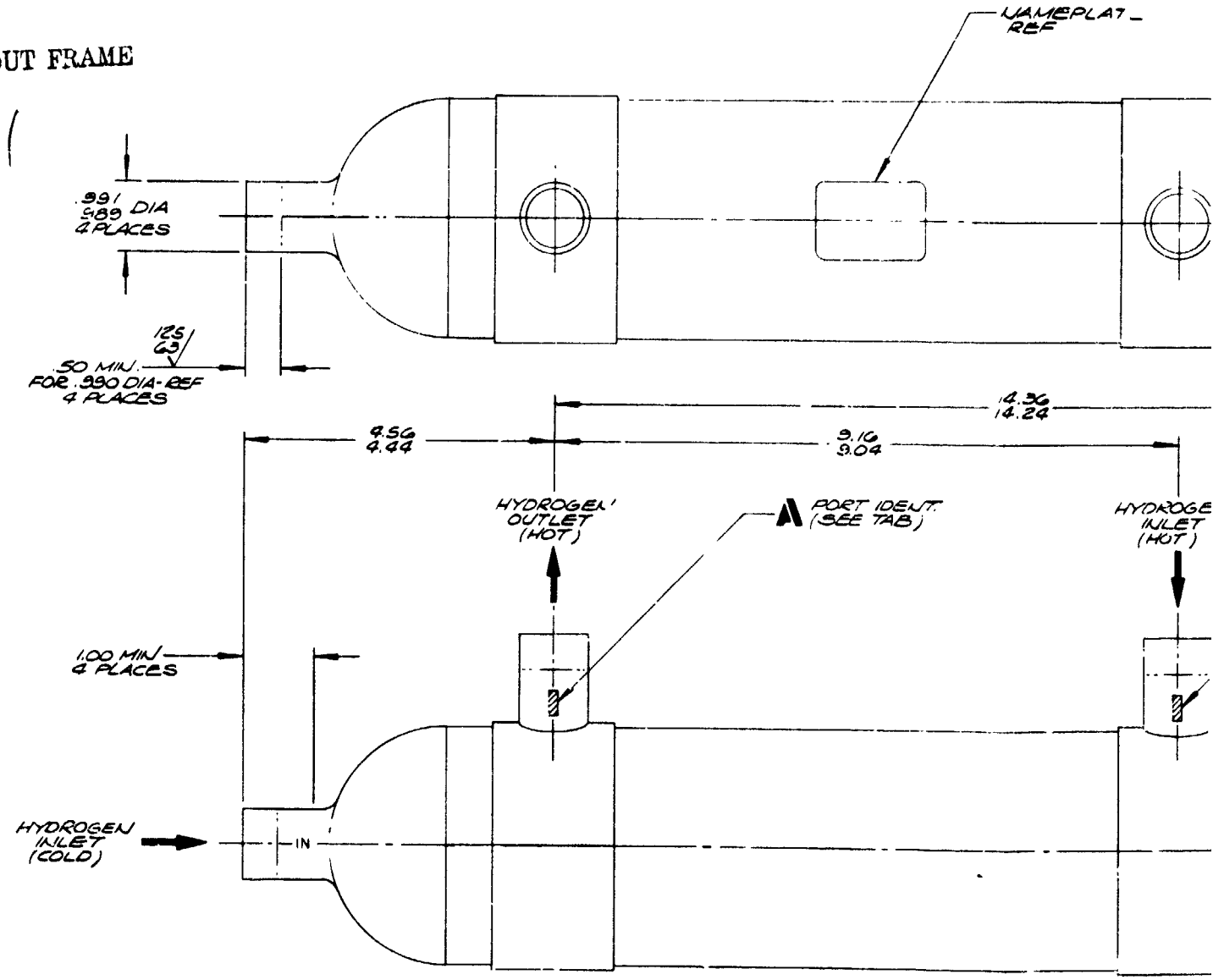

2. UNIT DESIGNED TO WITHSTAND SIMULTANEOUS PROOF PRESSURE ON BOTH CIRCUITS, OF 100 PSID ΔP MAX., CIRCUIT TO CIRCUIT.

1. ALL OPENINGS PROVIDED WITH SHIPPING COVERS. REMOVE ONLY AT TIME OF INSTALLATION

NOTES: UNLESS OTHERWISE SPECIFIED.

FOLDOUT FRAME 2

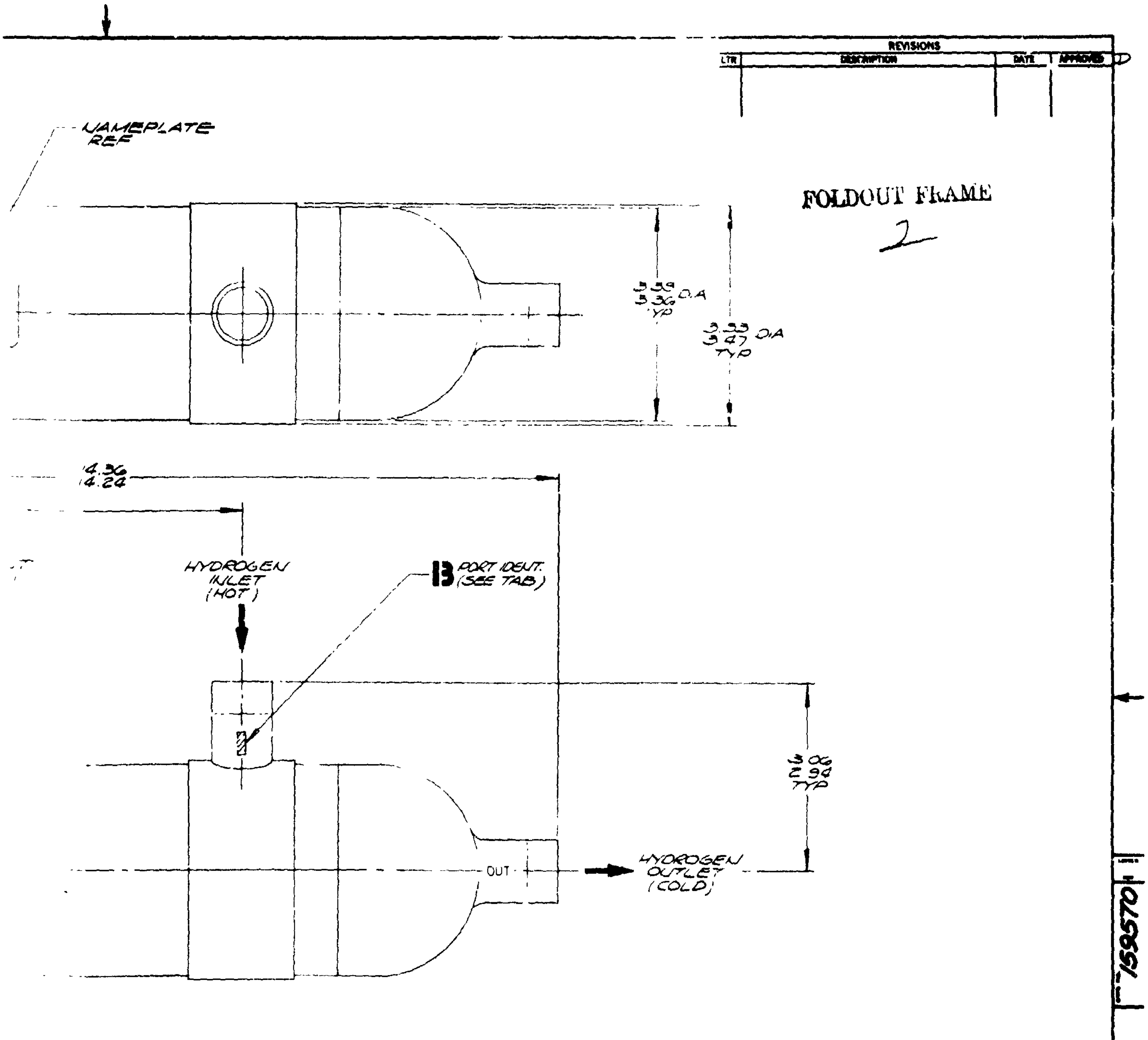

PART NO.	ASSY NO.	CALC. WEIGHT	REMARKS
159570-2-1	159571-2		REGENERATOR
159570-1-1	159571-1		PRE-HEATER

QTY REQD	ITEM NO.	CODE IDENT NO.	PART OR IDENTIFYING NO.	NOMENCLATURE OR DESCRIPTION	S/M
	← ASSY			PARTS LIST	

...AND SIMULTANEOUS CIRCUITS, OF 100 PSID ΔP

...TH SHIPPING COVERS. ...INSTALLATION.

...SPECIFIED.

NEXT ASSY	USED ON
	FINAL
	FINAL

APPLICATION

UNLESS OTHERWISE SPECIFIED: BURR CONTROL PER ...

IDENTIFICATION MARKING PER ...

STD INTERPRETATIONS PER ...

HEAT TREATMENT | PROCESS

5-31-73 · 6-5-73 · 6-15-73 · 6-2-73

AIRESEARCH MANUFACTURING COMPANY

HEAT EXCHANGER OUTLINE, HYDROGEN

SIZE	CODE IDENT NO.	DWG NO.
D	70210	159570

SCALE 1/1 — SHEET 1 OF 1

7-4?/7-44

The heat transfer design point occurs at a regenerator operating condition, whereas the most severe thermal environments exist when the heat exchanger is operated as the preheater.

This unit also was investigated in detail by use of the thermal analyzer computer program. Since the start and power change transients are expected to be much slower than the recuperator, only steady-state operating conditions were investigated. The nodal models utilized are depicted in figs. 7-16 and 7-17. The two models are essentially the same, except for the direction of shell-side fluid flow with respect to the flow inside of the tubes.

The steady-state results at both maximum power and idle when the unit is operated as the recuperator are presented in table 7-14. The temperature difference between various portions of the core are not extremely large.

The corresponding solutions when the unit is operated as the preheater are given in table 7-15. The temperature gradients are much greater for this mode of operation. These gradients necessitated the use of a bellows to compensate for the differential thermal expansion between the tube bundle and the shell, which operates at essentially hot fluid temperature.

The more severe pressure and temperature requirements of the preheater were used in the stress analysis. The analysis considered the proof and burst pressure conditions at temperature as well as the 1000 start-stop life cycle requirement. The analysis indicates that the design shown in dwg. 159570 will meet the specified structural requirements.

The tubular heat exchanger with a cylindrical shell and hemispherical caps is a configuration well suited for pressure containment. The design pressures and allowable stresses at temperature are shown in table 7-16. The allowable stresses are AiResearch-established minimums for type-347 stainless steel. Calculated stress conditions are shown in table 7-17 for proof and burst pressures.

The large temperature difference between the tube bundle and the shell dictated the structural design with a floating header and a bellows seal. The normal operating stresses in the tube bundle are low, and the shell is the primary structural consideration. The heat exchanger was analyzed for the specified operating conditions 14 and 15B, as shown in table 7-18.

A computer program for static analysis of thin elastic shells of revolution was used to calculate the thermal stresses in the shell and the cap. Only one-half of the shell and one cap were analyzed, because the shell is considered free to grow radially at its centerline, and the slope is considered as fixed

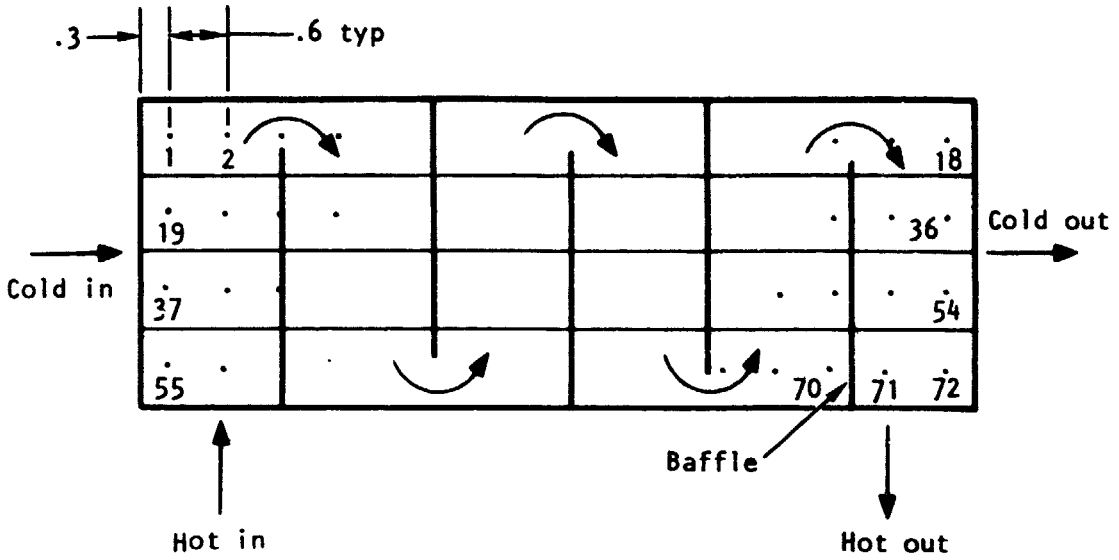

Figure 7-16. --Regenerator Nodal Model - Six-Pass, Cross-Parallel Flow.

Notes:
1. Node numbers refer to metal matrix
2. Each hydrogen fluid stream has a corresponding number of nodes
3. Shell fluid is mixed between each pass

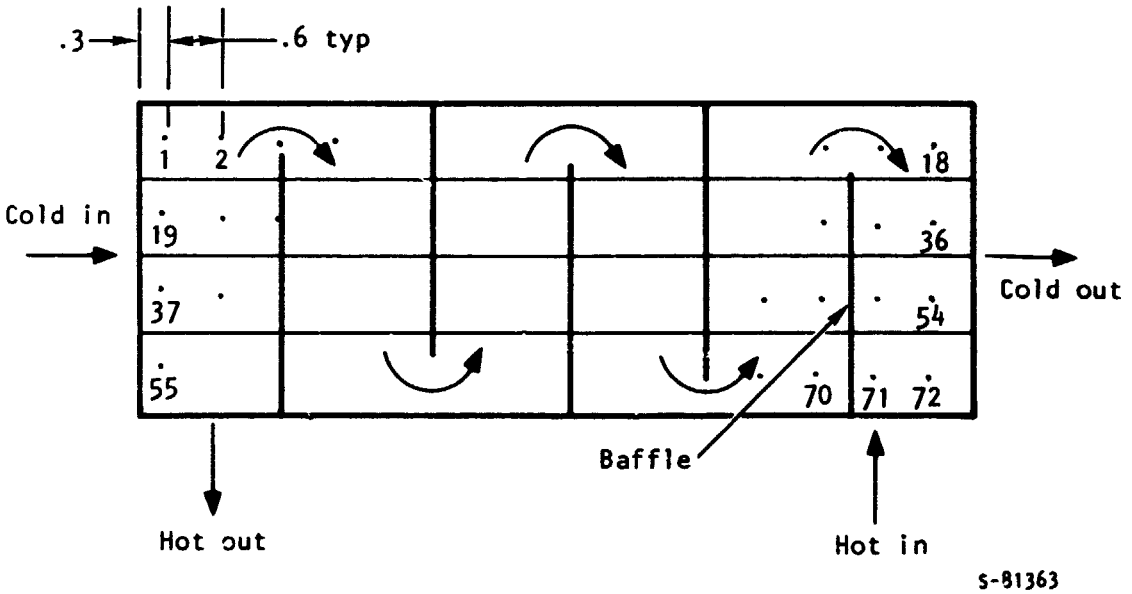

Figure 7-17. --Preheater Nodal Model, Six-Pass, Cross-Counterflow.

TABLE 7-14

REGENERATOR METAL NODE STEADY-STATE SOLUTION

Condition 14		Condition 15B	
NODE NO.	TEMP.	NODE NO.	TEMP.
1	458.86	1	454.45
2	461.27	2	464.56
3	463.54	3	466.74
4	463.65	4	454.43
5	465.36	5	463.52
6	466.94	6	473.40
7	461.85	7	411.37
8	462.98	8	418.10
9	464.04	9	424.85
10	464.13	10	422.45
11	464.92	11	425.95
12	465.66	12	429.09
13	463.42	13	416.65
14	463.93	14	418.29
15	464.42	15	419.53
16	463.79	16	417.46
17	464.14	17	418.28
18	464.48	18	419.05
19	460.59	19	497.10
20	462.93	20	488.66
21	465.21	21	489.27
22	462.71	22	438.06
23	464.37	23	448.28
24	465.94	24	458.91
25	462.51	25	415.82
26	463.74	26	422.92
27	464.60	27	429.69
28	463.73	28	418.79
29	464.50	29	422.40
30	465.23	30	425.67
31	463.77	31	417.24
32	464.29	32	418.98
33	464.78	33	420.57
34	464.09	34	417.87
35	464.44	35	418.72
36	464.77	36	419.50
37	462.34	37	523.43
38	464.68	38	514.52
39	466.95	39	514.16
40	461.83	40	425.13
41	463.47	41	435.62
42	465.03	42	446.99
43	463.43	43	422.84
44	464.56	44	429.82
45	465.62	45	436.37
46	463.38	46	416.77
47	464.14	47	420.33
48	464.85	48	423.56
49	464.16	49	416.96
50	464.68	50	420.66
51	465.17	51	422.19
52	464.42	52	419.03
53	464.77	53	419.81
54	465.10	54	420.52
55	464.18	55	551.30
56	466.52	56	541.75
57	466.78	57	540.91
58	461.04	58	414.08
59	462.65	59	425.08
60	464.19	60	436.57
61	464.30	61	430.86
62	465.43	62	437.39
63	466.49	63	443.60
64	463.09	64	415.60
65	463.83	65	418.93
66	464.53	66	422.08
67	464.60	67	421.07
68	465.11	68	422.68
69	465.60	69	424.11
70	464.78	70	420.41
71	465.12	71	421.09
72	465.44	72	421.71

Fluid conditions

Condition 14: Maximum power, sea level, 550°R bulk temperature of hydraulic fluid.

Hot flow, lb/min	8.33
T in, °R	505
T out, °R	469
Cold flow, lb/min	8.33
T in, °R	426
T out, °R	461

Condition 15B: Idle power, altitude

Hot flow, lb/min	1.17
T in, °R	716
T out, °R	422
Cold flow, lb/min	1.17
T in, °R	140
T out, °R	416

Note: See Fig. 7-16 for node locations.

TABLE 7-15

PREHEATER METAL NODE STEADY-STATE SOLUTION

Condition 14

NODE NO.	TEMP.
1	410.73
2	399.87
3	395.43
4	476.57
5	501.52
6	496.29
7	493.04
8	505.62
9	507.56
10	630.24
11	636.68
12	646.09
13	670.29
14	685.23
15	697.67
16	775.45
17	793.57
18	808.70
19	454.15
20	415.62
21	408.18
22	486.40
23	486.62
24	482.64
25	526.30
26	521.31
27	521.49
28	609.09
29	615.66
30	625.18
31	687.26
32	700.42
33	712.84
34	797.17
35	811.46
36	826.07
37	766.02
38	428.67
39	421.69
40	470.82
41	471.77
42	468.06
43	543.39
44	537.77
45	537.59
46	590.41
47	597.96
48	607.68
49	707.62
50	720.15
51	731.94
52	819.71
53	833.40
54	847.42
55	478.32
56	442.42
57	436.18
58	456.19
59	457.28
60	454.05
61	561.32
62	555.10
63	554.17
64	572.90
65	581.23
66	591.66
67	729.37
68	741.13
69	752.20
70	843.48
71	856.47
72	869.81

Condition 15B

NODE NO.	TEMP.
1	56.25
2	56.44
3	56.66
4	61.27
5	61.85
6	62.41
7	63.87
8	64.60
9	65.40
10	84.02
11	87.97
12	89.40
13	97.70
14	100.02
15	102.88
16	184.91
17	187.53
18	199.64
19	56.60
20	56.83
21	57.07
22	60.20
23	60.80
24	61.33
25	64.93
26	65.76
27	66.62
28	80.37
29	81.99
30	83.47
31	108.41
32	109.85
33	113.10
34	218.81
35	234.48
36	245.75
37	57.05
38	57.32
39	57.59
40	59.46
41	59.98
42	60.47
43	66.49
44	67.42
45	68.31
46	76.43
47	77.91
48	79.35
49	123.89
50	124.58
51	128.68
52	286.08
53	303.02
54	311.12
55	57.61
56	57.92
57	58.21
58	58.94
59	59.38
60	59.83
61	68.71
62	69.69
63	70.64
64	73.53
65	74.87
66	76.34
67	148.13
68	147.20
69	152.52
70	388.86
71	396.68
72	395.86

Fluid conditions

Condition 14: Maximum power, sea level, 550°R bulk temperature of hydraulic fluid.

Hot flow, lb/min	7.69
T in, °R	1152
T out, °R	561
Cold flow, lb/min	8.33
T in, °R	55
T out, °R	555

Condition 15B: Idle power, altitude

Hot flow, lb/min	0.147
T in, °R	875
T out, °R	59
Cold flow, lb/min	1.17
T in, °R	55
T out, °R	148

Note: See Fig. 7-17 for node locations.

TABLE 7-16

ALLOWABLE STRESSES

	Load conditions		
	Operating	Proof	Burst
Cold cap and tube pressure, psig	700	1050*	1750
Hot shell pressure, psig	600 to 700	900 to 1050	1500 to 1750
ΔP across passes, psig	100	150	250
Type 347 stainless steel at 630°F, F_{ty} ksi		21.5	
Type 347 stainless steel at 630°F, F_{tu} ksi			57.0

*Proof pressure revised to 900 psig after completion of analysis.

TABLE 7-17

CALCULATED STRESS CONDITIONS

	Tubes		Cylindrical shell		Spherical caps	
Testing condition	Proof	Burst	Proof	Burst	Proof	Burst
Pressure, psig	1050*	1750	1050*	1750	1050*	1750
Temperature, °F	360	360	630	630	630	630
Allowable stress, ksi	24.0	60.0	21.5	57.0	21.5	57.0
Tangential stress, ksi	16.4	17.6	13.65	22.6	11.0	18.3
Meridianal stress, ksi	21.2	35.3	7.0	11.0	7.8	11.0
Axial load, lb/tube	14.5					
Critical buckling, lb/tube	66.0					

*Proof pressure revised to 900 psig after completion of analysis.

TABLE 7-18

OPERATING CONDITIONS

	Condition	
	14	15B
Hot Flow, lb/min	7.693	0.147
T_{in}, ^{o}R	1152	875
T_{out}, ^{o}R	560.5	59.1
Pressure, psig	460 to 560	460 to 560
Cold Flow, lb/min	8.331	1.168
T_{in}, ^{o}R	55	55
T_{out}, ^{o}R	554.8	148
Pressure, psig	560	560

at the longitudinal midpoint (the shell is symmetric). The dimensions and temperature profile of this shell-cap structure are shown in fig. 7-18. The stresses for the shell and cap are plotted in figs. 7-19 and 7-20. The stress of 42.2 ksi at the joint of the branch duct and the shell is a theoretical value. This theoretical stress is very localized and may be regarded as a "singular point" of the computer model that will have a 14.2-ksi stress in the fabricated part. The joint at the branch duct, duct, and sphere will have an equivalent thickness of 3 times the 0.08 in. and a stress concentration factor $K_T = 3$. Therefore, the stress at this point will be 14.2 ksi instead of 42.5 ksi. Also, at one-half the shell thickness (X = 0.062 in.) from the joint, the meridianal stress in the branch duct has been reduced to 21 ksi. The maximum stress in this shell cap structure is the meridianal stress in the spherical shell at its joint to the duct, where the stress is 26.0 ksi. The number of cycles that type 347 stainless steel can take at 26.0 ksi at 630°F operating temperature should be more than 10^6 cycles; this provides a good margin of safety over the required thermal and pressure cycles of 10^3 cycles.

Temperature equalizer.--The temperature equalizer shown in dwg. 159580 is of a specialized type of plate-fin construction, with annular passages. A vented buffer zone is included between the oxygen and hydrogen passages to prevent mixing of the fluids in the event of a leak. The heat exchanger is of all-stainless-steel, brazed-and-welded construction. The alternate tubes and fin layers are assembled and then brazed to form a single unit, which is then pressure tested. Upon completion of leak checks, the manifolds are welded on, completing the assembly.

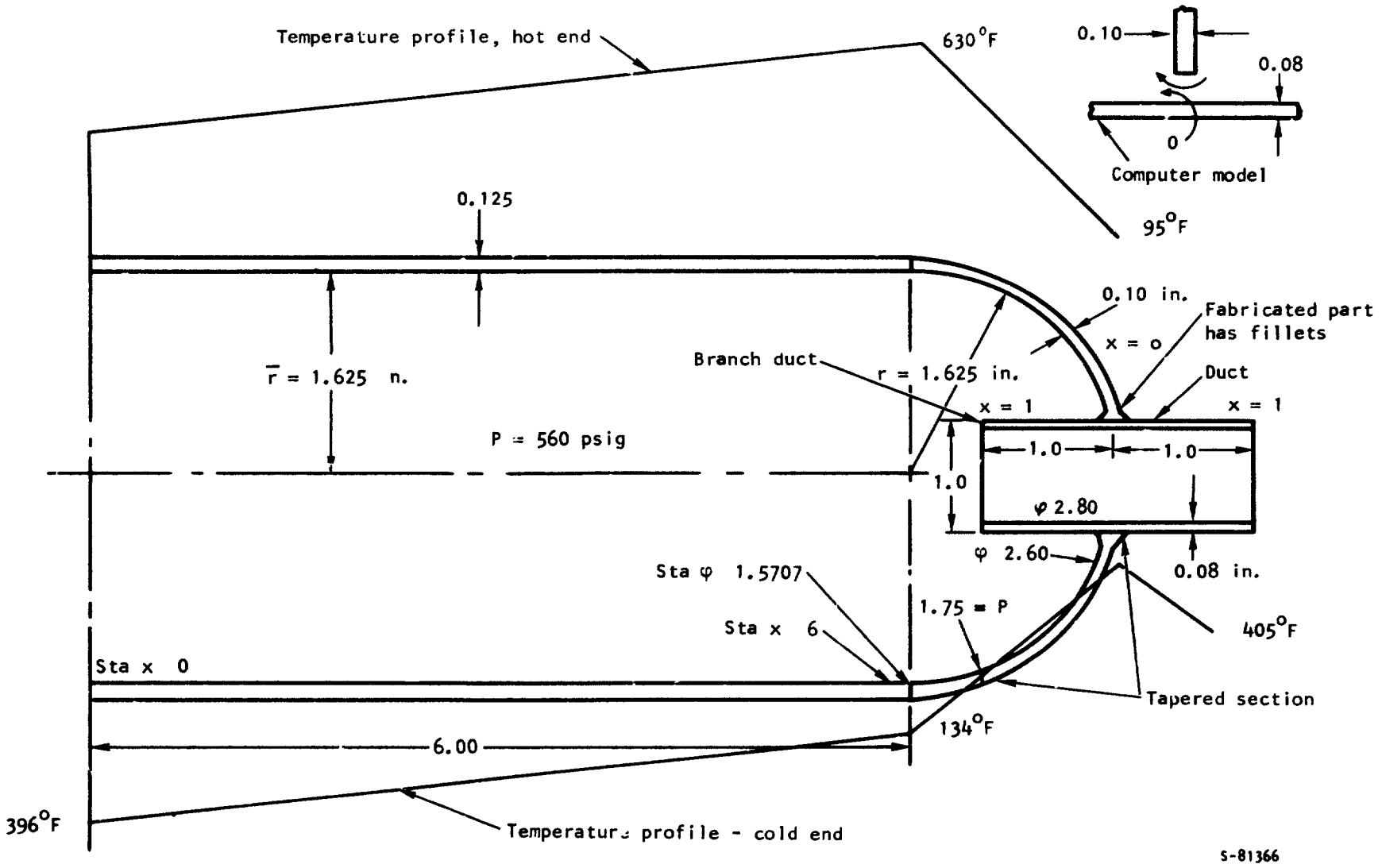

Figure 7-18.--Preheater Stress Model.

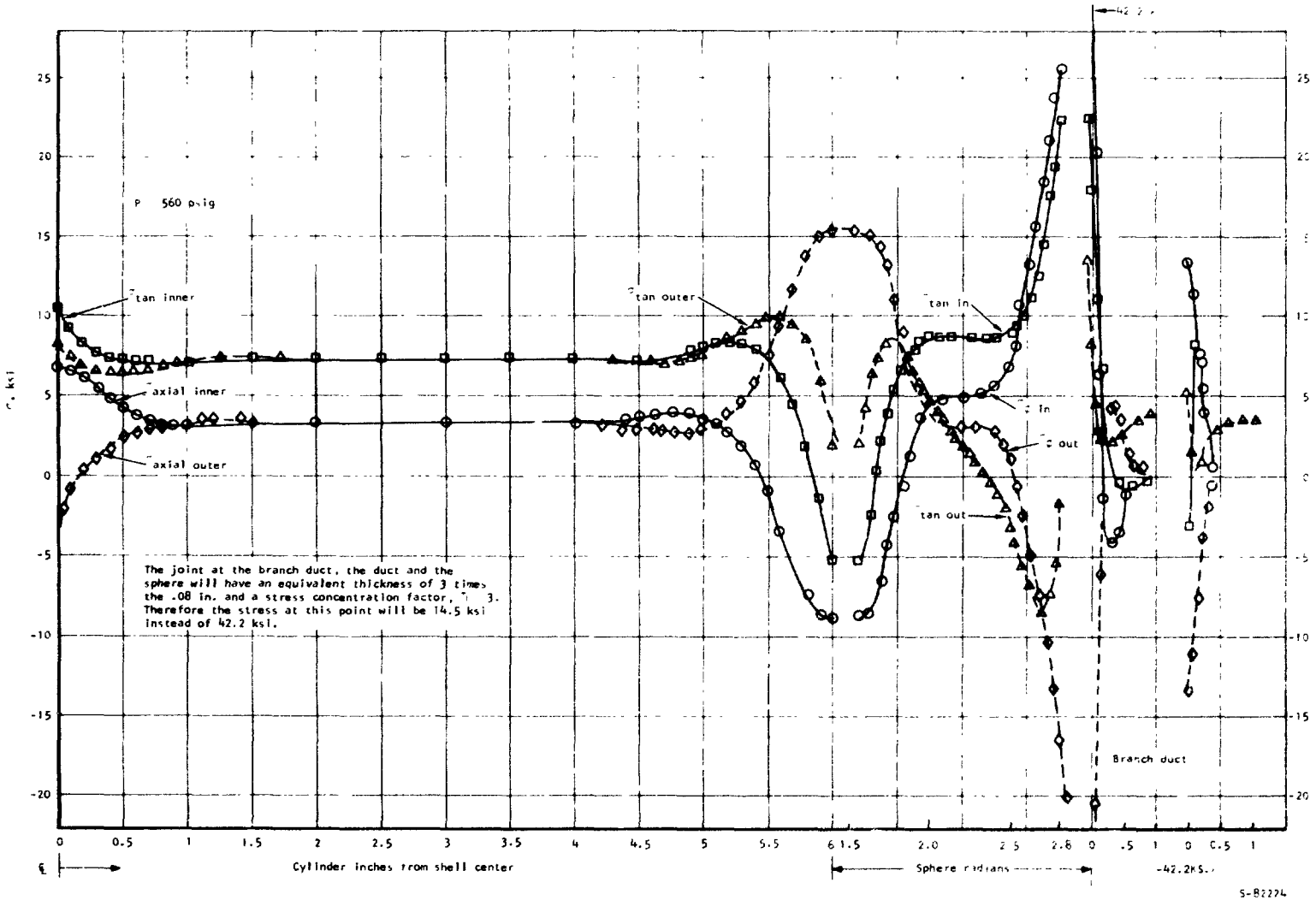

Figure 7-19. Condition 14: Pressure Stresses Plus Thermal Stresses

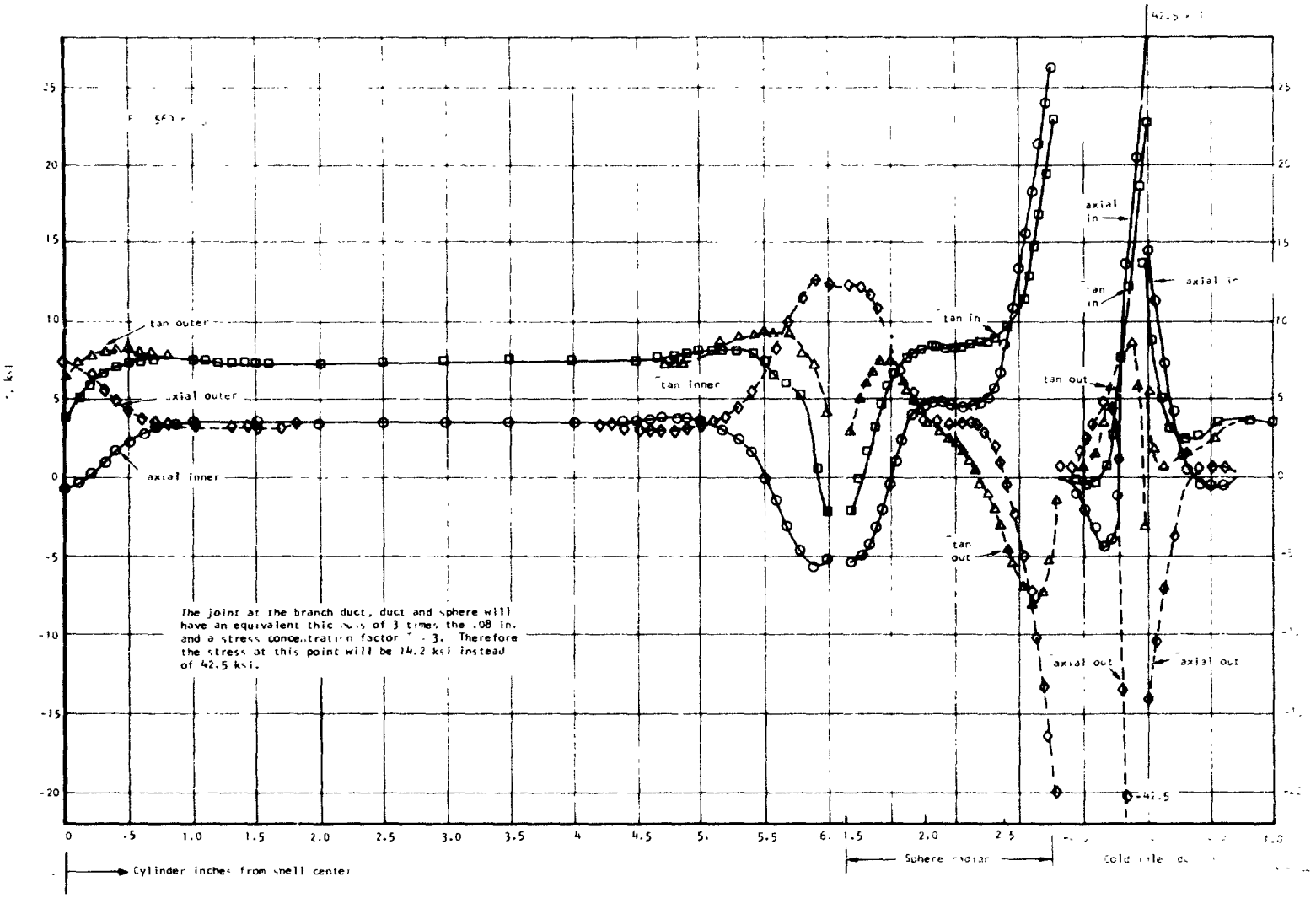

Figure 7-20. Condition 14: Pressure Stresses Plus Thermal Stresses

The pure parallel configuration of the temperature equalizer greatly simplifies the thermal analysis. All temperature gradients are linear and are estimated based on the relative magnitude of the heat transfer coefficients and the conduction resistances of the walls and buffer zone. Since no circumferential temperature gradients exist, the calculation of temperature distribution within the equalizer is relatively straightforward, and the use of the thermal analyzer computer program is not required.

The stress analysis of the temperature equalizer considered the loads imposed by pressure, temperature, and duct interface connections. The configuration and construction shown in dwg. 159580 were determined satisfactory for the specified loading conditions. Thermal stresses are summarized in tables 7-19 and 7-20, and pressure stresses are summarized in table 7-21.

The unit was analyzed for a proof pressure of 1050 psi at 250°F on the hydrogen side and 1350 psi on the oxygen side. The design was based on proof pressure rather than burst because the ratio of ultimate-to-yield stresses for type-347 stainless steel is larger than the ratio of ultimate-to-yield stresses for type-347 stainless steel is larger than the ratio of burst-to-proof pressure factors. Each side is considered pressurized while the other is at atmospheric pressure. Calculated stresses not exceeding 80 percent of the material yield stress were used as design criteria.

The 0.040-in.-thick inner shell is not loaded by pressure because the central cavity is vented to the oxygen flow passage. The 0.062-in.-thick outer shell is loaded by internal pressure only.

The buffer passage tube comprises two concentric cylindrical shells separated by fins and rings, and can be considered as a structure that can be under either external or internal pressure. Critical (buckling) pressure for the entire tube is in excess of the proof pressure. The actual hoop stress in the tube has a margin of safety of 0.74.

FOLDOUT FRAME

1

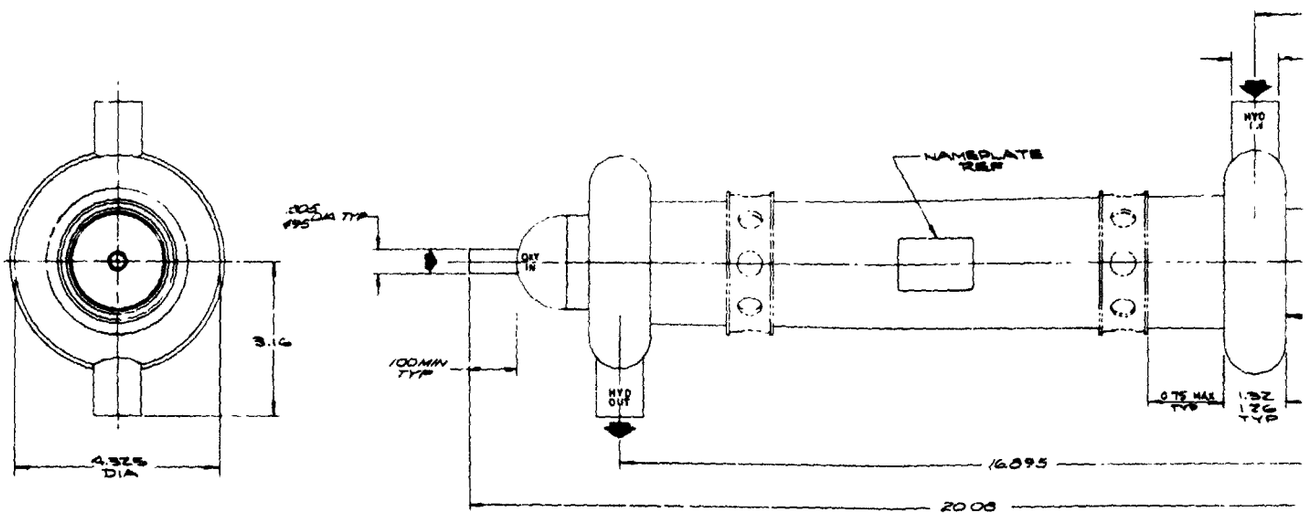

3. UNIT DESIGNED FOR PROOF PRESSURE OF:
   OXYGEN SIDE 1530 PSIG
   HYDROGEN SIDE 1030 PSIG
2. ALL OPENINGS PROVIDED WITH SHIPPING COVERS. REMOVE ONLY AT INSTALLATION
1. DIMENSION TOLERANCE ± .06

FOLDOUT FRAME

2

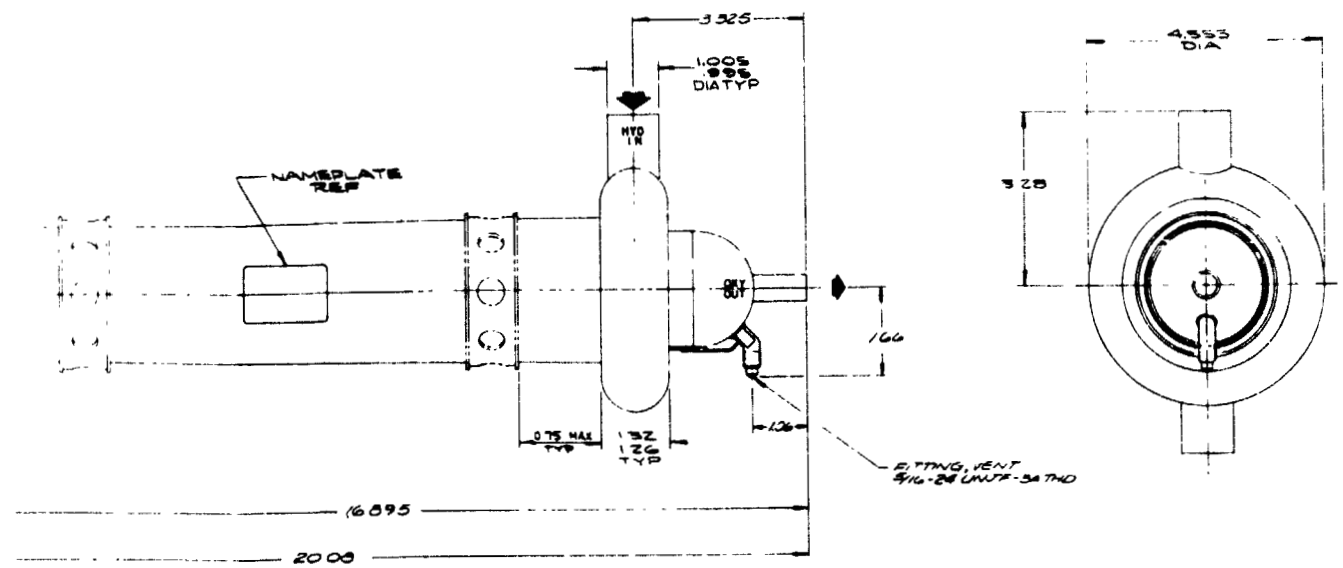

159580-1-1	159581-1	10.5 LBS	
PART NO.	ASSY NO	CALC WT	REMARKS

EQUALIZER OUTLINE, TEMPERATURE, HYDROGEN/OXYGEN

E	70210	159580

3. UNIT DESIGNED FOR PROOF PRESSURE OF OXYGEN SIDE 1320 PSIG HYDROGEN SIDE 1050 PSIG
2. ALL OPENINGS PROVIDED WITH SHIPPING COVERS REMOVE ONLY AT INSTALLATION
1. DIMENSION TOLERANCE ± .06

7-55/7-56

TABLE 7-19

MAXIMUM PROOF PRESSURE STRESSES AND MARGIN OF SAFETY

	Wall thickness t(in.)	Temperature, T (^{o}F)	Allowable stress, σ_{all} (psi)	Calculated maximum stress, σ (psi)	Margin of safety, M.S. = $\frac{\sigma_{all}}{\sigma} - 1$
Outer shell	0.062	230	21,200	21,170	0.0015
Tube					
Hydrogen side	0.045	200	21,600	12,400	0.74
Oxygen side	0.040				
Inner shell	0.040	-160	No pressure load		
Muff					
Torus	0.08	250	20,800	7900	1.63
Muff flange	0.10	250	20,800	19,650	0.06

*Critical (buckling) pressure of the tube: 5000 psi

TABLE 7-20

SHELL MAXIMUM THERMAL STRESSES AND LIFE

	Meridonal stress, σ_1 (psi)	Hoop stress σ_2 (psi	Combined stress, $\sigma_2 = \sigma_1^2 - \sigma_1\sigma_2 + \sigma_2^2$	Life*
Inner shell	+33,000	+47,200	42,000	Approximately 600,000 cycles
Oxygen side	+11,060	+9700	10,500	Infinite
Hydrogen side	-7000	-18,350	16,000	Infinite
Outer shell	-14,300	-30,900	26 00	Infinite

*Based on elastic-plastic analysis, using Wetzel-Morrow method (AiResearch computer program X0870) for type 347 stainless steel brazed at 200°F (R=0)

TABLE 7-21

FIN MAXIMUM STRESSES AND LIFE

	Direct stress, σ_1 (psi)	Shear stress, τ (psi)	Combined stress $\sigma_2 = \sqrt{\sigma_1^2 + 3\tau^2}$	Life**
Oxygen fin, S7053	12,160	6900	17,000	Infinite
Buffer fin, S 7052	13,700	8600	20,000	Infinite
Hydrogen fin, S7051	21,400	14,300	32,800	Approximately 100,000 cycles

**Based on fatigue data for OFHC copper (R = -1), from Cryogenic Matls. Data Handbook, by Air Force Matls. Lab., Wright-Patterson AFB, Ohio, AFML-TDR-64-280.

Thermal analysis.--The thermal stress analysis is based on the temperature distribution shown in fig. 7-21. To simplify the calculations, average shell metal temperatures were used. The analysis was concentrated around the oxygen and hydrogen inlet end of the equalizer because the temperature differences are the largest in this area. A radial and a longitudinal analysis were performed; the results are combined and shown in tables 7-20 and 7-21. A model for the radial analysis was constructed as shown below:

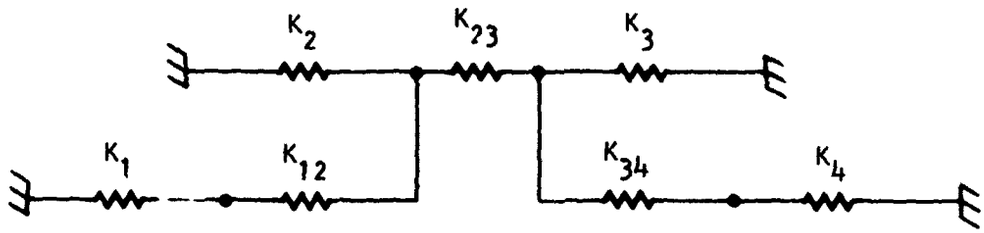

Model for radial analysis S-81352

Where K_1, K_2, K_3 and K_4 represent the radial spring rates of the shells starting from the inside shell, and K_{12}, K_{23} and K_{34} represent the spring rates of oxygen, buffer, and hydrogen fins, respectively. At operating temperature, each of these seven component springs will undergo some thermal expansion and an equilibrium will be reached. The difference between unrestricted length and length at equilibrium is necessary to calculate hoop stresses, and ultimately the cyclic life.

In a similar manner, the longitudinal analysis was performed. The model for the analysis is shown below:

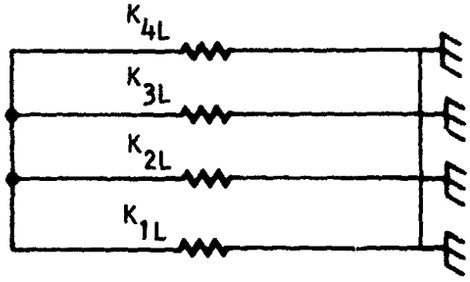

Model for longitudinal analysis S-81353

Where K_{1L}, K_{2L}, K_{3L}, and K_{4L} represent the longitudinal spring rates of the inner, tube (oxygen side, hydrogen side), and outer shell, respectively.

As shown in table 7-21, the hydrogen fin is the weakest component. This determines the life of the unit, which is predicted to be approximately 10,000 cycles from room temperature, to the operating temperatures shown in fig. 7-21.

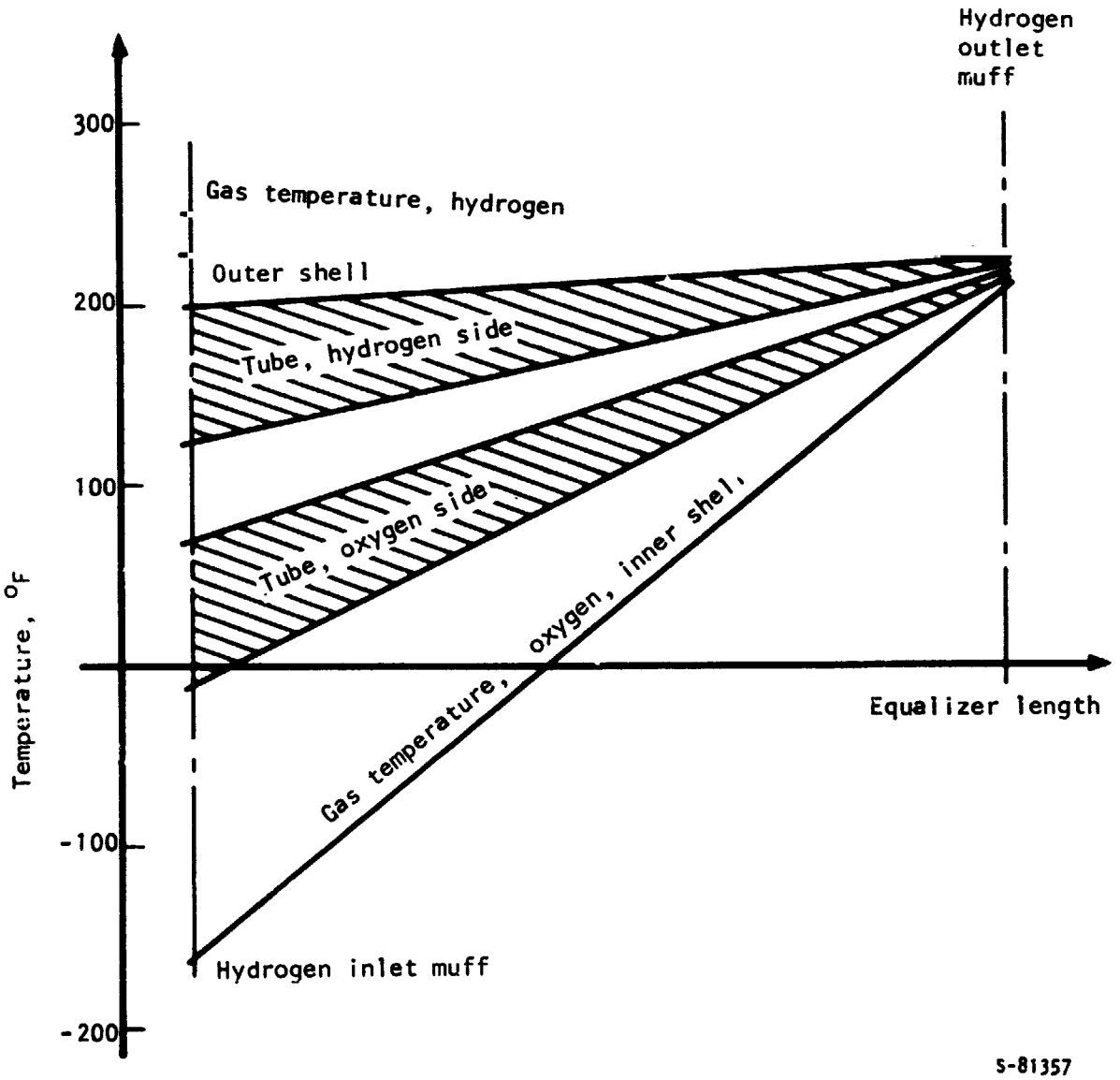

Figure 7-21.--Temperature Distribution Used in the Stress Analysis of the Hydrogen/Oxygen Temperature Equalizer (NASA APU, Space Shuttle).

SECTION 8

RESULTS AND CONCLUSIONS

SECTION 8

RESULTS AND CONCLUSIONS

Early studies of the NASA initial reference system (with jet pump) showed that, although the system was sensitive to component design and jet pump predicted performance, a system could be designed to meet program objectives. The NASA-directed feasibility analysis of an alternate APU system (without jet pump) showed, based principally upon steady-state computer modeling, that such a system also could meet the program objectives without the uncertainties associated with the prediction of jet pump performance. Further dynamic modeling and computer analysis resulted in minor system design changes and demonstrated analytically the feasibility of controlling the alternate within the desired limits. A mathematical model of the required controls was prepared and converted into a breadboard design for test and development of the test system.

The APU turbine design initially was envisioned to be essentially flight-type hardware. All anticipated design problems were solved. A major design effort was required for resolution of heat soakback and thermal transients. The resulting design was evaluated in regard to the test requirements of this technology program. This evaluation resulted in the decision by NASA to simplify the turbine design by deviating from some flight requirements to obtain a simpler and less costly development program. To this end, design changes were made without compromising the program test objectives. The resulting design has a speed of 63,000 rpm at a TIT of 1960°R, but can be retrofitted with higher performance turbine wheels at 2060°R and 70,000 rpm. The test gearbox design is a workhorse unit and is of secondary interest.

In the design of the heat exchangers it was found that the same mechanical design could be used for the hydrogen preheater and hydrogen regenerator, although the preheater is a counterflow installation and the regenerator a parallel flow installation. The same mechanical design also was used for the hydraulic and lube oil coolers. Due to high anticipated thermal stresses, the recuperator design uses a U-tube approach. Manufacturing drawings were completed for the test system components, and no unique or unusual designs were required to achieve design goals.

Early testing of the combustor showed its performance to be high and its operational characteristics very satisfactory.